Selective Oxidation and Oxidative Dehydrogenation Reactions Using Niobium Based Catalysts

Aled Mathew Davies

School of Chemistry, Cardiff University

ProQuest LLC
789 East Eisenhower Parkway
P.O. Box 1346
Ann Arbor, MI 48106-1346

Form: PGR_Submission_200701

NOTICE OF SUBMISSION OF THESIS FORM: POSTGRADUATE RESEARCH

CARDIFF UNIVERSITY
PRIFYSGOL CAERDYDD

DECLARATION

This work has not previously been accepted in substance for any degree and is not concurrently submitted in candidature for any degree.

Signed ..... (candidate) Date 5/2/09

STATEMENT 1

This thesis is being submitted in partial fulfillment of the requirements for the degree of .....(insert MCh, MD, MPhil, PhD etc, as appropriate)

Signed ..... (candidate) Date 5/2/09

STATEMENT 2

This thesis is the result of my own independent work/investigation, except where otherwise stated. Other sources are acknowledged by explicit references.

Signed ..... (candidate) Date 5/2/09

STATEMENT 3

I hereby give consent for my thesis, if accepted, to be available for photocopying and for inter-library loan, and for the title and summary to be made available to outside organisations.

Signed ..... (candidate) Date 5/2/09

STATEMENT 4: PREVIOUSLY APPROVED BAR ON ACCESS

I hereby give consent for my thesis, if accepted, to be available for photocopying and for inter-library loans **after expiry of a bar on access previously approved by the Graduate Development Committee.**

Signed ..... (candidate) Date .....

Abstract.

The selective oxidation of methanol to formaldehyde, the oxidative dehydrogenation of ethane and the oxidative dehydrogenation of propane have been investigated using niobium based catalysts. It has been shown that niobium oxides prepared by different methods show in general a low conversion of reactant in all probe reactions investigated. However, high selectivity to the desired products are maintained (i.e. formaldehyde, ethylene and propene) at elevated temperatures. The introduction of phosphorus into niobium based catalysts enhanced the catalytic performance of the catalyst. The aim was to maintain a high selectivity of desirable products whilst increasing conversion. Two sets on niobium and phosphorus based catalysts were investigated. The first set of catalyst was niobium oxide phosphates, $NbOPO_4$, prepared from a method which was analogous to VPO work.

Catalytic testing of the niobium oxide phosphates showed an increased conversion in both methanol oxidation and ethane oxidative dehydrogenation. However, there was little effect in using niobium oxide phosphates for the oxidative dehydrogenation of propane. Comparing niobium oxide phosphates to niobium oxides, the conversion doubled with respect to oxidative dehydrogenation of ethane and increased 18-fold with respect to methanol oxidation.

The second set of niobium and phosphorus based catalysts were niobium phosphates, $NbPO_5$. These were prepared from the reduction of niobium oxide phosphates. Catalytic testing showed an increased conversion in both methanol oxidation and ethane oxidative dehydrogenation. This is the first time that niobium phosphates and oxyphosphates have been investigated as catalysts and they demonstrate appreciable activity for a range of selective oxidation reactions.

Acknowledgements.

This thesis has only proved possible due to the help and support of many people. Firstly, thanks must go to Dr. Stuart Taylor for offering me the opportunity to study in Cardiff and all his help within this period. I am also grateful to Cardiff University for the funding of the project.

I would also like to express my gratitude to fellow group members who have provided support and help with work. In particular, I would like to thank Tom, Kieran, Ferg, Laura, Nick and Matt who have helped to make the time in Cardiff enjoyable.

Thanks to my family and friends who have supported me throughout the three years of my PhD. Mum and Dad, you have helped me to maintain my focus throughout my studies and ensure that I finished, without you this thesis would not be what it is.

List of Abbreviations.

XRD = X-Ray Diffraction

BET = Brauner-Emmett-Teller Surface area

XPS = X-Ray Photoelectron Spectroscopy.

SEM = Scanning Electron Microscopy

TPD = Temperature Programmed Desorption

TPR = Temperature Programmed Reduction

f.c.c. = Face centred cubic

b.c.c. = Body centred cubic

Raman = Laser Raman Spectroscopy

Nb = Niobium in the (+5) oxidation state

XANES – X-ray adsorption near edge spectrometry

FTIR – Fourier Transform Infrared

HDA - Hydroxylamine

Contents.

Contents.

1. Introduction and Literature Review.

1.1 Aims of Investigation.

The aim of the thesis involves investigating the structure and properties of niobium compounds as catalysts for different reactions. The reactions that will be studied are methanol oxidation, propane oxidative dehydrogenation and ethane oxidative dehydrogenation. As niobium has similar electronic structure and properties to vanadium. Both vanadium and niobium have an electronic configuration of d^5. Vanadium is in the 4^{th} period and niobium is in the 5^{th} period. It is beneficial to investigate whether using niobium in place of vanadium will offer any advantages catalytically.

1.2 Catalysis.

A catalyst is a substance that accelerates the rate of a chemical reaction, but undergoes no chemical change itself. It works by lowering the activation energy of the reaction by providing an alternative reaction pathway to form the products. Thus, an increased rate is observed at the same temperature. The catalyst does not affect the position of the equilibrium, only the rate at which it is approached.

The first time humans used catalysis is lost in prehistoric years. This was when they started to produce alcohol by fermentation. The use of an inorganic catalyst was used by Valerius Cordus in 1552, where sulfuric acid was used to catalyse the conversion of alcohol to ether[1].

In 1874, Fulhame presented the first principles of catalysis. She suggested that small quantities of water were required in order to oxidise carbon monoxide, and that water was unaffected by the chemical reaction. The first person to use the word catalysis was Berzelius in 1835 when studying the effect of sulfuric acid on ethanol to the decomposition of hydrogen peroxide and drawing analogies with the conversion of starch into sugar. It was found that addition of sulfuric acid to ethanol altered the decomposition of hydrogen peroxide

"I shall therefore call it the catalytic power of substances, and the decomposition by means of this power catalysis, just as we use this analysis to denote the separation of component parts of bodies by means of ordinary chemical forces. Catalytic power actually means that the substances are able to awake affinities which are asleep at this temperature by their mere presence and not by their own affinity".[2]

Catalysis was further advanced in 1877 by Lemoine when it was shown that a catalyst could change the rate at which a chemical equilibrium was reached, but the position of equilibrium remained unaltered. Langmuir presented his theories on adsorption in 1915, based on earlier work done by Haber[3]. The most significant step in catalysis modelling was made by Hinshelwood in 1927, where a kinetic theory was based on the earlier findings by Langmuir. Hinshelwood was awarded the Nobel-prize in 1932, and these theories are still being applied to catalysis modelling today.

Heterogeneous catalysis occurs when the catalyst and substrate are in different phases, typically the catalyst is solid and the substrate is in the gaseous phase. In this case, the gaseous substrate is adsorbed on to the solid catalyst surface, before reacting to form the product. Heterogeneous catalysis offers the advantage over homogeneous catalysis (catalyst and substrate are in the same phase) of separation. An example of heterogeneous catalysis is the exhaust gas catalyst system (the most common catalytic reactor in the world)[1]. This is summarised in Table 1.1.

Table 1.1 – Examples of homogeneous and heterogeneous catalysts.

Catalytic System	Phase	Example
Homogeneous	Liquid + Liquid	Acid/base catalysed hydrolysis of ethers
	Gas + Gas	Oxidation of sulphur dioxide catalysed by nitric oxide
Heterogeneous	Liquid + Gas	Phosphoric acid catalysed polymerisation of olefins
	Solid + Liquid	Gold catalysed hydrogen peroxide decomposition
	Solid + Gas	Iron catalysed production of ammonia (Haber process)

1.3 Kinetics of Catalysed Reactions.

The primary effect of a catalyst on a chemical reaction is to increase the rate of reaction – this means that the rate constant has to become larger.

According to collision theory:

$k = PZ \exp(-E/RT)$ (1)

where P is the steric factor, Z is the collision frequency, R is the gas constant and T is the temperature.

In terms of absolute rate theory:

$k = (\mathbf{k}T/h).\exp(-\Delta G^{\#}/RT)$ (2)

where **k** is the Boltzmann constant, $\Delta G^{\#}$ is the Gibbs free energy of activation and h is Planck's constant.

The Gibbs free energy of activation is composed of entropy and an enthalpy of reaction:

$$\Delta G = \Delta H^{\#} - T\Delta S^{\#} \qquad (3)$$

where ΔH is the enthalpy of activation and ΔS^{θ} is the entropy of reaction. The entropy of activation in a catalysed reaction will usually be less than in the corresponding uncatalysed reaction because the transition state is immobilised on the surface of the catalyst. There must also be a decrease in the enthalpy of activation to compensate. The figure below illustrates a potential energy profile for a catalysed and uncatalysed reaction.

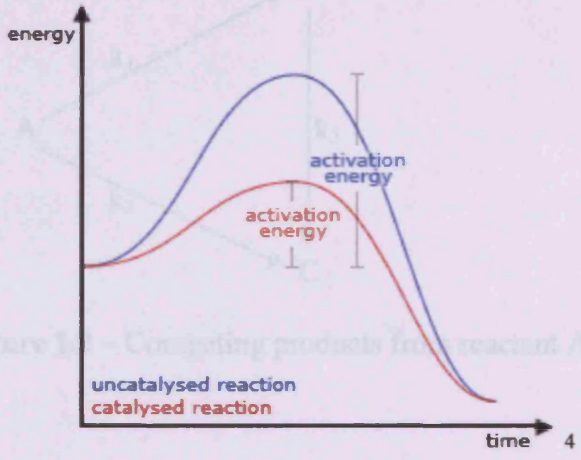

Figure 1.1 – potential energy profile for an exothermic reaction, showing lower activation energy of the catalysed reaction.

There are a wide range of properties of a catalyst that are required in order for it to be an efficient one for any particular reaction. There must be correct kinetic

parameters (i.e. high product yield per unit time) and the correct active phase must be present. In order for the yield to be optimised, the catalyst should usually have a high surface area exposed to the reactant[5].

In general, in catalysis, more than one product is formed from any particular reaction. Only one of these is the desired product. The objective, therefore is to design a catalyst with a high selectivity to the desired product, favouring one particular reaction pathway over any others, as shown in figure 1.2. This figure shows alternative reaction pathways in order to reach a product. For example, A is the starting material. Two different products could be formed, B and C. In order to form B, there is only one reaction pathway. In order to form C, there are two reaction pathways. The first is directly from A to C, the second is from A to B, then conversion of B to C.

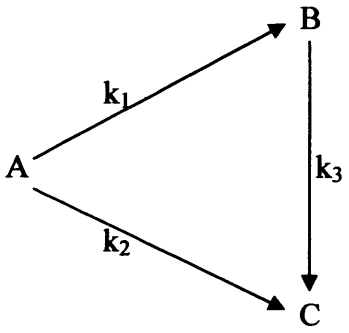

Figure 1.2 – Competing products from reactant A.

1.4 *Background Information of Niobium and Niobium Compounds.*

1.4.1 Niobium – Uses and Properties.

Niobium is a second row transition element, below vanadium and above tantalum. It has an atomic number of 41 with the electron configuration [Kr] $4d^4$ $5s^1$. Niobium is a rare, soft, grey, ductile transition metal, niobium is found in the minerals pyrochlore (the main source for niobium) and columbite. It is never found as a free element, but does occur in minerals. When separated from other elements in the minerals, the most likely form of niobium is niobium(V) oxide. Applications of niobium include steel production (<0.1%), super-alloys (5%), commemorative coins and superconducting magnets[6].

Niobium has attracted much attention in recent years in terms of catalysis. Vanadium oxides are widely used as a catalyst in selective oxidation reactions. Niobium oxide has a similar structure and properties to that of the vanadium oxide. It is therefore beneficial to study partial oxidation reactions using niobium (V) oxide catalysts and investigate the properties and structure change of the catalyst. By investigating these properties and testing the catalyst, better yields may be obtained. The most stable form of niobium is in the +5 state.

Figure 1.3 shows the different compounds of niobium that can be produced. These will be discussed in further detail in the following sections. The main points that will be discussed are niobium oxides and phosphates.

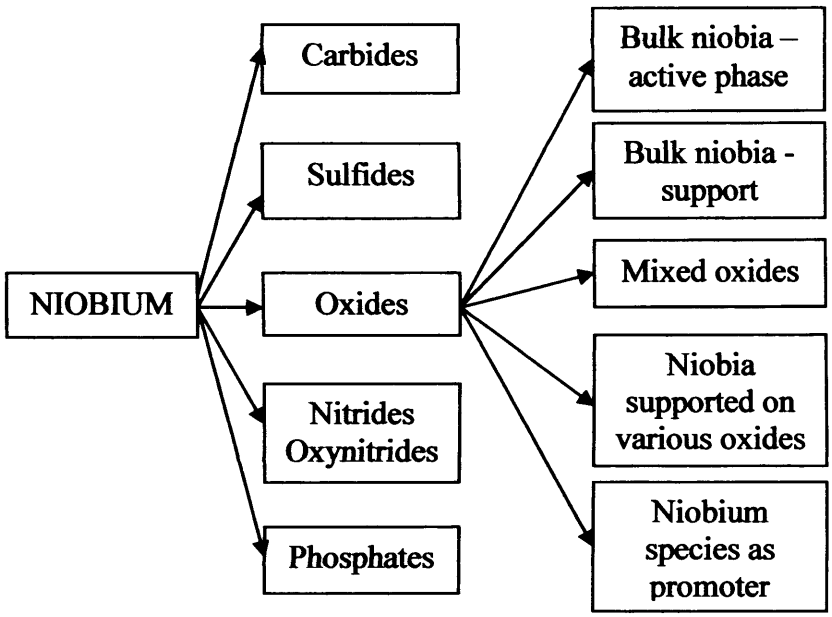

Figure 1.3 – Chemical nature and niobium species in heterogeneous catalysis[9].

1.4.2 Niobium(V) Oxide.

Niobium(V) oxide, otherwise known as niobium pentoxide, has the chemical formula Nb_2O_5. It is mainly used in the production of capacitors and optical glass[7]. Hydrated niobium pentoxide is known as niobic acid. Hydrated niobium oxide is interesting from a catalysis point of view because it retains a high acid strength (H_0=8.2) on the surface, even in the presence of water[8]. Niobium compounds are stable and have strong metal support interactions, which are very important for some catalysts[9].

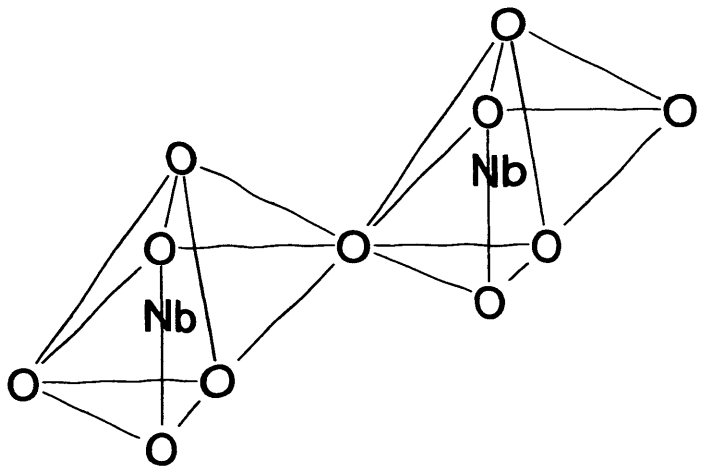

10

Figure 1.4 – Diagram of the type of bonding in Niobium(V) Oxide

As can be seen from the above diagram, only corner oxygen atoms are 'shared' between the niobium atoms. However, during partial oxidation reactions, when a reactant is oxidised, an oxygen atom is transferred from the catalyst to the reactant. This causes the metal:oxygen stoichiometry of the catalyst to alter. Instead of the oxygen atoms on the corner being shared, the both oxygen atoms on one of the edges are shared. The catalyst is then itself oxidised and the structure becomes corner sharing once again[11]. This is illustrated in the following diagram:

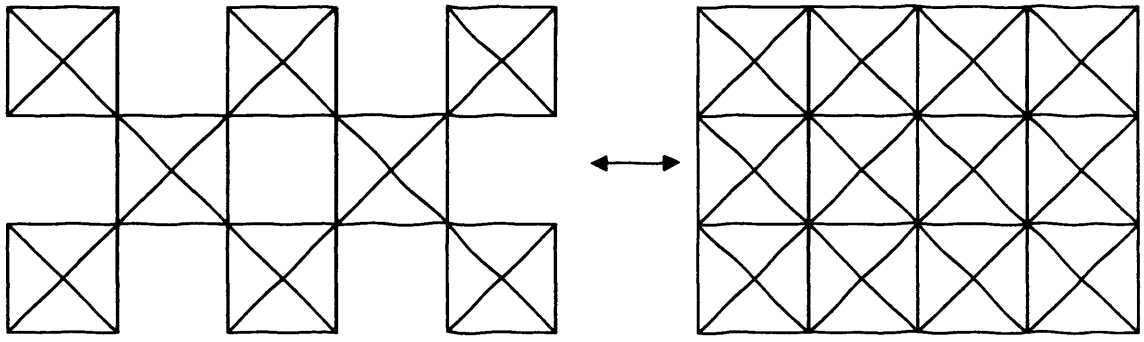

Figure 1.5 – Diagram of the change in structure in Niobium(V) Oxide when Participating in Oxidation Reactions.

This type of reaction is explained using the Mars van Krevelen mechanism. When niobium(V) oxide participates in an oxidation reaction, there are two different ways in which the substrate can be oxidised. The first is that oxygen adsorbed on the surface from the gas phase combines with the substrate and forms products. The second is that oxygen is donated from niobium(V) oxide, causing a structural change of the catalyst (as seen in Figure 1.4). The structure changes from corner sharing to edge sharing oxygen atoms. The catalyst is then re-oxidised and the structure of the catalyst goes back to the original structure (i.e. back to corner sharing, as shown in Figure 1.4 and Figure 1.5).

In its hydrated form, niobic acid is active for the vapour phase esterification of ethyl alcohol[12] and for ethylene hydration[13]. Most work involving niobium oxide focuses on using niobium oxide as a support for other materials[14] and as surface modifiers[15], often using a second component of the system in conjunction with it.

Early work carried out by Brauer identified three modifications of niobium pentoxide – low (L), medium (M) and high (H) temperature niobium pentoxide[3]. The structures of the various forms of Nb_2O_5 are complicated. According to XRD data, there are 20 different forms of niobium pentoxide[16]. Octahedral elements are the decisive factor for the structure of the oxides. The stoichiometric ratio of 2.5 can be achieved by combination of various octahedral linkages, and this is the reason for the multiplicity of the niobium pentoxide structures[17].

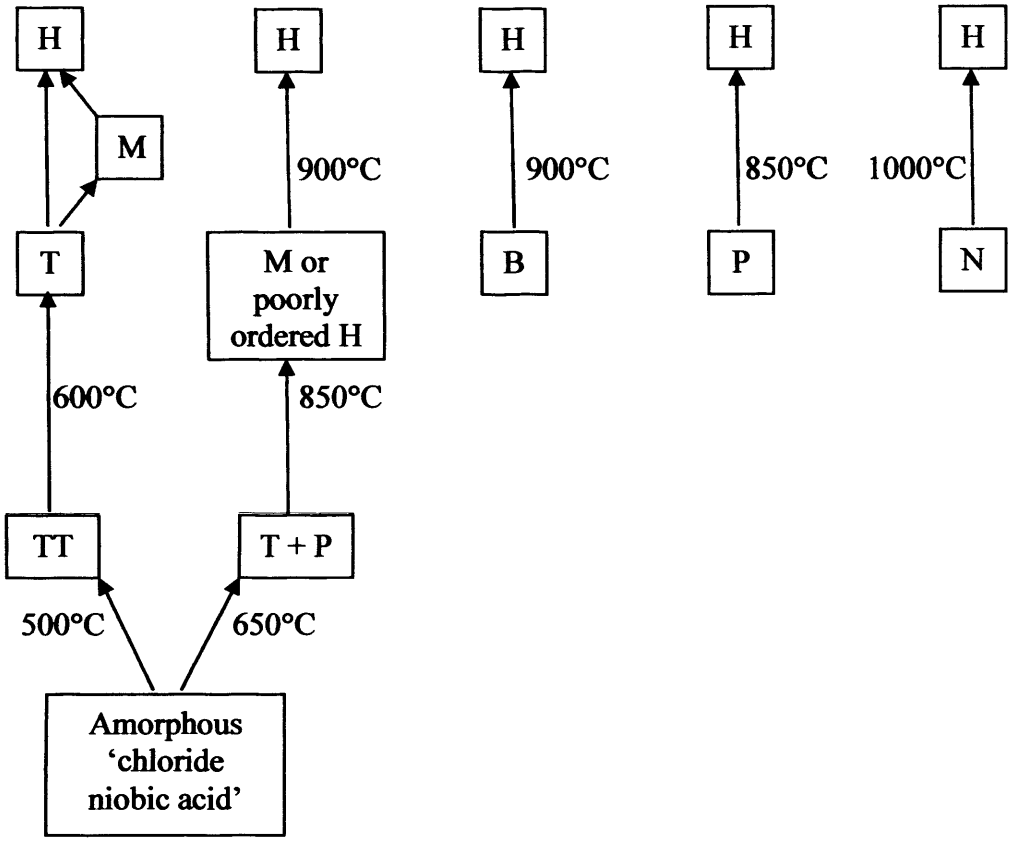

Figure 1.6 – Conversion of the forms of Nb_2O_5 on heating in air[18]. The various forms of niobium oxides are prepared using different calcination temperatures.

There is a strong interaction between niobia and silica. This interaction inhibits the crystallisation of a surface phase, and thus makes the niobium pentoxide layer more difficult to reduce. Temperature programmed reduction experiments were carried out by Burke *et al.* and found that niobium oxide reduces at 880°C, whereas a niobium pentoxide monolayer has a peak close to 1000°C[19].

The unfavourable feature of niobium oxides (which is the biggest branch of niobium compounds in heterogeneous catalysis) is the low reducibility of niobium species[9].

As described in figure 1.3, bulk niobium pentoxide exists as NbO_6 units. However, NbO_7 and NbO_8 units appear occasionally. Wachs *et al.*[20] compared some

features of group V metal oxides and found that, although the surface area of niobium oxide was lower than the surface area of vanadium oxide, bulk Nb_2O_5 possessed approximately five times greater number of specific surface active sites for methanol oxidation than bulk V_2O_5, due to the different surface morphologies of both oxides.

Niobium oxides exhibiting high surface areas have been investigated by Montes[21]. Surface areas of the samples varied from 27 to 132m^2/g. It was found that all of the materials investigated exhibited the Nb=O bond in a highly distorted octahedral NbO_6, indicated by a band in the IR near 850cm^{-1}. After calcination at 673K, acid sites were mostly Bronsted acid sites. However, at increased temperature, Lewis centres increased in importance. This was shown using the aldol condensation of acetone. The products mesytilene and acetic acid are controlled by acid centres. As the temperature of the reaction increased less products were observed, indicating Lewis acid sites were more important. Small amounts of niobium oxide species added to catalysts (usually mixed oxides) can also play a role of a promoter.

The preparation of niobium oxide exhibiting high surface area opened up new possibilities in their application as supports for other active catalysts. Previous work has studied supporting metals such as Pt[22,23], V[24] and Fe[25], to name just a few. These elements improve the conversion of reactant, while the niobium oxide support maintains its high selectivity.[22-25]

The main approach to use mixed oxides containing niobium and niobia supported on various oxides is the catalytic application of their redox properties as well as Lewis acidity of niobium species[9]. The catalytic properties of niobia supported on metal oxides depend on the nature of the support. Most frequently, silica, titania and alumina are used as supports for niobium oxides. The addition of niobia to alumina increases the acidity of the alumina[26]. Lewis acidity was found in all of the

supported niobium oxide systems, while Bronsted acid sites were only detected in niobium supported on alumina and silica.

Niobium oxides change phases at different temperatures, according to Schafer *et al.*[27]. At 320 °C, a TT phase niobium(V) oxide is formed from the oxidation of NbO_2. When this is heated to 410°C, a T phase of niobium(V) oxide is formed. Further heating to 817°C produces a B phase of niobium(V) oxide and heating to 960°C forms a H phase of niobium(V) oxide.

1.4.3 Niobium, Oxygen and Phosphorous Containing Compounds.

Both niobic acid and niobium phosphate catalysts are highly acidic solid catalysts in fructose dehydration[28]. Niobium containing materials have found applications in several catalytic processes, where strong acid properties are required. Niobium phosphates and oxides have attracted interest due to their strong acid properties, which can be preserved in polar liquids[29,30]. Hydrated niobium oxide is interesting from a catalysis point of view because it retains a high acid strength (H_0=8.2) with a higher ratio of Lewis/Bronsted acid sites[17]. This exhibits a higher acid strength than niobic acid.

Hydrated niobium phosphate, $NbOPO_4.nH_2O$, consists of NbO_6 distorted octahedra which are connected in their equatorial planes by PO_4 tetrahedra via sharing corners[31]. Work was carried out by Carlini *et al.* and it was found that in both niobic acid and niobium phosphate, niobium is octahedral. However, when niobium is impregnated with phosphoric acid, niobium is a higher coordinated species.

All phosphate containing samples investigated by Carlini bulk and impregnated indicated the presence of both terminal POH and NbOH groups. High

activity of all of the catalysts is achieved in the dehydration of fructose to 5-hydroxymethyl-2-furaldehyde. However, niobium phosphate exhibits polymerisation, making it more promising practically.

Work has been carried out on mixed vanadium phosphorus – niobium phosphorus catalysts[32]. Nb in VPO phases and V in NbPO phases were observed, resulting in V^{5+}/V^{4+}. From a catalytic point of view, this is advantageous due to the catalyst having good redox properties and the catalyst having a good ability to donate oxygen to form the product.

1.4.4 Other Niobium Compounds.

Small atoms such as carbon, nitrogen or oxygen dissolved interstitially in the lattice of early transition metals produce a class of compounds with unique physical and chemical properties[33] for electronic, magnetic and refractory purposes. Such compounds are called (oxy)nitrides and (oxy)carbides. Although little research has been carried out on these types of materials, early investigations suggest that their catalytic activity compares to those of noble metals.

Niobium nitride does not reach the +5 oxidation state. The following compounds exist: Nb_2N-β-phase (hexagonal), Nb_4N_3-γ-phase (tetragonal) and NbN-δ-phase (cubic)[34].

Nitrides are commonly prepared by the direct interaction between transition metals and dinitrogen or ammonia[27]. Brayner *et al.* prepared extruded niobium oxynitrides with macropores and then tested them in cyclohexane dehydrogenation reactions[33]. These were active, but less stable than their molybdenum and tungsten counterparts.

Niobium carbides can be prepared by a variety of methods, including direct union of the elements at high temperature (e.g. in a solar furnace) or by self-propagating high-temperature reaction, carburization of oxides by carbon or methane-hydrogen mixtures or by plasma-chemical processes[35].

Five solid systems exist in the niobium carbon system: a solid solution of carbon in niobium (b.c.c.), Nb_2C (h.c.p.), NbC (f.c.c.), ζ-Nb_4C_{3-x} and ζ-NbC_{1-x}[36]. The composition range of Nb_2C is very limited at low temperatures, whereas NbC varies from $NbC_{0.7}$ to $NbC_{0.99}$.

1.5 Study of Catalytic Systems.

The reaction systems that have been chosen for catalytic study are methanol selective oxidation to formaldehyde, propane oxidative dehydrogenation and ethane oxidative dehydrogenation. These reactions have been chosen as vanadium is known to be an effective catalyst in these reactions from previous work. Niobium has similar structure and properties to that of vanadium, therefore if vanadium is a good catalyst for these reactions, then a direct comparison can be made to niobium being used as a catalyst.

1.5.1 Methanol – Uses, Properties and Recent Work.

Methanol is a starting material for a number of useful organic products. Much is converted by catalytic processes to formaldehyde, either by oxidative dehydrogenation or by direct dehydrogenation. The former reaction proceeds with

good selectivity to formaldehyde over iron molybdate but is quite exothermic (ΔH = -159kJ/mol), and heat removal is therefore a problem[2].

Haagblad *et al.* investigated a number of $FeAlVO_4$ (with varying concentrations of Fe) catalysts for the oxidation of methanol[37]. It was shown that conversion and selectivity to formaldehyde increased with time on-line studies up to 16 hours. It was also shown that the stability of the bulk phases improved when Al was substituted for Fe in the structure. Using different characterisation techniques such as XRD and XANES, it was found that the $FeVO_4$ post reaction showed that it had transformed into a cation-vacant spinel-type $Fe_{1.5}V_{1.5}O_4$ phase, whereas the AlVO4 phase showed no change in bulk structure. Selectivity to formaldehyde was about 90% for all samples at high methanol conversion. In comparison to pure vanadia, the vanadates had lower activity per V atom and a slightly higher selectivity to formaldehyde. As a result, it was concluded that the role of Al and Fe on the catalyst surface can be described as that of a spacer, decreasing the surface concentration of active V sites and the number of less reactive V-O-V sites.

House *et al.* investigated the selective oxidation of methanol to formaldehyde over iron molybdate catalysts[38]. The reaction of an iron molybdate catalyst (Mo:Fe = 2.2:1) with methanol was studied with a pulsed-flow microreactor. Typical reaction conditions were pulses of 1µl of methanol every 2 minutes into a continuous flow of 10% oxygen in helium at a flow of 30mL/minute. Analysis was carried out continuously in real-time using an on-line quadropole mass spectrometer.

The catalyst was prepared by acidification of a solution of ammonium heptamolybdate to pH2 using nitric acid, before dropwise addition of iron nitrate with stirring at 60°C. The resulting solid was dried overnight at 120°C, before being calcined at 500°C for 48 hours.

The first pulse of methanol showed similar conversion and selectivity to formaldehyde in both aerobic and anaerobic conditions. The conclusion was made that gaseous oxygen was not directly involved in the reaction, but was used to re-oxidise the catalyst surface. Conversion of methanol reached 95% with selectivity to formaldehyde of 90 at 265°C.

Reduction of the catalyst took place under 250°C under anaerobic conditions, which resulted in no conversion of methanol. However, above 250°C, it was found that oxygen migration through the catalyst occurred. The process of oxygen migration led to the formation of new phases, such as $FeMoO_4$, MoO_2, and Mo_4O_{11}. Selectivity of the catalyst during reduction initially changed to CO, but at elevated temperatures, it shifted to CO_2. It was concluded that iron oxide appeared at the surface of the catalyst.

Further work by House *et al.* investigated varying the cation ratio within iron molybdate catalysts for methanol partial oxidation[39]. Mixed cation catalysts with molybdenum and iron were prepared by acidification of solutions of ammonium heptamolybdate to pH2 using nitric acid, before dropwise addition of iron nitrate with stirring at 60°C. A yellow precipitate formed, which was dried at 90°C.

In catalysts with Mo/Fe ratios 1:1 or below, the yellow precipitate redissolved upon continued stirring. The precipitate was then evaporated to dryness at 90°C, which resulted in a brown gel being formed. The solids were dried overnight at 120°C and then calcined in air at 500°C for 48 hours.

The particles were pressed to 10T before being sieved to yield particles between 600 and 850μm. 500mg of each catalyst was tested, except in the case of Mo/Fe 0.5/1 catalyst, where an additional separate loading of 100mg was also tested.

Catalysts were tested in a pulsed flow microreactor. The reactor consisted of a 6mm stainless steel U-tube mounted on an oven. To establish the catalytic performance of the catalyst, 1μL of liquid methanol were passed over the catalyst every 2 minutes in a flow of 30mL/minute, 10% O_2/He, while the temperature was ramped up to 400°C at a rate of 8°C/minute.

From the characterisation data, it can be seen that all catalysts with both molybdenum and iron presented a phase of $Fe_2(MoO_4)_3$ combined with a phase of MoO_3 for high molybdenum ratios and a highly dispersed Fe_2O_3 phase for low ratios. Raman studies showed Mo-O-Mo stretches and terminal Mo=O vibrations present in the sample. Surface areas varied greatly with cation ratios, 1-65m^2/g. As the Mo level increased, the surface area diminished.

Methanol conversion varied greatly for catalysts low in molybdenum, showing the greatest conversion. Using Mo/Fe 0.2/1, 50% conversion occurred at 185°C, whereas using Mo/Fe 2.2/1, 50% conversion occurred at 205°C. Formaldehyde selectivity was above 50% at low temperatures. Using the Fe_2O_3 catalyst, the dominant product was CO_2, with little selectivity to formaldehyde. Catalysts containing low ratios of Mo maintain their high selectivity, however as the ratio of Mo increased, conversion of methanol decreased.

Dias also investigated supported catalysts for the oxidation of methanol[40]. Catalysts were prepared by contacting the support material with a hot, aqueous solution of both Mo and Fe precursors with citric acid. Ammonium heptamolybdate was used as the molybdenum precursor and iron precursors used were chloride, sulfate, phosphate and pyrophosphates.

All catalysts were prepared with Mo/Fe atomic ratio 3, similar to unsupported industrial catalysts[41]. The mixture was a slurry, which was heated to 100°C with

vigorous stirring until dry. No precipitation occurred in this step as this was prevented by citric acid. The catalyst was left to dry overnight, and then calcined at 300°C in air for 5 hours.

Catalytic testing was carried out in a continuous flow reactor at atmospheric pressure. Catalytic behaviour was studied in steady state conditions. Liquid methanol was injected into the air flow. The catalyst was diluted with SiC to avoid adverse thermal effects.

It was found that surface areas, measured by nitrogen adsorption analysis were 60-90m^2/g, depending on the precursor used. Results showed that during the reaction, molybdenum migrated to the catalyst surface. It was also shown that methanol oxidation proceeded via a partial reduction followed by reoxidation of the active phase which segregates MoO_3.

All catalysts prepared displayed high activity and selectivity towards formaldehyde for both low and high methanol conversions. The catalyst prepared from iron pyrophosphate was the most active. The presence of heteropolymolybdates, containing phosphorus, or its Mo rich surface can perhaps explain its enhanced catalytic behaviour. By-products were produced with considerable selectivity at high temperatures and high methanol conversion. This indicated that the combustion products resulted from the consecutive oxidation of formaldehyde.

Wang and Maddix investigated a vanadia on titania catalyst for the oxidation of methanol[42]. Vanadia adlayers of different coverage were prepared on TiO_2(1 1 0) by codosing $VOCl_3$ and water. It was found that with increasing vanadia coverage, the rate of methoxy dehydrogenation to formaldehyde increased until monolayer coverage was reached. It was found that the V-O-Ti bond and the oxidation state of the vanadium cation play an important part in the oxidation process.

Isaguliants and Belomestnykh investigated methanol oxidation over V-Mg-O catalysts[43]. It was researched that using silver catalysts, it was possible to reach a selectivity of 90% towards formaldehyde with almost complete conversion at around 600°C.

Catalysts were prepared by suspending MgO powder in a solution of ammonium vanadate at 40-60°C under stirring. This was rotary evaporated and dried in air at 120°C. The powder formed was pressed into tablets and crushed to the required size before testing.

Catalytic testing took place in a continuous flow fixed bed reactor at atmospheric pressure and tested between 250 and 450°C. This was connected to a gas chromatography instrument for on-line analysis.

Results from catalytic testing showed that methanol oxidation proceeds selectively between 250 and 450°C with the major reaction product being formaldehyde. It was also concluded that the activity and selectivity of the catalyst depends on the vanadium loading. Higher vanadium loading up to monolayer coverage resulted in higher methanol conversion.

Time on-line studies were also conducted in this investigation. Testing the V-Mg-O catalyst revealed that on a 60 hour operation, methanol conversion was 95% with 91% selectivity to formaldehyde.

1.5.2 Propane – Uses, Properties and Recent Work.

Propane is a 3-carbon alkane. It is derived from larger alkanes such as octane during processing. Propane can be used as a fuel for engines, barbecues and home heating systems[44]. When used as a fuel in vehicles, it is referred to as liquefied

petroleum gas (LPG). This is a mixture of propane and ethanethiol, this is added in order for people to smell the gas in the event of a gas leak. Propane remains a popular choice for barbecues and portable stoves because its low boiling point (-42°C) allows it to vaporize once it is released from its pressurized container. In many rural areas of North America, propane is used in furnaces, cooking stoves, water heaters, laundry dryer and other heat-producing appliances. As of 2000, 6.9 million American households use propane as their primary heating fuel[45]. The main hazard associated with propane is that it is highly flammable, with explosive limits of 3-10%.

Many studies involving the oxidative dehydrogenation of short chain alkanes has been carried out in the last couple of decades. In 2004, Liu *et al.* investigated vanadium oxide supported on SBA-15[46]. It was suggested that vanadium oxide species containing terminal V=O groups were the active sites for the selective formation of propylene[47]. It was found by Corma[48] that MCM-41 supports have high surface areas and were well ordered hexagonal channels with controllable uniform pore sizes of 2-8nm. Solsona *et al.* showed that a higher concentration of isolated tetrahedral vanadium species was achieved using this support in comparison to other conventional supports such as silica, alumina and titania. This resulted in a greater number of surface active sites available[49].

Liu and co-workers prepared the support by hydrothermal treatment of a complex solution at 95°C for 3 days. This was filtered and dried. A methanol solution of NH_4VO_3 was added to the SBA-15 support to achieve different vanadium content and then dried and calcined.

Results from catalyst characterization showed that all of the catalysts prepared by this method had ordered hexagonal mesostructures. UV-vis spectrometry was

carried out on the samples also. Peaks were observed which corresponded to isolated V sites in tetrahedral coordination and polymeric V-O-V species. The presence of V_2O_5 crystallites were observed due to polymerisation of the vanadium species.

Catalytic tests were carried out in a fixed bed quartz tubular flow reactor at atmospheric pressure. 300mg of the catalyst was introduced into the sample and diluted with 300mg of quartz powder. Propylene and carbon oxides (CO and CO_2) were the main products for the oxidative dehydrogenation of propane. The introduction of vanadium into the catalyst enhanced propane conversion and the selectivity of partial oxidation products. Using SBA-15 alone produced a conversion of 9% with 23% selectivity to propene. Conversion of propane was maximized with 2.8% vanadium on SBA-15; conversion of propane was 42% with 57% selectivity to propene.

It was also reported in this investigation that vanadium supported SBA-15 had a higher conversion and selectivity than using MCM-41 and SiO_2 as a support. Using MCM-41 as a support with 2.8% vanadium loading produced a propane conversion of 31% with a 57% selectivity to propene. Using SiO_2 as a support with 2.8% vanadium loading produced a propane conversion of 26% and 54% selectivity to propene. The conclusions from this work were that the amount of dispersed vanadium ions could be increased on a different support, namely SBA-15, yielding more selective vanadium based catalyst for the ODH of propane.

Segura *et al.* also investigated vanadia-titania supported systems[50]. Vanadium and titanium oxide were deposited on a mesoporous SBA-15. Different characterisation techniques were used to determine the nature of the vanadia on the support. The catalytic performance for the oxidative dehydrogenation of propane was

investigated by steady-state experiments in a fixed bed micro multi-tubular reactor. Catalytic data showed that with increasing vanadium loading up to the monolayer coverage, the conversion increased with high selectivity to propene. It was also shown that Ti acts as a promoter in the catalytic system.

In a study by Banares and Khatib[51], alumina supported molybdena-vanadia catalysts were investigated for propane ODH. Alumina supported Mo-V catalysts were prepared with different Mo + V loadings, which were co-impregnated by a solution of NH_4VO_3 and $(NH_4)_6Mo_7O_{24}.4H_2O$, which was dried and calcined at 450°C for 5 hours.

Catalytic activity was performed using a conventional microreactor connected to gas chromatography equipment. 300mg of the catalyst sample was placed into the microreactor, yields and selectivities in products were determined on the basis of moles of propane feed and products.

Raman spectroscopy showed bands for *x*MoVAl catalysts which were characteristic of Mo=O stretching modes of surface monooxo molybdenum oxide species. Introducing V into the catalyst showed bands which were characteristic of V=O and V-O-V stretching modes. It was also found that surface Mo and surface V were sensitive to hydration.

0.5%MoAl exhibited the highest selectivity to propene but was less active than the other catalysts. 0.5%VAl exhibited a lower selectivity to propene but a higher conversion of propane. When combining Mo, V and Al, the selectivity to propene increased whilst the conversion of propane also increased.

Solsona *et al.* investigated siliceous ITQ-6 as a support for vanadia in the ODH of propane[52]. It was shown in previous studies that low vanadium loadings presented the highest activity to olefins. However, as the loading was low, there were few active sites in the selective catalysts. This work focused on using a delaminated material with a high surface area of $632m^2/g$ as support for vanadium oxide on the ODH of propane.

For catalyst preparation, silica, NH_4F, HF, 4-amino-2,2,6,6-tetramethylpiperidine and MiliQ deionised water were mixed. This was stirred at room temperature for 90 minutes, producing a gel. This was heated in an autoclave at 175°C for 5 days, then washed and dried. ITQ-6 supported vanadia catalysts were prepared by the wet impregnation method. An ethanolic solution of vanadyl acetyl acetonate was added to the support at 80°C and rotaevaporated until complete dryness and dried in an oven at 100°C. This was then calcined at 600°C in static air for 6 hours.

Catalytic testing was carried out at atmospheric pressure in a fixed bed quartz tubular flow reactor up to 550°C. 500mg of catalyst was used with varying total flow in order to achieve different propane conversions. Analysis of reactants and products was carried out using gas chromatography equipment, using both the thermal conductivity detector and flame ionization detector.

Results from the study showed that catalysts with low V-loading presented isolated or highly dispersed tetrahedrally coordinated VO_x species whilst V_2O_5 crystallites and isolated VO_4 units coexist on the catalysts with highest loadings. The most selective catalyst was 1%V supported ITQ-6. This gave a conversion of propane of 40% with selectivity to propene of 37%. This achieved a yield of 15%.

It was found by Perez-Ramirez *et al.* that steam activated iron-zeolites are highly efficient catalysts for the ODH of propane to propene[53]. Propene yields of 25% were seen at 723K, but coking caused deactivation. In a system with 2 fixed bed reactors running in parallel with each other, propene yields of over 20% were achieved using 'reaction and regeneration' of the catalyst at 723K and 823K respectively. This leads to the simultaneous valorization of C_3H_8 and N_2O, which can be economically applied for on-site propylene production using a low-cost source of N_2O.

Barsan carried out kinetic investigations on the ODH of propane over Ni-Co catalysts[54]. This study focussed on the influence of propane and oxygen partial pressures, space-time velocity and reaction temperature. Several kinetic models were investigated. Experimental results were in good agreement with two surface oxido-reduction models for the propane ODH reaction. The difference between the models exists in the surface reduction step in which one O atom is involved for the first model, while two 'O' are required for the second model.

Niobium(V) oxide was used as a support in the ODH of propane by Cherian[55]. Chromium oxide was supported on niobium oxide. Several loadings of Cr_2O_3 on Nb_2O_5 prepared by incipient wetness were investigated. It was observed that surface chromium oxide species were formed similar to those on other oxide supports and similar monolayer coverage was achieved. The ODH of propane over the Cr_2O_3/Nb_2O_5 catalysts revealed that the activity increased up to monolayer coverage and then decreased due to the presence of Cr_2O_3 crystals. There was a similar trend with V_2O_5:Nb_2O_5 and MoO_3:Nb_2O_5 catalysts. Propene selectivity was constantly high for Cr_2O3/Nb_2O_5. The yield for this catalyst was higher in comparison to Cr_2O_3/Al_2O_3 and Cr_2O_3/TiO_2 catalysts.

In a study by Jibril, Mn-P-O catalysts were investigated[56]. This was an extension of previous work, which concentrated on vanadium phosphate catalysts. The activity of V-P-O catalysts was considered to be among the best. The aim of the work was to find a metal ion that could be easily reduced as this is a crucial part of ODH catalysts.

Catalysts were prepared by a precipitation method. 1g of the catalyst was placed into a micro-reactor which was connected to gas chromatography apparatus. The surface areas of the catalysts were low, typically $6m^2/g$. FTIR analysis showed the presence of $P_2O_7^{4-}$ in the catalyst.

At 450°C, the conversion of propane was 4% with 41% selectivity to propene. At 550C, the conversion increased to 40%, however the selectivity to propene did not change. Generally, olefin selectivity decreases with an increase in alkane conversion. This is dependent on reducibility, acid-base character and oxygen mobility[57]. It was thought that there may be different types of lattice oxygen responsible for respective production of propene and CO_x and other oxygen containing products.

The authors found that Mn-P-O is active and selective as a catalyst for the oxidative dehydrogenation of propane. Propane conversion increased, especially at high temperature. It was suggested that different types of oxygen species determine the conversion and product distribution, depending on the propane and oxygen partial pressure.

1.5.3 Ethane – Uses, Properties and Recent Work.

Ethane is a 2 carbon alkane. It is the only 2 carbon alkane available – it is an aliphatic hydrocarbon. Ethane is a colourless, odourless gas at standard temperature

and pressure. Ethane is produced from natural gas during petroleum refining. The primary use of ethane is for ethylene production[58]. Ethane is favored for ethylene production because the steam cracking of ethane is fairly selective for ethylene. Steam cracking yields a lower selectivity to ethylene and richer in heavier olefins such as propylene and butadiene, and in aromatic hydrocarbons.

Ethane is a flammable gas at standard temperature and pressure, with explosive limits of 3-13%. When stored as a cryogenic liquid, direct contact with liquid ethane can result in severe frostbite. Vapors evaporating from liquid ethane are, until they warm to room temperature, heavier than air and can creep along the ground or gather in low places, and if they encounter an ignition source, can flash back to the body of ethane from which they evaporated.

Solsona *et al.* investigated the ODH of ethane on promoted VPO catalysts[59]. It was recognised that vanadium phosphorus mixed oxide catalysts attracted considerable attention as they were one of the few groups of catalysts capable of selective alkane activation[60]. It was reported that the incorporation of some promoters into VPO catalysts enhances catalytic behaviour in the oxidation of alkanes. Previous work around this subject involved work which saw bismuth doped VPO catalysts, which presented higher activity and selectivity to ethylene in comparison to the undoped catalyst.

Metal doped (Bi, La-Bi, Zr) catalysts were synthesised in a butanol medium with the addition of vanadium oxide, ortho-phosphoric acid and the corresponding metal nitrate. The catalysts were dried in vacuum with of increasing temperature step-by-step to 270°C. The catalysts were activated in-situ at 500°C for 4 hours in the reaction conditions. After catalytic reaction, the samples were cooled in inert gas flow.

Catalytic tests were carried out in a fixed bed quartz tubular reactor at atmospheric pressure. 500mg of the catalyst sample was placed into the reaction vessel and the reaction was studied at 400-500°C. Analysis of the reactants and products were carried out using a gas chromatography instrument. It was found that the addition of metal into the VPO catalyst lead to an increase in surface area, as measured by nitrogen adsorption analysis. Also, there was P-enrichment on the surface of the catalysts after incorporation of the doped metal.

Catalytic testing showed reaction products of ethylene, CO and CO_2 as the main reaction products in the ODH reaction. It was found that an increase in Bi content in the Bi-VPO samples lead to an increase in both conversion of ethane and selectivity to ethylene. The optimum doping amount of Bi was 0.04. This produced conversion of ethane of 10% with selectivity to ethylene of 80%.

Ethane ODH has attracted much interest over the past two decades[61,62]. In recent studies, Bortella and co-workers investigated using MoVTeNbO catalysts for the ODH of ethane to ethylene. This was built on previous work which found that these catalysts could operate at temperatures lower than 450°C[63] and showed ethane conversions of 73% with selectivity to ethylene of 71%. Bortella aimed to report on the catalytic performance of Mo-V-Te-Nb catalysts which were prepared by hydrothermal synthesis with varying compositions.

Briefly, the catalysts were prepared from aqueous gels of vanadyl sulphate, niobium oxalate, ammonium heptamolybdate and telluric acid. These were autoclaved at 175°C for 60 hours. The resulting solids were filtered, washed and dried at 80°C for 16 hours. Finally, the catalysts were heat treated in nitrogen at 600°C for 2 hours.

Catalytic testing was carried out using a fixed bed quartz tubular reactor at atmospheric pressure. Flow rates varied from 25-100mL/minute and the mass of

catalyst varied from 500-2000mg. Experiments were carried out between 325 and 425°C. The reactants and products were analyzed using gas chromatography instrumentation. Products were ethylene, CO and CO_2.

Results from the study showed that conversion of ethane increased with increasing V/Mo atomic ratio. At a V/Mo atomic ratio of 0.4, conversion of ethane reached 15% with selectivity to ethylene of 80%. The catalytic activity strongly decreased on the catalyst prepared from synthesis gels with V/Mo atomic ratios higher than 0.4. It was suggested that there was a linear correlation between catalytic activity and ethylene formation with the V/Mo ratio in the catalyst.

It was shown by Thornsteinson *et al*[64]. that Mo-V-Nb based catalysts appeared to be one of the most promising materials at reaction temperature lower than 450°C. An extension of this work was done by Ueda *et al.*, in which hydrothermal synthesis of the catalysts were carried out. This resulted in high selectivity catalysts being formed, with low conversion of ethane. The paper reported on hydrothermally prepared Mo-V-Te-Nb oxide catalysts on the effect it had on the ODH of ethane to ethylene[65].

Catalysts were prepared using vanadyl sulphate, niobium oxalate, ammonium hexamolybdotellurate and water. The gels were autoclaved at 175°C for 60 hours. This was then filtered, washed and dried at 80°C, before being calcined at different temperatures in a stream of nitrogen.

Catalytic measurements were carried out in a fixed bed quartz reactor at atmospheric pressure. Reaction temperatures ranged from 340-400°C. Ethylene, CO and CO_2 were the reaction products. It was found that the catalytic performance of the catalysts. When the catalyst was calcined at 500°C, 27% ethane conversion was observed with 94% selectivity to ethylene. When the catalyst was calcined at 650°C,

49% ethane conversion was observed with 95% selectivity to ethylene. When the catalyst was calcined at 700°C, 38% ethane conversion was observed with 95% selectivity to ethylene.

Proposals were put forward for V sites being the active sites in the oxidative activation of ethane, however it was also mentioned that there were different V sites in the catalysts[66]. Small differences in the selectivity to ethylene were observed at low ethane conversions on MoVTeNbO catalysts. Te-free catalysts showed both the lowest selectivity to ethylene at low ethane conversion but the highest deep oxidation of ethylene at high conversion. Yields of ethylene of 60-75% were achieved at ethane conversions higher than 80% using $MoV_{0.14\text{-}0.39}Te_{0.18\text{-}0.25}Nb_{0.17\text{-}0.19}$ atomic ratios.

The results in this paper showed that MoVTeNb mixed metal oxide catalysts were active and selective in the ODH of ethane. The hydrothermal synthesis route favours the formation of new crystalline phases, which are not completely observed in the corresponding ternary systems. The evidence provided showed that V^{5+} species should be the active sites in alkane activation.

In other work, TiO_2 supported vanadium phosphates were investigated by Casaletto[67]. TiO_2 supported $VOPO_4$ catalysts were prepared by direct impregnation of TiO_2 with $VOPO_4$ or by dispersing a V_2O_5 precursor on previously phosphate titania. It was found that the preparation method influences the surface composition of the sample. The V^{+5} oxide was favoured over V^{4+} oxide in the reaction, where a comparable fraction of $VOPO_4$ was formed using both preparation techniques. It was concluded from catalytic testing that the presence of V^{4+} strongly improves performances, leading to higher ethylene yields.

Liu *et al.* investigated a new class of catalyst for ethane ODH at low temperature[68]. This was built on to previous work, which established a strong

correlation between catalysts prepared as thin films for the ODH of ethane to ethylene[69]. The authors investigated catalysts containing Ni, Nb and Ta or Co mixed oxides. The ternary systems were first screened in a thin film, and then scaled up. Optimal conditions were $Ni_{0.62}Ta_{0.10}Nb_{0.28}O_x$. This catalyst produced 20.5% conversion with 86% selectivity to ethylene at 300°C. This is much greater in comparison to 3.3% conversion with 83% selectivity to ethylene $Mo_{0.72}V_{0.26}Nb_{0.02}O_x$ – a state-of-the-art catalyst, under identical testing conditions.

Another supported catalyst, alumina supported vanadyl phosphate, was investigated for the ODH of ethane and characterised by XPS[70]. The surface chemical composition of the sample and the modifications induced by different calcination temperatures and catalysis were determined. Calcination of the catalysts was carried out in air at 550°C and 650°C and catalytic measurements were carried out at 450°C and 550°C. It was found that the presence of V^{4+} oxide in the sample enhanced the catalytic performance.

Yamada *et al.* investigated the ODH of ethane over the mixed oxide of nickel and iron[71]. This was evaluated using a selective olefin sensor, which determined the concentration of ethylene in ethane. Catalytic results showed high conversion of ethane but a low selectivity to ethylene.

In other studies, Argyle *et al.* investigated the identity and reversibility of elementary steps involved in the ODH of ethane[72]. The catalysts investigated were VO_x/Al_2O_3 and VO_x/ZrO_2. It was concluded from the study that C-H bond cleavage in ethane and ethane is an irreversible and kinetically relevant step in ODH reactions. Kinetic analysis suggests that surface oxygen, OH groups and oxygen vacancies are the most abundant reactive intermediates during ethane ODH on active VO_x domains.

The ODH of ethane was investigated on metal oxide-based sulphated zirconia catalysts between 400°C and 600°C. The activity and selectivity depended on the nature of the metal oxide being used. The highest observed ethylene yield was using nickel oxides and vanadium oxides[73]. Nickel oxides gave an ethane conversion of 18.2% with 72% selectivity to ethylene. Vanadium oxides gave an ethane conversion of 17.6% with 84% selectivity to ethylene.

1.6 Aims of the Investigation.

A number of catalysts have been previously studied for methanol oxidation, propane oxidative dehydrogenation and ethane oxidative dehydrogenation. Some research has been carried out using niobium in catalytic systems, but no work has been carried out using only niobium as the metal in the catalyst.

Niobium has similar structure and properties to that of vanadium. Vanadium is used in oxidation and oxidative dehydrogenation reactions. The aim of the project is to investigate whether niobium catalysts offer any advantages over vanadium catalysts. All of the catalysts that are investigated in this work are niobium based catalysts. There are no other metals in any of the catalysts.

Relatively little work has been carried out on niobium(V) compounds for oxidation reactions. A variety of niobium oxides, niobium oxide phosphates and niobium phosphates will be made and the structure and properties will be investigated.

There are three probe reactions that will be investigated. The first is methanol partial oxidation to formaldehyde. Other effective catalysts for this reaction are iron molybdates. The second probe reaction is propane oxidative dehydrogenation, where

vanadia catalysts are used. The final probe reaction is ethane oxidative dehydrogenation, where supported metal oxide catalysts are used.

Any trends involving niobium oxides, niobium oxide phosphates and niobium phosphates will be recorded, and comparisons will be made according to the preparation technique, calcination temperature and type of precursor used. Comparisons will also be made with non-phosphorus containing catalysts and phosphorus containing catalysts.

References.

[1] Lindstroem, B.; Pattersson, L. J. *Cattech* **2003**, 7, 130.

[2] Bond, G. C.; Heterogeneous Catalysis Principles and Applications 2nd Edition, Oxford Science Publications.

[3] Langmuir, I. *Physical Review* **1915**, 6, 79.

[4] http://content.answers.com/main/content/wp/en/a/af/Catalyst_effect.png

[5] The Basis and Applications of Heterogeneous Catalysis, Bowker, M.; Oxford chemistry Primers **1998**.

[6] http://en.wikipedia.org/wiki/Niobium

[7] Cardarelli, F.; *Materials Handbook*, **2008** Springer London.

[8] Ushikubo, T., Koike, Y., Wada, K., Xie, L., Wang, D., Guo, X.; *Catalysis Today*, 28, **1996**, 59-69.

[9] Ziolek, M.; *Catalysis Today*, 78, **2003**, 47-64.

[10] Jehng, J. M., Wachs, I. E.; *Chem. Mater.*, 3, **1991**, 100.

[11] Guenin, M., Frety, R., Garbowski, E.; *Journal of Materials Science*, 23, **1988**, 1009-1013.

[12] Chen, Z., Jizuka, T., Tanabe, K.; *Chem. Lett.* **1984**, 1085.

[13] Ogasawara, K., Iizuka, Tanabe,Kk.; *Chem. Lett*, **1984**, 645.

[14] Bafrali, R., Nuhfer, N. T., Wagner, N. J., Ko, E. I.; *J. Catal.*, 95, **1985**, 260.

[15] Asakura, K., Iwasawa, Y.; *Chem. Lett.*, **1988**, 633.

[16] JCPDS Database Version 2.2.

[17] Schafer, H., Gruehn, R., Schulte, F.; Angew. *Chem. Internat. Edit*, Vol. 5, **1966**, No. 1.

[18] Angew. Chem. Internat. Edit. Vol. 5, **1966**, No. 1.

[19] Burke, P. A., Weissman, J. G., Ko, E. I., Wynblatt, P.; J. W. Wards (Ed.), *Catalysis*, **1987**, 457-467.

[20] Wachs, I. E., Briand, l. E., Jehng, J. M., Burcham, L., Gao, X.; *Catal. Today*, 57, **2000**, 323.

[21] Paulis, M., Martin, M., Soria, D.B., Diaz, A., Odriozola, J. A., Montes, M.; *Appl. Catal. A.*, 180, **1999**, 411.

[22] Brown, R., Kemball, C. H.; *J. Chem. Soc., Faraday Trans.*, 92, **1996**, 281.

[23] Aranda, D. A. G., Ramos, A. L. D., Passos, F. B., Schmal, M.; *Catal. Today*, 57, **2000**, 283.

[24] Smitts, R. H. H., Seshan, K.,Ross, J. R. H.; Symposium on Catalytic Selective Oxidation, *American Chemical Society*, Washington DC, **1992**, p.1121.

[25] Phadke, M. D., Ko, E. I.; *J. Catal.*, 100,**1986**, 503.

[26] Weissman, J. G.; *Catal. Today*, 28, **1996**, 159.

[27] Schafer, H., Gruehn, R., Schulte, F., Angew. Chem. Internat. Edit., 5, **1966**, 40-52.

[28] Carniti, P., Gervasini, A., Biella, S., Auroux, A.; *Catalysis Today*, **2006**, 118, 373-378.

[29] Nowak, I., Ziolek, M.; *Chem. Rev.*; **1999**, 99, 3603.

[30] Ziolek, M.; C*atal. Today*, **2003**, 78, 47.

[31] Armaroli, T., Busca, G., Carlini, C., Guittari, M., Galletti, A. M. R., Busca, G.; *J. Mol. Catal. A.*, 151, **2000**, 233.

[32] Duarte de Farias, A. M., Gonzales, W. A., Pries de Oliveira, P. G., Eon, J. G., Hermann, J. M., Aouine, M., Loridant, S, Volta, J. C.; *J. Catal.*, 208, **2002**, 238.

[33] Brayner, R., Rodrigues, J. A. J., Cruz, J. M.; *Catal. Today*, 57, **2000**, 219.

[34] Yang, D. S., Hackett, P. A.; *J. Electr. Spectr. Related Phenom.*, 106, **1999**, 100.

[35] Kim. H. S., Bugli, G, Djega-Mariadassou, G; *J. Solid State Chem.*, 142, **1999**, 100.

[36] Ettmayer, P., Lengauer, W., in: R. B. King (Ed.), *Encyclopedia of Inorganic Chemistry, Wiley, Chichester*, **1994**, p.519.

[37] Häggblad, R., Wagner, J. B., Hansen, S., Andersson, A.; *J. Catal.*, 258(2), **2008**, 345-355.

[38] House, M. P., Carley, A. F., Bowker, M.; *J. Catal.*, 252(1), **2007**, 88-96.

[39] House, M. P., Carley, A. F., Valda, R. E., Bowker, M.; *J. Phys. Chem. C*, **2008**, 112, 4333-4341.

[40] Dias, A. P. S., Rozanov, V. V., Waerenborgh, J. C. B., Portela, M. F.; *Applied Catalysis A*, 345(2), **2008**, 185-194.

[41] Soares, A. P. V., Portela, M. F., Kiennemann, A.; *Catal. Rev. Sci. Eng.*, 47, **2005**, 125.

[42] Wang, Q., Madix, R. J.; *Surface Science*, 496(1-2),**2002**, 51-63.

[43] Isaguliants, G. V., Belomestnykh, I. P.; *Catalysis Today*, 100, **2005**, 441-445.

[44] http://en.wikipedia.org/wiki/Propane

[45] U. S. Census Bureau, U.S. Departments of Energy and Transportation statistics (2000).

[46] Liu, Y. M., Cao, Y., Yi, N., Feng, W. L., Dai, W. L., Yan, S. R., he, H. Y., Fan, K. N.; *Journal of Catalysis*, 224, **2004**, 417-428.

[47] Blasco, T., Nieto, J. M. L.; *Appl. Catal. A*; 157, **1997**, 117.

[48] Corma, A.; *Chem. Rev.*, 97, **1997**, 2373.

[49] Solsona, B., Blasco, T., Nieto, J. M. L., Pena, M. L., Rey, F., Vidal-Moya, A.; *J. Catal.*, 203, **2001**, 443.

[50] Segura, Y., Paul, J. S., Huyghe, K., Vermandel, W., Cool, P., Vansant, E. F., Sels, B. F., Jacobs, P. A.; *Studies in Surface Science and Catalysis*, 156, **2005**, 733-740

[51] Banares, M. A., Khatib, S. J.; *Catalysis Today*, 96, **2004**, 251-257.

[52] Solsona, B., Nieto, J. M. L., Diaz, U.; Microporous and Mesoporous Materials, 94, **2006**, 339-347.

[53] Perez-Ramirez, J., Gallardo-Llamas, A., Daniel, C., Mirodatos, C.; *Chemical Engineering Science*, 59(22-23), **2004**, 5535-5543.

[54] Barsan, M. M., Thyrion, F. C.; *Catalysis Today*, **2003**, 81, (2) 159-170.

[55] Cherian, M.; *Catalysis Today*, 78, **2003**, 397-404.

[56] Jibril, B. Y.; *Ind. Eng. Chem. Res.*, 44, **2005**, 702-706.

[57] Centi, G., Cavani, F., Trifiro, F.; *Selective Oxidation by Heterogeneous Catalysis*, Kluwer Academic/Plunum: London **2001**.

[58] http://en.wikipedia.org/wiki/Ethane

[59] Solsona, B., Zazhigalov, V. A., Nieto, J. L. M., Bacherikova, I. V., Diyuk, E. A.; *Applied Catalysis A*, 249, **2003**, 81-92.

[60] Cavani, F., Trifiro, F.; *Catal. Today*, 51, **1999**, 561.

[61] Alboneti, S., Cavani, F., Trifiro, F.; *Catal. Rev.-Sci. Eng.*, 38, **1996**, 413.

[62] Grasselli, R. K.; *Top. Catal.*, 15, **2001**, 93.

[63] Bortella, P., Nieto, J. M. L., Dejoz, A., Vazquez, M. I., Arias, A. M.; *Catal. Today*, 78, **2003**, 507.

[64] Thornsteinson, E. M., Wilson, T. P., Young, F. G., Kasai, P. H.; *J. Catal.*, **1978**, 52, 116.

[65] Nieto, J. M. L., Botella, P., Vasquez, M. I., Dejoz, A.; *Chem. Commun.*, **2002**, 1906-1907.

[66] Bortella, P., Nieto, J. M. L., Solsona, B., Mifsud, A., Marquez, F., *J. Catal.*, 209, **2002**, 445.

[67] Casaletto, M. P.; *Catalysis Today,* **2004**, 91-92, (15), 271-274.

[68] Liu, Y., Cong, P., Doolen, R. D., Guan, S., Markov, V., Woo, L., Zey, S., Dingerdissen, U.; *Applied Catalysis A:* 254 (1), **2003**, 59-66.

[69] Proceedings by the National Academy of Sciences, U.S.A. 96 **1999** 11077.

[70] Casaletto, M. P., Mattogno, G., Massucci, M. A.; *Applied Surface Science*, 211(1-4), **2003**, 216-226.

[71] Yamada, Y., Ueda, A., Zhao, Z., Maekawa, T., Suzuki, K., Takada, T., Kobayashi, T.; *Catalysis Today*, 67(4), **2001**, 379-387.

[72] Argyle, M. D., Chen, K., Bell, A. T., Iglesia, E.; *J. Phys. Chem*, **2002**, 869-898.

[73] Wang, S., Murata, K., Hayakawa, T., Hamakawa, S., Suzuki, K.; *J. Catal.*, 305, **1999**, 8565.

2.Experimental.

2.1 Preparation of Niobium (V) Oxide Catalysts.

2.1.1 Co-Precipitation Reaction of Niobium (V) Chloride and Sodium Carbonate.

Aqueous niobium (V) chloride (16.91g in 50mL water, 0.25M) was placed in a 250mL round bottomed flask. The pH of the solution was measured. Sodium carbonate (53.00g in 250mL water, 2M) as added drop-wise to the niobium (V) chloride until a precipitate was formed. This was filtered and left to dry in an oven at 110°C for 16 hours. The product was calcined in air at 500°C for 3 hours at a ramp rate of 15°C/minute.

$$2NbCl_5\,(aq) + 5Na_2CO_3\,(aq) \rightarrow Nb_2(CO_3)_5\,(s) \xrightarrow{\text{Calcined in air, 500°C, 3 hours}} Nb_2O_5\,(s) + 5CO_2\,(g)$$

2.1.2 Co-Precipitation Reaction of Niobium (V) Chloride and Urea.

Aqueous niobium (V) chloride (16.91g in 50mL water, 0.25M) was placed in a 250mL round bottomed flask. The pH of the solution was measured. This was then heated to 80°C and stirred. Urea (30.03g in 250mL water, 2M) as added drop-wise and left to stir for 3 hours. This was filtered and left to dry in an oven at 110°C for 16 hours. The product was calcined at 500°C for 3 hours at a ramp rate of 15°C/minute.

2.1.3 Oxidation of Niobium Metal.

Niobium metal was calcined at 500°C in air for 3 hours at a ramp rate of 15°C/minute.

2.1.4 Oxidation of Niobium (V) Ethoxide.

A solution of niobium ethoxide in absolute ethanol (10mL) was added drop-wise to a 30mL mixture of ethanol water, under rapid stirring. A white precipitate was formed and was filtered and oven dried for 16 hours. This was then calcined at 450°C in air for 3hours at a ramp rate of 15°C/minute.

2.1.5 Niobium (V) Oxide, Purchased from Aldrich.

Niobium (V) oxide, purchased from Aldrich was calcined at 600°C in air for 3hours at a ramp rate of 15°C/minute

2.2 Preparation of Niobium (V) Phosphate Catalysts.

2.2.1 Preparation of Niobium Oxide Phosphate, NbOPO4.

Niobium (V) chloride (13.52g, 0.25M) was placed in a 250mL round bottomed flask and phosphoric acid (30mL) and water (120mL) was added and left to stir for 30 minutes. A condenser was then added to the flask and refluxed for 24 hours. The resulting solution was white. This was filtered, washed and dried at 110°C for 16 hours. A white product was collected. The P:Nb ratio was calculated to be 8:1. This was then calcined at 500°C for 3 hours at a ramp rate of 15°C/minute. Ortho-phosphoric acid and pyro-phosphoric acid was used.

$$NbCl_5\,(aq) + H_3PO_4\,(aq) + \tfrac{1}{2}O_2 \rightarrow NbOPO_4\,(s) + 3HCl + Cl_2$$

2.2.2 Preparation of Niobium Phosphate, $NbPO_5$.

Niobium oxide phosphate, prepared previously was reduced at 500°C under hydrogen for 3 hours at a ramp rate of 15°C/minute.

Calcined in H_2,
500°C, 3 hours

$NbOPO_4 \rightarrow NbPO_5$

2.2.3 Preparation of Niobium Phosphate, $NbPO_5$.

Niobium oxide phosphate (1g,) was placed in a 250mL round bottomed flask. Isobutanol (30mL) was added to the solid. This was left to reflux for 24 hours, then was filtered and dried at 110°C for 16 hours. This was then calcined at 500°C in air for 3 hours at a ramp rate of 15°C/minute.

Refluxed with Isobutanol,
Calcined 500°C in air, 3 hours

$NbOPO_4 \rightarrow NbPO_5$

2.2.4 Preparation of Niobium Phosphate, $Nb_2P_4O_{15}$.

Niobium chloride (10mmol, 2.7g) was added to water (50mL) and phosphoric acid (20mmol, 1.2mL) and left to stir for 30 minutes. Ammonia hydroxide solution was added until the pH reached 2.6 and remained constant. This was filtered and washed with distilled water. Water (10mL) and hydroxylamine (6mmol, 0.18mL) was added to the precipitate. Phosphoric acid (8mmol, 0.46mL) was added and the resulting suspension was kept at pH 3.88 for 30 minutes using ammonia hydroxide solution. The resulting gel was placed in a Teflon-lined stainless steel liner and heated

at 65°C and autogenous pressure for 48 hours. This was filtered, washed and dried at 110°C for 15 hours and then calcined at 450°C at a ramp rate of 15°C/minute [1].

2.3 Characterisation Techniques.

2.3.1 X-Ray Diffraction.

1. Theory.

X-ray diffraction is a method used to characterise materials according to their specific unit cells. XRD is a method of determining the structure of the powder. In order to produce a powder XRD pattern, the sample must be crystalline and have long range order. More, specifically, powder XRD requires there to be many small crystals orientated randomly.

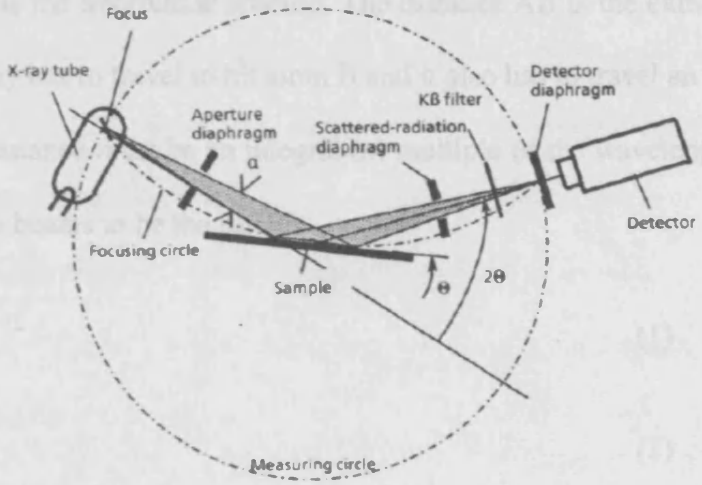

Figure 2.1 – Schematic of an X-ray Diffractometer[2]

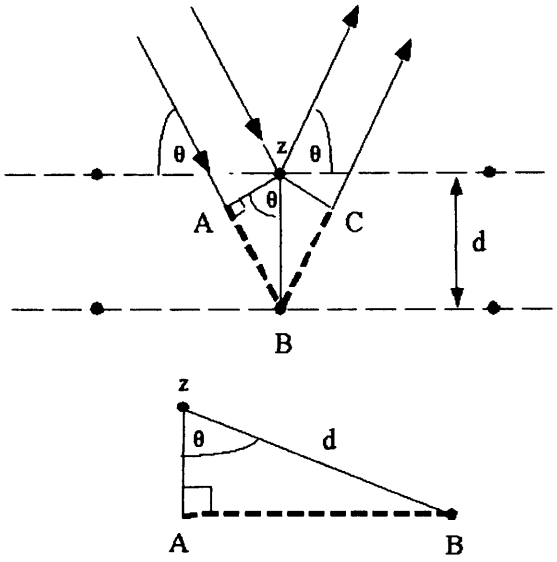

Figure 2.2 – Deriviation of Bragg's Law

Bragg's Law can be derived from the above diagrams. The arrows pointing downwards are the incident rays and the rays pointing upwards are the reflected rays. The distance, d, is the interplanar spacing. The distance AB is the extra distance that the adjacent X-ray has to travel to hit atom B and it also has to travel an extra distance BC. This extra distance must be an integral (n) multiple of the wavelength (λ) for the phases of the two beams to be the same:

$$n\lambda = AB + BC \quad (1)$$

$$AB = d \sin\theta \quad (2)$$

Because AB = BC equivalent (1) becomes,

$$n\lambda = 2AB \quad (3)$$

Substituting equation (2) in equation (3) we have the Bragg equation:

$$n\lambda = 2\, d \sin\theta$$

2. Experimental.

The X-Ray diffractometer used was Enraf Nonius FR590 Powder Diffractometer. The sample was ground up into a fine powder. It was then was placed on to a metal disc, making sure that the disc was completely covered by the sample and placed on to the rotating anode. The X-rays were turned on and a sample was run. A pattern was obtained in about 30 minutes. Another X-Ray diffractometer used was PanAlytical XRD. This worked on the same basis as the other machine, but involved using 2 nickel filters and 2 monochromators.

2.3.2 Laser Raman Spectroscopy.

1. Theory.

At the molecular level, photons can interact with matter by scattering or adsorption. There are two ways in which scattering can occur – Elastically (change in vibrational energy level and decays back into the same energy level) or inelastically (does not decay back into the same energy level). The inelastic process is termed Raman scattering. Raman scattering occurs when the system exchanges energy and the final vibrational energy is above or below that of the initial energy. This is called ΔE. A plot of the defected number of photons vs. Raman shift of the incident laser energy gives a Raman spectrum.

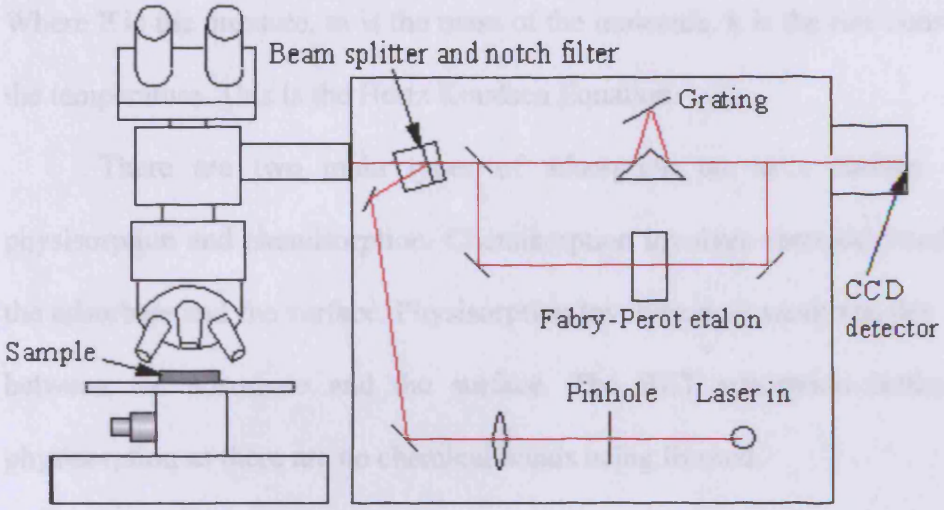

Figure 2.3 – Schematic of Laser Raman Spectrometer

2. Experimental.

The Raman spectrometer used is the Renishaw Ramascope Raman spectrometer. A sample of the catalyst was spread on to a metal plate and placed underneath the diode argon laser beam with a wavelength of 516nm. Experimental conditions were run as 10 accumulations for 10 seconds.

2.3.3 BET Surface Area.

1. Theory.

This information is important for comparing the adsorption properties of different surfaces. There are various types of isotherms; the isotherm that is relevant to the type of surface area being studied is the BET (Brunauer, Emmett, and Teller) adsorption isotherm. The type II and type IV adsorption isotherm is used to measure BET surface area.

The rate of collision of gas molecules with a surface is

$$r = P/\sqrt{(2\pi mkT)}$$

Where P is the pressure, m is the mass of the molecule, k is the rate constant and T is the temperature. This is the Hertz Knudsen Equation.

There are two main types of adsorption on to a surface – these are physisorption and chemisorption. Chemisorption involves chemical bonding between the adsorbate and the surface. Physisorption involves only weak van der Waals forces between the adsorbate and the surface. The BET adsorption isotherm involves physisorption as there are no chemical bonds being formed.

There are two instances that can occur when a molecule collides with a surface. The first instance is that nothing happens and the molecule deflects back off the surface. The second instance is that the molecule feels an attractive force, normally weak, to the surface and is adsorbed.

$$\text{Sticking Probability} = \frac{\text{Number of molecules that stick}}{\text{Number of molecular impacts}}$$

The recognised BET adsorption isotherm is as follows:

$$\frac{P}{\upsilon (P_0 - P)} = \frac{c-1}{\upsilon_m c}\left(\frac{P}{P_0}\right) + \frac{1}{\upsilon_m c} \qquad (1)$$

where: υ is the volume of gas adsorbed, P_0/P is specific pressure, c is a constant value and υ_m is the monolayer volume. The values of P_0/P are usually in the range of 0.05 to 0.35[3]. Methods used to evaluate mesopore size distributions are DH and BJH methods.

This is a straight line equation in the form of $y = mx + c$.[1]

2. Experimental.

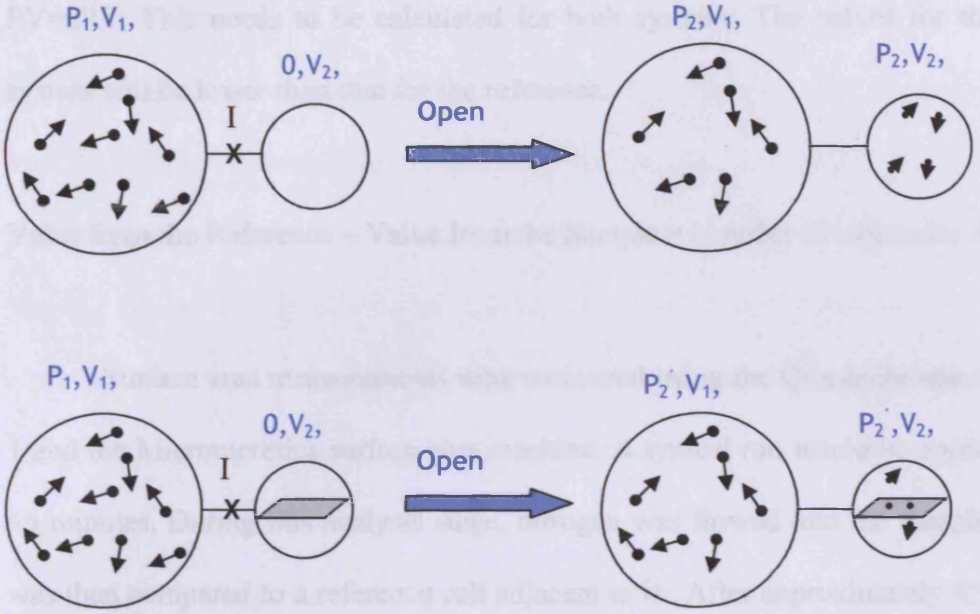

Figure 2.5 - Schematic of Adsorption on to a Surface[2].

In Figure 2.5, the top half of the diagram shows no surface present – this is the reference. When valve I is opened, some of the gas molecules move into the smaller vessel and thus the pressure equilibrates. Hence,

$$P_1 V_1 = P_2 (V_1 + V_2)$$

In the bottom half of Figure 2.5, a surface is added to the second vessel. Because of this the pressure in the second vessel changes as some molecules will be adsorbed by the surface. The value of P_2' is now smaller than the value of P_2.

From this, the number of gas molecules adsorbed can be calculated because the following information is known:

- P_1, the pressure before the valve is opened;
- V_1 and V_2, the volumes of each of the vessels;
- T, the temperature of the system.

Firstly, the number of moles of gas needs to be calculated by using the formula PV=nRT. This needs to be calculated for both systems. The values for the second system will be lower than that for the reference.

Value from the Reference – Value from the Sample = Number of molecules Adsorbed

Surface area measurements were measured using the Quantachrome Autosorb-1 and the Micromeretics surface area machine. A typical run would be approximately 45 minutes. During this analysis stage, nitrogen was flowed into the sample and this was then compared to a reference cell adjacent to it. After approximately 45 minutes, a surface area of $12m^2/g$ was obtained.

2.3.4 Scanning Electron Microscopy.

1. Theory.

When electrons penetrate the sample, the electrons get scattered. This causes a change in energy. This energy change between the electron beam and the catalyst sample results in the emission of electrons and electromagnetic radiation which can be detected to produce an image, this is known as scanning electron microscopy.

Scanning electron microscopy (SEM) is a technique used to observe the physical, chemical and structural aspects of different samples. SEM uses electrons, instead of light to form an image. This is a surface sensitive technique. Electrons are emitted from a tungsten filament and accelerated towards an anode. The electron beam is then focussed by lenses to form a focal spot. The electron beam under normal conditions is 30keV. This beam then passes over the sample surface and the electrons get deflected. This type of deflection is known as back-scattering, and forms an image

with bright spots where mere electrons get emitted. Darker spots show few electrons getting detected.

Another type of scattering of electrons is when an electron collides with another electron and causes a movement of the electron. An image is then formed by the secondary electrons as these electrons have a different energy to those in the electron beam. The brightness of the signal depends on the number of secondary electrons reaching the detector. If the electron beam enters the sample and a bright surface is observed, this is an indication that more secondary electrons have been emitted or a build up of surface charge.

The magnitude of the interaction depends on the sample density, the beam accelerating voltage and the atomic number of the sample.

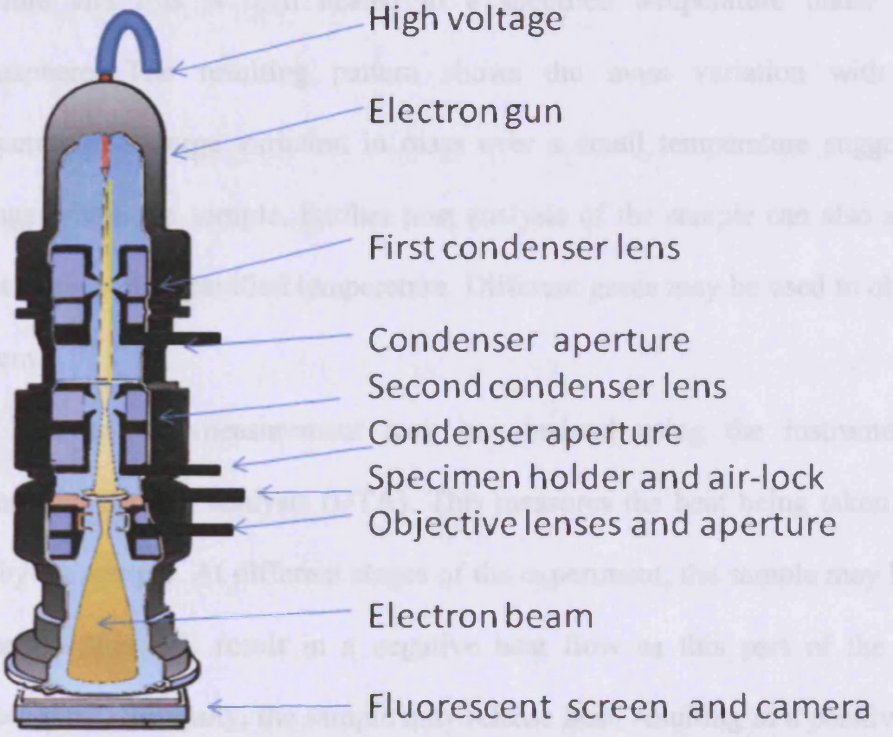

Figure 2.6 – Schematic of a Scanning Electron Microscope[4]

2 Experimental.

Samples of catalyst were placed on to an adhesive carbon disc. The excess sample was removed by gentle knocking. A thin layer resulted on the carbon strip. This was placed in the holder and the vacuum was initialised. Once a high vacuum had been achieved, the electron beam was switched on.

2.3.5 Thermal Gravimetric Analysis.

1. Theory.

Thermal gravimetric analysis (TGA) is a technique used to investigate weight changes in a sample. A specified mass of sample is placed into an aluminium oxide crucible and this is then heated to a specified temperature under a specified atmosphere. The resulting pattern shows the mass variation with respect to temperature. A large variation in mass over a small temperature suggests a phase change within the sample. Further post analysis of the sample can also show rate of mass change at a specified temperature. Different gases may be used to obtain a TGA pattern.

A second measurement may be obtained using the instrument. This is differential thermal analysis (DTA). This measures the heat being taken in or given out by the sample. At different stages of the experiment, the sample may have to take in heat – this will result in a negative heat flow as this part of the reaction in endothermic. Similarly, the sample may release heat, resulting in a positive heat flow, i.e. an exothermic reaction.

All of the information obtained from the instrument gives evidence of possible phase changes, the type of reaction i.e. exothermic or endothermic at a particular

temperature and also how fast the mass varies with temperature. The TGA curve plots the TGA signal, converted to percent weight change on the Y-axis against the reference material temperature on the X-axis.

2 Experimental.

Patterns were obtained using a Setaram Setsoft TG/DTA machine. A typical example for obtaining a TGA pattern is as follows. 50mg of a sample of $Nb_2(CO_3)_5$ was placed into an aluminium oxide crucible for analysis. The analysis was performed in air. The temperature programme that was used was to have an isothermal time period at 30°C for 6 minutes, then a temperature ramp to 900°C at a ramp rate of 20°C/min.

2.3 Gas Chromatography.

1. Theory.

Gas chromatography is a technique used to test the catalytic activity of the materials produced by separating different compounds with different retention times.

One of the test reactions being investigated is the oxidative dehydrogenation of propane to propene. A specific method has been set up in order to accurately examine the effectiveness of the catalyst.

$$C_3H_8 + 0.5\ O_2 \rightarrow C_3H_6 + H_2O$$

In this reaction, there is half the number of moles of oxygen as propane. The limiting factor in this reaction is oxygen. If there were an excess of oxygen, then there is a high probability of complete oxygen to carbon dioxide and water. However, as there is a stoichiometric amount of oxygen entering the system, there is a possibility of propene being formed in the reaction.

The flows of gases into the system can be controlled by using mass flow controllers (MFC). These are calibrated before use and can therefore control the volumes of different gases flowing through the system. The gases flowing into the reactor are helium, oxygen and propane. A constant flow rate of 23mL/min must flow through the system at all times.

When the gases flow into the reactor bed, at elevated temperatures, reactants will turn to products. The product that is most desirable in the reaction is propene. However, other products are also formed. For example, carbon dioxide and carbon monoxide forms, as do other C_3 products such as acrolein and acrylic acid. These are separated according to the temperature at which they condense in the column. The temperature profile below is used in the reaction.

Table 2.1 - Method programme for the separation of the eluted products and there analysis

Time	Temperature (°C)	Rate (°C/min)	Hold (min)	Total (min)
Initial	80.0	-	2.00	2.00
1	120.0	20.0	2.00	6.00
2	160.0	5.0	1.00	16.50

Within the GC, there are 2 valves, which control what is happening within the system. When the reactor is idle, gases only flow through the bypass and no compounds go through the columns. When the first valve opens, gases are able to pass into the first column, the Molecular Sieve. The Molecular Sieve is responsible for

separating compounds such as oxygen, carbon monoxide, carbon dioxide and other C_3 products. When the second valve opens, gases are able to flow into both columns. The reason for keeping the second valve closed is because if carbon dioxide enters the HasepQ, the column would become irreversibly adsorbed.

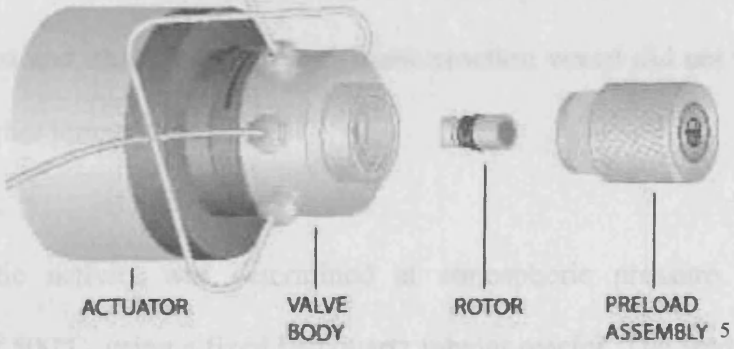

Figure 2.41 – Diagram of valve on GC[6].

Table 2.2 – List of retention times for propane ODH reaction.

Compound	Retention Time (minutes)
Propane	7.3
Propene	7.1
Oxygen	2.9
Carbon monoxide	3.1
Carbon dioxide	1.3
Other C3 products	11 to 15

1. Experimental.

Propane ODH.

Glass wool was placed into the centre of a quartz tube. 250mg of the catalyst was then placed on the glass wool in the quartz tube. This was then attached to the

MFC and the GC. Surrounding the quartz tube was a furnace. The flowmeter was adjusted to allow 17mL helium, 4mL propane and 2mL oxygen (2:1 by volume) through the system. The joints were checked for leaks. A gas chromatograph was obtained after 16 minutes. This was repeated three times at a specific temperature. The temperature was then increased in 25°C increments until product peaks were observed. The maximum temperature reached was 500°C. Conversion and selectivity were calculated and used for analysis. A blank reaction vessel did not become active until much higher temperatures.

Ethane ODH.

Catalytic activity was determined at atmospheric pressure at a reaction temperature of 500°C, using a fixed bed quartz tubular reactor. The feed consisted of a mixture of $C_2H_6/O_2/He$ (with ethane = 9mL/minute and oxygen = 3mL/minute. The amount of catalyst was varied from 1 to 10 g in order to obtain several contact times. The bed volume was kept constant in all cases by dilution using SiC when appropriate. The total flow was fixed in all cases between 15 and 30 ml min^{-1}. Flow rate varied due to the data acquired required varying flow rates, as shown in chapter 6. Two analyses at each reaction condition were carried out with a stabilization time of 60 minutes. Reactant and products were analysed by gas chromatography using two packed columns: i) Molecular sieve 5Å (2.5m) and ii) Porapak Q (3m). For comparative purposes a blank run using 15 ml min^{-1} was also conducted at 500°C. An ethane conversion lower than 0.4 % was obtained. A blank reaction vessel did not become active until much higher temperatures.

Methanol Oxidation.

Glass wool was placed into the centre of a quartz tube. 500mg of the catalyst was then placed on the glass wool in the quartz tube. This was then attached to the

MFC and the GC. Surrounding the quartz tube was a furnace. The flowmeter was adjusted to allow 30mL helium, 10mL methanol and 15mL oxygen (2:3 by volume) through the system. The joints were checked for leaks. A gas chromatograph was obtained after 60 minutes. This was repeated three times at a specific temperature. The temperature was then increased in 20°C increments until product peaks were observed. The maximum temperature reached was 400°C. Conversion and selectivity were calculated and used for analysis. Blank quartz tubes showed no activity until 500°C.

References.

[1] Mal, N. K., Fujiwara, M.; *Chem. Commun.*, **2002**, 2702-2703.

[2] Course Notes, Cardiff University.

[3] Autosorb-1 Operating Manual Ver. 1.51 Page 68.

[4] www.biologie.uni-hamburg.de/b-online/ge03/14.gif

[5] http://www.vici.com/vval/images/vwssaex.jpg

[6] www.vici.com

3. Characterisation Data.

A wide variety of catalysts were prepared in this study, and they were characterised using a variety of techniques. The characterisation techniques employed were X-ray diffraction, Raman spectroscopy, nitrogen adsorption analysis, X-ray photoelectron spectroscopy and scanning electron microscopy. The range of techniques was selected as they probe a range of properties of the catalysts, such as bulk structure, elemental composition, surface composition and physical and textural properties. This chapter describes the results of the characterisation studies.

3.1 Characterisation of Niobium(V) Oxides.

Different phases of niobium(V) oxide are present, according to X-Ray Diffraction (XRD) databases (JCPDS Version 2.2c). Some of these include monoclinic (00-019-0864, JCPDS) and orthorhombic (00-027-1105, JCPDS) niobium(V) oxide.

3.1.1. XRD Data.

The catalyst surface areas and crystalline phases identified by powder XRD are summarised in Table 1. Niobium oxides, prepared from precipitation reactions using sodium carbonate and urea both produced a monoclinic phase (00-019-0864 and 00-007-0061 respectively). Niobium oxides, prepared from oxidation methods produced an orthorhombic phase.

Table 3.1 – Summary of phases of niobium oxides produced.

Catalyst	Phase	Reference Number
Precipitation of $NbCl_5$ and Na_2CO_3	Monoclinic	00-019-0864
Precipitation of $NbCl_5$ and Urea	Monoclinic	00-007-0061
Niobium(V) Oxide, Purchased from Aldrich	Orthorhombic	00-027-1105
Oxidation of Niobium Ethoxide	Orthorhombic	00-030-0873
Oxidation of Niobium Metal	Orthorhombic	00-027-1103

Niobium oxides produced from precipitation reactions were calcined in air at different temperatures to investigate the possible differences of the catalysts catalytically. Figures 3.1 and 3.2 show the products calcined at different temperatures in air for 3 hours.

It can be seen from Figure 3.1 that the product which was calcined at 500°C is different to the products which were calcined at 400°C and 600°C. An extra peak at 48 and 70 degrees 2-theta appeared on the product which was calcined at 500°C, however this peak was not observed in the other calcined products.

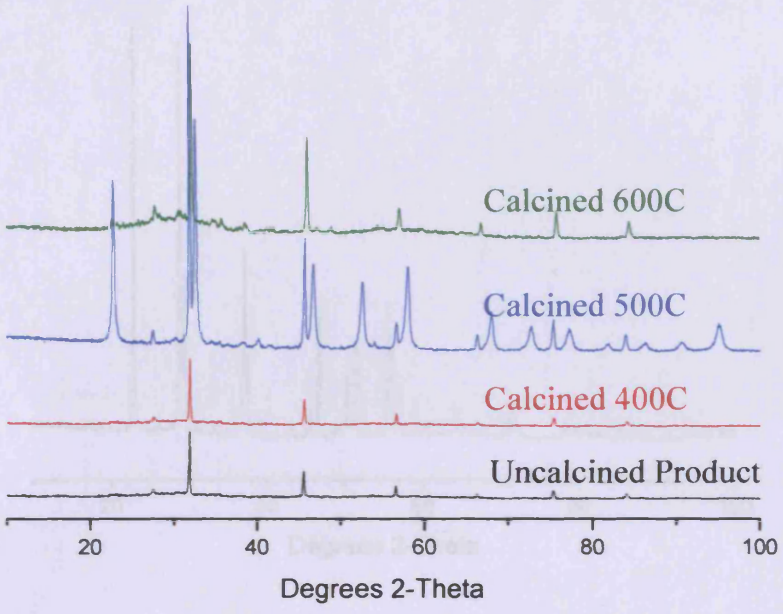

Figure 3.1 – XRD pattern for the precipitation reaction of niobium(V) chloride and sodium carbonate, calcined in air at different temperatures.

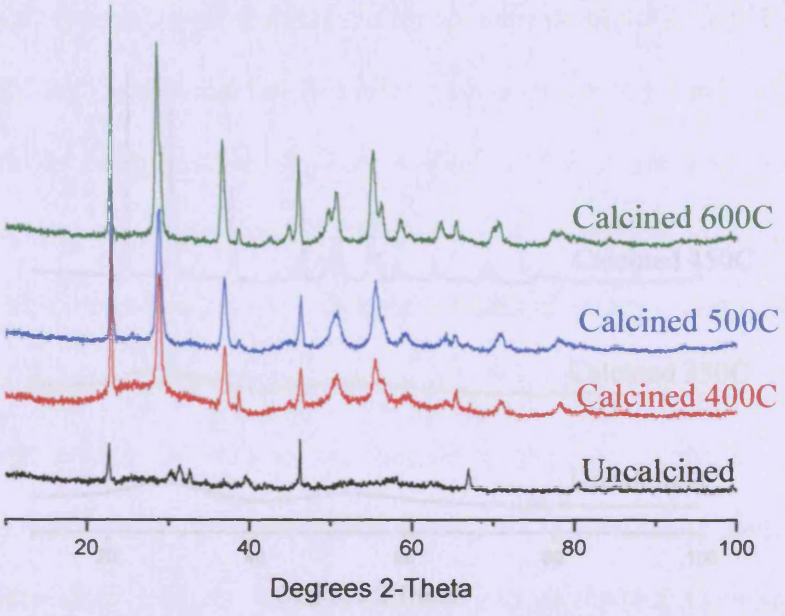

Figure 3.2 – XRD pattern for the precipitation reaction of niobium(V) chloride and urea, calcined in air at different temperatures.

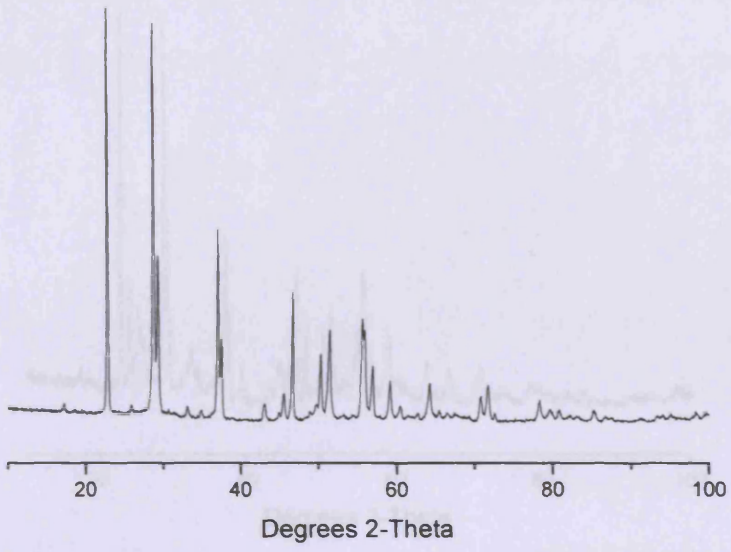

Figure 3.3 – XRD pattern for niobium(V) oxide, purchased from Aldrich.

The preparation involving the oxidation of niobium ethoxide to produce niobium oxide was followed from a previous method[1].

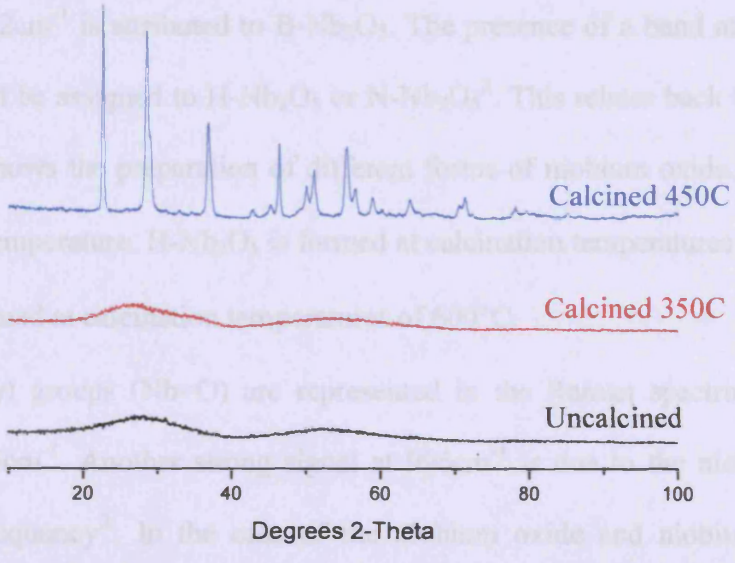

Figure 3.4 – XRD pattern for niobium(V) oxide, produced from the oxidation of niobium ethoxide, calcined in air at different temperatures.

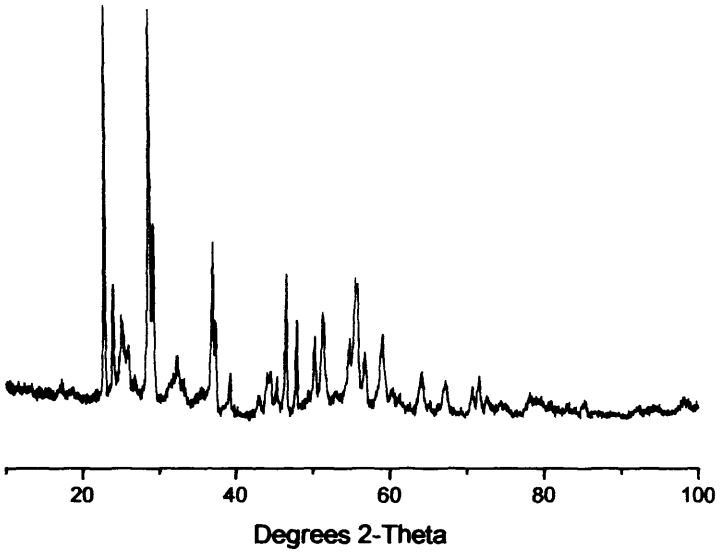

Figure 3.5 – XRD pattern for the oxidation of niobium metal, calcined in air at 500°C.

3.1.2 Raman Data.

Raman spectra for all niobium oxides are shown below. A band in the Raman spectra at 232cm^{-1} is attributed to B-Nb_2O_5. The presence of a band at 625cm^{-1} and 995cm^{-1}could be assigned to H-Nb_2O_5 or N-Nb_2O_5[2]. This relates back to Figure 1.6. The figure shows the preparation of different forms of niobium oxide, according to calcination temperature. H-Nb_2O_5 is formed at calcination temperatures of 800°C. N-Nb_2O_5 is formed at calcination temperatures of 600°C.

Niobyl groups (Nb=O) are represented in the Raman spectra by a strong signal at 805cm^{-1}. Another strong signal at 996cm^{-1} is due to the niobium-oxygen stretching frequency[3]. In the case of the niobium oxide and niobium phosphate catalysts the Raman results confirmed the phases identified from XRD data. A band in the Raman spectra at 377cm^{-1} is attributed to O-Nb-O deformation. Niobyl groups

$(Nb=O)^4$ are represented in the Raman spectra by a strong signal at 805cm^{-1}. Another strong signal at 988cm^{-1} may be due to an external mode or, more likely, the stretching mode becoming active when the NbO_6 octahedron is distorted[2,5,6].

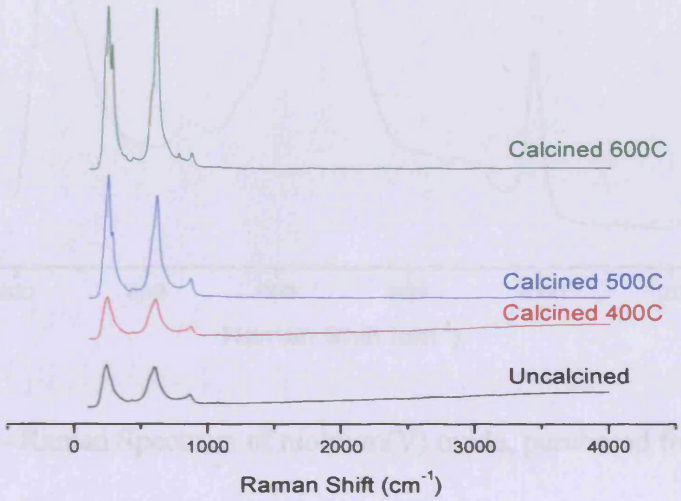

Figure 3.6 – Raman Spectrum from the precipitation reaction of niobium(V) chloride and sodium carbonate, calcined in air at different temperatures.

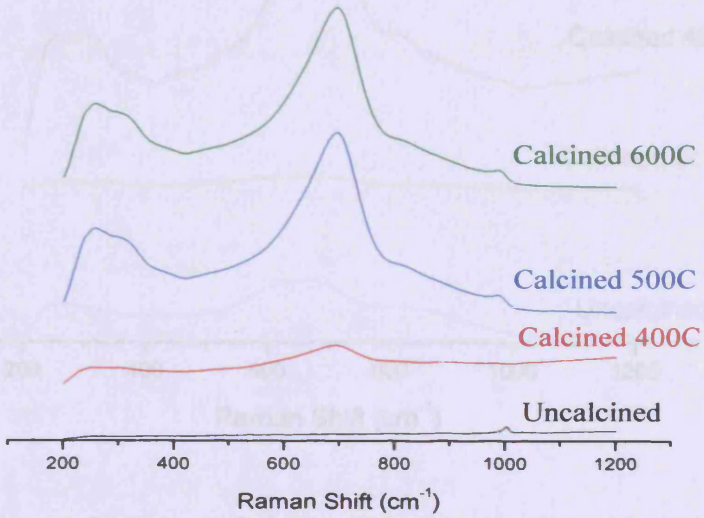

Figure 3.7 – Raman Spectrum from the precipitation reaction of niobium(V) chloride and urea, calcined in air at different temperatures.

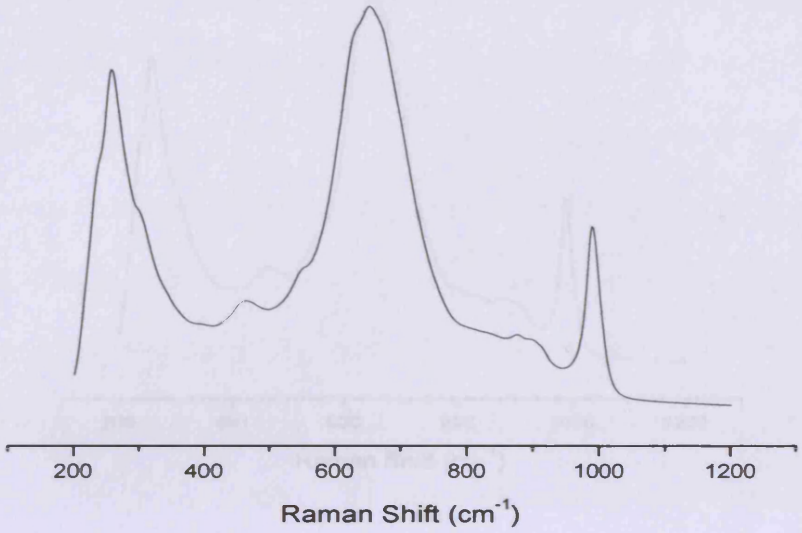

Figure 3.8 – Raman Spectrum of niobium(V) oxide, purchased from Aldrich.

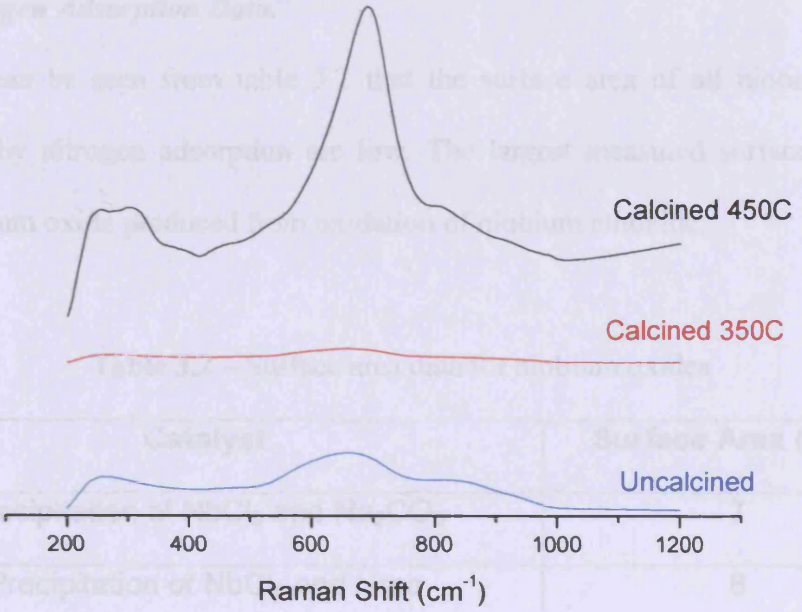

Figure 3.9 – Raman Spectrum of niobium(V) oxide, produced from the oxidation of niobium ethoxide, calcined in air at different temperatures.

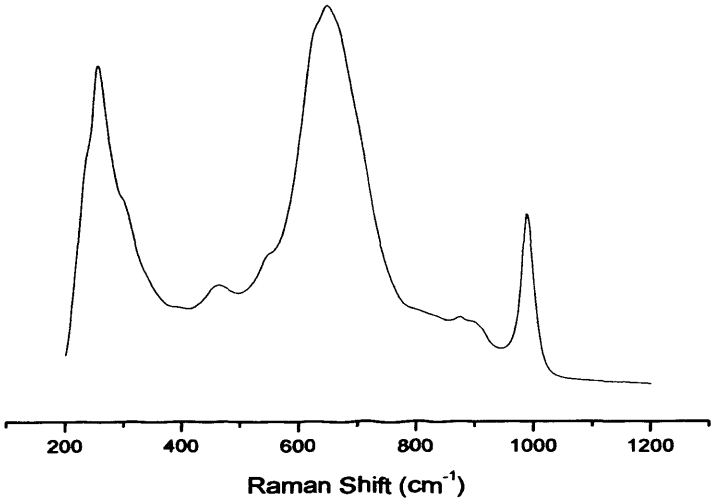

Figure 3.10 – Raman Spectrum of niobium(V) oxide produced as a result of oxidation of niobium metal.

3.1.3 Nitrogen Adsorption Data.

It can be seen from table 3.2 that the surface area of all niobium oxides measured by nitrogen adsorption are low. The largest measured surface area was from niobium oxide produced from oxidation of niobium ethoxide.

Table 3.2 – Surface area data for niobium oxides

Catalyst	Surface Area (m^2/g)
Precipitation of $NbCl_5$ and Na_2CO_3	7
Precipitation of $NbCl_5$ and Urea	8
Niobium(V) Oxide, Purchased from Aldrich	4
Oxidation of Niobium Ethoxide	18
Oxidation of Niobium Metal	12

3.1.4 SEM Data.

Figures 3.11 to 3.15 show SEM images of niobium oxides produced from different preparation techniques. Figure 3.11 and 3.12 show niobium oxides prepared from precipitation methods. The inset in Figure 3.11 quotes the crystal size. Both images show that the samples produce large, globular structures with typical particle sizes of 100-200μm in both samples. Figure 3.13 shows an SEM image of niobium oxide purchased from Aldrich. This produced much finer particles. Figures 3.14 and 3.15 produced niobium oxide as a result of oxidation reactions. It can be seen that particle sizes are large. The graph on 3.14 is a depth analysis technique used to show that the surface of the crystal is not flat.

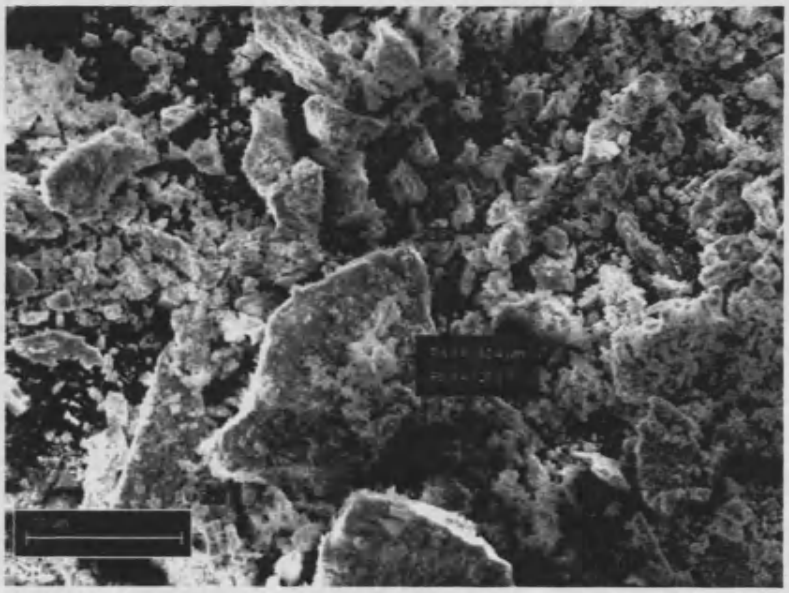

Figure 3.11 – SEM image of niobium oxide produced from the precipitation reaction of niobium(V) chloride and sodium carbonate.

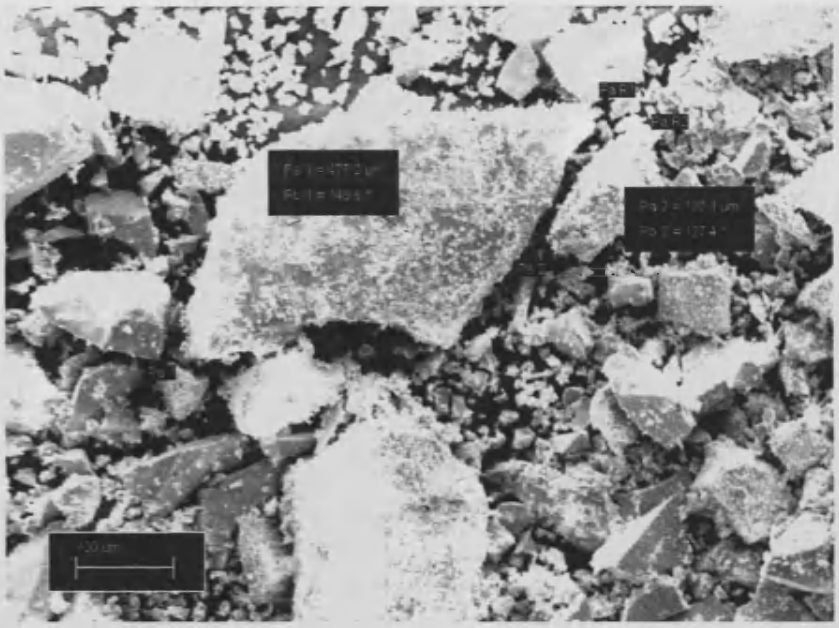

Figure 3.12 – SEM image of niobium oxide produced from the precipitation reaction of niobium(V) chloride and urea.

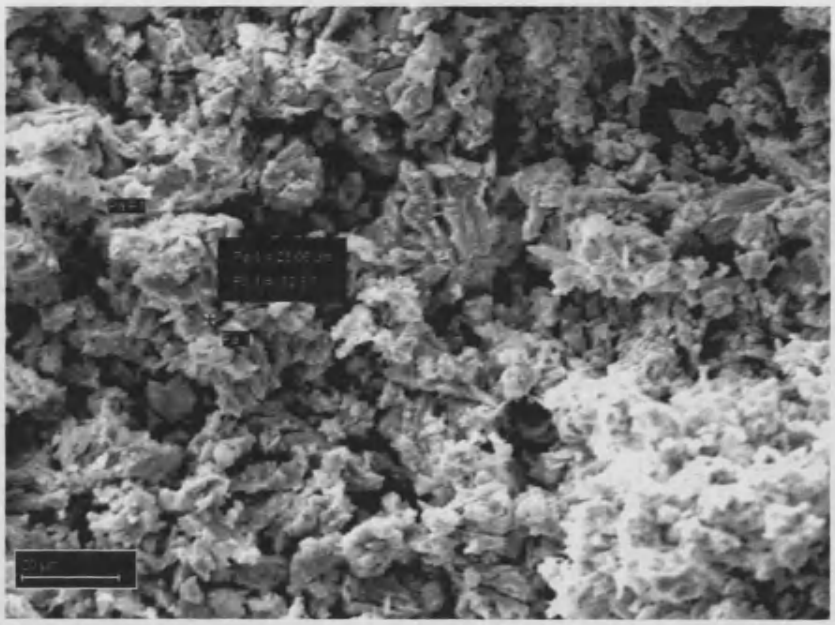

Figure 3.13 – SEM image of niobium(V) oxide, purchased from Aldrich.

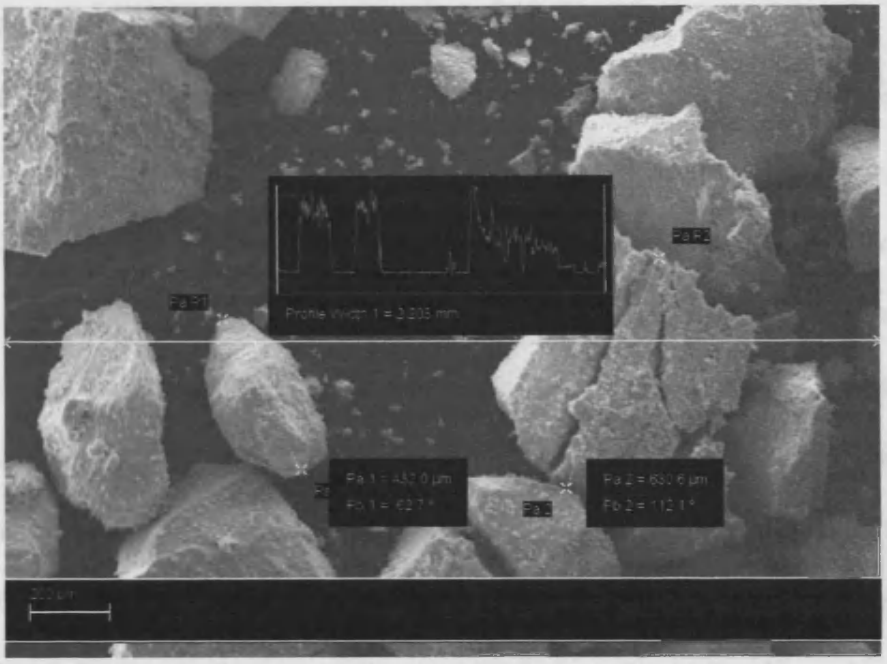

Figure 3.14 – SEM image of niobium(V) oxide, produced from the oxidation of niobium ethoxide.

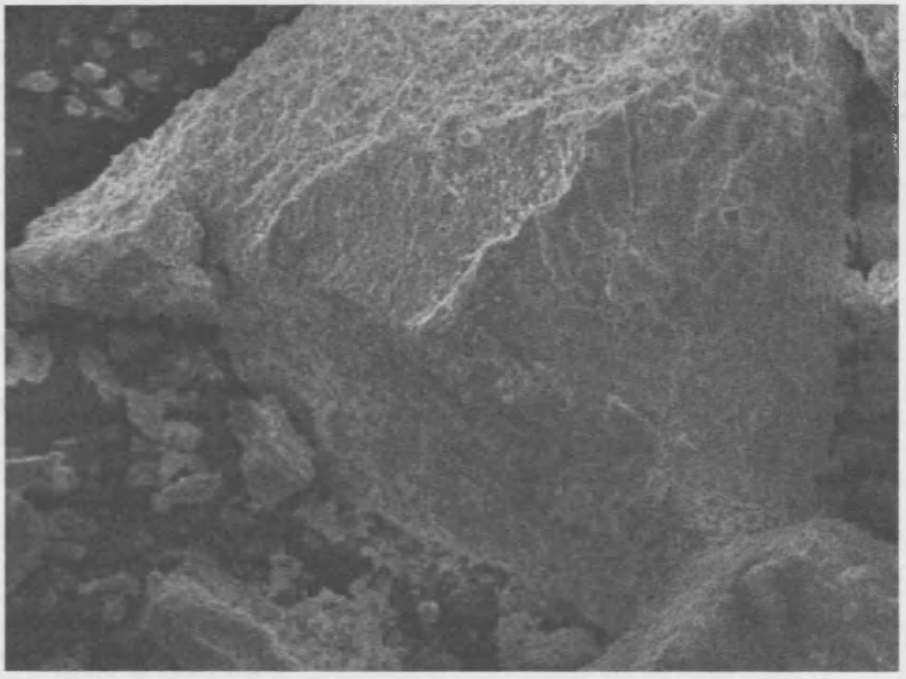

Figure 3.15 – SEM image of niobium oxide produced from the oxidation of niobium metal.

3.1.5 TGA Data.

Figure 3.16 shows TGA analysis for niobium oxide produced from the precipitation of niobium chloride and sodium carbonate. A temperature program of 10°C/minute up to 900°C was set, with the following result. At approximately 400°C, there is a large decrease in mass, possibly due to loss of carbonate in the sample. At 550°C, there is a large increase in mass, possibly due to oxidation of the sample.

Figure 3.17 shows TGA analyses for niobium oxide produced from the precipitation of niobium chloride and urea. A temperature program of 10°C/minute up to 600°C was set. At approximately 250°C, there is a decrease in mass, possibly due to loss of water from the sample. At 350°C, there is another large decrease in mass, and at 450°C, there is a decrease in mass.

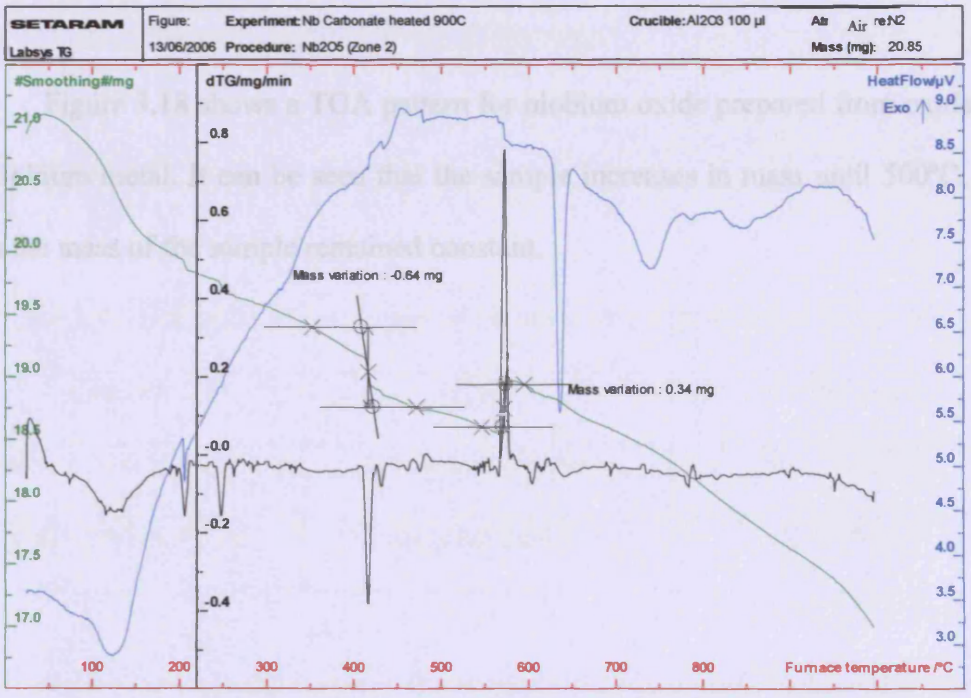

Figure 3.16 – TGA pattern of the precipitation reaction with niobium(V) chloride and sodium carbonate.

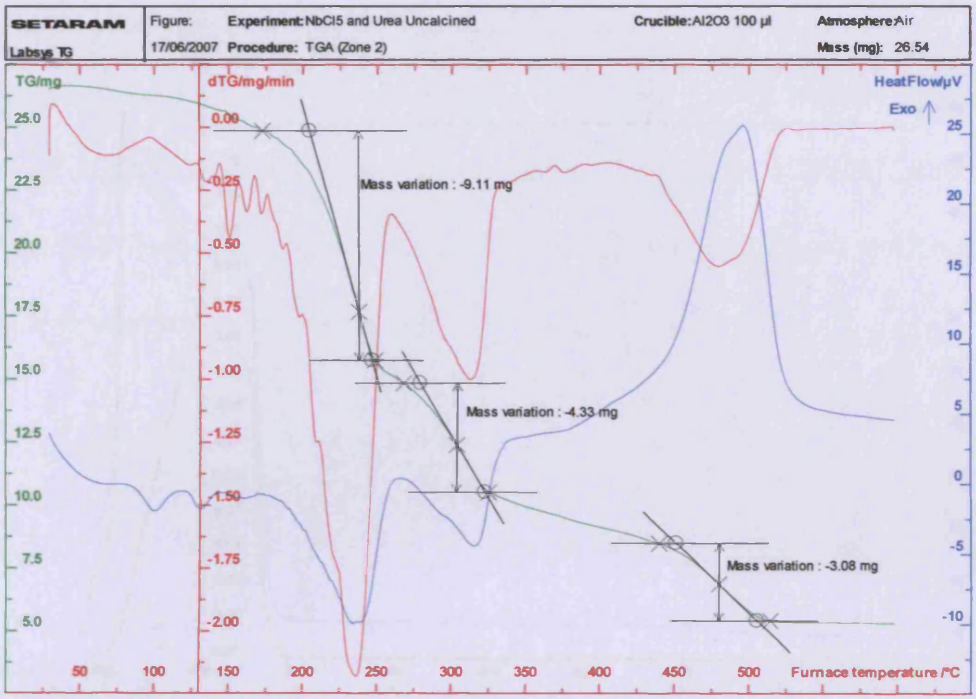

Figure 3.17 – TGA Data for the precipitation reaction between $NbCl_5$ and urea in air up to 550°C.

Figure 3.18 shows a TGA pattern for niobium oxide prepared from oxidation of niobium metal. It can be seen that the sample increases in mass until 500°C, and then the mass of the sample remained constant.

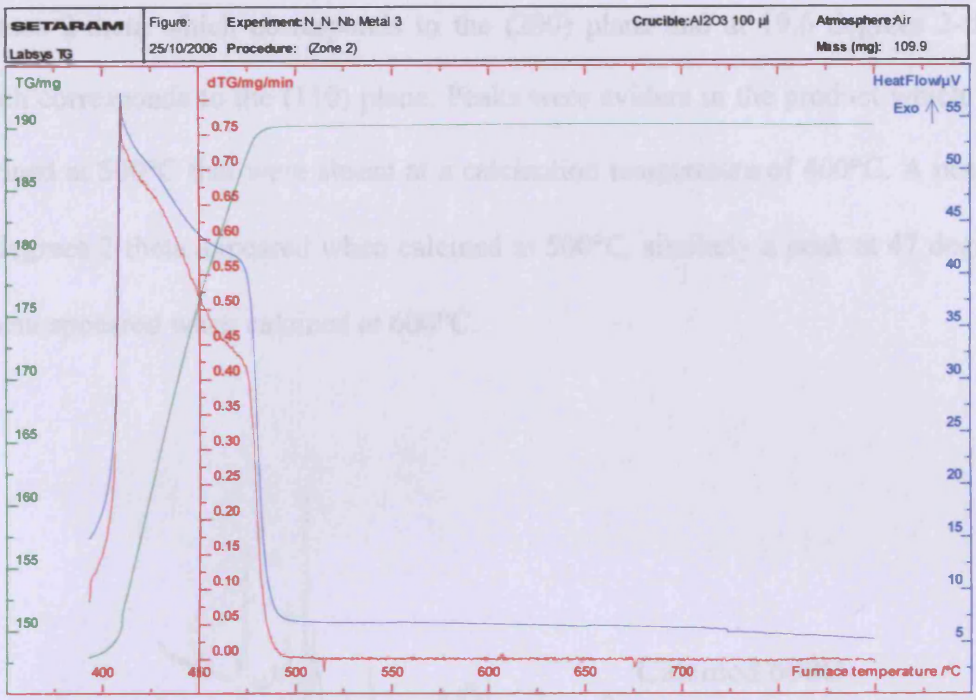

Figure 3.18 – TGA Pattern for the Oxidation of Niobium Metal.

3.2 ***Characterisation of Niobium Oxide Phosphate.***

3.2.1. XRD Data.

Table 3.3 – Summary of the phases of niobium oxide phosphate phases formed.

Catalyst	Phase	Reference
$NbCl_5$ and H_3PO_4	Tetragonal $NbOPO_4$	01-070-2652
$NbCl_5$ and $H_4P_2O_7$	Tetragonal $NbOPO_4$	01-073-1609

α-Niobium oxide phosphate (Reference 01-070-2652, JCPDS) prepared from using ortho-phosphoric acid was tetragonal with a space group of $P4/_{nmm}$. All angles were 90°, a = b = 6.4043Å and c = 4.1217Å. The most intense peak was at 25.7 degrees 2-theta, which corresponds to the (101) plane. Other planes were at 27.8

degrees 2-theta which corresponds to the (200) plane and at 19.6 degrees 2-theta which corresponds to the (110) plane. Peaks were evident in the product which was calcined at 500°C that were absent at a calcination temperature of 400°C. A peak at 38 degrees 2-theta appeared when calcined at 500°C, similarly a peak at 47 degrees 2-theta appeared when calcined at 600°C.

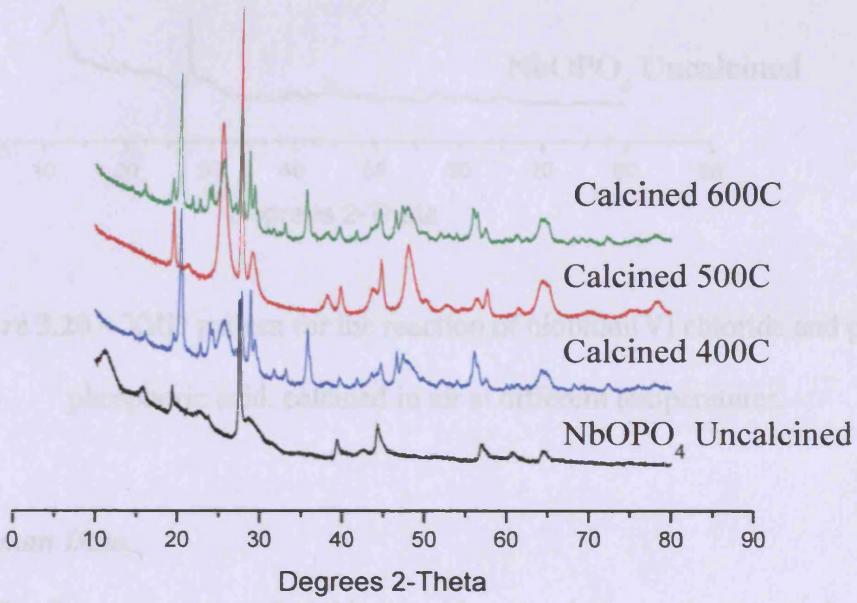

Figure 3.19 – XRD pattern for the reaction of niobium(V) chloride and ortho-phosphoric acid, calcined in air at different temperatures.

α-Niobium oxide phosphate (Reference 01-073-1609, JCPDS) prepared from using pyro-phosphoric acid was tetragonal with a space group of $P4/_n$, with all angles 90°, a = b = 6.3873Å and c = 4.1037Å. The most intense peak was at 25.8 degrees 2-theta, which corresponds to the (101) plane. Other planes were at 27.9 degrees 2-theta which corresponds to the (200) plane and at 19.6 degrees 2-theta which corresponds to the (110) plane.

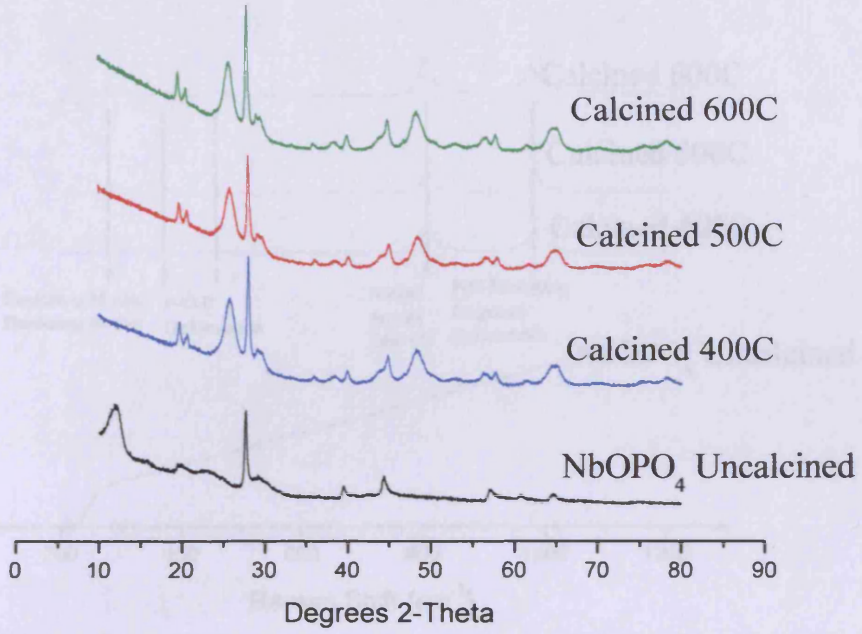

Figure 3.20 – XRD pattern for the reaction of niobium(V) chloride and pyro-phosphoric acid, calcined in air at different temperatures.

3.2.2 Raman Data.

The Raman spectra of niobium oxide phosphate catalysts contained peaks which were characteristic of niobium and phosphorus catalysts. A band in the Raman spectra at 377cm^{-1} is attributed to O-Nb-O deformation. The presence of a weak band at 460cm^{-1} indicates P-O-P deformation. Niobyl groups (Nb=O) are represented in the Raman spectra by a strong signal at 805cm^{-1}. Another strong signal at 988cm^{-1} may be due to the stretching mode becoming active when the NbO_6 octahedron is distorted[2,3,4].

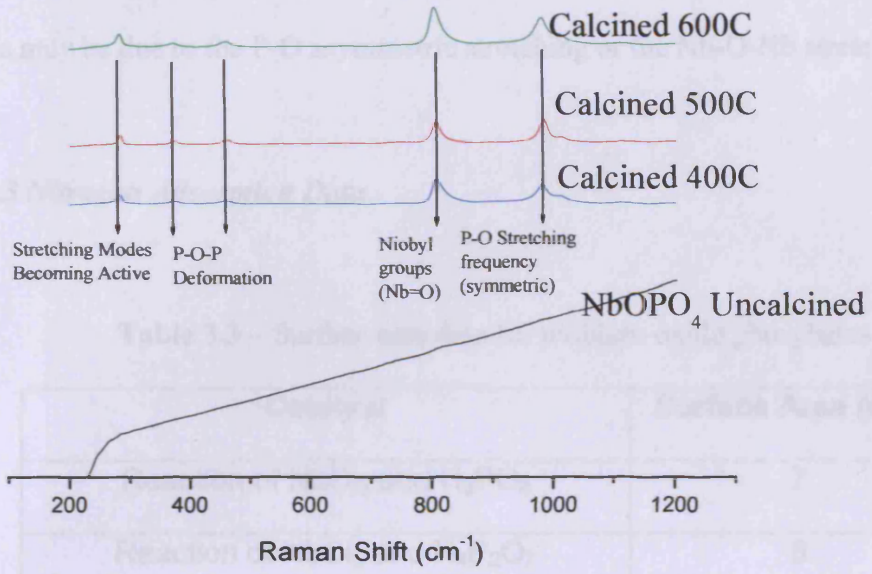

Figure 3.21 – Raman spectrum for the reaction of niobium(V) chloride and ortho-phosphoric acid, calcined in air at different temperatures.

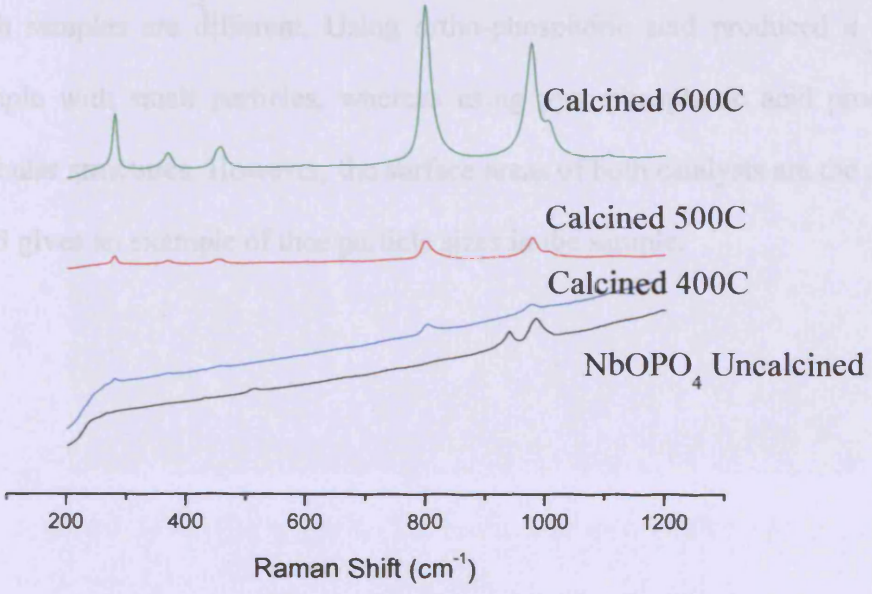

Figure 3.22 – Raman spectrum for the reaction of niobium(V) chloride and pyro-phosphoric acid, calcined in air at different temperatures.

It can be seen from Figure 3.22 that the Raman spectrum of the product which was calcined at 600°C contained two extra peaks at 600cm^{-1} and 1100cm^{-1}. This may be due to the P-O asymmetric stretching or the Nb-O-Nb stretching bonds.

3.2.3 Nitrogen Adsorption Data.

Table 3.3 – Surface area data for niobium oxide phosphates

Catalyst	Surface Area (m^2/g)
Reaction of $NbCl_5$ and H_3PO_4	7
Reaction of $NbCl_5$ and $H_4P_2O_7$	8

3.2.4 SEM Data.

Figures 3.23 and 3.24 show SEM images of niobium oxide phosphate catalysts prepared from using different types of phosphoric acid. The morphology of both samples are different. Using ortho-phosphoric acid produced a fine powder sample with small particles, whereas using pyro-phosphoric acid produced large, globular structures. However, the surface areas of both catalysts are the same. Figure 3.23 gives an example of thee particle sizes in the sample.

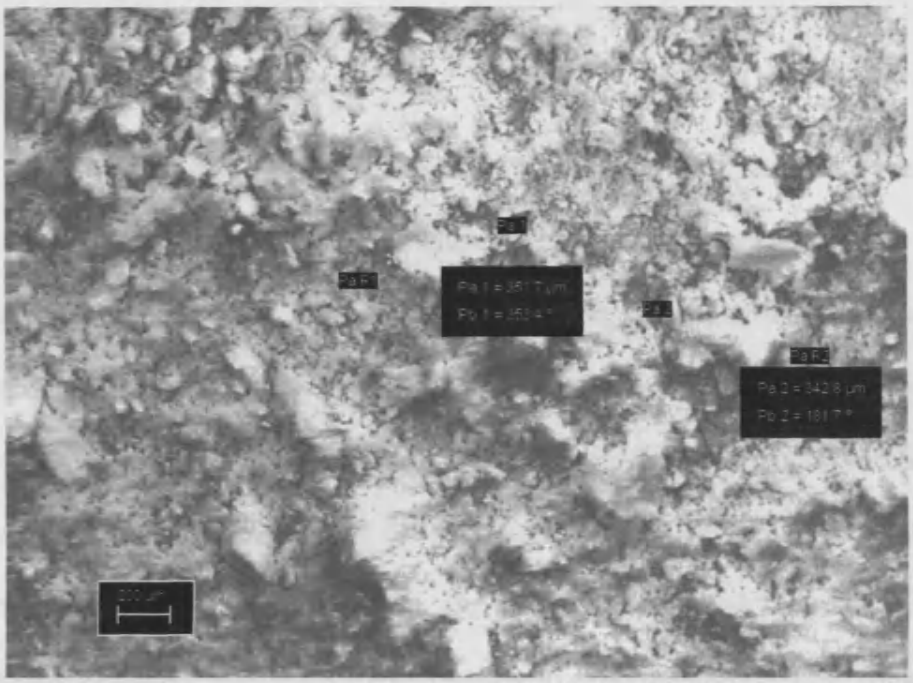

Figure 3.23 – SEM image for the reaction of niobium(V) chloride and ortho-phosphoric acid, calcined in air at 500°C.

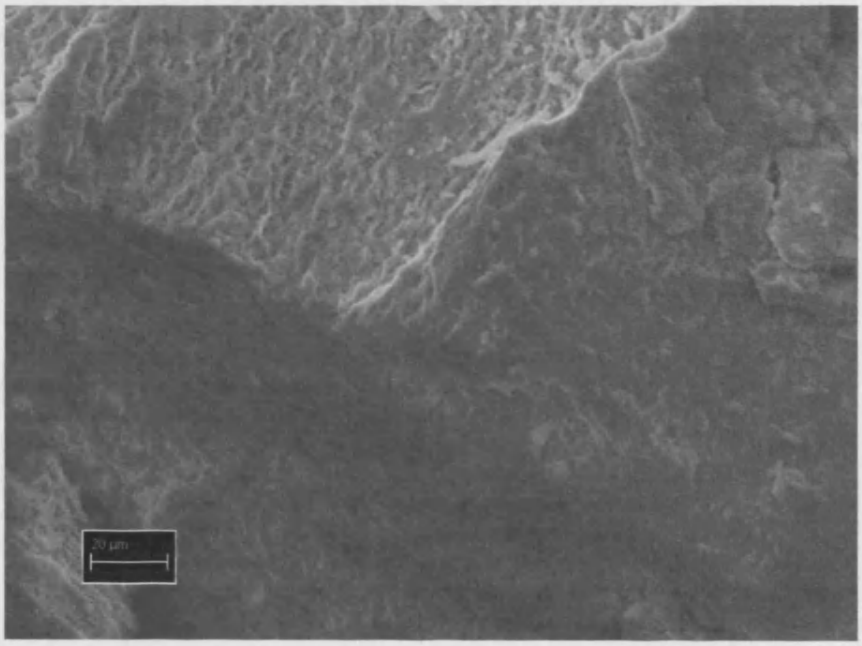

Figure 3.24 – SEM image for the reaction of niobium(V) chloride and pyro-phosphoric acid, calcined at 500°C.

3.1.5 TGA Data.

Niobium oxide phosphate was reduced in hydrogen for 3 hours. No previous work could be found using this type of method to produce niobium phosphate. In order to find out the best calcination temperature, a TGA was performed on niobium oxide phosphate. This is shown in figure 3.25. Initially, the mass of the sample decreased, due to loss of water from the sample and possibly loss of PH_3. After water was lost, the sample gained in mass. It was determined that the optimum calcination temperature for this reaction was 500°C. The sample was run and TG (mass of sample) was obtained. This had a rough line due to experimental error, so smoothing had to take place.

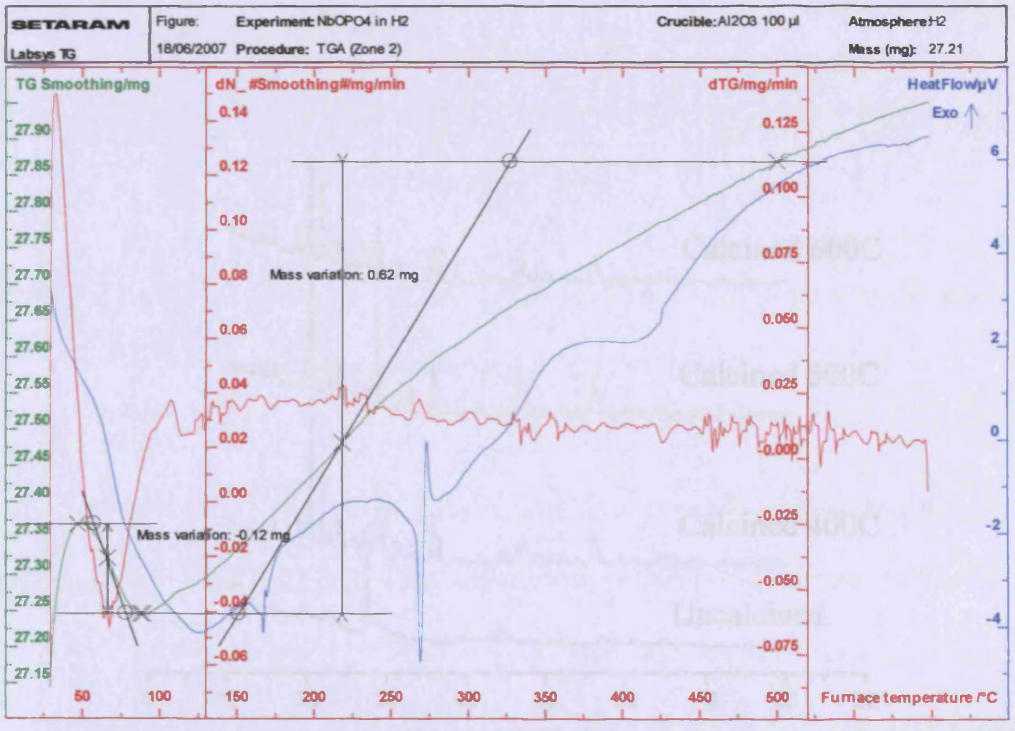

Figure 3.25 – TGA data for the reaction of niobium(V) chloride and ortho-phosphoric acid, heated to 600°C in hydrogen.

3.3 Characterisation of Niobium Phosphate.

3.3.1. XRD Data.

Niobium oxide phosphate reduced with hydrogen produced ε-niobium phosphate (00-040-0124, JCPDS) which is orthorhombic and is in the space group Pn^*_a. All angles were 90°, a = 8.7520Å, b = 12.0900Å and c = 8.6740Å. The most intense peak was at 20.5 degrees 2-theta and corresponds to the (121) plane. Other peaks were 35.8 degrees 2-theta which corresponds to the (123) plane and another at 36.1 degrees 2-theta, which corresponds to the (240) plane.

Figure 3.26 showed evidence of peaks absent in the sample which was calcined at 500°C which were present in the sample calcined at 400°C and 600°C – this was the peak at 17 and 36 degrees 2-theta.

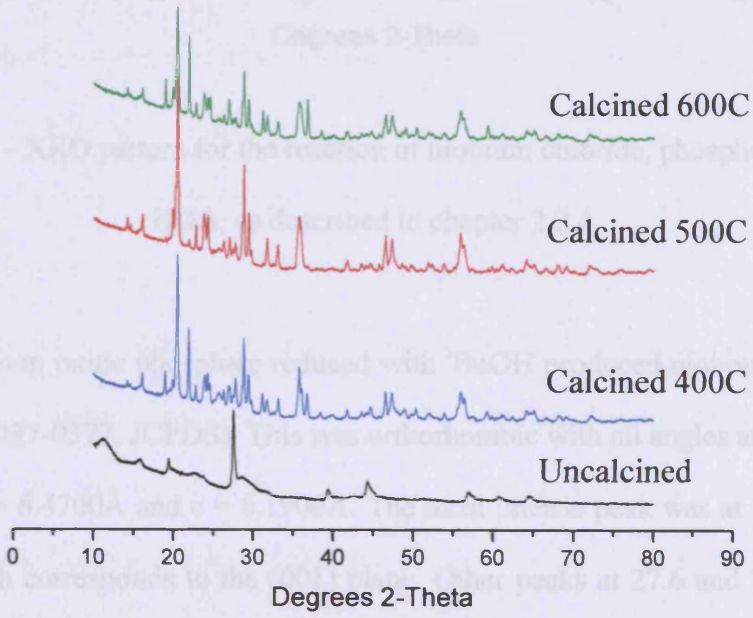

Figure 3.26 – XRD pattern for the reaction of niobium oxide phosphate calcined with H_2 at different temperatures.

Niobium phosphate, $Nb_2P_4O_{15}$ (00-028-0715, JCPDS), was cubic pre-reaction and post-reaction. All angles were 90°, a = b = c = 8.0660Å. The most intense peak was at 22 degrees 2-theta corresponds to the (200) plane. Other peaks were 36.9 degrees 2-theta which corresponds to the (311) plane and another at 31.4 degrees 2-theta, which corresponds to the (220) plane.

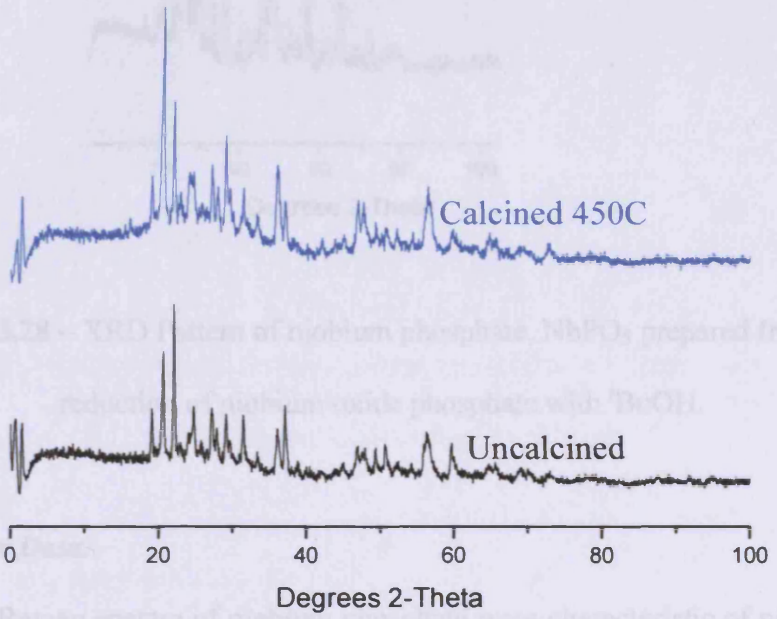

Figure 3.27 – XRD pattern for the reaction of niobium chloride, phosphoric acid and HDA, as described in chapter 2.2.4.

Niobium oxide phosphate reduced with ^{i}BuOH produced niobium phosphate hydrate (00-037-0377, JCPDS). This was orthorhombic with all angles at 90° and a = 6.2600Å, b = 6.4700Å and c = 6.1900Å. The most intense peak was at 14.4 degrees 2-theta which corresponds to the (001) plane. Other peaks at 27.6 and 28.6 degrees 2-theta, which correspond to the (020) and (002) planes respectively.

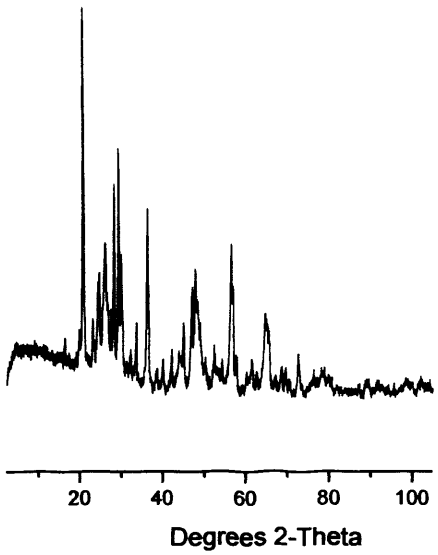

Figure 3.28 – XRD Pattern of niobium phosphate, $NbPO_5$ prepared from the reduction of niobium oxide phosphate with $^{i}BuOH$.

3.3.2 Raman Data.

The Raman spectra of niobium phosphate were characteristic of niobium and phosphorous catalysts. The Raman spectra of niobium oxide phosphate catalysts contained peaks which were characteristic of niobium and phosphorus catalysts. A band in the Raman spectra at $377cm^{-1}$ is attributed to O-Nb-O deformation. The presence of a weak band at $460cm^{-1}$ indicates P-O-P deformation. Niobyl groups (Nb=O) are represented in the Raman spectra by a strong signal at $805cm^{-1}$. Another strong signal at $988cm^{-1}$ may be due to an external mode or, more likely, the stretching mode becoming active when the NbO_6 octahedron is distorted[2,3,4].

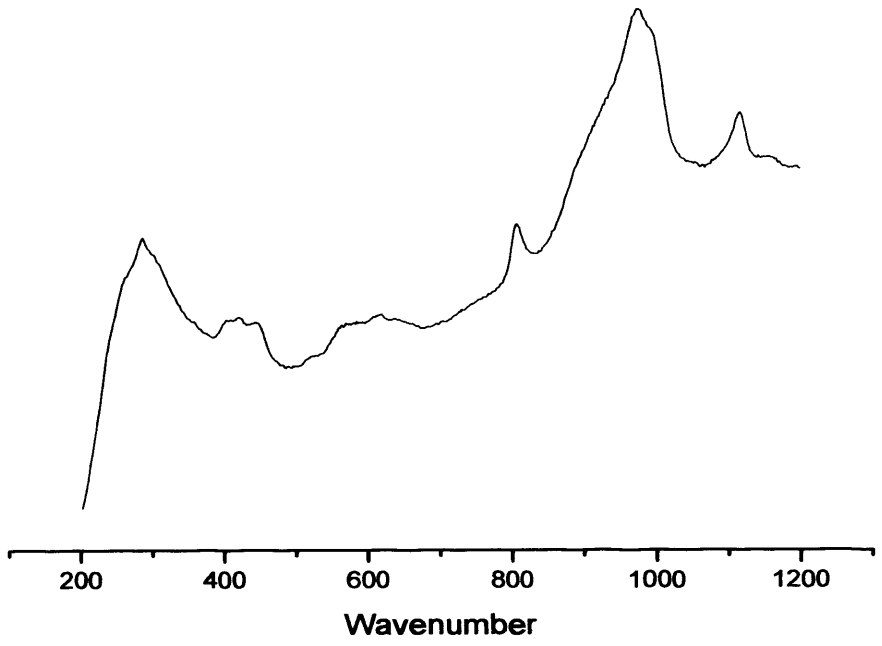

Figure 3.29 – Raman spectra for the reaction of niobium chloride, phosphoric acid and hydroxylamine, as described in chapter 2.2.4.

3.3.3 Nitrogen Adsorption Data.

Table 3.4 – Surface area data for niobium phosphates.

Catalyst	Surface Area (m^2/g)
$NbOPO_4.xH_2O$ Reduced with H_2	6
Reaction of $NbOPO_4.xH_2O$ with ^tBuOH	5
Reaction of $NbOPO_4.xH_2O$ with 1-BuOH	6
Reaction of niobium chloride, phosphoric acid and HDA.	12

3.3.4 SEM Data.

Figures 3.30 to 3.32 show SEM images of niobium phosphates prepared by different methods. Particle sizes are smaller than other catalysts described previously.

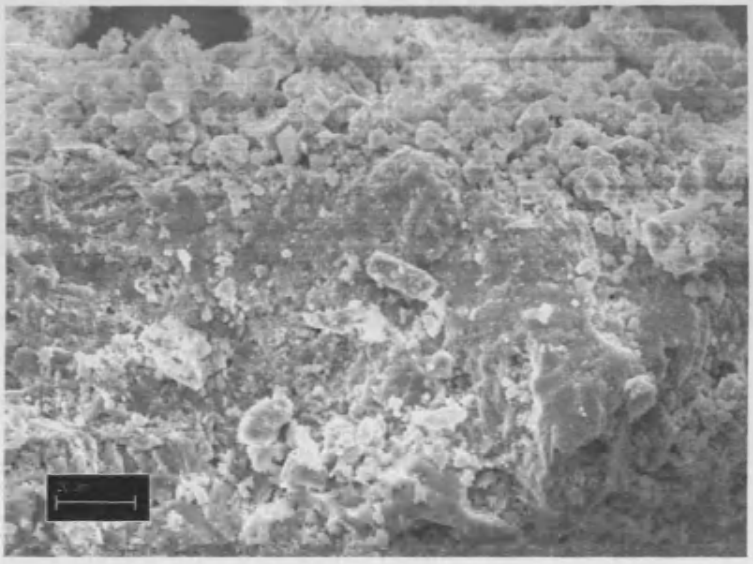

Figure 3.30 – SEM image of the product from the reaction of niobium oxide phosphate calcined in H_2 at 500°C.

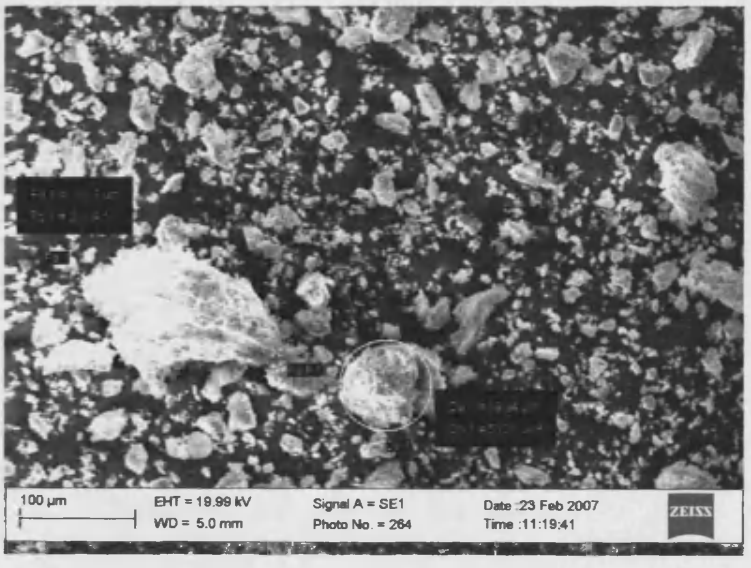

Figure 3.31 – SEM image of the product from the reaction of niobium oxide phosphate reduced with ^{i}BuOH calcined at 500°C.

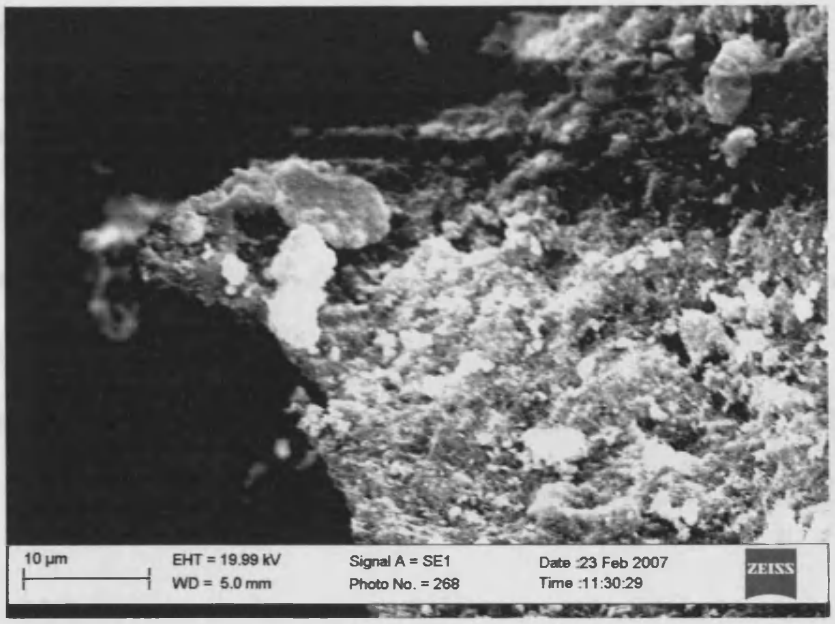

Figure 3.32 – SEM Image of $Nb_2P_4O_{15}$.

References.

[1] Licoccia, S., Polini, R., D'Ottavi, C., Fiory, F. S., Di Vona, M. L., Traversa, E.; *Journal of Nanoscience and Nanotechnology*, 5, **2005**, 592-595.

[2] Da Silva, J. C. G., Viera, M. D., Oliveira Andrade, W.; *Journal of Material Science*, 40, **2005**, 4455-4460.

[3] A. A. McConnell, J. S. Anderson, C.N.R. Rao, *Spectrochim. Acta*, 32, **1976**, 1067.

[4] Mazali, I. O., Alves, O. L.; *Journal of Materials Science Letters*, 20, **2001**, 2113-2117.

[5] B. Huang, K. Wang, J. S. Church, Y-S. Li, *Electrochimica Acta*, 44, **1999**, 2571-2577.

[6] J. C. G. Da Silva, M. D. Viera, W. De Oliveira Andrade, *J. Mater. Science*, 40, **2005**, 4455-4460.

4. Methanol Partial Oxidation.

4.1 Introduction to Methanol Oxidation.

This chapter investigates methanol oxidation over niobium based catalysts. Effects of preparation method and the introduction of phosphorus are tested to gain insight into the requirements for a good formaldehyde production catalyst.

Iron molybdates are used as commercial catalysts for the partial oxidation of methanol to formaldehyde. A large number of investigations have been performed into the properties of iron molybdates for the oxidation of methanol. This includes Liberti, Pernicone and Soattini, who investigated an $Fe_2(MoO_4)_3$ prepared by calcination of a mixed phase ($Fe_2(MoO_4)_3$ and MoO_3 to sublime excess MoO_3) catalyst which was calcined at 700°C for one week, and found it to be active to methanol oxidation[1]. A review by Trifiro of molybdate based catalysts described some important aspects of preparation of iron molybdate catalysts[2], such as:

- Species of molybdenum ions within aqueous solution.
- Formation of heteropolyanions.
- The transformation of the amorphous precipitate to crystalline structure.
- Solid-state reaction with oxide impurities during calcination.

4.1.1. Methanol.

Methanol is a naturally occurring substance and is the simplest of the alcohol family with the formula CH_3OH. Methanol is colourless, tasteless and is poisonous.

The density of methanol is 0.7914 g/cm^3 at room temperature and pressure. It has a melting point of -93.9°C and a boiling point of 65.0°C at standard pressure[3].

Methanol is used in a wide range of applications. It can be used as a fuel source for internal combustion engines, for example high powered cars such as Drag racing and American Indy cars. It has been suggested that methanol can be used as a renewable substitute for petroleum, as methanol can be produced from organic materials[10]. However, current petrol engines would require significant alteration in order for methanol to be used widely as a fuel for vehicles.

Methanol is used as a solvent, it is added to ethanol as a denaturant because it is poisonous and is used in antifreeze in pipelines. The largest use for methanol is the production of other chemicals, such as DME (dimethyl ether), which is used in aerosols. However, the largest product is formaldehyde, which accounts for 40% of methanol usage[4].

4.1.2. Formaldehyde.

Formaldehyde is rarely found in the monomeric form (H_2CO) and is most likely to be found in a polymeric form. Dry monomeric formaldehyde is a colourless gas at room temperature, with a melting point of -92°C and a boiling point of -21°C[5].

Gaseous formaldehyde is hazardous, even at concentrations of 20 ppm, with a pungent odour and is an irritant to the eyes, nose and throat. Formaldehyde exists in several forms aside from H_2CO: the cyclic trimer trioxane and the polymer paraformaldehyde.[6]

Formaldehyde has been produced commercially for over 100 years, its initial use being as a disinfectant and an embalming agent. The first person to prepare

formaldehyde was Alexander M Butlerov in 1859[7]. It was first produced from methanol in 1868 when August W. Von Hoffman passed methanol vapour and air over a heated platinum spiral[8].

The first industrial catalysts involved dehydrogenation over a copper gauze. These were later replaced by silver catalysts, due to the higher yield achieved, also, these catalysts possess a greater resistance to poisoning. In the 1950's, an alternative process was designed involving the selective oxidation of methanol over an Fe-Mo oxide catalyst. At present, the silver and oxide processes each account for approximately half of the total production of formalin (aqueous solution of formaldehyde). However, in the last ten years, the oxide process has been favoured. The advantages of this process are summarised as follows[9]:

a. Higher yield – allows production of solutions with low methanol content.
b. Higher resistance to poisoning – no purification methods are required.
c. Longer lifetime of catalyst.
d. Low fire and explosion hazards.

4.2. Catalytic Cycle for Methanol Oxidation.

The following reaction scheme shows the cycle for the selective oxidation of methanol to formaldehyde using silver catalysts[10]. This follows the Mars van Krevelen mechanism, where oxygen from the lattice is used and then replaced by gaseous oxygen. Oxygen is adsorbed after the formaldehyde reaction to re-oxidise the reduced surface. The Mars van Krevelen mechanism was discovered by Mars and van Krevelen in 1954[11], this has been a mechanism that is widely accepted for various catalytic reactions.

$CH_3OH \rightarrow CH_3OH\ (a)$ Eq. 4.1

$CH_3OH\ (a) + O\ (a) \rightarrow CH_3O\ (a) + OH\ (a)$ Eq. 4.2

$CH_3OH\ (a) + OH\ (a) \rightarrow CH_3O\ (a) + H_2O$ Eq. 4.3

$CH_3O\ (a) \rightarrow H_2CO\ (a) + H\ (a)$ Eq. 4.4

$2H\ (a) \rightarrow H_2$ Eq. 4.5

$H\ (a) + OH\ (a) \rightarrow H_2O$ Eq. 4.6

$H_2CO\ (a) \rightarrow H_2CO$ Eq. 4.7

House *et al.* showed that surface oxygen is used in the mechanism for the oxidation of methanol to formaldehyde over iron molybdates[12]. It was found that surface oxygen is used in the mechanism, whilst bulk oxygen diffuses to the surface and became active at a significant rate above 250°C. Depending upon the speed of bulk oxygen diffusion, this may also be contributing to the low activity of niobium oxide catalysts. Carlinsey investigated niobium oxide microstructures via potentiostatic anodisation (where a potential difference i.e. voltage is put across a conductor) and found that niobium oxides have slow oxygen diffusion rates (i.e. oxygen does not readily diffuse from bulk to surface)[13]. Recent studies by Ubago-Perez *et al.* concentrated on using carbon supported Pt and Pd crystals[14]. It was found that conversion of methanol increased up to 70% at 220°C, whilst selectivity to formaldehyde was less than 50% at 220°C. The other product in the reaction was carbon dioxide.

In other studies, Islam *et al.* studied Pt/Ru alloys for methanol oxidation[15]. Pt was added in different amounts to Ru. It was found that, although Pt increased the conversion of methanol, the selectivity achieved by high ratios of Ru decreased as conversion of methanol increased.

In this chapter, attempts will be made to compare niobium based catalysts with other catalysts tested within the literature and understand the comparisons between them. From previous work involving propane oxidative dehydrogenation, it has been shown that niobium based catalysts have a high selectivity for propene. The aim of this work is to examine whether the selectivity to formaldehyde from methanol can be maintained with high conversions. The selectivity and activity of methanol oxidation is sensitive to the structure of the catalytic surface making it an excellent probe reaction[16 17].

4.3 Methanol Oxidation Using Niobium(V) Oxide Catalysts.

Niobium oxides, prepared by different methods were tested for the oxidation of methanol, the desired product being formaldehyde. Catalysts prepared from precipitation reactions, oxidation reactions and niobium oxide which has been purchased (as described in chapter 2) was all tested.

4.3.1 Effect of Preparation Techniques.

Figure 4.1 shows that the majority of niobium catalysts produce a low conversion up to 400°C, except for niobium oxide produced from the oxidation of niobium ethoxide. Niobium oxide, produced from the oxidation of niobium ethoxide started to show activity at 200°C. Niobium oxides produced by all other methods became active at 240°C.

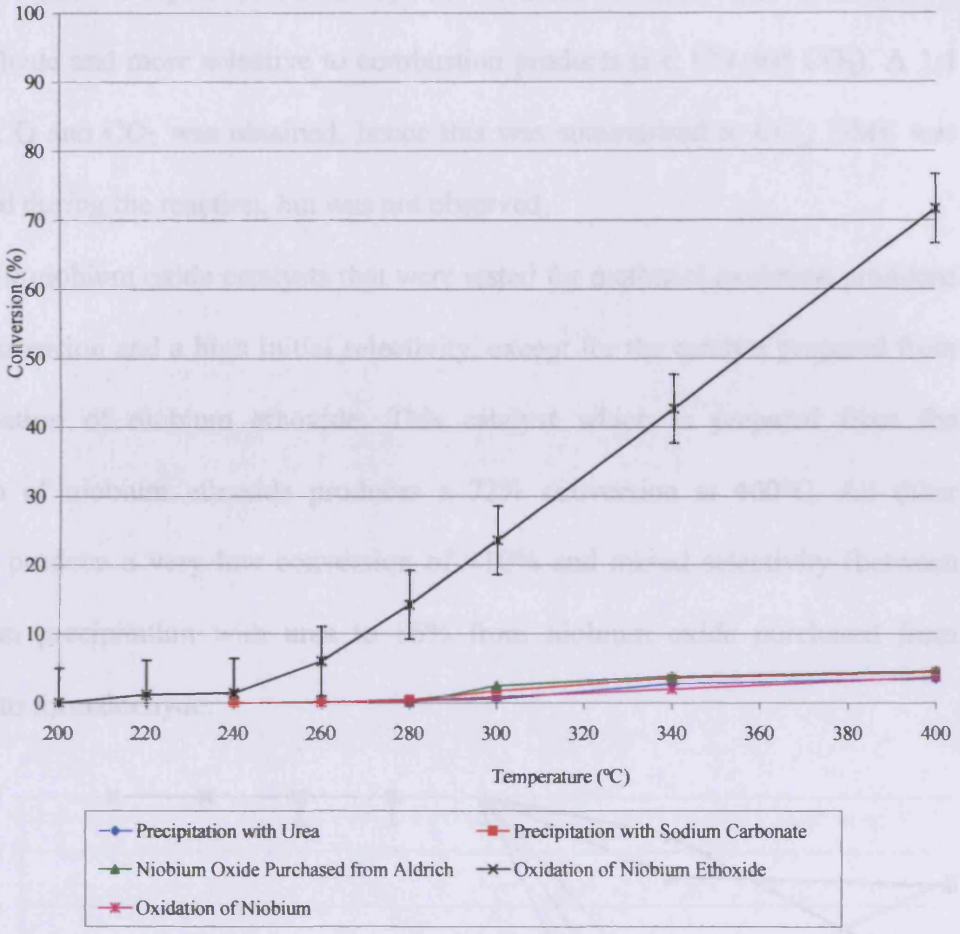

Figure 4.1 – Methanol conversion as a function of temperature using niobium oxides prepared by different methods.

Possible products from the oxidation of methanol are CO, CO_2 and DME. No DME is observed, while at higher temperatures CO and CO_2 are produced as a product. The selectivity to formaldehyde decreased with each catalyst due to the formation of combustion products. Formic acid and methyl formate could also have been produced, but these were not observed in the analysis.

Figures 4.2 and 4.3 shows the selectivity to formaldehyde and combustion products for the various niobium oxide catalysts. All niobium oxide catalysts were entirely selective to formaldehyde when the catalysts first became active. At 340°C,

niobium oxide catalysts prepared by all methods become less selective to formaldehyde and more selective to combustion products (i.e. CO and CO_2). A 1:1 ratio of CO and CO_2 was obtained, hence this was summarised to CO_x. DME was monitored during the reaction, but was not observed.

All niobium oxide catalysts that were tested for methanol oxidation produced a low conversion and a high initial selectivity, except for the catalyst prepared from the oxidation of niobium ethoxide. This catalyst which is prepared from the oxidation of niobium ethoxide produces a 72% conversion at 400°C. All other catalysts produce a very low conversion of <10% and mixed selectivity (between 40% from precipitation with urea to 85% from niobium oxide purchased from Aldrich) to formaldehyde.

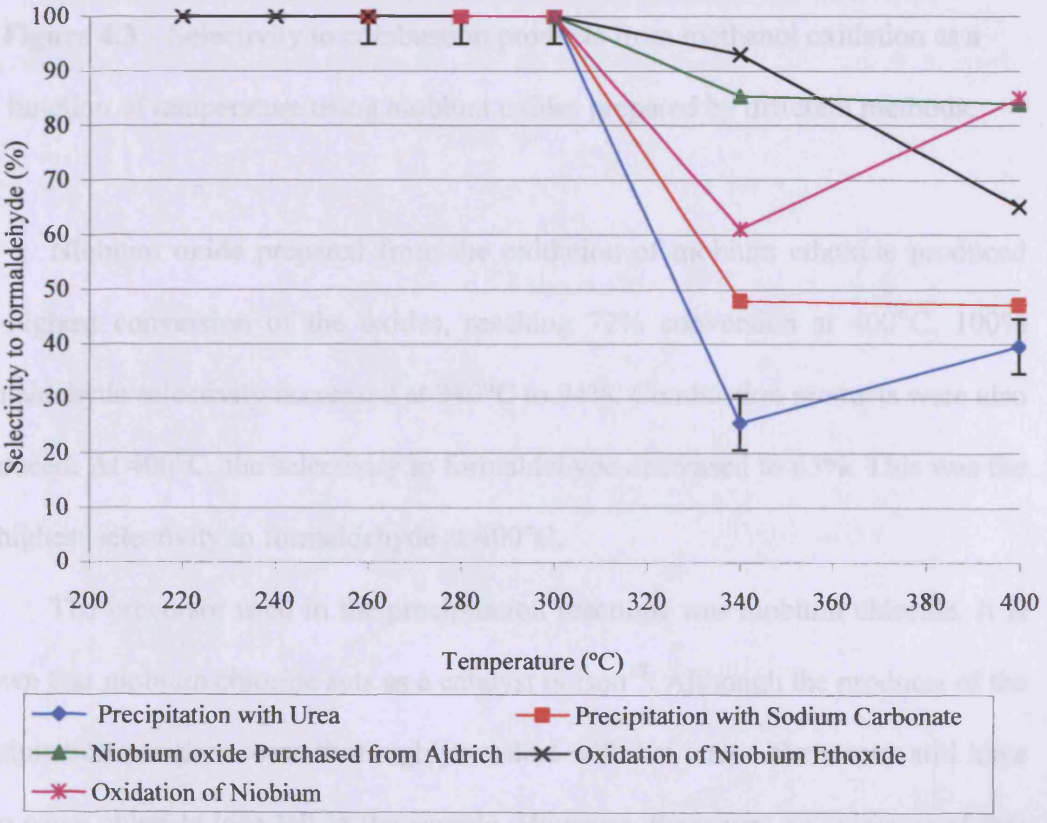

Figure 4.2 – Selectivity to formaldehyde from methanol oxidation as a function of temperature using niobium oxides prepared by different methods.

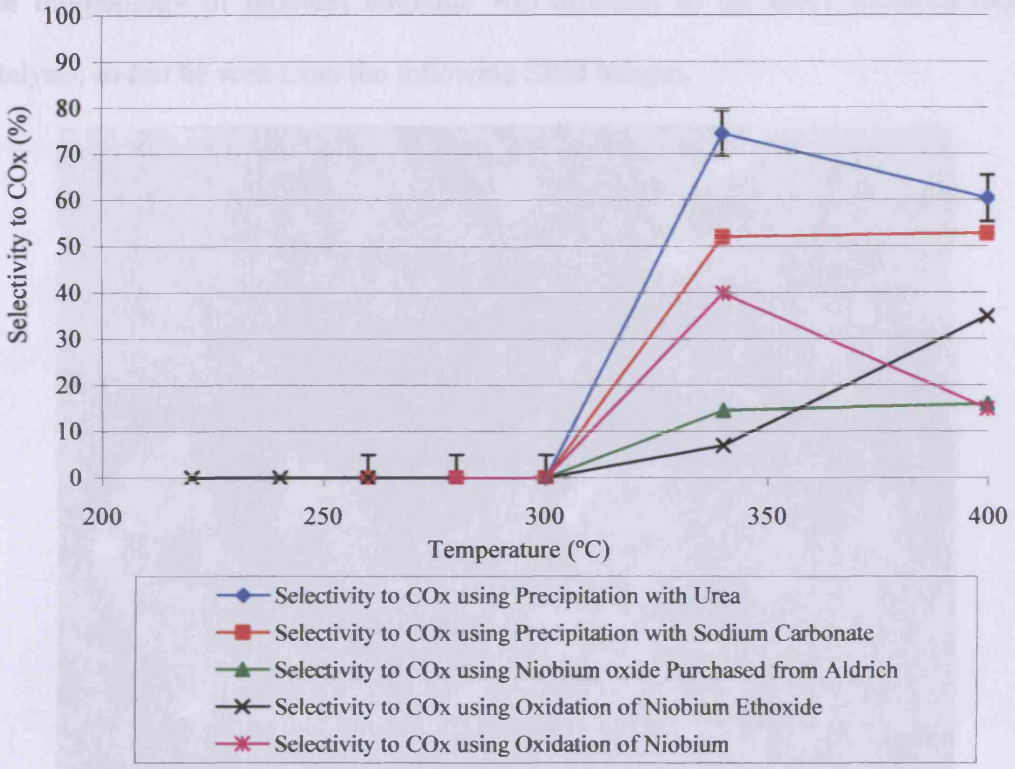

Figure 4.3 – Selectivity to combustion products from methanol oxidation as a function of temperature using niobium oxides prepared by different methods.

Niobium oxide prepared from the oxidation of niobium ethoxide produced the highest conversion of the oxides, reaching 72% conversion at 400°C. 100% formaldehyde selectivity decreased at 340°C to 94%. Combustion products were also produced. At 400°C, the selectivity to formaldehyde decreased to 65%. This was the 3rd highest selectivity to formaldehyde at 400°C.

The precursor used in the precipitation reactions was niobium chloride. It is known that niobium chloride acts as a catalyst poison[18]. Although the products of the precipitation reactions were thoroughly washed with hot water, there may still have been some chloride ions left in the sample. However, there was no evidence of this from XPS studies. Further discussion of XPS results are found in chapter 4.3.3.3.

The morphology of niobium ethoxide was different to the other niobium oxide catalysts, as can be seen from the following SEM images.

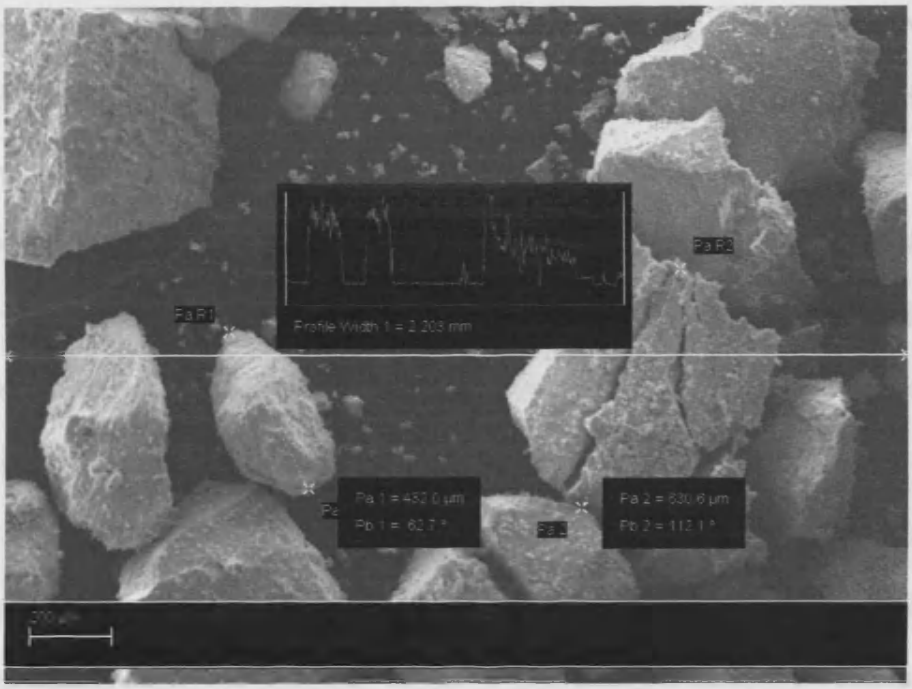

Figure 4.4 – SEM image of niobium oxide produced from the oxidation of niobium ethoxide.

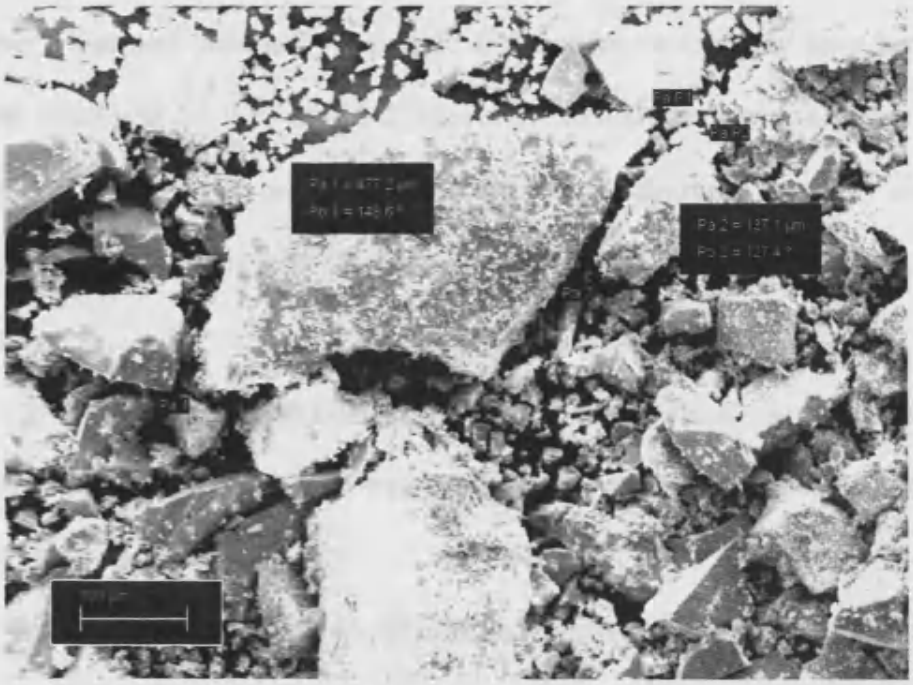

Figure 4.5 – SEM image of niobium oxide produced from the precipitation reaction of niobium chloride and urea.

Niobium oxide catalysts which were produced from precipitation reactions both decrease to <50% selectivity to formaldehyde at 340°C. Niobium oxide produced from the precipitation with sodium carbonate produced a selectivity of 48% to formaldehyde, and this selectivity was maintained up to 400°C. However, in the precipitation reaction with urea, selectivity to formaldehyde of 26% was achieved at 340°C. One would expect an increase in temperature to result in a lower selectivity, however, the selectivity to formaldehyde increased to 40% at 400°C. This was initially considered as an anomaly, the process was repeated another three times and the same result was obtained.

Niobium oxide formed from the oxidation of niobium metal also gave a similar result for selectivity to formaldehyde as the precipitation reactions discussed. This catalyst became active at 300°C. 100% formaldehyde selectivity decreased at 340°C, where 60% selectivity to formaldehyde resulted. At 400°C, 85% selectivity to formaldehyde was achieved. This, as before, was tested another three times and the same result was obtained. A possible explanation for this may have been that niobium metal was not fully oxidised. However, thermal gravimetric analysis (up to 700°C) was performed on the sample, and showed that the metal was fully oxidised at 500°C. Results for this type of niobium oxide were also repeated and an average was taken.

The selectivity to formaldehyde of niobium oxide which was purchased from Sigma-Aldrich decreased from complete selectivity to formaldehyde at 300°C to 86% at 340°C and 84% at 400°C.

It can be seen from the experimental data above that niobium oxide produced from the oxidation of niobium ethoxide has a higher conversion of methanol in comparison to niobium oxides produced by other methods. Licoccia *et al.*[19] reported

that the substitution of bulkier propoxide groups with ethoxides enhances the reaction kinetics of hydrogen abstraction from the adsorbed methoxy species, leading to faster nucleation, thus favouring the formation of nanoparticles. Niobium oxide prepared by this method produced particle dimensions of 20-50nm[14]. This is in good agreement of crystallite size calculated by XRD peak broadening. This may be another explanation for the large difference in reactivity of niobium oxides produced by different methods.

From XRD data (Figure 3.3), orthorhombic niobium oxide was produced as a result of the oxidation of niobium ethoxide. Orthorhombic niobium oxide was also produced as a result of oxidation of niobium metal and the commercial niobium oxide was in this form. Both precipitation reactions produced monoclinic niobium oxide. At 400°C, the catalyst from the precipitation with urea produced the lowest selectivity to formaldehyde, followed by the precipitation with sodium carbonate. From this data, it can be determined that orthorhombic niobium oxide maintains a higher selectivity than using monoclinic niobium oxide.

Surface areas measured by nitrogen adsorption data are all very low for all niobium oxides discussed (Table 3.2). The surface area of niobium oxide prepared by the oxidation of niobium ethoxide is the largest, having a surface area of $18m^2/g$. All other surface areas are approximately $10m^2/g$. This is likely to be part of the explanation as to why the activity of niobium oxide produced from oxidation of niobium ethoxide is more active. There must, however, be other factors which correspond to the significant increased activity of the catalyst, as the surface area is approximately doubled, while the conversion is 14 times larger.

4.3.2 Effect of Calcination Temperature.

Catalysts prepared by precipitation methods were calcined at 400°C, 500°C and 600°C and tested for methanol oxidation (Figure 4.6). Calcination temperature did not affect the phase of niobium oxide according to XRD data (Figure 3.1). Catalysts prepared by precipitation using sodium carbonate and niobium chloride were calcined at 400°C, 500°C and 600°C for 3 hours and tested for the oxidation of methanol. The highest observed activity for all catalysts was the catalyst calcined at 500°C.

The conversion under reaction conditions at 400°C was 4%, at 500°C, the conversion was 5% and at 600°C, the conversion was 4%. The selectivity to formaldehyde at 400°C was 30%, at 500°C, the conversion was 47% and at 600°C, the selectivity to formaldehyde was 46%.

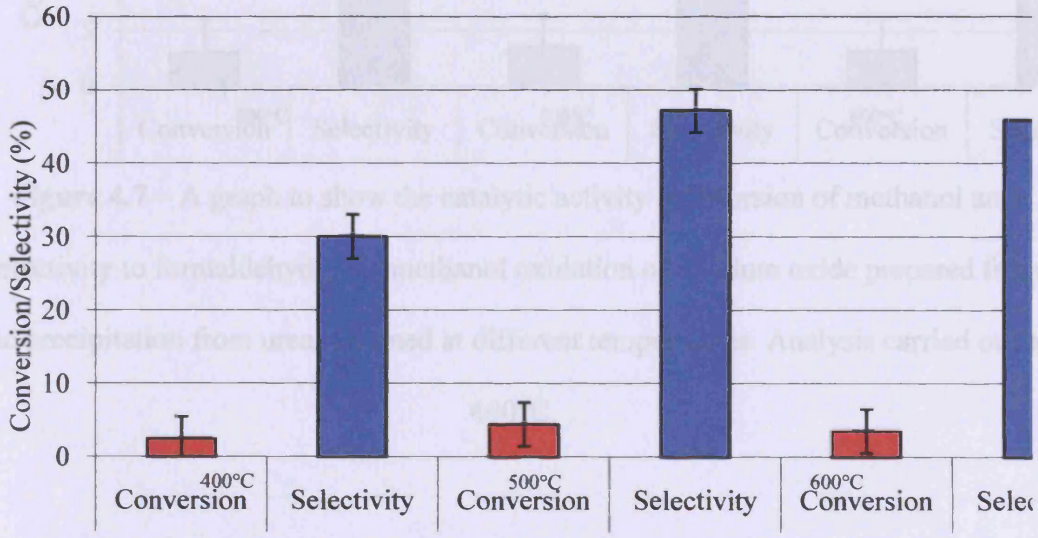

Figure 4.6 – A graph to show the catalytic activity (conversion of methanol and selectivity to formaldehyde) for methanol oxidation of niobium oxide prepared from the precipitation from sodium carbonate, calcined at different temperatures. Analysis carried out at 400°C.

The second precipitation method used was between sodium carbonate and urea. These data are shown in Figure 4.7. Conversions for catalysts calcined at all temperatures are low. The catalyst calcined at 400°C showed 3% conversion with 35% selectivity to formaldehyde. The catalyst calcined at 500°C produced 4% conversion with 39% selectivity to formaldehyde and the catalyst calcined at 600°C produced 3% conversion with 37% selectivity to formaldehyde.

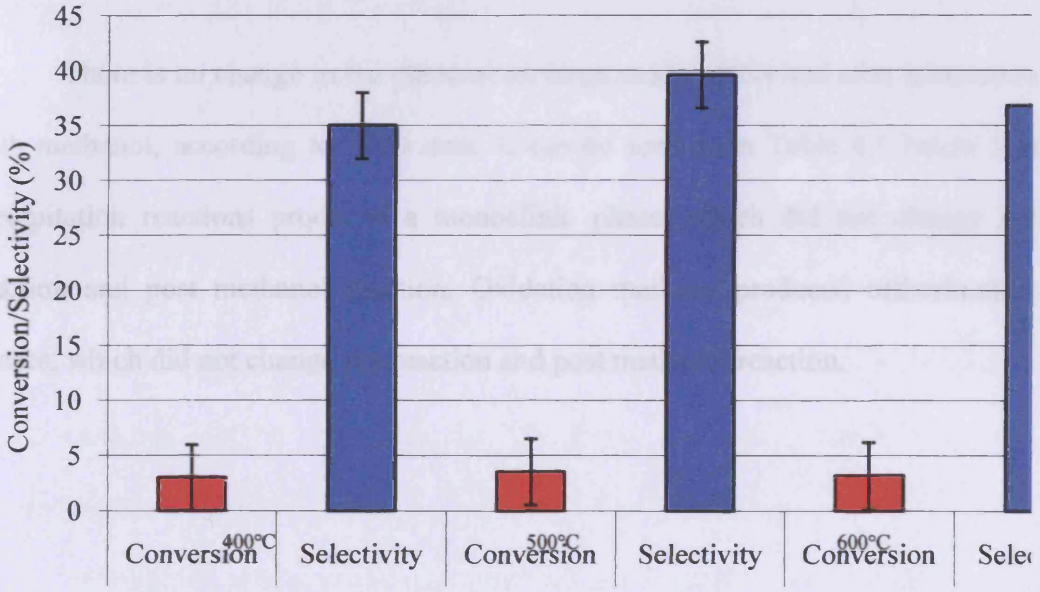

Figure 4.7 – A graph to show the catalytic activity (conversion of methanol and selectivity to formaldehyde) for methanol oxidation of niobium oxide prepared from the precipitation from urea, calcined at different temperatures. Analysis carried out at 400°C.

A possible explanation for the higher activity of the catalyst prepared from urea, calcined at 500°C compared to 400°C may be due to the crystallinity of the catalyst (evident from the XRD patterns). Amorphous and crystalline samples have different types of surface sites, which would result in differences in activity[20]. Surface areas were the same, 7-8m^2/g. As can be seen from the error bars on the

graph, both conversion of methanol and selectivity to formaldehyde are within experimental error.

4.3.3Catalysts pre-reaction compared to post-reaction.

4.3.3.1 XRD data.

There is no change in the phase of niobium oxide before and after interaction with methanol, according to XRD data. It can be seen from Table 4.1 below that precipitation reactions produced a monoclinic phase, which did not change pre reaction and post methanol reaction. Oxidation methods produced orthorhombic phases, which did not change pre reaction and post methanol reaction.

Table 4.1 – Summary of XRD data for niobium(V) oxides pre and post methanol reactor.

	Pre Reaction		Post Reaction	
Preapration Method	Phase	Space Group	Phase	Space Group
Precipitation with Na_2CO_3	Monoclinic	P_{2m}	Monoclinic	P_{2m}
Precipitation with Urea	Monoclinic	P_{2m}	Monoclinic	P_{2m}
Nb_2O_5 Purchased from Aldrich	Orthorhombic	P_{mm}	Orthorhombic	P_{mm}
Oxidation of $Nb(OEt)_5$	Orthorhombic	P_{mm}	Orthorhombic	P_{mm}
Oxidation of Nb	Orthorhombic	P_{mm}	Orthorhombic	P_{mm}

4.3.3.2 SEM.

There are no obvious differences pre-reactor and post-reactor. SEM images of all catalysts can be found on the CD ROM included. Particle sizes and morphology are similar.

All catalysts produced globular structures pre reactor. Post methanol reaction, particles appeared larger in all niobium oxide catalysts. A possible explanation for this could be attrition.

4.3.3.3 XPS data.

Niobium in all niobium oxides was present in the +5 oxidation state both pre and post reactor (from the Nb 3d spectrum). All XPS data was compared to the NIST online database[21]. Pre- reactor, peaks at binding energies of 529.7 and 530.6eV (from the O 1s spectrum) were due to the presence of oxide and OH^-. Post-reactor, peaks at

529.9 and 531.0eV were due to the presence of oxide and OH^- [Appendix A1, 3, 5, 7, 9 (a-c)].

Niobium oxide prepared from the precipitation reaction using sodium carbonate had the same peaks at 529.3 and 531.1eV (from the O 1s spectrum), due to the presence of oxide and OH^-. Additionally, this had high energy binding peaks pre-reaction due to the presence of sodium (Na-O Auger). No other Na/O peaks were observed [Appendix A1 (a-c)]. Post reaction, binding energies of 529.4 (oxide), 530.9eV (OH^- or CO_3^{2-}) and high binding energy where peaks were due to the presence of sodium. Carbonate peaks were also present in the sample. [Appendix A2, 4, 6, 8, 10 (a-c)]. Carbonates and hydroxide species are needed for the active surface.

Table 4.2 – XPS data for niobium oxides pre reaction and post reaction with methanol.

	Pre Reaction			
	Nb(V)		O	
Preparation method	Binding Energy (eV)	Assignment	Binding Energy (eV)	Assignment
Precipitation with Na_2CO_3	206.6	Nb +5	529.1, 531.1, High binding enregy peaks	Oxide, OH, Na-O auger
Precipitation with Urea	207.2	5	530.1, 531.2	Oxide, OH
Nb_2O_5 Purchased from Aldrich	206.7	5	529.7, 530.6	Oxide, OH
Oxidation of $Nb(OEt)_5$	206.8	5	529.7, 530.8	Oxide, OH
Oxidation of Nb	206.8	5	529.6, 530.5	Oxide, OH
	Post Reaction			
	Nb(V)		O	
	Binding Energy (eV)	Assignment	Binding Energy (eV)	Assignment
Precipitation with Na_2CO_3	206.4	Nb +5	529.4, 530.9, other high energy binding peaks	Oxide, OH, due to the presence of sodium
Precipitation with Urea	206.9	5	529.9, 531.1	Oxide, OH
Nb_2O_5 Purchased from Aldrich	206.6	5	529.9, 531.0	Oxide, OH
Oxidation of $Nb(OEt)_5$	206.9	5	529.9, 532.8	Oxide, SiO_2 from quartz wool
Oxidation of Nb	206.8	5	529.9, 531.0	Oxide, OH

Table 4.3 shows rate of formaldehyde production per unit area for niobium oxides tested for the partial oxidation of methanol. Surface areas and conversion of methanol are low for all catalysts, except for niobium oxide produced from the oxidation of niobium ethoxide. The surface area is approximately twice the value of the other catalyst, and the conversion is approximately 10 times as much as the other

catalysts. As a result, the rate of formaldehyde production per unit area is much greater than for other niobium oxide catalysts.

Table 4.3 – Data to show Rate of formaldehyde production/m^2 for niobium oxides. Surface area is mass normalised.

Catalyst	Surface Area (m^2)	Conversion (%)	Rate/m^2 (10^{-11}) (mol/s/m^2)
Bottle Nb_2O_5	4	5	5
Precipitation with Na_2CO_3	4	4	4
Precipitation with Urea	3.5	4	4
Oxidation of Niobium	6	4	3
Oxidation of $Nb(OEt)_5$	9	72	34

4.4 Methanol Oxidation Using Niobium Oxide Phosphate Catalysts.

4.4.1 Effect of Preparation Technique.

Two preparation techniques were used with the only difference being the type of phosphoric acid used. One method involved the refluxing of niobium chloride with ortho-phosphoric (H_3PO_4) acid and the other involved the reflux of with pyro-phosphoric acid ($H_4P_2O_7$) for 24 hours. Both produced a niobium oxide phosphate phase, α-$NbOPO_4$, according to XRD data. SEM data shows a difference in morphology, with the use of ortho-phosphoric acid producing jagged edges in the catalyst, whereas using pyro-phosphoric acid produced smooth edges in the catalyst (APPENDIX).

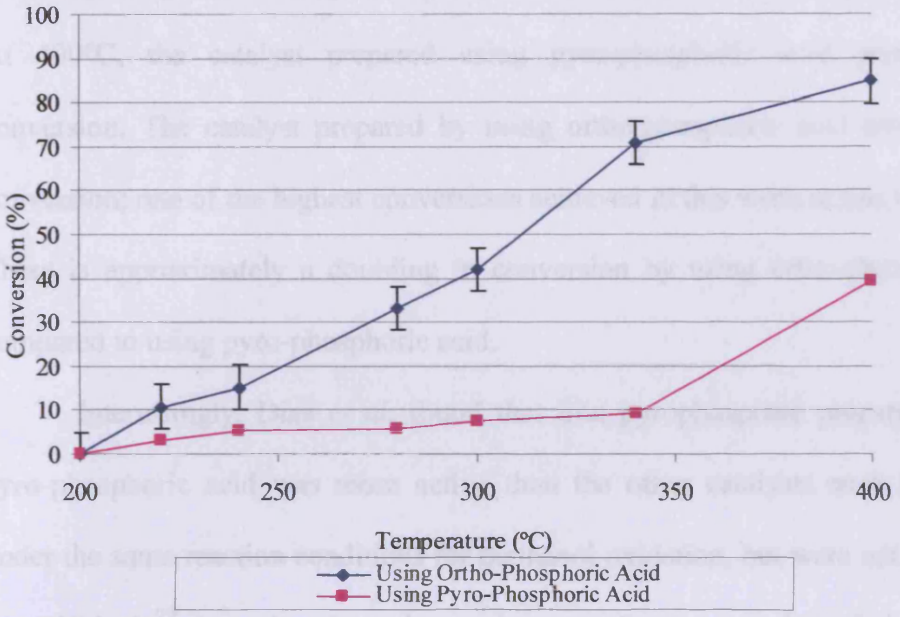

Figure 4.8 – Methanol conversion as a function of temperature using niobium oxide phosphates prepared by different methods.

Figure 4.8 above shows the conversion of methanol as a function of temperature. Although XRD data indicated no difference in the phase of the catalysts, there is a vast difference in the conversion from the two catalysts. Both catalysts become active at the same temperature, (200°C). The conversion increased using ortho-phosphoric acid almost linearly from 200°C to 400°C. At 280°C, the conversion of methanol using ortho-phosphoric acid was 33%. The surface areas of the two samples were similar (8-12m^2/g), also the Raman bands present within both samples were the same (figure 3.21 and 3.22). Although none of the samples were porous, particle sizes using otho-phosphoric acid were slightly smaller (shown on SEM images in appendix) than using pyro-phosphoric acid. Comparing this to using pyro-phosphoric acid, the conversion of methanol at the same temperature was 8%.

The morphology of the samples may have an influence on the activity of the catalyst. At 400°C, the catalyst prepared using pyro-phosphoric acid produced 39% conversion. The catalyst prepared by using ortho-phosphoric acid produced 85% conversion; one of the highest conversions achieved in this work at this temperature. There is approximately a doubling in conversion by using ortho-phosphoric acid compared to using pyro-phosphoric acid.

Interestingly, Dias *et al.* found that iron pyrophosphate prepared by using pyro-phosphoric acid was more active than the other catalysts such as platinum under the same reaction conditions for methanol oxidation, but were not selective to formaldehyde[22]. Iron phosphates have a lower surface area to that of niobium oxide phosphates with the same acid strength. Niobium oxide phosphates are more amorphous in character in comparison to iron phosphates[23]. This is unlike the work presented above. Using pyro-phosphoric acid to produce niobium oxide phosphate has approximately half of the activity compared to using ortho-phosphoric acid.

Both niobium oxide phosphate catalysts were initially entirely selective to formaldehyde when they became active at 200°C. Both catalysts began to become less selective to formaldehyde at 400°C. The catalyst produced using ortho-phosphoric acid produced 88% selectivity at 400°C, whereas the catalyst produced using pyro-phosphoric acid produced 98% selectivity to formaldehyde. Side products were CO and CO_2. There is the possibility of a second oxidation step, which would result in a lower selectivity of formaldehyde using ortho-phosphoric acid. This may result in a greater activity of the catalyst.

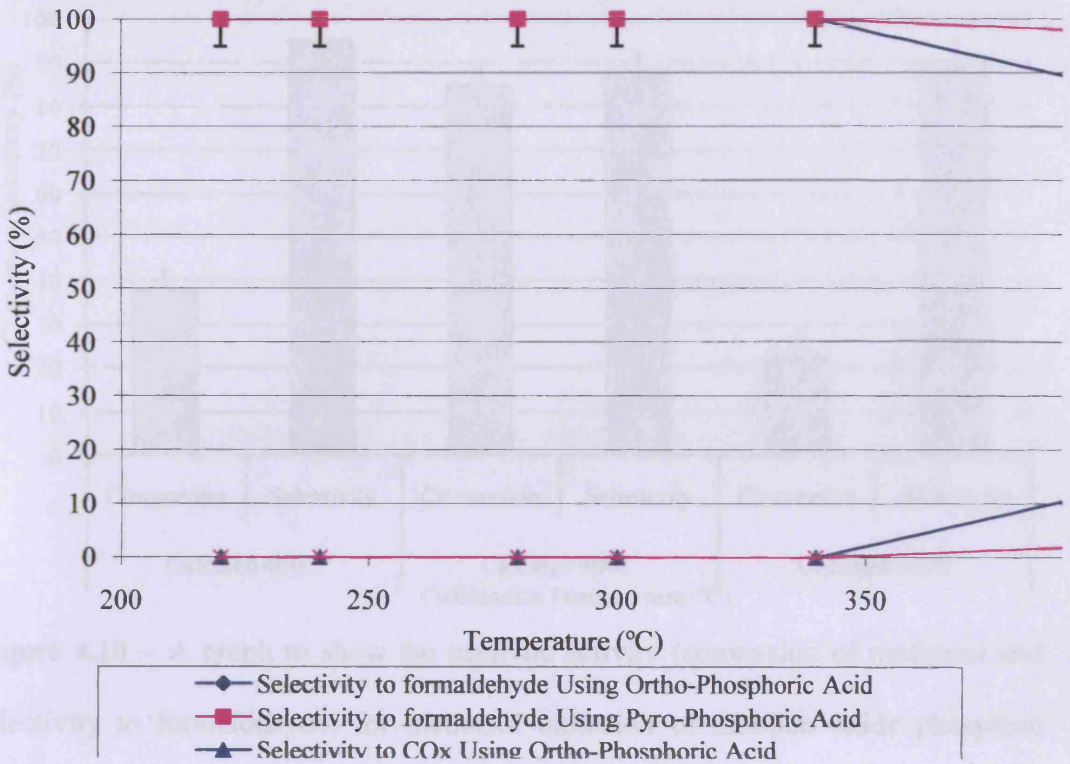

Figure 4.9 – Selectivity to products as a function of temperature using niobium oxide phosphates prepared by different methods.

4.4.2 Effect of Calcination Temperature.

Calcination temperature does not affect the bulk phase of niobium oxide phosphate, according to XRD data (figure 3.20 and 3.21). All catalysts were calcined at 400°C, 500°C and 600°C and tested for the oxidation of methanol. The highest observed conversion for $NbOPO_4$ produced from H_3PO_4 was the catalyst calcined at 500°C. However, using $H_4P_2O_7$, the highest conversion was observed at 400°C. At 500°C, the conversion decreased and then at 600°C, the conversion increased, but not to the extent with the catalyst calcined at 400°C. Selectivities for all of these catalysts remained extremely high throughout, which can be seen from the figures below.

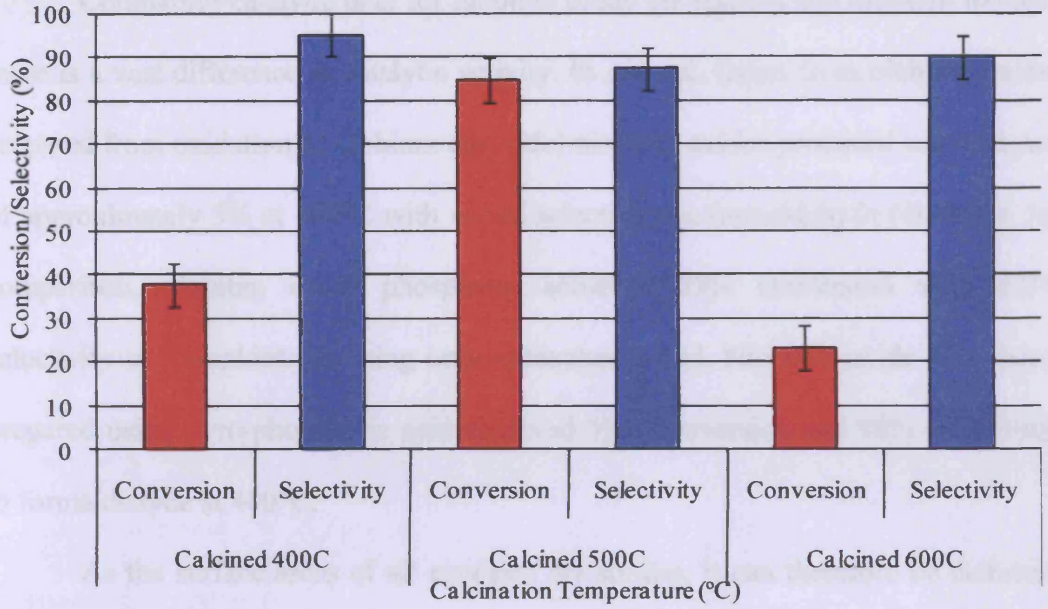

Figure 4.10 – A graph to show the catalytic activity (conversion of methanol and selectivity to formaldehyde) for methanol oxidation of niobium oxide phosphate prepared from ortho-phosphoric acid, calcined at different temperatures. Analysis carried out at 400°C.

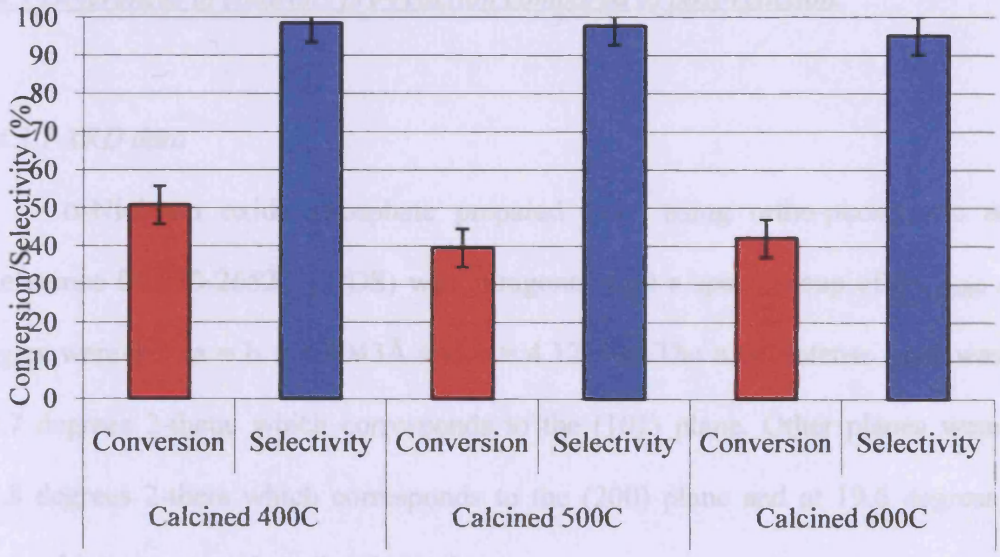

Figure 4.11 – A graph to show the catalytic activity (conversion of methanol and selectivity to formaldehyde) for methanol oxidation of niobium oxide phosphate prepared from pyro-phosphoric acid, calcined at different temperatures. Analysis carried out at 400°C.

Comparing catalytic data for niobium oxide phosphates and niobium oxides, there is a vast difference in catalytic activity. In general, (apart from niobium oxide prepared from oxidation of niobium ethoxide) niobium oxides produced conversions of approximately 5% at 400°C with varied selectivity to formaldehyde (40-85%). In comparison, niobium oxide phosphates achieved 85% conversion with 87% selectivity to formaldehyde using ortho-phosphoric acid. Niobium oxide phosphate prepared using pyro-phosphoric acid achieved 39% conversion and 98% selectivity to formaldehyde at 400°C.

As the surface areas of all catalysts are similar, it can therefore be deduced that introducing phosphorus into the catalyst enhances the catalyst and makes it more active. A possible reason as to why introducing phosphorus enhances the catalyst may be more due to phosphorus making the catalyst more acidic.

4.4.3 Differences in catalysts pre-reaction compared to post-reaction.

4.4.3.1 XRD data

α-Niobium oxide phosphate prepared from using ortho-phosphoric acid (Reference 01-070-2652, JCPDS) was tetragonal with a space group of $P4/_{nmm}$. All angles were 90°, a = b = 6.4043Å and c = 4.1217Å. The most intense peak was at 25.7 degrees 2-theta, which corresponds to the (101) plane. Other planes were at 27.8 degrees 2-theta which corresponds to the (200) plane and at 19.6 degrees 2-theta which corresponds to the (110) plane.

Post methanol reaction, the same phase of α-niobium oxide phosphate was identified (01-070-2654, JCPDS). There was a slight difference in the value of a b and c pre reactor compared to post reactor, indicating a height displacement. After

interaction with methanol, a = b = 6.4035Å and c = 4.1281Å. It can also be seen that pre-reaction, there is no peak at 35 degree 2-theta. However, post methanol-reaction, there is a small peak present in the XRD pattern.

Table 4.4 – XRD data for niobium oxide phosphate catalysts pre- and post-methanol reaction.

	Pre Reaction		Post Reaction	
Preapration Method	Phase	Space Group	Phase	Space Group
Using ortho-phosphoric acid	Tetragonal	$P4/_{nmm}$	Tetragonal	$P4/_{nmm}$
Using pyro-phosphoric acid	Tetragonal	$P4/_{n}$	Monoclinic	$P4/_{n}$

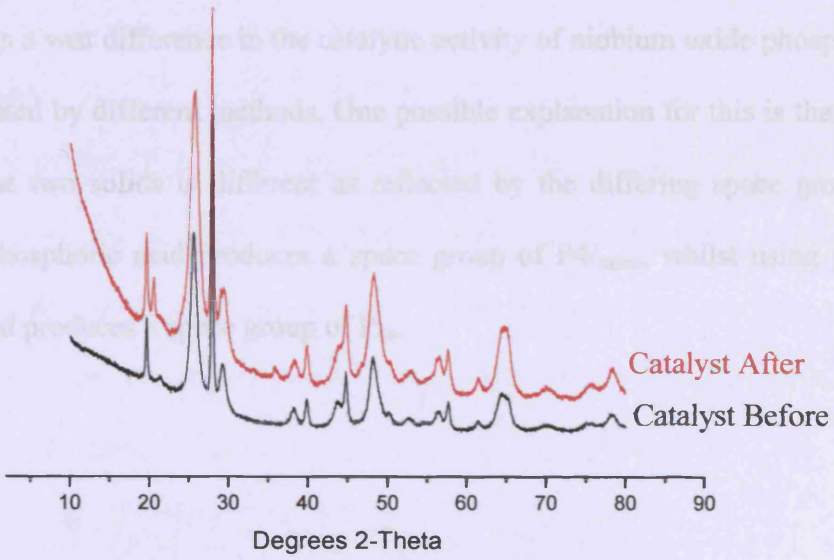

Figure 4.12 – XRD pattern of $NbOPO_4$ prepared using ortho-phosphoric acid before and after use in the methanol oxidation reactor.

α-Niobium oxide phosphate prepared from using pyro-phosphoric acid (Reference 01-073-1609, JCPDS) was tetragonal with a space group of $P4/_{n}$, with all

angles 90°, a = b = 6.3873Å and c = 4.1037Å. The most intense peak was at 25.8 degrees 2-theta, which corresponds to the (101) plane. Other planes were at 27.9 degrees 2-theta which corresponds to the (200) plane and at 19.6 degrees 2-theta which corresponds to the (110) plane.

Post methanol reactor, the same phase of niobium oxide phosphate was identified (01-070-2652, JCPDS). The space group was $P4/_{nmm}$. This is a different space group to pre reaction. There was a slight difference in the value of a b and c pre reactor compared to post reactor. After interaction with methanol, a = b = 6.4043Å and c = 4.1217Å. There is also a difference in the background of the XRD patterns before and after reaction with methanol. Pre-reaction, the background is relatively low between 10 and 20 degrees 2-theta. However, post-reaction, the background of the sample in this range is significantly increased.

There is a vast difference in the catalytic activity of niobium oxide phosphate catalysts prepared by different methods. One possible explanation for this is that the structure of the two solids is different as reflected by the differing space groups. Using ortho phosphoric acid produces a space group of $P4/_{nmm}$, whilst using pyro phosphoric acid produces a space group of P_{4n}.

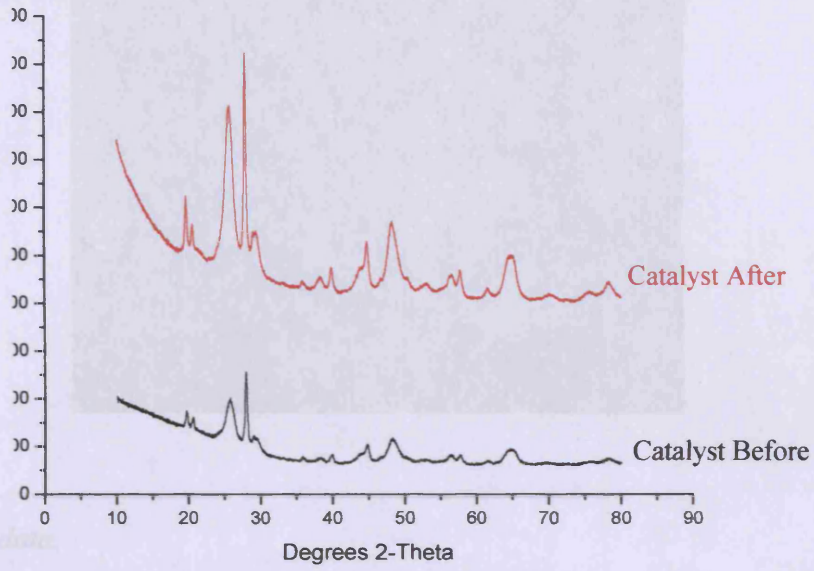

Figure 4.13 – XRD pattern of $NbOPO_4$ prepared using pyro-phosphoric acid before and after use in the methanol oxidation reactor.

4.4.3.2 SEM data.

SEM images of all catalysts can be found on the CD ROM included. The SEM image below shows niobium oxide phosphate produced using ortho phosphoric acid pre- (top) and post- (bottom) reaction. It can be seen that niobium oxide phosphate particles are larger post reaction. Also, it can be seen that there is SiO_2 wool in the sample post-reaction.

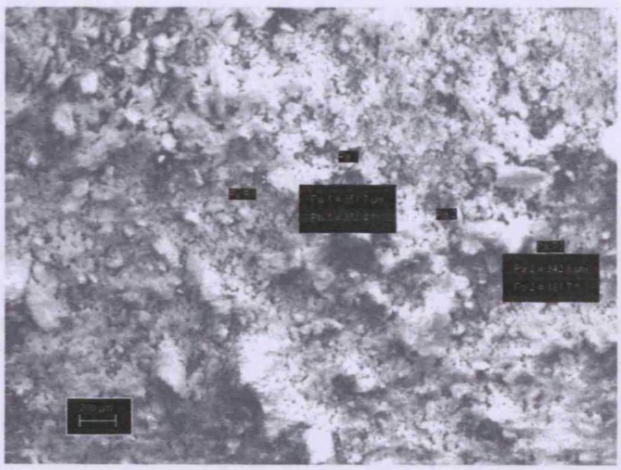

4.3.3.3 XPS data.

Niobium in niobium oxide phosphate prepared from using ortho-phosphoric acid was in a +5 oxidation state both pre-reaction and post-reaction with a binding energy of 208.0eV. Pre-reaction, a binding energy of 531.5eV (in the O 1s spectrum) was probably due to PO_x [Appendix A11 (a-c)]. Post reaction, binding energies of 531.5 and 533.2eV may be due to PO_4^- and OH^- on the surface of the catalyst. In the P 2p spectrum, a binding energy of 133.9eV was assigned to PO_x. Pre reaction, the Nb:P ratio was 1:6, whereas post reaction, the Nb:P ratio was 1:8 [Appendix A12 (a-c)].

Niobium in niobium oxide phosphate prepared from using pyro-phosphoric acid was in a +5 oxidation state both pre-reaction and post-reaction with a binding energy of 208.0eV [Appendix A13 (a-c)]. Pre-reaction, a binding energy of 531.5eV (in the O 1s spectrum) was probably due to PO_x and OH^-. Post reaction, binding energies of 531.6 and 533.1eV may be due to CO_3^{2-}, PO_4^- and OH^- on the surface of the catalyst. In the P 2p spectrum, a binding energy of 134.0eV was assigned to PO_x. Both pre reaction and post reaction, the Nb:P ratio was 1:6. [Appendix A14 (a-c)]

Table 4.4 – XPS data for niobium oxide phosphates pre and post reaction with methanol.

	Pre Reaction					
	Nb		O		P	
Preaparation method	Binding Energy (eV)	Assignment	Binding Energy (eV)	Assignment	Binding Energy (eV)	Assignment
Using H_3PO_4	208	5	531.5, 533.4	POx	133.9	POx
Using $H_4P_2O_7$	207.9	5	531.5, 533.2	CO_3^{2-}, PO_4^{3-}, OH^-	134	POx
	Post Reaction					
	Nb		O		P	
	Binding Energy (eV)	Assignment	Binding Energy (eV)	Assignment	Binding Energy (eV)	Assignment
Using H_3PO_4	208.1	5	531.5, 533.2	CO_3^{2-}, PO_4^{3-}, OH^-	134	POx
Using $H_4P_2O_7$	208	5	531.6, 533.1	CO_3^{2-}, PO_4^{3-}, OH^-	134	POx

4.5 Methanol Oxidation Using Reduced Niobium Phosphate Catalysts.

4.5.1 Effect of Preparation Techniques.

All niobium phosphate catalysts were tested for the oxidation of methanol. Unlike with niobium oxide and niobium oxide phosphate catalysts, niobium phosphate catalysts became active at different temperatures. The catalyst produced from the reduction of niobium oxide phosphate with ^{i}BuOH became active at 125°C.

The catalyst produced from the reduction of niobium oxide phosphate with 1-BuOH became active at 160°C. The catalyst produced from the reduction of niobium oxide phosphate with hydrogen became active at 200°C and $Nb_2P_4O_{15}$ became active at 240°C.

The most unstable catalyst was niobium oxide phosphate reduced with 1-butanol. This is because the conversion fluctuated quite dramatically as the temperature increased. As this was an anomaly, it was repeated twice in order to obtain reproducible results. The result was a pattern very similar to the pattern above. A possible explanation for this may be that the catalyst was re-oxidising during the reaction.

Conversion data for $Nb_2P_4O_{15}$ increased almost linearly up to 63% conversion at 400°C.

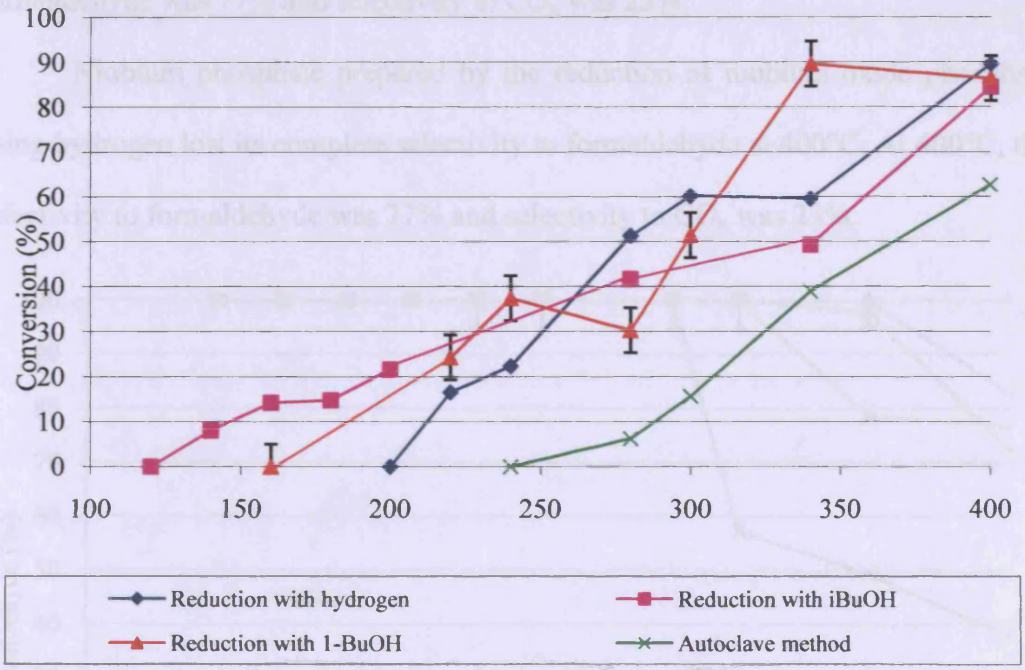

Figure 4.14 – Methanol conversion as a function of temperature using niobium phosphates prepared by different methods.

All niobium phosphate catalysts show selectivity to formaldehyde as the only product at low temperatures. Niobium phosphate, $Nb_2P_4O_{15}$, prepared using the autoclave method lost its complete selectivity to formaldehyde at 300°C and instead

produces some CO and CO_2. At 400°C, selectivity to formaldehyde using $Nb_2P_4O_{15}$ was 34%. This catalyst was 66% selective to CO and CO_2 as shown in Figure 4.14. A 1:1 ratio of CO: CO_2 was observed with all catalysts, hence this was summarised to CO_x.

Using ^{i}BuOH as the reducing agent produced a catalyst which is more selective to formaldehyde. This catalyst lost its complete selectivity to formaldehyde at 350°C. At 400°C, this catalyst was 63% selective to formaldehyde and 37% selective to CO_x. Replacing ^{i}BuOH with 1-BuOH as reductant resulted in an increased selectivity to formaldehyde at 400°C. At 400°C, selectivity to formaldehyde was 77% and selectivity to CO_x was 23%.

Niobium phosphate prepared by the reduction of niobium oxide phosphate using hydrogen lost its complete selectivity to formaldehyde at 400°C. At 400°C, the selectivity to formaldehyde was 77% and selectivity to CO_x was 23%.

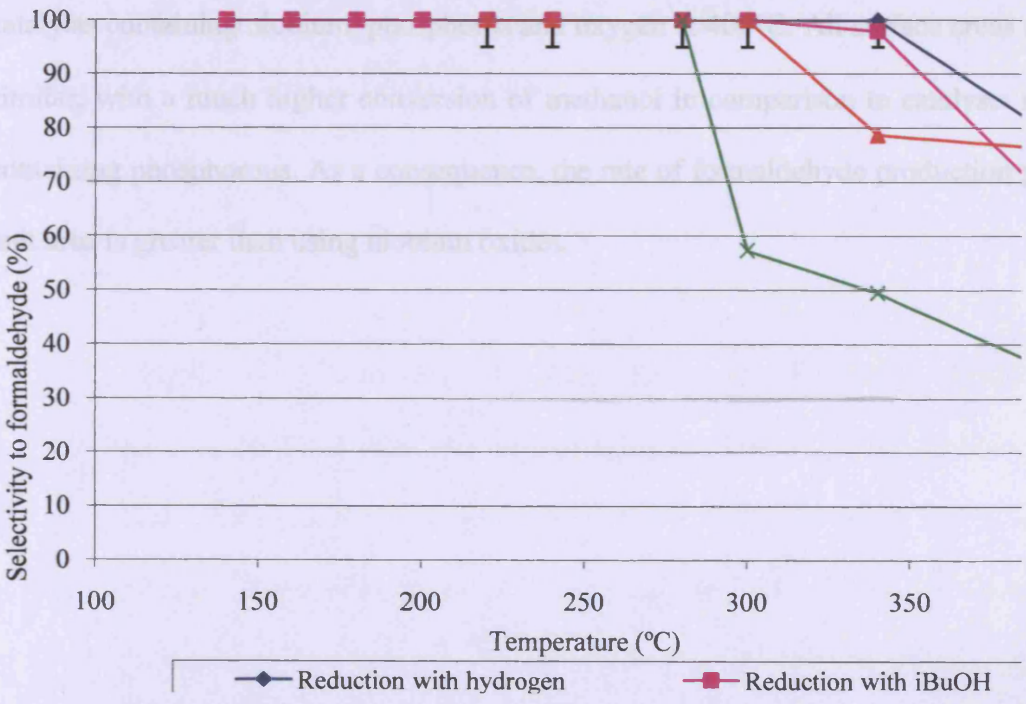

Figure 4.15 – Selectivity to formaldehyde from methanol oxidation as a function of temperature using niobium phosphates prepared by different methods.

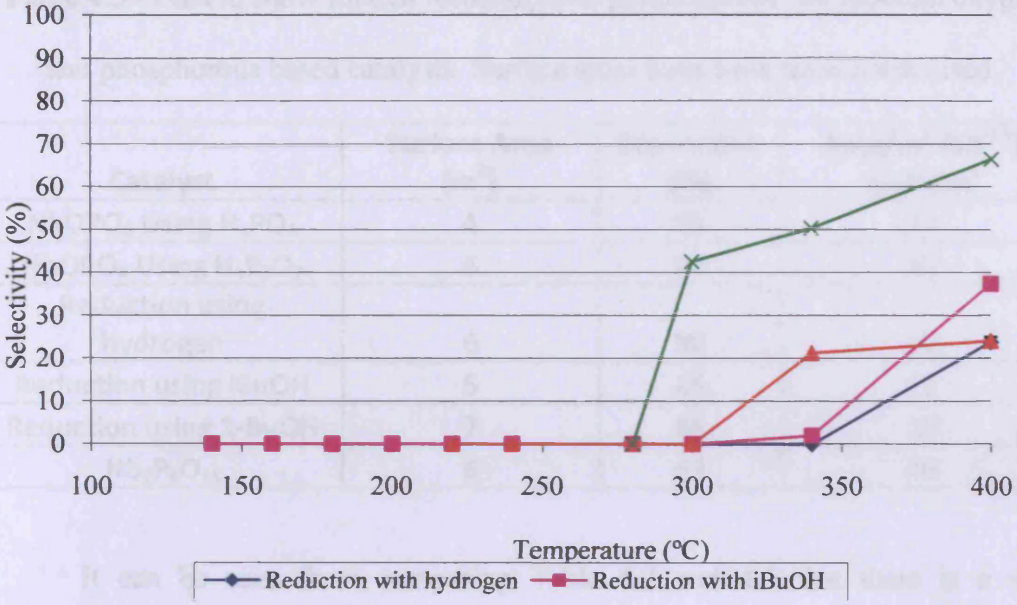

Figure 4.16 – Selectivity to combustion products from methanol oxidation as a function of temperature using niobium phosphates prepared by different methods.

Table 4.5 shows the rate of formaldehyde production per unit area for catalysts containing niobium, phosphorus and oxygen at 400°C. All surface areas are similar, with a much higher conversion of methanol in comparison to catalysts not containing phosphorous. As a consequence, the rate of formaldehyde production per unit area is greater than using niobium oxides.

Table 4.5 - Data to show Rate of formaldehyde production/m^2 for niobium oxygen and phosphorous based catalysts. Surface areas have been mass normalised.

Catalyst	Surface Area (m^2)	Conversion (%)	Rate/m^2 (10^{-11}) mol/s/m^2
$NbOPO_4$ Using H_3PO_4	4	85	97
$NbOPO_4$ Using $H_4P_2O_7$	6	40	13
Reduction using hydrogen	6	90	60
Reduction using iBuOH	5	85	75
Reduction using 1-BuOH	7	86	20
$Nb_2P_4O_{15}$	6	63	46

It can be seen from comparing Table 4.2 and 4.5 that there is a vast difference in the conversion of methanol and the resulting rate/m^2 of the catalyst. Natani *et al.* investigated the effect of adding phosphorus into a Pt/Ru catalyst and found that there was approximately a 10-fold increase in activity in adding phosphorus into the catalyst. Adding phosphorus into the catalyst increases the acidity of the catalyst. Addition of phosphorus was effective for downsizing PtRu particles and improving their catalytic activity[24].

4.5.2 Effect of Calcination Temperature.

Calcination temperature does not affect the phase of niobium phosphate formed according to XRD data. All catalysts (except for $Nb_2P_4O_{15}$ – this was prepared from a previous method) were calcined and tested at 400°C, 500°C and 600°C. The highest observed conversions for all catalysts were the catalysts calcined at 500°C. Conversions of catalysts calcined at 400°C and 600°C were lower than catalysts calcined at 500°C.

4.5.3 Differences in catalysts pre-reaction compared to post-reaction.

4.5.3.1 XRD data.

Table 4.5 – Summary of XRD data for niobium phosphates pre and post methanol reactor.

	Pre-Reaction		Post-Reaction	
Preapration Method	Phase	Space Group	Phase	Space Group
Reduction with hydrogen	Orthorhombic $NbPO_5$	P_{n*a}	Orthorhombic $Nb_{1.91}P_{2.82}O_{12}$	P_{bcn}
Reduction with iBuOH	Orthorhombic $NbPO_5$	P_{n*a}	Tetragonal $NbPO_5$	$P_{4/n}$
Reduction with 1-BuOH	Orthorhombic $NbPO_5$	P_{n*a}	Tetragonal $NbPO_6$	$P_{4/n}$
Autoclave Reaction	$Nb_2P_4O_{15}$	P_{mm}	$Nb_2P_4O_{15}$	P_{mm}

Niobium oxide phosphate reduced with hydrogen produced ε-niobium phosphate (00-040-0124, JCPDS) which is orthorhombic and is in the space group P_{n*a}. All angles were 90°, a = 8.7520Å, b = 12.0900Å and c = 8.6740Å. The most intense peak was at 20.5 degrees 2-theta and corresponds to the (121) plane. Other peaks were 35.8 degrees 2-theta which corresponds to the (123) plane and another at 36.1 degrees 2-theta, which corresponds to the (240) plane.

Post- reactor, the catalyst changed phase. The new phase of the catalyst was $Nb_{1.91}P_{2.82}O_{12}$ (00-051-1738, JCPDS). The ratios of Nb:P:O changed pre-reaction compared to post-reaction. This was orthorhombic with a space group of P_{bcn}. All angles were 90° and a = 12.0819Å, b = 806848Å and c = 8.7452Å. The most intense peak was at 20.6 degrees 2-theta, which corresponds to the (211) plane. Other peaks were 20.4 degrees 2-theta which corresponds to the (020) plane and another at 29.0 degrees 2-theta, which corresponds to the (022) plane.

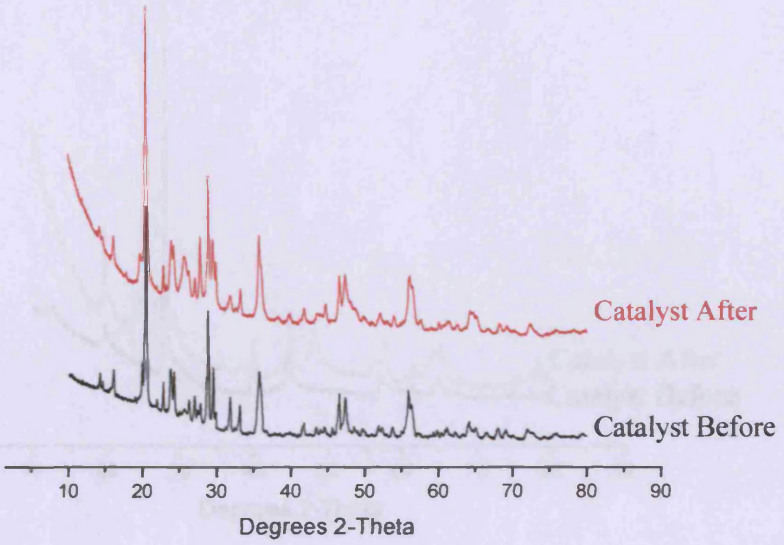

Figure 4.17 – XRD Pattern of $NbPO_5$ produced from the reduction of $NbOPO_4$ with H_2 Before and after use in the methanol oxidation reactor.

Niobium oxide phosphate reduced with ^{i}BuOH produced niobium phosphate hydrate (00-037-0377, JCPDS). This was orthorhombic with all angles at 90° and a = 6.2600Å, b = 6.4700Å and c = 6.1900Å. The most intense peak was at 14.4 degrees 2-theta which corresponds to the (001) plane. Other peaks at 27.6 and 28.6 degrees 2-theta, which correspond to the (020) and (002) planes respectively.

Post-reaction, niobium phosphate is formed (01-070-2650, JCPDS). The old phase is still present in addition to the new phase. This was tetragonal with a space group of $P_{4/n}$. All angles were 90°, with a = b = 6.4038Å, and c=4.1056Å. New peaks were present in the post-reactor catalyst. The peaks were present at 22, 27 46 and 77 degrees 2-theta. The most intense peak was at 25.7 degrees 2-theta which corresponds to the (101) plane. Other peaks at 27.8 and 19.6 degrees 2-theta correspond to the (200) and (110) planes respectively.

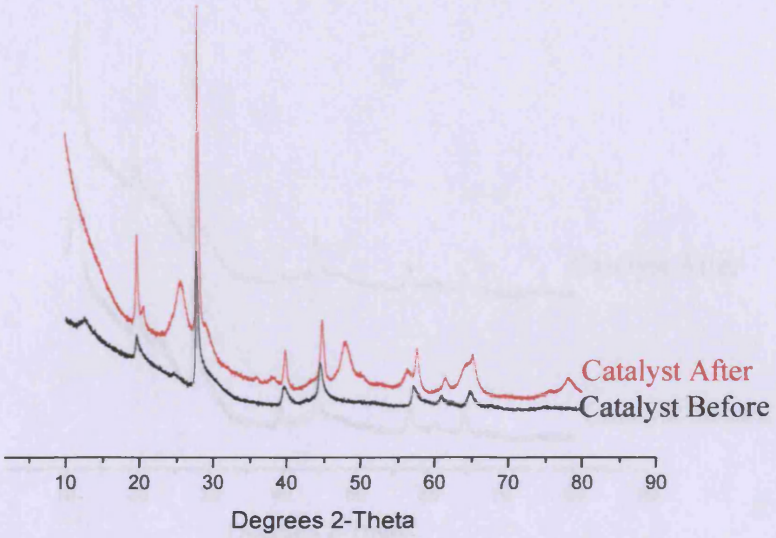

Figure 4.18 – XRD Pattern of $NbPO_5$ produced from the reduction of $NbOPO_4$ with $^{i}BuOH$ before and after use in the methanol oxidation reactor.

Niobium oxide phosphate reduced with 1-BuOH produced niobium phosphate hydrate (00-037-0377, JCPDS). This was orthorhombic with all angles at 90° and a = 6.26Å, b = 6.47Å and c = 6.19Å. The most intense peak was at 14.4 degrees 2-theta corresponding to the (001) plane. Other peaks at 27.6 and 28.6 degrees 2-theta correspond to the (020) and (002) planes respectively.

Post-reaction, niobium oxide phosphate is formed (01-070-2650, JCPDS). This was tetragonal with a space group of $P_{4/n}$. All angles were 90°, with a = b = 6.4038Å. The most intense peak at 25.7 degrees 2-theta corresponds to the 101 plane. Other peaks at 27.8 and 19.6 degrees 2-theta correspond to the 200 and 110 planes respectively.

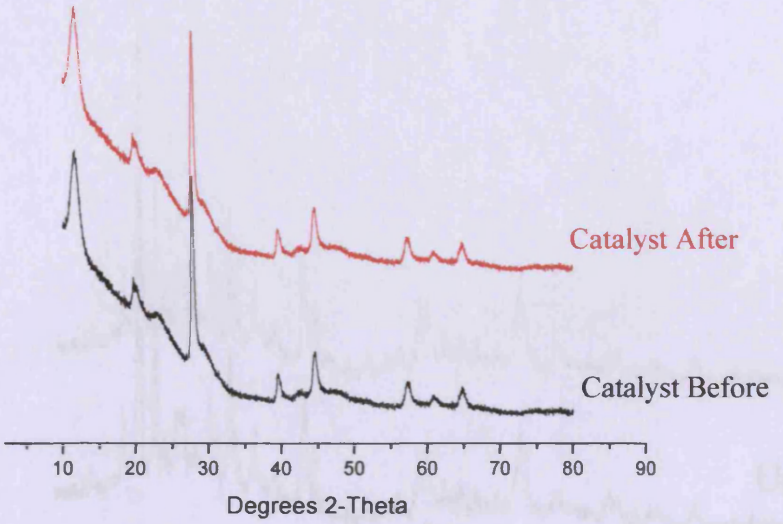

Figure 4.19 – XRD Pattern of $NbPO_5$ produced from the reduction of $NbOPO_4$ with 1-BuOH before and after use in the methanol oxidation reactor.

Niobium phosphate, $Nb_2P_4O_{15}$ (00-028-0715, JCPDS), was cubic pre-reaction and post-reaction. All angles were 90°, a = b = c = 8.0660Å. The most intense peak was at 22 degrees 2-theta corresponds to the (200) plane. Other peaks were 36.9 degrees 2-theta which corresponds to the (311) plane and another at 31.4 degrees 2-theta, which corresponds to the (220) plane.

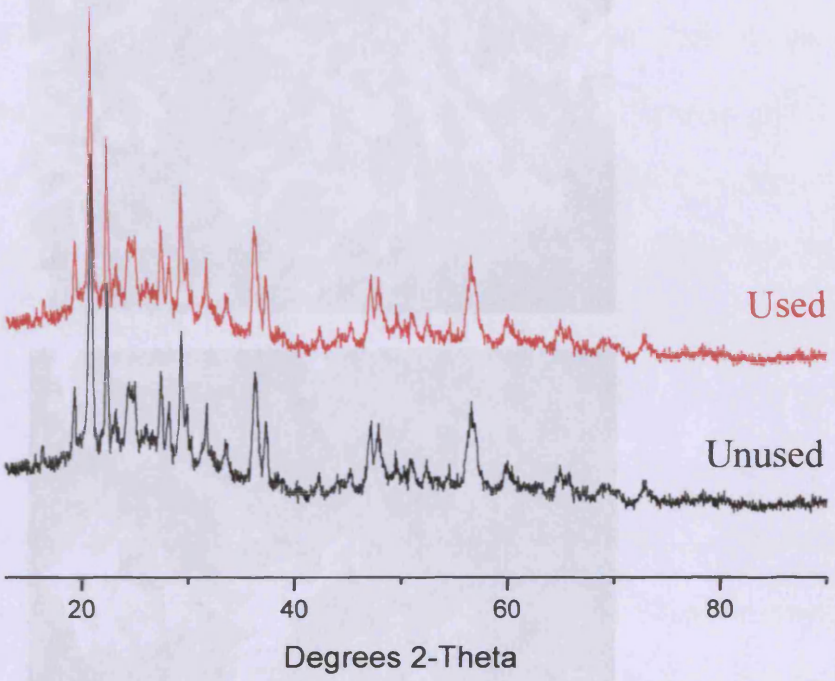

Figure 4.20 – XRD Pattern of $Nb_2P_4O_{15}$ before and after reaction in the methanol oxidation reactor.

4.5.3.2 SEM data.

SEM images of all catalysts can be found on the CD ROM included. The SEM images below show niobium phosphate prepared from the reduction of niobium oxide phosphate with hydrogen. Pre-reactor (top), the catalyst is in a layered structure, whereas post-reaction (bottom), the catalyst is in more of a globular structure. It appears globular structures are less active than layered structures.

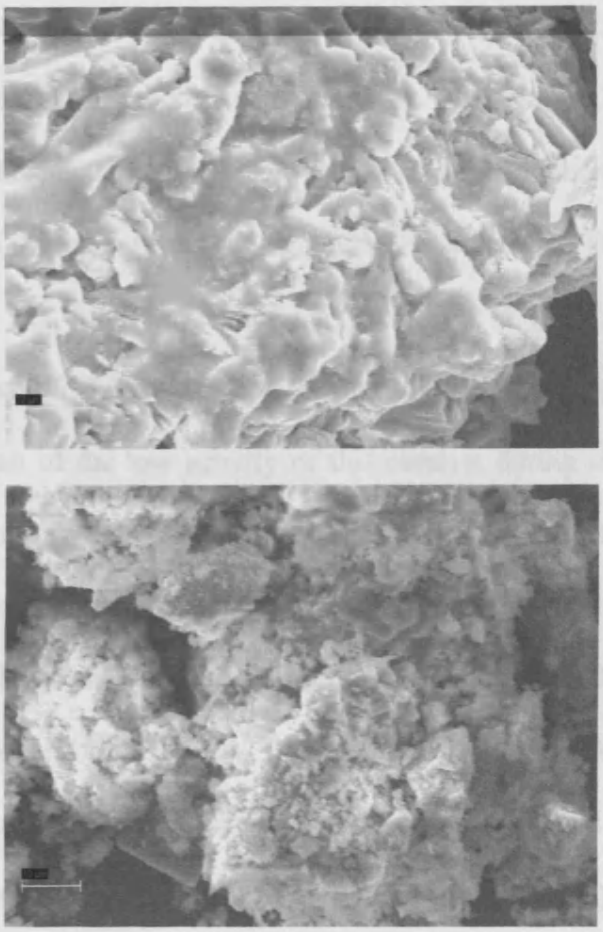

4.5.3.3 XPS data.

Niobium in all niobium phosphates was in the +5 oxidation state, both pre and post reactor. Pre-reactor, niobium phosphate prepared from the reduction using ^{i}BuOH had binding energies of 531.5eV (in the O 1s spectrum), which could be due to CO_3^{2-}, PO_4^{3-} and OH^- species. In the P 2p spectrum, a binding energy of 133.8eV was assigned to PO_x [Appendix A15 (a-c)]. Post-reaction, the presence of a peak at 533.3eV was due to impurities in the sample, such as SiO_2. This may be a possible explanation of the low activity of this catalyst during methanol oxidation. Contamination of the sample decreases the activity of the catalyst. In the P 2p spectrum, a binding energy of 134.5eV was assigned to PO_x, P_2O_5 and PO(OH). The

Nb:P ratio pre-reaction was 1:7, compared to post-reaction of 1:5. The catalyst had lost phosphorus through the reaction with methanol. [Appendix A16 (a-c)]

Niobium phosphate prepared from the reduction of niobium oxide phosphate using 1-BuOH had the same peaks at 531.5 and 532.9eV (in the O 1s spectrum), due to the presence of PO_4^{3-} and OH^- species [Appendix A17 (a-c)]. Post reaction, the presence of a peak at 533.3eV was due to impurities in the sample. This may be a possible explanation of the low activity of this catalyst during methanol oxidation. Contamination of the sample decreases the activity of the catalyst. The Nb:P ratio pre-reaction was 1:6, compared to post-reaction of 1:6. [Appendix A18 (a-c)]

Niobium phosphate prepared from an autoclave-type method, i.e. $Nb_2P_4O_{15}$, showed binding energies of 531.41eV, due to CO_3^{2-}, PO_4^{3-} and OH^- binding energy. In the P 2p spectrum, a binding energy of 133.7eV was assigned to PO_x [Appendix A19 (a-c)]. Post reactor, a peak at 531.8eV (in the O 1s spectrum) was due to CO_3^{2-}, PO_4^{3-} and OH^- binding. A peak at 532.8eV was due to SiO_2 contamination. In the P 2p spectrum, a binding energy of 133.8eV was assigned to PO_x. The Nb:P ratio pre reaction was 1:9, compared to post reaction of 1:9. [Appendix A20 (a-c)].

Niobium phosphate prepared from the reduction of niobium oxide phosphate using hydrogen had a peak at 208.2eV, responsible for niobium in the +5 oxidation state as with all the other catalysts. However, there is another peak at 209.4eV (in the O 1s spectrum), this is due to niobium being in a highly electron withdrawing environment. This could be a possible explanation for niobium phosphate prepared from the reduction of niobium oxide phosphate using hydrogen being a better catalyst than other catalysts [Appendix A21 (a-c)]. These peaks occur both pre-reaction and post-reaction. In the P 2p spectrum, a binding energy of 134.0eV was

assigned to PO_x. The Nb:P ratio pre reaction was 1:20, compared to post reaction of 1:10. [Appendix A22 (a-c)]

Table 4.6 – XPS data for niobium phosphates prepared by different methods.

	Pre Reaction			
	Nb(V)		O	
Preaparation method	Binding Energy (eV)	Assignment	Binding Energy (eV)	Assignment
Reduction with hydrogen	206.6	5	529.1, 531.1, High binding enregy peaks	Oxide, OH^-, Na-O Auger
Reduction with iBuOH	207.2	5	531.5	PO_x, P_2O_5, PO(OH)
Reduction with 1-BuOH	206.7	5	531.5, 532.9	PO_4^{3-}, OH^-
$Nb_2P_4O_{15}$	206.8	5	531.4, 531.8	CO_3^{2-}, PO_4^{3-}, OH^-
	Post Reaction			
	Nb(V)		O	
	Binding Energy (eV)	Assignment	Binding Energy (eV)	Assignment
Reduction with hydrogen	206.4	5	529.4, 530.9, other high energy binding peaks	Oxide, OH^-, due to the presence of sodium
Reduction with iBuOH	206.9	5	531.5	POx, P_2O_5, PO(OH)
Reduction with 1-BuOH	206.6	5	531.5, 532.9	$PO4^{3-}$, OH^-
$Nb_2P_4O_{15}$	206.9	5	531.4, 531.8	CO_3^{2-}, PO_4^{3-}, OH^-, SiO_2 contamination

4.6 Time On-Line Studies.

Niobium phosphate which was prepared from the reduction of niobium oxide phosphate was tested for stability with time on-line studies, as shown in Figure 4.21. it can be seen that there is a slight decrease in conversion over 50 hours, however after 50 hours, the conversion was >70%. Research was carried out using V-Mg-O catalysts for prolonged run experiments[25] for methanol oxidation. It was found that

over 60 hours, of operation in the methanol reactor, the average formaldehyde yield was approximately 90% and the selectivity to formaldehyde was 97%.

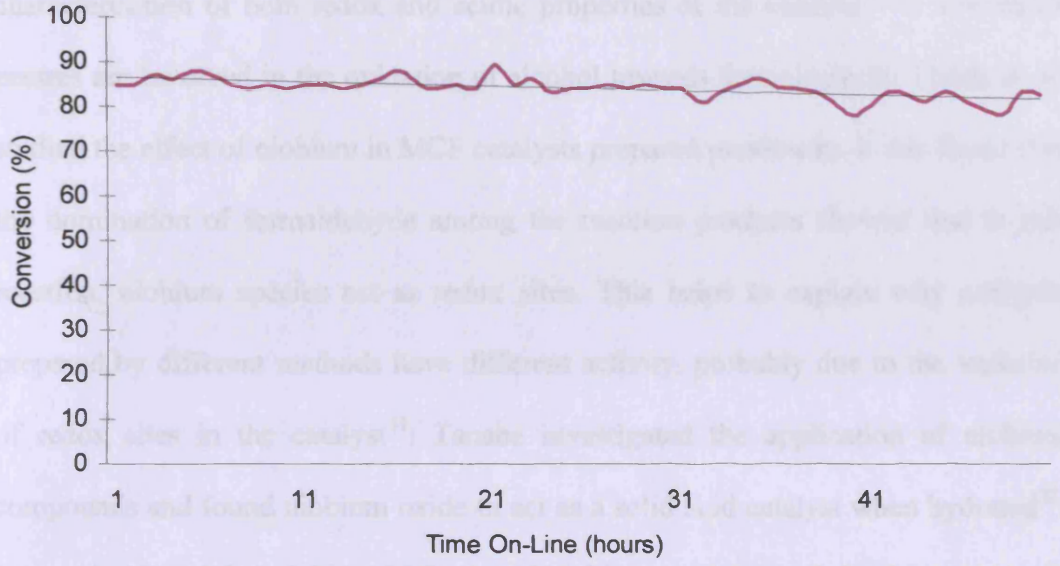

Figure 4.21 – Time on-line data showing methanol conversion as a function of time using niobium phosphate prepared using the reduction of niobium oxide phosphate with hydrogen.

The addition of another element, such as P, in niobium phosphate structures, has led to a remarkable increase in both conversion and selectivity to formaldehyde. The explanation for the observed promoter effect of phosphorus in this reaction is not straightforward. The addition of P modifies both the acidic and the redox characteristics of the niobium oxide. For example, niobium (V) oxides have an acid strength ($H_0 \leq -5.6$), whereas niobium phosphate has a higher acid strength of $H_0 \leq -8.2$ [26 27]. In particular, the acidity of the support used to produce supported vanadium oxide catalysts is an important factor for the selective oxidation of methanol to

formaldehyde, as increased acidity was beneficial for formaldehyde production in terms of selectivity[28].

The use of the methanol oxidation process is a good choice for the characterisation of both redox and acidic properties of the catalyst[29 30]. The redox centres are involved in the oxidation of alcohol towards formaldehyde. Trejda *et al.* studied the effect of niobium in MCF catalysts prepared previously. It was found that the domination of formaldehyde among the reaction products showed that in this reaction, niobium species act as redox sites. This helps to explain why catalysts prepared by different methods have different activity, probably due to the variation of redox sites in the catalyst[31]. Tanabe investigated the application of niobium compounds and found niobium oxide to act as a solid acid catalyst when hydrated[32]. It was also found that niobic acid (hydrated niobium oxide) containing large amounts of water exhibited high catalytic performances for acid catalysed reactions in which water molecules participate or are liberated. It would be expected that dimethyl ether (DME) would be produced at low temperatures. However, with the catalysts that were tested, no DME was observed.

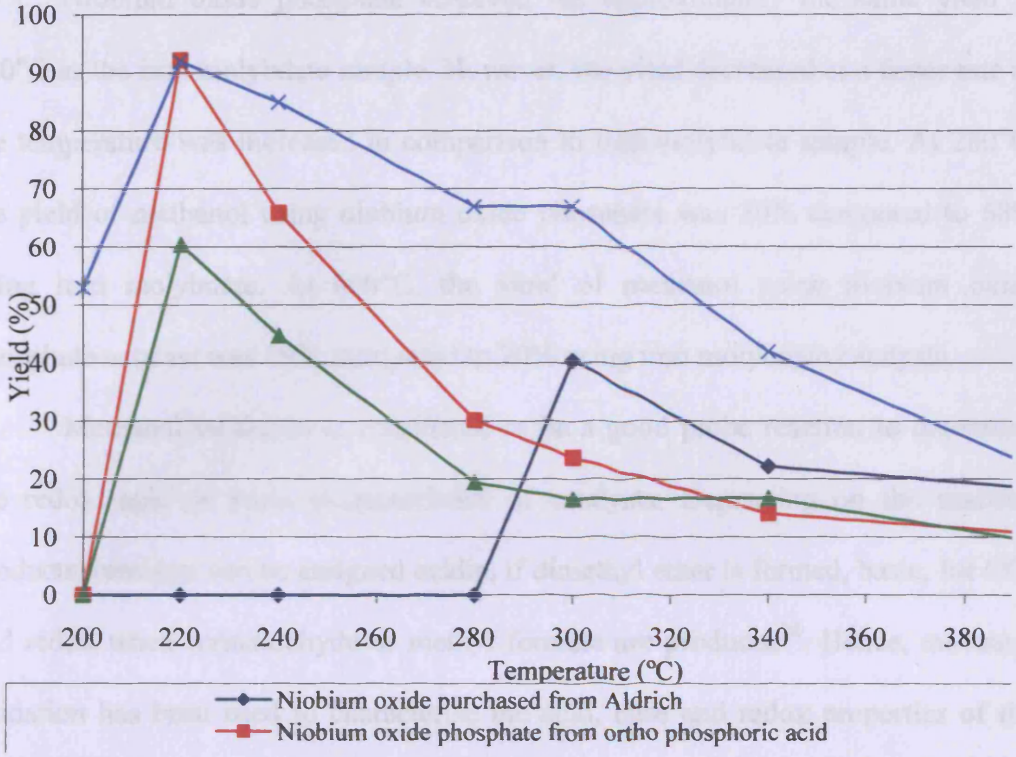

Figure 4.22 – A graph to show yield as a function of temperature using niobium oxide, niobium oxide phosphate and niobium phosphate prepared from the reduction of niobium oxide phosphate using hydrogen. These are all compared to an iron molybdate catalyst.

Figure 4.22 shows a yield graph for niobium catalysts, this is compared to an iron molybdate catalyst. It can be seen from figure 4.22 that the yield of methanol with the iron molybdate[33] is higher than with all of the niobium catalysts shown. It can clearly be seen from the graph that niobium oxides do not become active until >250°C. At 300°C, the yield reached 40%. An increase in temperature decreased the yield to 18% at 400°C.

Niobium phosphate prepared from the reduction of niobium oxide phosphate with hydrogen became active at 220°C. A 60% yield was achieved at 220°C. The yield then decreased to 20% at 280°C and then <10% at 400°C.

Niobium oxide phosphate achieved the approximately the same yield at 220°C as the iron molybdate sample. However, the yield decreased at a faster rate as the temperature was increased in comparison to iron molybdate sample. At 280°C, the yield of methanol using niobium oxide phosphate was 30% compared to 68% using iron molybdate. At 400°C, the yield of methanol using niobium oxide phosphate catalyst was 10%, compared to 20% using iron molybdate catalysts.

Methanol oxidation is considered to be a good probe reaction to determine the redox, acid or basic characteristics of catalysts. Depending on the reaction products, catalysts can be assigned acidic, if dimethyl ether is formed, basic, for CO_2 and redox when formaldehyde or methyl formate are produced[34]. Hence, methanol oxidation has been used to characterise the acid, base and redox properties of the niobium phosphate catalysts.

Iron molybdates are more effective catalysts in the oxidation of methanol to formaldehyde at higher temperatures due to iron molybdate catalysts being more selective than niobium based catalysts.

The addition of another element, such as P, in niobium phosphate structures, has led to a remarkable increase in both conversion and selectivity to formaldehyde. The explanation for the observed promoter effect of phosphorous in this reaction is not straightforward. The addition of P modifies both the acidic and the redox characteristics of the niobium oxide. For example, niobium (V) oxides have an acid strength ($H_0 \leq -5.6$), whereas niobium phosphate has a higher acid strength of $H_0 \leq -8.2$ [35 36]. In particular, the acidity of the support used to produce supported vanadium oxide catalysts is an important factor for the selective oxidation of methanol to formaldehyde, as increased acidity was beneficial for formaldehyde production[37].

The increased acidity on the addition of P has an influence on activity, but modification of the redox properties of the catalyst is a more important factor.

4.7 Conclusions.

It was observed that there was high selectivity to formaldehyde (reaction product associated to the presence of redox sites) obtained for all the catalysts. It was especially high for $NbPO_5$ prepared from the reduction using hydrogen and $NbOPO_4$ prepared using ortho-phosphoric acid.

Niobium oxides in general have a low activity for the partial oxidation of methanol to formaldehyde. All catalysts, except for one niobium oxide have low conversion of methanol. Niobium oxide prepared from the oxidation of niobium ethoxide produced a high conversion of methanol.

Adding phosphorus into the catalyst greatly enhanced the activity of the catalyst. The most active catalysts were niobium oxide phosphate produced using ortho-phosphoric acid, and the reduction of this catalyst with hydrogen. Other catalysts were less active, but it is evident that addition of phosphorus increases the activity of the catalyst.

References.

[1] Liberti, G.; Pernicone, N.; Soattini, S.; *Journal of Catalysis*, **1972**, 27, 52.

[2] Trifiro, F.; *Catalysis Today*, **1998**, 41, 21.

[3] Twigg, M. V.; *Catalysis Handbook 2nd Ed.; Wolfe Publishing*, **1989**.

[4] Ohno, Y., Inoue, N., Ogawa, T., Ono, M., Shikada, T., Hayashi, H.; *NKK Technical review No. 85*, **2001**.

[5] Weast, R. C.; *Handbook of Chemistry and Physics, 55th Edition, CRC Press*, **1974**.

[6] Walker, J. F. *Formaldehyde*, 3rd Ed.; Reinhold, **1964.**

[7] Butlerov, A. *Ann.*, **1959**, *111*, 242.

[8] Von Hoffman, A. W. *Ann.* **1868**, *145*, 357.

[9] Pernicone, N., *Journal of Less Common Metals*, **1974**, *36*, 289.

[10] Bowker, M., Holroyd, R., Elliott, A., Morrall, P., Alouche, A., Entwistle, C., Toerncrona, A., *Cat. Letters* **2002**, 83, 3-4.

[11] van Krevelen, Mars.; *Spec. Suppl. Chem. Eng Sci.*, 3 **1954**, 41.

[12] House, M. P., Carley, A. F., Bowker, M., *Journal of Catalysis*, 252, **2007**, 88-96.

[13] Carlinesy, R.; *Electrochemistry Communications*, 7, 12, **2005**, 1190-1194.

[14] Ubago-Perez, R., Carrasco-Marin, F., Morena-Castilla, C.; *Catalysis Today*, 123, **2007**, 158-163.

[15] Islam, M., Basnayake, R., Korzeniewski, C.; *Journal of Electroanalytical Chemistry*, 599(1), **2007**, 31-40.

[16] Wang, Q., Madix, R. J., *Surface Science*, 496, **2002**, 51-63.

[17] Deshmukh, S. A. R. K., van Sint Annaland, M., Kuipers, J. A. M., *Appl. Cat. A*, 289, **2005**, 240-255.

[18] Broqvist, P., Molina, L. M., Grönbeck, H., Hammer, B.; *Journal of Catalysis*, 227(1), **2004**, 217-226.

[19] Lioccia, S.; *Journal of Nanoscience and Nanotechnology*, **2005**, 5, 292-295.

[20] http://ecsmeet2.peerx-press.org/ms_files

[21] http://srdata.nist.gov/gateway

[22] Dias, A. P. S.; *Appl. Catal A: Gen* **2008**, doi:10.1016/j.apcata.2008.04.040.

[23] Srilakshmi, C., Lingaiah, N., Nagaraju, P., Prasad, P. S. S., Kalevaru, V., Martin, A, d.o.i. 10.1016/j.apcata.2006.05.005.

[24] Natani, H., Nakagawa, T., Daimon, H., Kurobe, Y., Ono, T., Honda, Y., Koizumi, A., Senio, S., Yamamoto, T. A., *Appl. Catal. A*, 326(2), **2007**, 194-201.

[25] Isaguliants, G. V., Belomestnykh, I. P., *Catalysis Today*, 100, **2005**, 441-445.

[26] I.E. Wachs, I.E. Briand, J.M. Jehng, L. Burcham, X. Gao, *Catal. Today*, 57, **2000**, 323.

[27] H.H. Kung, M.C. Kung, *Appl. Catal. A: General*, 157, **1997**, 105.

[28] T. Blasco, J.M. López Nieto, *Appl. Catal. A: General*, 157, **1997**, 117.

[29] Tatibouet, J. M., *Appl. Catal. A Gen* 148, **1997**, 219.

[30] Gao, X., Wachs, I. E., Wong, M. S., Ying, J. Y., *J. Catal*, 203, **2001**, 18.

[31] Trajeda, M.; *Catal. Today*, **2008**, doi, 10.1016/j.cattod.2008.04.006.

[32] Tanabe, K.; *Catalysis Today*, 78, **2003**, 65-77.

[33] House, M. P., Carley, A. F., Echeverria, R., Bowker, M., *J. Phys. Chem. C*, **2008** 112, 4333-4341.

[34] M. Badlani, I.E. Wachs, *Catalysis Letters*, 75, **2001**, 137.

[35] I.E. Wachs, I.E. Briand, J.M. Jehng, L. Burcham, X. Gao, *Catal. Today*, 57 **2000**, 323.

[36] H.H. Kung, M.C. Kung, *Appl. Catal. A*: General 157, **1997**, 105.

[37] T. Blasco, J.M. López Nieto, *Appl. Catal. A*: General, 157 **1997**, 117.

5. Propane Oxidative Dehydrogenation.

5.1 Introduction to Propane Oxidative Dehydrogenation.

Oxidative dehydrogenation reactions provide an alternative route than steam cracking for the production of alkenes[1]. The oxidative dehydrogenation of lower alkanes is believed to proceed via a Mars van Krevelen redox mechanism on metal oxide surfaces. The catalyst surface is reduced due to surface oxygen atoms abstracting hydrogen from the alkane, forming olefins and water. Gas phase oxygen then adsorbs on to the surface and undergoes a series of electron transfer processes before being incorporated back into the lattice, restoring the working oxidation state of the catalyst. When in equilibrium with the gas phase, the surface is populated with a number of short lived oxygen species. Oxygen facilitates the conversion into water and shifts the equilibrium towards the products[2].

$$C_3H_8 + \tfrac{1}{2} O_2 \rightarrow C_3H_6 + H_2O$$

Intense research has taken place in the last 20 years in an attempt to develop catalysts for the oxidative dehydrogenation of propane due to the following reason[3]:

- In steam cracking, ethylene is the preferred product, but the demand for propylene is growing faster than for ethylene[4].

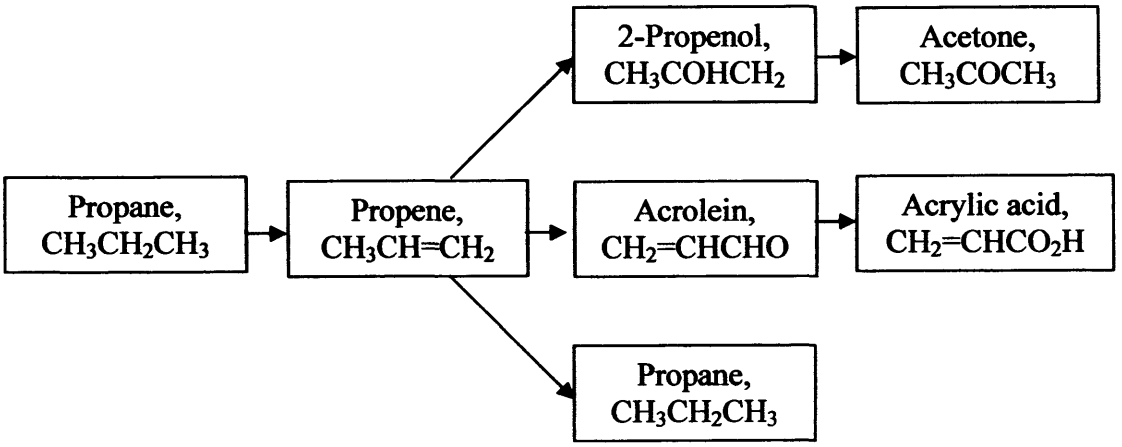

Figure 5.1 – Oxygenated products of propane[5].

Propene is formed from the oxidative dehydrogenation of propane. CO_x is formed from the direct combustion of propane and/or the total oxidation of propene. Figure 5.2 illustrates this.

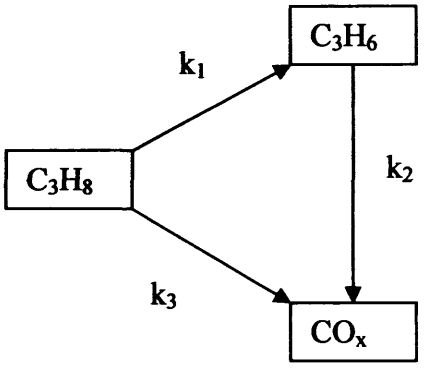

Figure 5.2 – Reaction scheme for the oxidative dehydrogenation of propane.

For a selective oxidation reaction, the k_3/k_1 ratio is low. In general, with increasing conversion, the selectivity of the alkene decreases. Weak allylic bonds in alkenes bind more strongly to the metal oxide surface and as a result, are susceptible to further oxidation[6].

Propane oxidative dehydrogenation involves redox cycles, where the organic molecule is oxidised by lattice oxygen resulting in a reduced centre which is then re-oxidised[7-10], [8910]i.e. the Mars van Krevelen mechanism. When in equilibrium with the gas phase, the surface is populated by short lived oxygen species capable of breaking the methylene C-H bond in the propane molecule[8]. A second hydrogen abstraction then takes place before desorption of the propene molecule and re-oxidation of the catalyst.

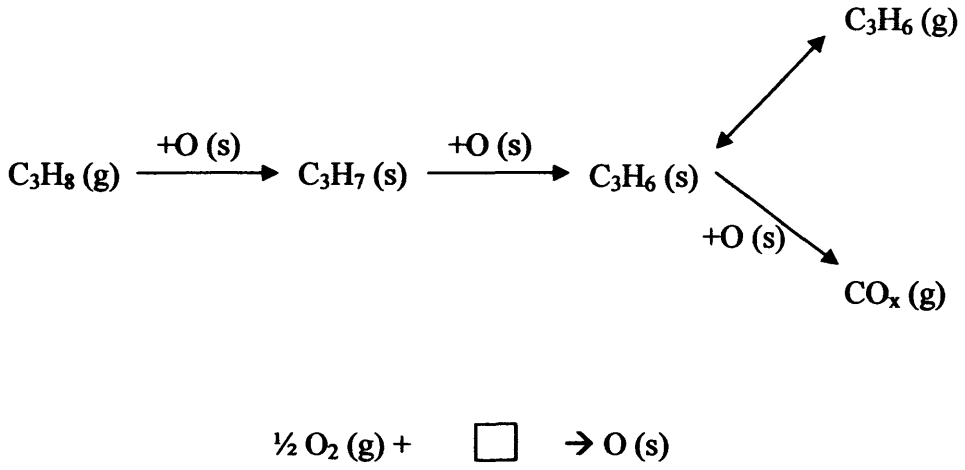

Figure 5.3 – Proposed reaction scheme for the oxidative dehydrogenation of propane[3]. (g) is gaseous substrate and product, (s) is adsorbate on the surface, □ is an oxygen vacancy.

The acid-base character of the catalyst has an influence on the selectivity to oxydehydrogenation products[11]. In this chapter, catalysts were tested for the oxidative dehydrogenation of propane using niobium oxides, niobium oxide phosphates and niobium phosphate catalysts. The catalytic data was compared to other catalysts which are used in the oxidative dehydrogenation of propane. Amongst the catalysts that have been developed, vanadia catalysts are some of the most active and selective[12]. Niobium has similar structure and properties to that of vanadium. It

is interesting to explore whether niobium offers any advantages over other catalysts in the oxidative dehydrogenation of propane.

5.2 Propane Oxidative Dehydrogenation Using Niobium(V) Oxide Catalysts.

5.2.1 Effect of Preparation Techniques.

Figures 5.4 and 5.5 show catalytic data for niobium oxides for the oxidative dehydrogenation of propane. It can immediately be seen that the conversion of propane is low. All catalysts are inactive below 300°C. The catalyst which became active at the lowest temperature was niobium oxide prepared from the oxidation of niobium ethoxide. This catalyst became active at 300°C and reached a conversion of 0.7% at 500°C. Selectivity to propene decreased almost linearly from 300°C to 450°C, reaching 28% selectivity to propene at 500°C. The major products were combustion products at higher temperatures i.e. CO_2. No CO was observed at any temperature.

The highest observed conversion from the different niobium oxides was the catalyst prepared by precipitation from niobium chloride and urea. At 500°C, a conversion of 1.2% was achieved. This catalyst became active at 350°C. Initially, complete selectivity to propene was achieved. However, 60% selectivity was observed at 400°C. Between 400°C and 475°C, conversion remained constant at approximately 0.3%, as did selectivity to propene at approximately 60%. When the temperature was increased to 500°C, conversion doubled. However, selectivity to propene remained constant even though there was a large relative increase in conversion. Carbon dioxide was the major product at higher temperatures. Looking

at oxygen conversion, it is clear that the reaction is not oxygen limited as combustion products are dominant at higher temperatures.

Niobium oxide prepared by precipitation from niobium chloride and sodium carbonate also became active at 350°C. Conversion over this catalyst increased almost linearly with conversion reaching 0.4% at 500°C. Complete selectivity to propene was observed initially. At 425°C, selectivity to propene decreased to 30%. As the temperature increased, selectivity did not change. Carbon dioxide was the major product at higher temperatures.

The lowest observed conversion of niobium oxides was from oxidation of niobium metal. This became active at 400°C, and reached 0.3% conversion of propane at 500°C. Selectivity to propene decreased from 100% to 36% at 500°C. Carbon dioxide was the major product at higher temperatures. No CO was detected.

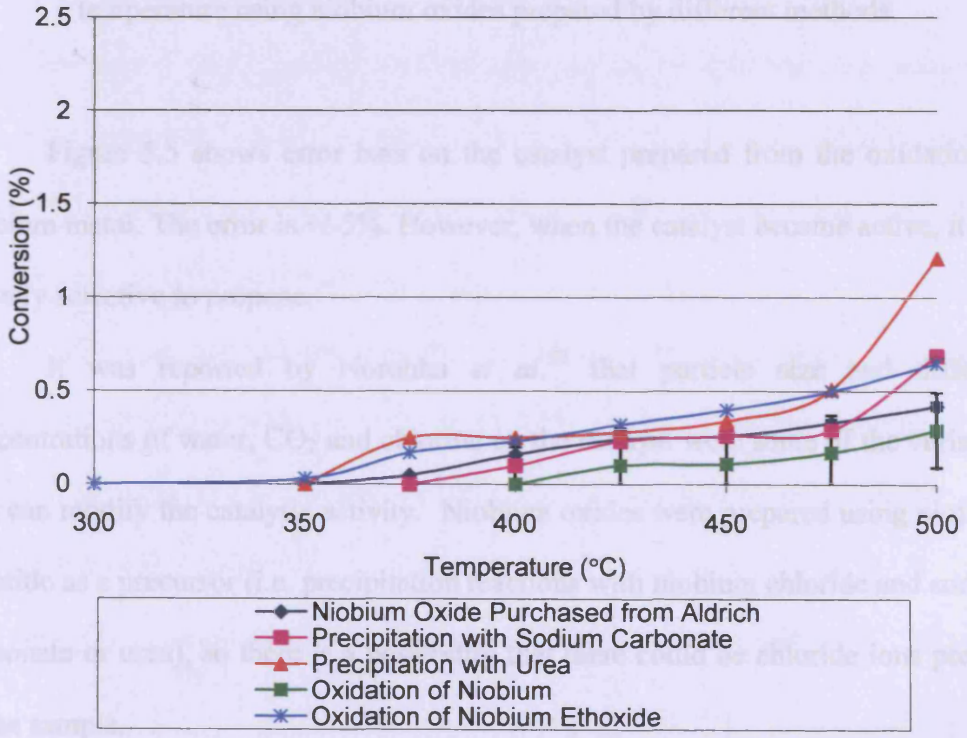

Figure 5.4 – Propane conversion as a function of temperature using niobium oxides prepared by different methods.

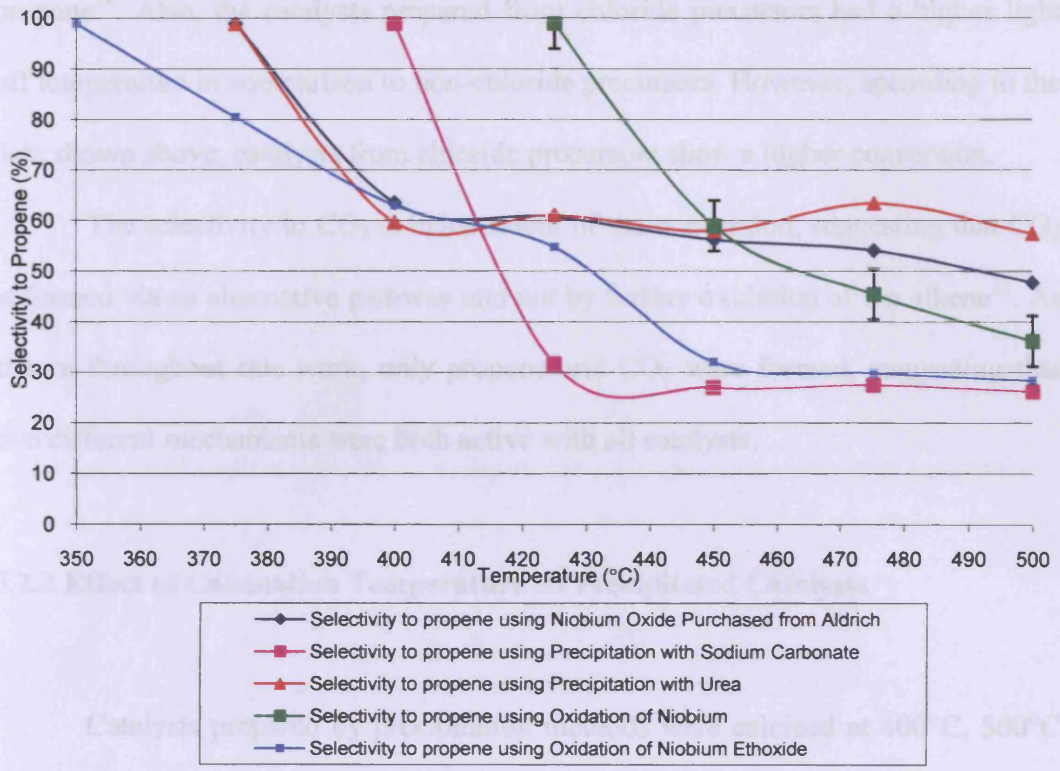

Figure 5.5 – Selectivity to propene and combustion products as a function of temperature using niobium oxides prepared by different methods.

Figure 5.5 shows error bars on the catalyst prepared from the oxidation of niobium metal. The error is +/-5%. However, when the catalyst became active, it was entirely selective to propene.

It was reported by Noronha *et al.*[13] that particle size and different concentrations of water, CO_2 and chlorine on the catalyst were some of the variables that can modify the catalytic activity. Niobium oxides were prepared using niobium chloride as a precursor (i.e. precipitation reactions with niobium chloride and sodium carbonate or urea), so there is a possibility that there could be chloride ions present in the sample.

It was shown by Sarzi-Amade *et al.* that catalysts from niobium chloride precursors gave a low conversion and selectivity to propene for the ODH of

propane[14]. Also, the catalysts prepared from chloride precursors had a higher light off temperature in comparison to non-chloride precursors. However, according to the data shown above, catalysts from chloride precursors show a higher conversion.

The selectivity to CO_2 is independent of the conversion, suggesting that CO_2 is formed via an alternative pathway and not by further oxidation of the alkene[15]. As shown throughout this work, only propene and CO_2 were formed, suggesting that two different mechanisms were both active with all catalysts.

5.2.2 Effect of Calcination Temperature on Precipitated Catalysts.

Catalysts prepared by precipitation methods were calcined at 400°C, 500°C and 600°C. The highest observed activity for all catalysts was the catalyst calcined at 500°C. A possible explanation for this is that at 500°C, the catalyst is more crystalline than at 400°C, which could explain why the catalyst was more active at a higher temperature. At 600°C, a possible reason for lower activity could be that the pores of the catalyst may have started to collapse, this causes less active sites to be available for the ODH of propane.

The conversion of the catalyst calcined at 400°C was 0.1%. The 500°C calcined catalyst displayed a conversion of 0.7% and at 600°C, the conversion was 0.05%. The selectivity to propene at 400°C, 500°C and 600°C was 25%, 27% and 26% respectively. When this was compared to the blank data, activity for the blank data was only observed at 600°C. This was 100°C above the reaction temperature.

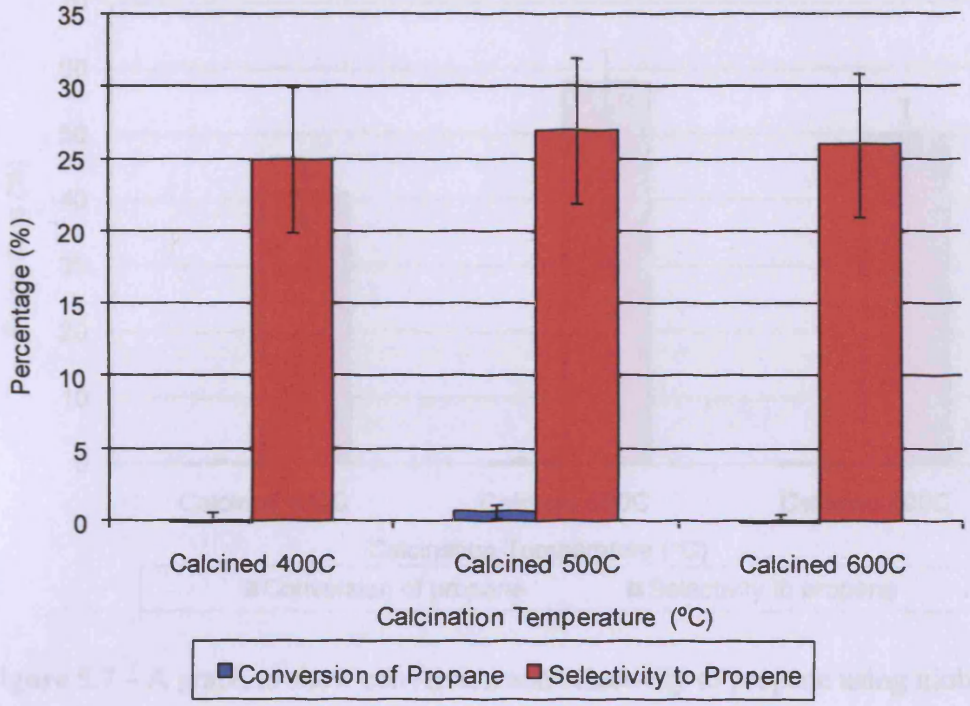

Figure 5.6 – A bar chart to show the catalytic activity of niobium oxide prepared from the precipitation from sodium carbonate, calcined at different temperatures.

Analysis carried out at 500°C.

The data shown in Figure 5.7, which shows data for the catalyst prepared by precipitation of niobium chloride and urea, shows a similar trend to that of using sodium carbonate as seen in Figure 5.6. Although the catalyst which was calcined at 500°C appeared to be more active, the conversion is so low that it can be assumed that the conversion of all catalysts are the same.

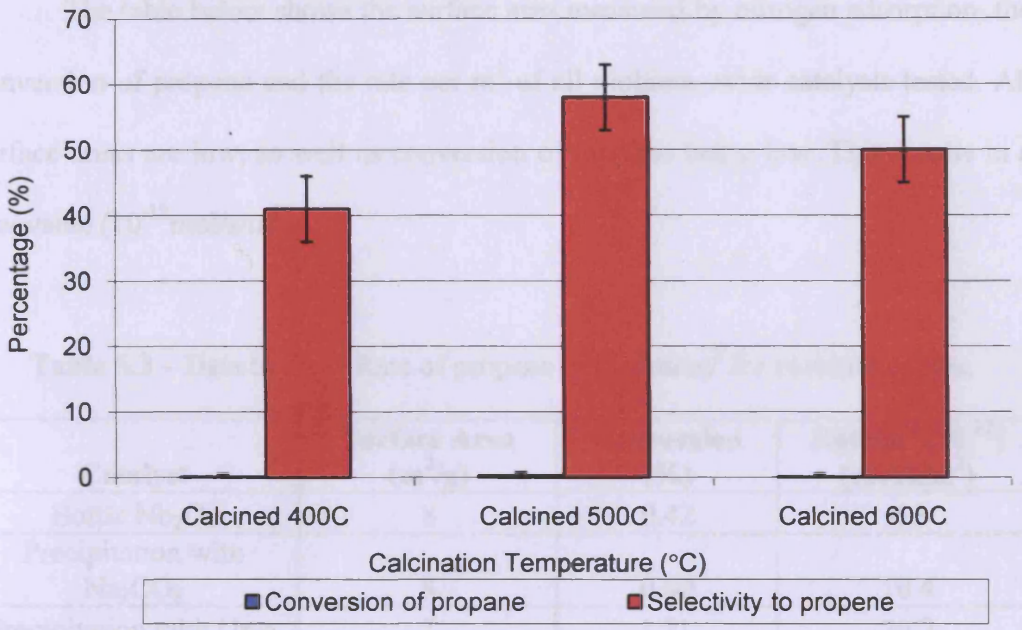

Figure 5.7 – A graph to show conversion and selectivity to propene using niobium oxide prepared from the precipitation from urea, calcined at different temperatures. Analysis carried out at 500°C.

In conclusion, all of the catalysts were poor for the oxidative dehydrogenation of propane. This may be due to the inability of the catalyst to give up oxygen from the lattice or to be re-oxidised. TPR studies were carried out by Lewandowsa and Banares, they found that niobium oxide does not reduce from the +5 to the +4 state until at 1117K[16]. It was also shown that when niobium was added to a vanadium catalyst, vanadium was less easily reduced in the studies. Vanadium oxide reduces at much lower temperatures in comparison to niobium oxide – it reduces at 772K. This is because the niobium-oxygen interactions in niobium oxide are stronger than the vanadium-oxygen interaction in vanadium oxide. Further evidence of this is shown in chapter 3.1.2. This shows the Raman spectra for niobium oxides. Metal-oxygen bond peaks are shifted to higher wavenumbers in comparison to vanadium- oxygen bond peaks.

The table below shows the surface area measured by nitrogen adsorption, the conversion of propane and the rate per m^2 of all niobium oxide catalysts tested. All surface areas are low, as well as conversion of propane being low. This results in a low value (10^{-12}mol/s/m^2).

Table 5.3 – Data to show Rate of propane oxidation/m^2 for niobium oxides.

Catalyst	Surface Area (m^2/g)	Conversion (%)	Rate/m^2 (10^{-12}) (mol/s/m^2)
Bottle Nb_2O_5	8	0.42	6.3
Precipitation with Na_2CO_3	8	0.69	10.4
Precipitation with Urea	7	1.21	20.7
Oxidation of Niobium	12	0.29	2.9
Oxidation of $Nb(OEt)_5$	17	0.65	4.6

5.2.3 Differences in catalysts pre-reaction compared to post-reaction.

5.2.3.1 XRD data of Used Catalysts.

There is no change in the phase of niobium oxide before and after interaction with propane, according to XRD data.

Table 5.1 - Summary of XRD data for niobium(V) oxides pre and post propane reactor.

	Pre Reaction		Post Reaction	
Preapration Method	Phase	Space Group	Phase	Space Group
Precipitation with Na_2CO_3	Monoclinic	P_{2m}	Monoclinic	P_{2m}
Precipitation with Urea	Monoclinic	P_{2m}	Monoclinic	P_{2m}
Nb_2O_5 Purchased from Aldrich	Orthorhombic	P_{mm}	Orthorhombic	P_{mm}
Oxidation of $Nb(OEt)_5$	Orthorhombic	P_{mm}	Orthorhombic	P_{mm}
Oxidation of Nb	Orthorhombic	P_{mm}	Orthorhombic	P_{mm}

5.2.3.2 SEM data.

There are no obvious differences pre-reactor and post-reactor. SEM images of all catalysts can be found on the CD ROM included. The images below show niobium oxide purchased from Aldrich pre- (top) and post- (bottom) reaction with propane. The particle sizes are similar and there appears to be no change in morphology.

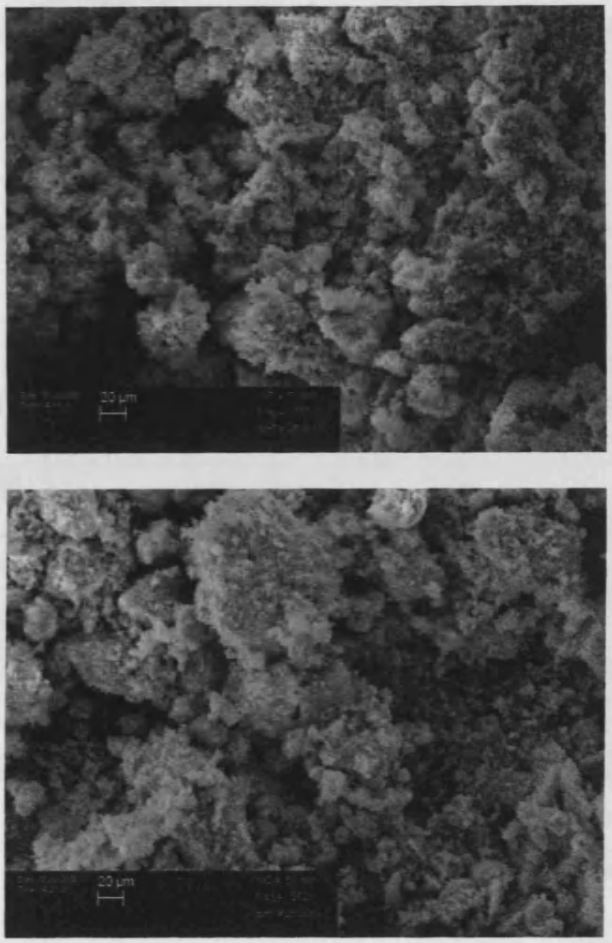

5.2.3.3 XPS data.

Table 5.2 shows the XPS data for niobium oxide catalysts prepared by different methods both pre- and post-reaction with propane. Data shows in all cases that the oxidation state of niobium does not change.

Table 5.2 – XPS data for niobium oxides pre reaction and post reaction with propane.

	Pre Reaction			
	Nb		O	
Preaparation method	Binding Energy (eV)	Assignment	Binding Energy (eV)	Assignment
Precipitation with Na_2CO_3	206.6	5	529.1, 531.1, High binding energy peaks	Oxide, OH^-, Na-O Auger
Precipitation with Urea	207.2	5	530.1, 531.2	Oxide, OH^-
Nb_2O_5 Purchased from Aldrich	206.7	5	529.7, 530.6	Oxide, OH^-
Oxidation of $Nb(OEt)_5$	206.8	5	529.7, 530.8	Oxide, OH^-
Oxidation of Nb	206.8	5	529.6, 530.5	Oxide, OH^-
	Post Reaction			
	Nb		O	
	Binding Energy (eV)	Assignment	Binding Energy (eV)	Assignment
Precipitation with Na_2CO_3	206.4	5 / +4	529.4, 530.9, other high energy binding peaks	Oxide, OH^-, due to the presence of sodium
Precipitation with Urea	206.9	5	529.9, 531.1	Oxide, OH^-
Nb_2O_5 Purchased from Aldrich	206.6	5	529.9, 531.0	Oxide, OH^-
Oxidation of $Nb(OEt)_5$	206.9	5	529.9, 532.8	Oxide, SiO_2
Oxidation of Nb	206.8	5	529.9, 531.0	Oxide, OH^-

Niobium in all niobium oxides was in the +5 oxidation state pre- and post-reaction. Pre- reaction, peaks at binding energies of 529.7 and 530.6eV were due to the presence of oxide and OH. Post-reactor, peaks at 529.9 and 531.0eV were due to the presence of oxide and OH [Appendix A2, 4, 6, 8, 10, 23, 24, 25 (a-c)].

Niobium oxide prepared from the precipitation reaction using sodium carbonate post-reaction had binding energies of 529.4 (oxide), 530.9 (OH or CO_3) and high binding energy peaks were due to the presence of sodium. Carbonate peaks were also present in the sample [Appendix A 23 (a-c)].

Niobium oxide prepared from the precipitation reaction with urea post-reaction had no variation in the XPS pattern.

The oxidation of niobium produced post-reaction oxide and hydroxide binding energies of 529.9 and 531.0eV with no other impurities present [Appendix A24 (a-c)].

The oxidation of niobium ethoxide produced post reaction peaks of oxide binding energy of 529.9eV. There were, however, traces of glass wool within the sample, indicated by a binding energy of 532.8eV [Appendix A25 (a-c)].

In a review by Mamedov and Corberan[17] it was discussed that catalytic activity/selectivity and reducibility was dependent on the redox cycle between V^{5+} and V^{4+}. According to TPR data, niobium(V) oxide does not reduce from Nb^{5+} to Nb^{4+} up to 850°C. The inability of the redox cycle between Nb^{5+} and Nb^{4+} is a possible explanation for low conversions of propane in the ODH reaction.

Unsupported vanadium pentoxide displays lower activity than supported vanadium oxide. It was found that selectivity to propene was enhanced using supported vanadium catalysts compared to unsupported vanadium oxide. One catalyst which is used for the ODH of propane is vanadia on titania. Corma *et. al.* reported high activity of the V_2O_5/TiO_2 catalysts at relatively low temperatures (500-600K)[18], however, selectivity to propene was low (<30%). It was also found that the reaction rate was proportional to the amount of V=O species in the catalyst. Titania has been used as a support in the oxidative dehydrogenation of propane[19] with quite

promising results, however niobium oxide catalysts are not very active for the oxidative dehydrogenation of propane.

5.3 Propane Oxidative Dehydrogenation Using Niobium Oxide Phosphate Catalysts.

5.3.1 Effect of Preparation Techniques.

Figures 5.8 and 5.9 show catalytic data for niobium oxides prepared by using different forms of phosphoric acid. It can be seen that conversion of propane using each catalyst is low; using pyro-phosphoric acid achieves a greater conversion. Catalytic activity was measured 3 times and an average was taken from these results.

Both niobium oxide catalysts became active at 400°C. Using pyro-phosphoric acid, conversion increased linearly up to 500°C, reaching a conversion of 0.3%. Selectivity to propene for this catalyst decreased from 100% at 425°C to 36% at 500°C. The major product was carbon dioxide at higher temperatures – no carbon monoxide was observed.

Using ortho-phosphoric acid, conversion increased from 0.15% at 425°C to 0.7% at 500°C. This followed the same trend as using pyro-phosphoric acid, i.e. a linear increase to 475°C. However, there is a tripling of activity in the conversion from 475°C to 500°C. Selectivity followed the same trend as using pyro-phosphoric acid. Selectivity to propene decreased from 100% at 425°C to 67% at 500°C.

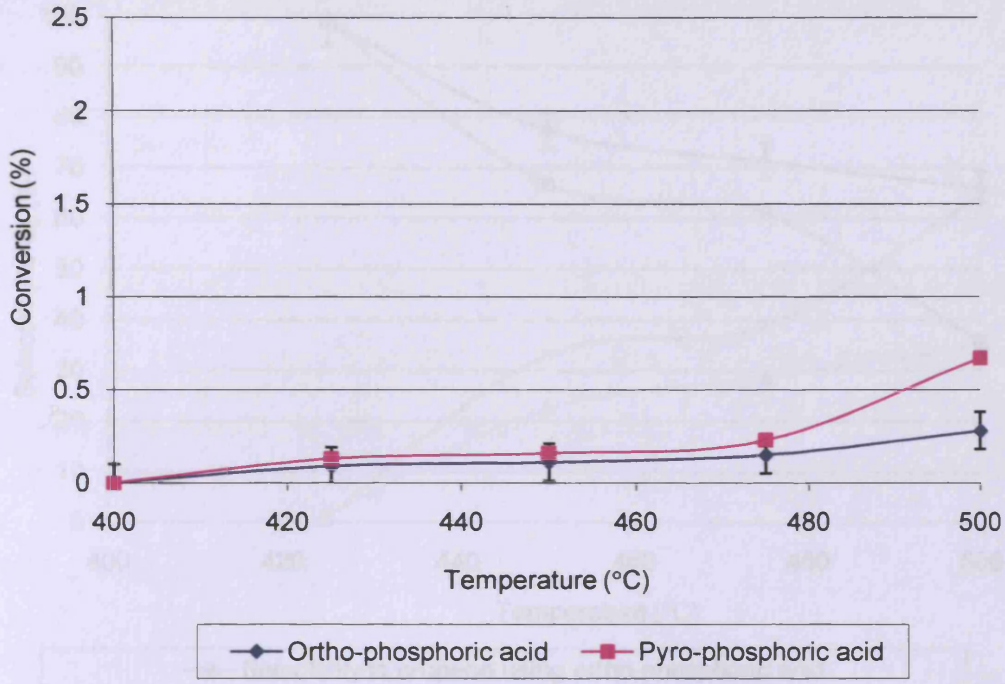

Figure 5.8 – Propane conversion as a function of temperature using niobium oxide phosphates prepared by different methods.

Singh *et. al.* investigated the effect of modifying vanadia-titania systems with phosphorus[20]. Addition of phosphorus increased the number of Bronsted acid sites available.

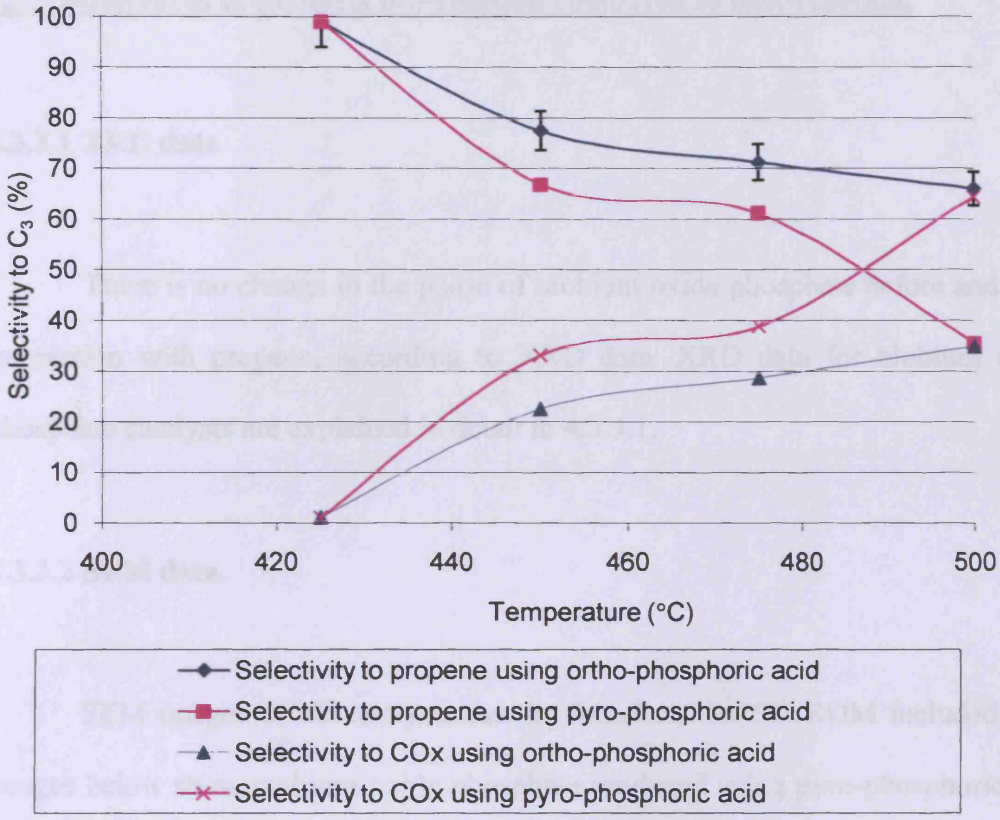

Figure 5.9 – Selectivty of propene and combustion products as a function of temperature using niobium oxide phosphates prepared by different methods.

5.3.2 Effect of Calcination Temperature.

Calcination temperature did not affect the bulk phase of niobium oxide phosphate, according to XRD data. All catalysts were calcined at 400°C (Nb-400), 500°C (Nb-500) and 600°C (Nb-600) and tested. The highest observed conversion for $NbOPO_4$ produced from H_3PO_4 was the using Nb-500. However, using $H_4P_2O_7$, the highest conversion was observed using Nb-400. Using Nb-500, the conversion decreased. Using Nb-600, conversion increased, but not to the extent as Nb-400.

5.3.3 Differences in catalysts pre-reaction compared to post-reaction.

5.3.3.1 XRD data

There is no change in the phase of niobium oxide phosphate before and after interaction with propane, according to XRD data. XRD data for niobium oxide phosphate catalysts are explained in detail in 4.3.3.1.

5.3.3.2 SEM data.

SEM images of all catalysts can be found on the CD ROM included. The images below show niobium oxide phosphate produced using pyro-phosphoric acid pre- (top) and post- (bottom) reaction with propane. The particle size pre-reactor is much larger than post-reactor.

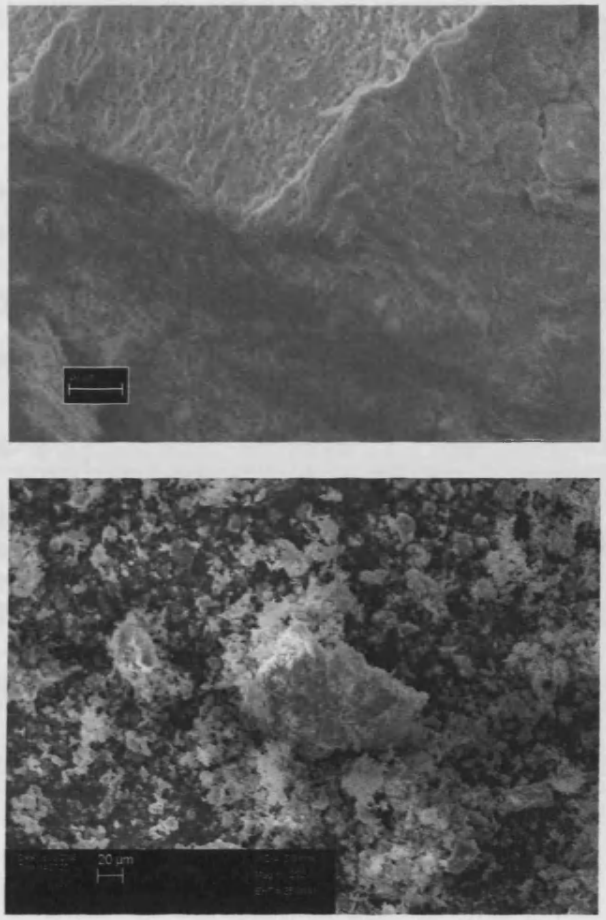

5.3.3.3 XPS data.

Table 5.4 shows XPS data for both niobium oxide phosphates both pre and post reaction with propane. Data shows in all cases that the oxidation state of niobium does not change.

Table 5.4 – XPS data for niobium oxide phosphates pre and post reaction with propane.

	Pre Reaction					
	Nb		O		P	
Preaparation method	Binding Energy (eV)	Assignment	Binding Energy (eV)	Assignment	Binding Energy (eV)	Assignment
Using H_3PO_4	208	5	531.5, 533.4	PO_x	133.9	PO_x
Using $H_4P_2O_7$	207.9	5	531.5, 533.2	CO_3^{2-}, PO_4^{3-} OH^-	134	PO_x
	Post Reaction					
	Nb		O		P	
	Binding Energy (eV)	Assignment	Binding Energy (eV)	Assignment	Binding Energy (eV)	Assignment
Using H_3PO_4	208.1	5	531.5, 533.2	CO_3^{2-}, PO_4^{3-} OH^-	134	PO_x
Using $H_4P_2O_7$	208	5	531.6, 533.1	CO_3^{2-}, PO_4^{3-} OH^-	134	PO_x

Niobium in niobium oxide phosphate prepared from using ortho-phosphoric acid post reaction had binding energies of 531.5 and 533.2eV may be due to CO_3^{2-}, PO43- and OH^- on the surface of the catalyst [Appendix A26 (a-c)].

Niobium in niobium oxide phosphate prepared from using pyro-phosphoric acid post reaction had binding energies of 531.6 and 533.1eV may be due to CO_3^{2-}, PO_4^{3-} and OH^- on the surface of the catalyst [Appendix A27 (a-c)].

5.4 Propane Oxidative Dehydrogenation Using Niobium Phosphate Catalysts.

5.4.1 Effect of Preparation Techniques.

Figures 5.10 and 5.11 show catalytic data for the oxidative dehydrogenation of propane using niobium phosphate catalysts. Once again, it can be seen that conversion of propane is low; for all catalysts, conversion is less than 0.5% at 500°C.

The catalysts that became active at the lowest temperature were niobium phosphate prepared from the autoclave type reaction (as described in2.2.4) and niobium phosphate prepared from the reduction of niobium oxide phosphate with hydrogen – these became active at 400C. Niobium phosphate prepared from the reduction using hydrogen produced 0.4% conversion and 56% selectivity to propene at 500°C. Niobium phosphate prepared from the autoclave type reaction produced conversion of 0.25% and 48% selectivity to propene. The only other product observed was carbon dioxide.

Catalysts prepared from the reduction of niobium oxide phosphate with alcohols became active at 450°C and produced conversion of 0.1% with no selectivity to propane. These catalysts produced carbon dioxide only.

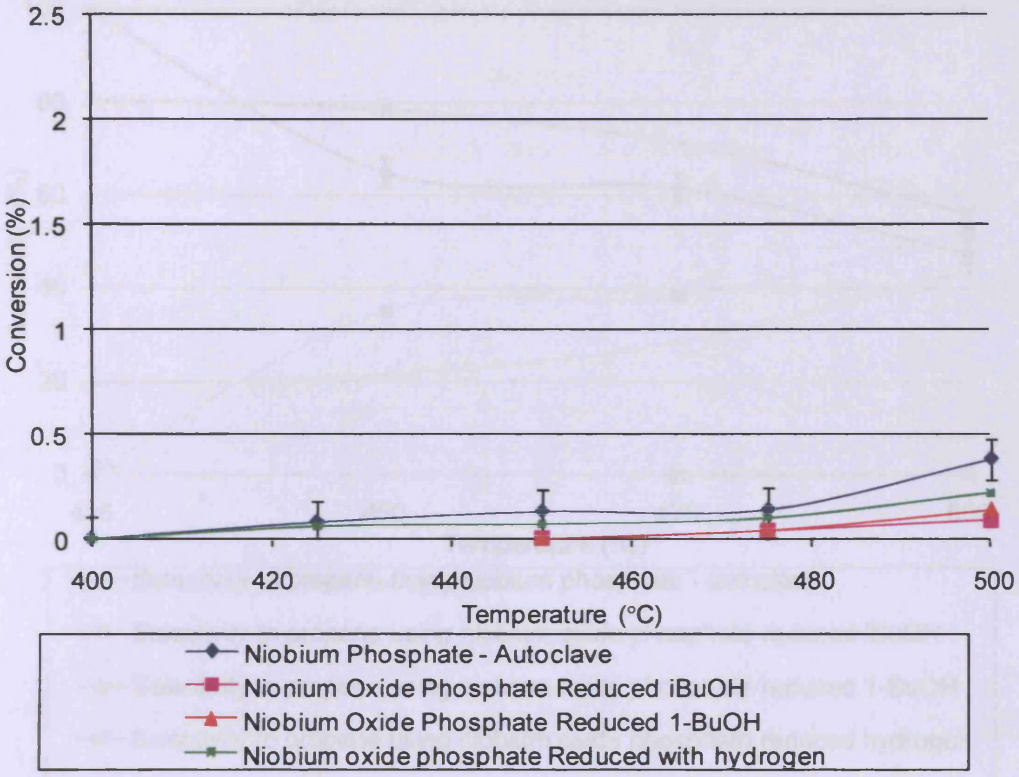

Figure 5.10 – Conversion of propane as a function of temperature using niobium phosphates prepared by different methods.

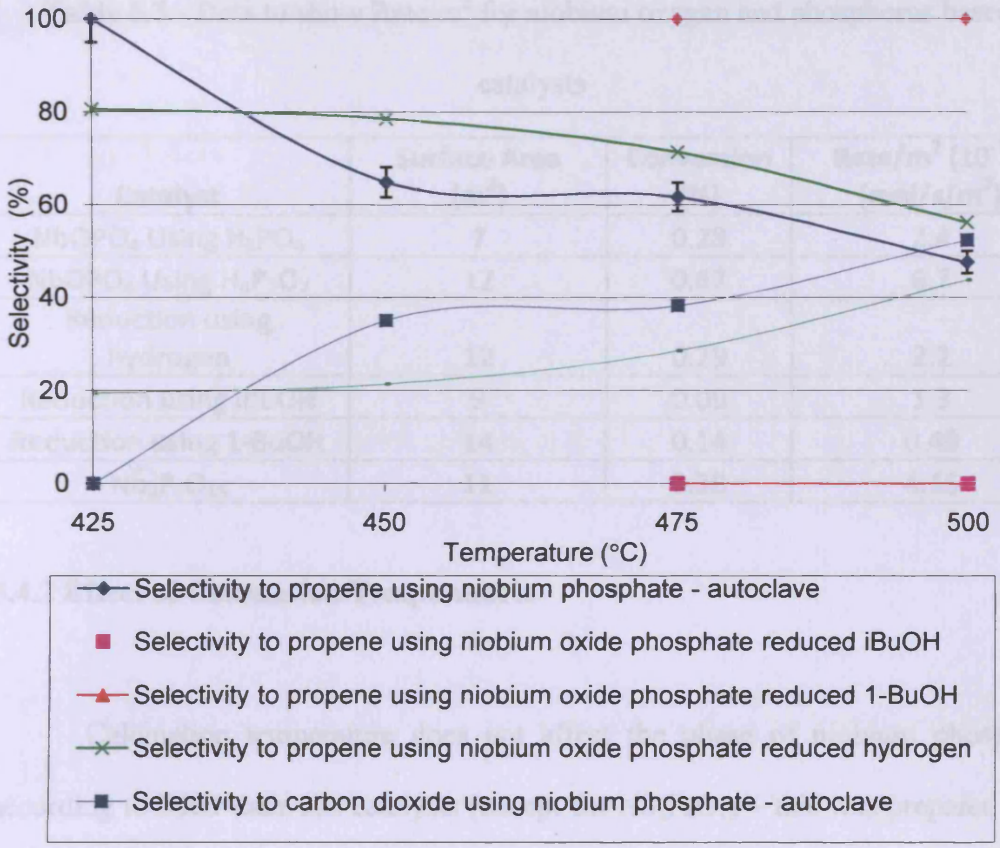

Figure 5.11 – Selectivity to propene and combustion products as a function of temperature using niobium phosphates prepared by different methods.

Table 5.5 shows data for niobium, oxygen and phosphorus based catalysts. As can be seen from surface area measurements measured by nitrogen adsorption analysis, the surface areas of all catalysts are low. Also, the conversion of propane is low, which results in a low rate per unit area. The largest conversion of propane is achieved by $Nb_2P_4O_{15}$. Further evidence that phosphorus increases the activity of the catalyst is provided as this catalyst has twice the Nb:P ratio as the other niobium, oxygen and phosphorus based catalysts.

Table 5.5 - Data to show Rate/m^2 for niobium oxygen and phosphorus based catalysts

Catalyst	Surface Area (m^2)	Conversion (%)	Rate/m^2 (10^{-12}) (mol/s/m^2)
$NbOPO_4$ Using H_3PO_4	7	0.28	2.4
$NbOPO_4$ Using $H_4P_2O_7$	12	0.67	6.7
Reduction using hydrogen	12	0.29	2.2
Reduction using iBuOH	9	0.09	1.3
Reduction using 1-BuOH	14	0.14	0.49
$Nb_2P_4O_{15}$	11	0.38	4.15

5.4.2 Effect of Calcination Temperature.

Calcination temperature does not affect the phase of niobium phosphate, according to XRD data. All catalysts (except for $Nb_2P_4O_{15}$ – this was prepared from a previous method) were calcined and tested at 400°C, 500°C and 600°C. The highest conversion for all catalysts was the catalysts calcined at 500°C. As conversion for all catalysts were low (<1%), it can be assumed that all catalysts have approximately the same conversion. There was no difference in conversion or selectivity. Selectivity using alcohols was completely selective to CO and CO_2. Selectivity to propene using $Nb_2P_4O_{15}$ was 45-50% at 500°C and selectivity to propene using reduction with hydrogen was 50-60% at 500°C.

5.4.3 Differences in catalysts pre-reaction compared to post-reaction.

5.4.3.1 XRD data

There is no change in the phase of niobium oxide phosphate before and after interaction with propane, according to XRD data. XRD data for niobium oxide phosphate catalysts are explained in detail in 4.4.3.1.

5.4.3.2 SEM data.

SEM images of all catalysts can be found on the CD ROM included. The images below show niobium phosphate prepared using the reduction of nibouim oxide phosphate with hydrogen pre- (top) and post- (bottom) reaction with propane. Pre-reaction, there is a layered structure compared to post-reaction there is a block globular structure.

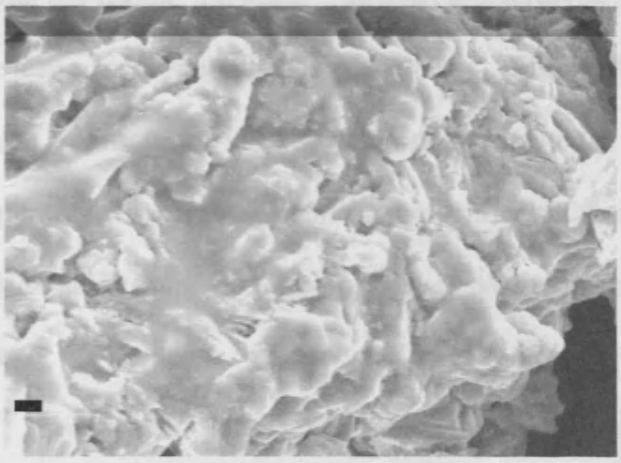

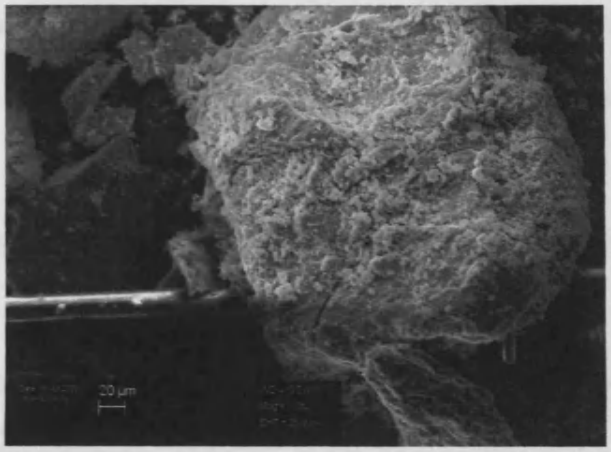

5.4.3.3 XPS data.

Niobium in all niobium oxides were in the +5 oxidation state pre-and post-reactor. There was no difference in XPS spectra pre- and post-reaction with propane for any catalysts. [Appendix A11, 12, 15, 17, 19, 21, 28, 29, 30, 31 (a-c)].

It was discussed in the review by Mamedov and Corberan that the oxygen of the vanadia species bonded to aluminium is more nucleophilic and is, therefore more reactive in activating the alkane molecule[13] through a heterolytic dissociation of the C-H bond than the same species bonded to phosphorus. Adding phosphorus into the catalyst increases the acidity of the catalyst. This should make the catalyst polarise a C-H bond to a greater extent. Hence, phosphorus aids activation of the alkane molecule. Conversion data is similar for phosphorus containing and non-phosphorus containing catalysts.

Centi *et al*[21] investigated the effect of vanadyl pyrophosphate on the ODH of propane and found the catalyst to produce mostly combustion products. This is similar to the work investigated here, where using niobium phosphates and oxide phosphates produces combustion products. Relating this back to Figure 5.2, this

indicates that the major reaction pathway is not proceeding via the alkene. The value of k_2 is larger than the value of k_1 and hence CO and CO_2 are the major products.

5.5 Comparison of Niobium Catalysts to VMgO Catalysts.

Figure 5.12 shows the comparison of niobium catalysts tested in comparison to other high activity catalysts, VMgO[22]. It can be seen that niobium catalysts have a lower yield than VMgO catalysts. This is because conversion of propane for all niobium catalysts is less than 2%. It can therefore be understood that niobium oxide, niobium oxide phosphate and niobium phosphate catalysts offer no advantages over other catalysts for the oxidative dehydrogenation of propane.

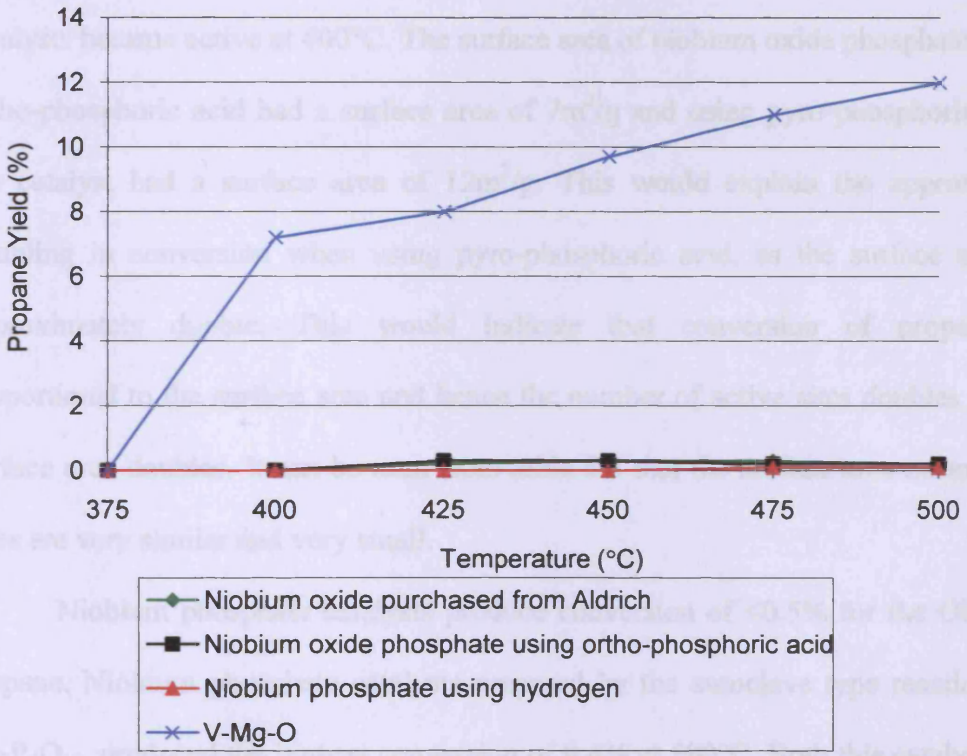

19

Figure 5.12 – A graph to show the yield of niobium based catalysts in comparison to other catalysts.

5.6 Conclusions.

It can be seen that all niobium catalysts which have been tested for the ODH of propane have a very low activity. Using niobium oxides, comparing preparation techniques, the highest conversion is using the catalyst prepared from the precipitation reaction of niobium chloride and urea. This produced approximately double the conversion at 500°C compared to the other niobium oxide catalysts tested. This catalyst became active at 375°C and selectivity to propene decreased from 100% to 60% at 400°C. At 500°C, selectivity further decreased to 55%. Surface areas of all niobium oxide catalysts were similar, 7-12m^2/g.

Niobium oxide phosphate catalysts also have a low activity. The two niobium oxide phosphate catalysts that were tested showed conversion of <1% at 500°C. Both catalysts became active at 400°C. The surface area of niobium oxide phosphate using ortho-phosphoric acid had a surface area of 7m^2/g and using pyro-phosphoric acid, the catalyst had a surface area of 12m^2/g. This would explain the approximate doubling in conversion when using pyro-phosphoric acid, as the surface area is approximately double. This would indicate that conversion of propane is proportional to the surface area and hence the number of active sites doubles as the surface area doubles. It can be seen from table 5.5 that the surface area normalised rates are very similar and very small.

Niobium phosphate catalysts produce conversion of <0.5% for the ODH of propane. Niobium phosphate catalysts prepared by the autoclave type reaction i.e. $Nb_2P_4O_{15}$, produced the highest conversion of 0.4% at 500°C. Both this catalyst and niobium phosphate prepared from the reduction of niobium oxide phosphate using

hydrogen was selective to propene. Niobium phosphates prepared from the reduction of niobium oxide phosphate using alcohol were not selective to propene.

References.

[1] Murgia, V., Sham, E., Gottifredi, E. C., Farfan Torres, E. M., *Latin American Applied Research*, 34, **2004**, 75-82.

[2] Woods, M. P., Liu, C., Wotson, R. B., *The 2005 Annual Meeting, Cincinnati*, **2005**, Monday 31st October, 12.30, 63a.

[3] Cavani, F., Ballarini, N., Creicola, A.; *Catalysis Today*, 127, **2007**, 113-131.

[4] http://pubs.acs.org/cen/coverstory/83/8312petrochemicals.html

[5] Bowker, M.; *The Basics and Applications of Heterogeneous Catalysis, Oxford University Primers*, **1998**.

[6] Creaser, D., Andersson, B.; *Appl. Catal. A. Gen*, 141, **1996**, 131.

[7] Michaels J. N., Stern D. L., Grasselli R. K.; *Catal. Lett*, 125, **1996**, 132.

[8] Patel D., Andersen P. J., Kung H. H.; *J. Catal.*, 125, **1990**, 132.

[9] Mars, P., van Krevelen, D. W.; *Chem Eng Sci*, 3, **1954**, 41.

[10] Heracleous, E., Machli, M., Lemonidou, A. A., Vasalos, I. A., *Journal of Molecular Catalysis A*, 232, **2005**, 29-39.

[11] Blasco, T., Galli, A., Lopez Nieto, J. M., Trifiro, F., *J. Catal.*, 169, **1997**, 203.

[12] Karakoulia, S. A., Triantafyllidis, K. S., Lemonidou, A. A., *Microporous and Mesoporous Materials*, 110, **2008**, 157-166.

[13] Noronha, F. B., Aranda, D. A. G., Ordine, A. P., Schmal, M., *Catalysis Today*, 57, **2000**, 275-282.

[14] Sarzi-Amade, M Morselli, S., Moggi, P., Maione, A., Ruiz, P., Devillers, M., *Applied Catalysis A*, 284, **2005**, 11-20.

[15] Klisinka, A., Samson, K., Gressel, I., Grzybowska, B., *Applied Catalysis A.*; 309, **2006**, 10-16.

[16] Lewandowska, A. E., Banares, M. A., *Catalysis Today*, 126, **2006**, 323-331.

[17] Mamedov, E. A., Corberan, V. C., *Applied Catalysis A;* 127, **1995**, 1-40.

[18] Corma, A., Lopez Nieto, J. M., Paredes, N., Perez, M., Shen, Y., Cao, H., Suib, S. L., *Surface Science Catalysis*, 72, **1992**, 213.

[19] http://dx.doi.org/10.1016/S0926-860X(01)00498-7

[20] Singh, R. P., Banares, M. A., Deo, G., *J. Catal.*, 233, **2005**, 388-398.

[21] Centi, G., Trifiro, F., *Catalysis Today*, 3, **1988**, 151.

[22] Parmaliana, A., Sokolovskii, V., Miceli, D., Giordano, N., *Applied Catalysis A*,; 135, **1996**, L1-L5.

6. Ethane Oxidative Dehydrogenation Using Niobium Based Catalysts.

6.1 Introduction to Ethane Oxidative Dehydrogenation.

Ethylene is one of the most important building blocks in chemistry. It ranks as the highest volume organic chemical produced in the world[1]. Olefin demand is commercially met through steam cracking of hydrocarbons, mainly naphtha and ethane[2]. Oxidative dehydrogenation (ODH) is a chemical process that offers both energy and cost effective advantages over traditional cracking technologies. Before ethane oxidative dehydrogenation can be considered as a viable alternative process, a catalyst producing a high ethylene yield needs to be developed.

In recent years there has been increased research effort to identify new catalysts for the oxidative dehydrogenation of ethane. In some cases yields to ethylene even higher than those obtained by steam cracking[3] have been achieved. Reactivity data for catalysts made of supported vanadium oxide are consistent both with kinetically relevant steps involving the dissociation of C–H bonds and with a Mars-van Krevelen redox mechanism involving lattice oxygen in C–H bond activation. The resulting alkyl species desorb as olefin and the remaining O–H group recombines with neighbouring O–H groups in order to form water and reduced V centres; the latter are re-oxidized by irreversible dissociative chemisorption of O_2. Surface oxygen, O–H groups and, especially, oxygen vacancies are the most abundant reactive intermediates during ODH.

However, ethylene manufacturers have been reluctant to adopt the ODH process, and currently there are no commercial plants using the approach. This is most likely due to the familiarity and trust in the tried and tested steam cracking process

and economic reasons. Therefore, if catalytic ODH is to become a viable competing route for ethylene production the identification and development of improved catalysts is required.

In this chapter, attempts will be made to compare niobium based catalysts with other catalysts and understand their applicability. From previous work involving oxidative dehydrogenation of propane, it has been shown that niobium based catalysts have a high selectivity[4]. The aim of this work is to examine whether the selectivity to ethylene from ethane can be maintained with high conversions.

6.2 Studying the Effect of Different Concentrations of Ethane, Propane and Helium for the ODH Process.

Certain catalysts were tested for the oxidative dehydrogenation of ethane to ethylene. These catalysts were tested in Valencia University by Dr. Benjamin Solsona.

Three catalysts were tested for the ODH of ethane using 30% ethane, 30% oxygen and 40% helium. It can be seen from Figure 6.1 that Nb-2 (niobium oxide prepared from the precipitation with urea) became active at 375°C, compared to Nb-5 (niobium oxide purchased from Aldrich) and NbP-3 ($NbPO_5$ prepared from the reduction with hydrogen) becoming active at 425°C. However, only a 2% conversion is achieved at 475°C. At 500°C, there is almost a 3-fold increase in conversion for Nb-2. Nb-5 achieved a lower conversion at 500°C. The conversion increased almost linearly from when it became active at 425°C and a conversion of 2.5% was achieved with this catalyst at 500°C.

NbP-3 also became active at 425°C. At 450°C, the conversion was at 1% (higher than Nb-5 and lower than Nb-2). At 475°C, there was a dramatic increase in

conversion; a conversion of 5% was obtained. The catalyst gained stability and the conversion remained relatively constant at 500°C, a conversion of 5.5% was achieved.

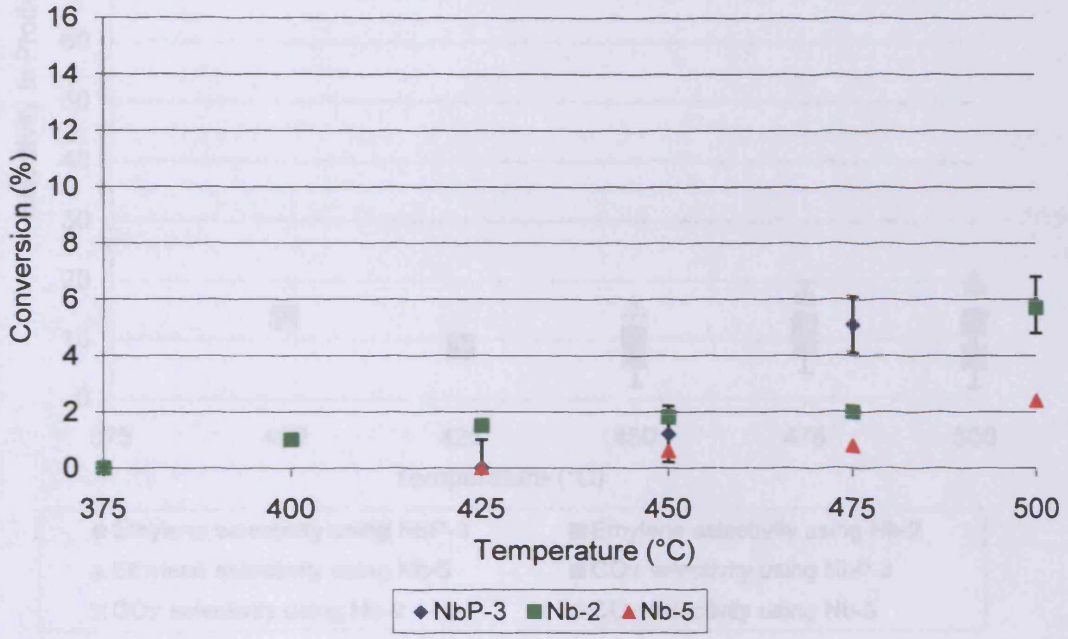

Figure 6.1 – A graph to show the conversion of ethane as a function of temperature using 30% ethane, 30% oxygen and 40% helium.

Figure 6.2 shows the selectivity to products in the ODH reaction. The products seen were ethylene (the desirable product) and carbon oxides i.e. CO and CO_2 in approximately a 1:1 ratio.

Nb-5 produced a high selectivity to combustion products. Less than 20% selectivity to ethylene was achieved using this catalyst, and 80% selectivity to combustion products was achieved at 500°C. A similar pattern was shown when using Nb-2. This catalyst was less than 15% selective to ethylene and 85% selective to combustion products.

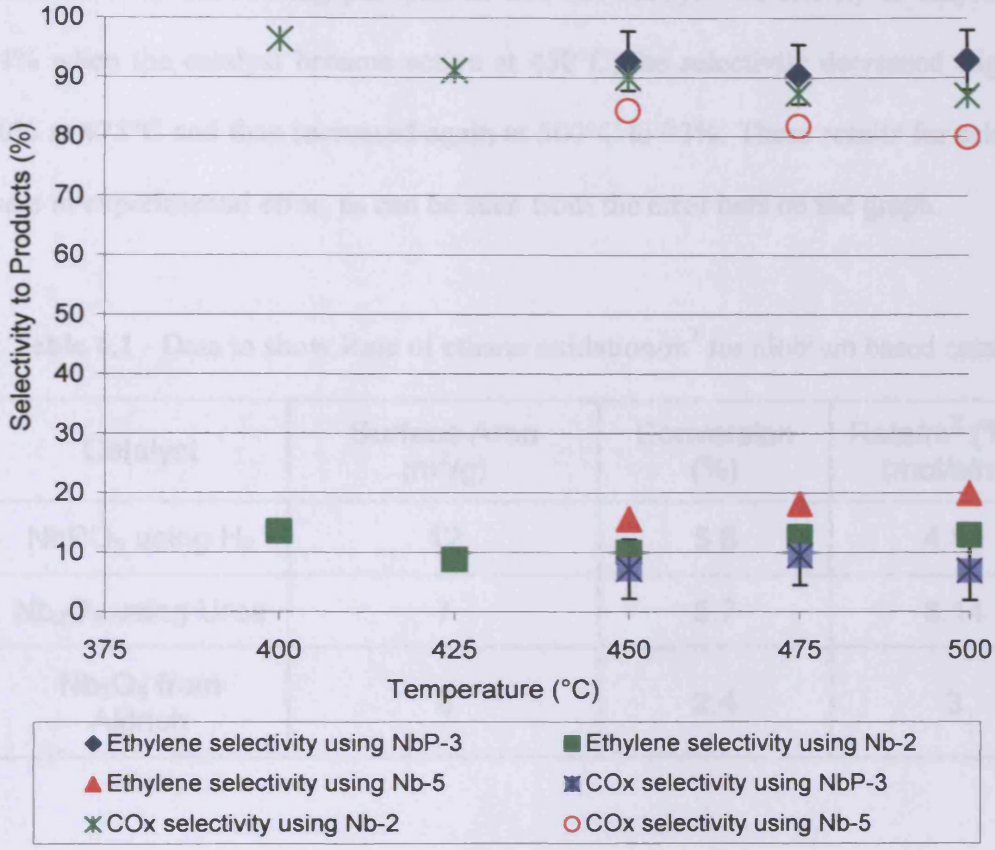

Figure 6.2 – A graph to show the selectivity to ethylene and CO_x as a function of temperature using 30% ethane, 30% oxygen and 40% helium.

Niobium(V) chloride was used as a precursor for all catalysts tested. It is known that chlorine acts as a catalyst poison. In the precipitation reaction with urea (Nb-2), the catalyst was washed thoroughly with hot and cold water in order to remove chloride ions. It is not clear as to how niobium oxide purchased from Aldrich (Nb-5) is produced, however, this may also use a niobium chloride precursor. XPS analysis shows no traces of chloride ions.

Niobium phosphate prepared from the reduction of niobium oxide phosphate using hydrogen (NbP-3) show a different trend to niobium oxide catalysts which have been discussed up to this point. A high selectivity to ethylene is achieved and

maintained by introducing phosphorus into the catalyst. Selectivity to ethylene was 94% when the catalyst became active at 450°C, the selectivity decreased slightly to 90% at 475°C and then increased again at 500°C to 93%. These results for selectivity were in experimental error, as can be seen from the error bars on the graph.

Table 6.1 - Data to show Rate of ethane oxidation/m^2 for niobium based catalysts.

Catalyst	Surface Area (m^2/g)	Conversion (%)	Rate/m^2 (10^{-11}) (mol/s/m^2)
$NbPO_5$ using H_2	12	5.8	4.83
Nb_2O_5 using Urea	7	5.7	8.14
Nb_2O_5 from Aldrich	8	2.4	3

Four catalysts were tested for the ODH of ethane using 30% ethane, 10% oxygen and 60% helium. It can be seen from Figure 6.3 that niobium phosphate prepared from the reduction of niobium oxide phosphate using hydrogen became active at 300°C. This is the same catalyst which was tested under different concentrations above. This catalyst was active at a different temperature using 30% ethane, 30% oxygen and 40% helium concentrations in comparison to using 30% ethane, 10% oxygen and 60% helium. The selectivity remained constant regardless of reaction conditions. The selectivity of the catalyst to ethylene slightly decreased from 98% at 350°C to 90% at 500°C. This again was within experimental error. The selectivity of the catalyst to combustion products was 10% at 500°C.

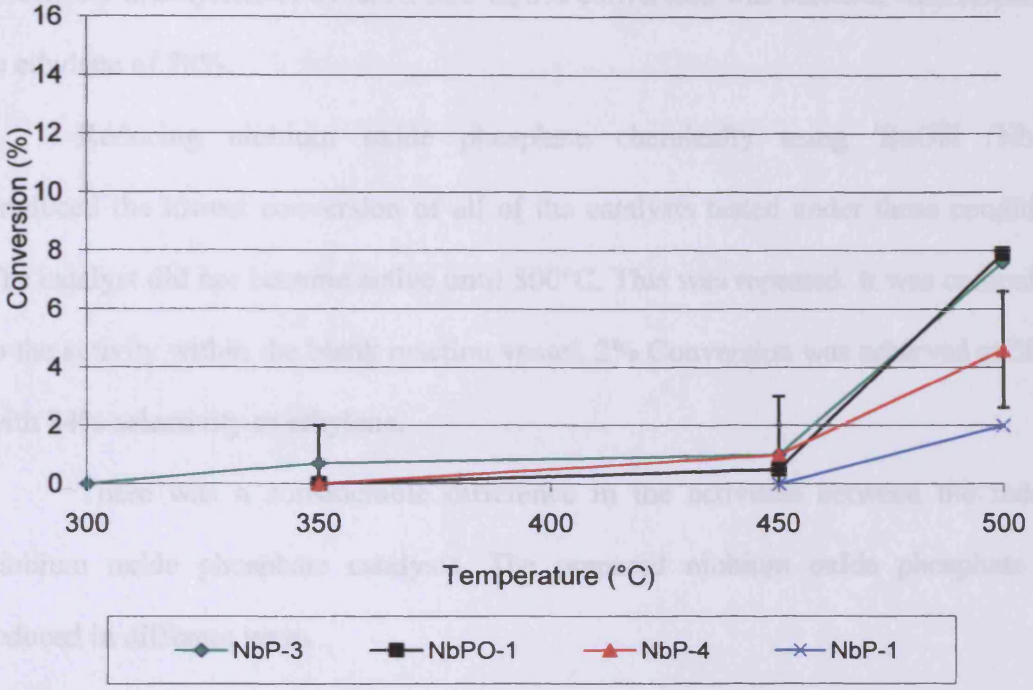

Figure 6.3 – A graph to show the conversion of ethane as a function of temperature using 30% ethane, 10% oxygen and 60% helium.

Niobium oxide phosphate which was calcined in air (NbPO-1) was also tested using 30% ethane, 10% oxygen and 60% helium. This catalyst became active at 350°C. This is 50°C greater than niobium phosphate discussed above. Conversion was less than 1% at 450°C, but at 500°C, conversion was slightly greater to that of NbP-3. Conversion reached 8.9% at 500°C. As conversion is slightly higher than NbP-3, one would expect the selectivity to ethylene to be lower, and this is the case. At 450°C the selectivity to ethylene was 92% with 8% selectivity to combustion products. At 500°C, the selectivity to ethylene was 79% with 21% selectivity to combustion products.

NbP-4 ($Nb_2P_4O_{15}$), which was prepared from an autoclave reaction (see chapter 2.2.4) also became active at 350°C. 1% conversion was reached at 450°C with

selectivity to ethylene of 81%. At 500°C, 5% conversion was reached, with selectivity to ethylene of 78%.

Reducing niobium oxide phosphate chemically using ^{i}BuOH (NbP-1) produced the lowest conversion of all of the catalysts tested under these conditions. The catalyst did not become active until 500°C. This was repeated. It was comparable to the activity within the blank reaction vessel. 2% Conversion was achieved at 500°C with 84% selectivity to ethylene.

There was a considerable difference in the activities between the reduced niobium oxide phosphate catalysts. The prepared niobium oxide phosphate was reduced in different ways

(i) Reduction using alcohols.

(ii) Reduction using hydrogen.

Using hydrogen to reduce niobium oxide phosphate decreased the temperature at which the catalyst became active. Using alcohol to reduce the catalyst increased the temperature at which the catalyst became active. Although selectivity to ethylene was high for all catalysts discussed in this section, the catalyst with the highest yield was niobium phosphate prepared from the reduction of niobium oxide phosphate reduced in hydrogen (entry ii).

Table 6.2 Selectivity to ethylene at different temperatures over Nb catalysts using 30% ethane, 10% oxygen and 60% helium

Entry	Catalyst	Temperature (°C)		
		350	450	480
1	NbP-3	98	96	90
2	NbPO-1	0	90	80
3	NbP-4	0	80	78
4	NbP-1	0	0	83

Table 6.3 - Data to show Rate of ethane oxidation/m^2 for niobium based catalysts.

Catalyst	Surface Area (m^2/g)	Conversion (%)	Rate/m^2 (10^{-11}) (mol/s/ m^2)
NbP-3	12	6	6
NbPO-1	7	6	11
NbP-4	8	2	42
NbP-1	9	2	2

6.3 Investigating the Effect of Contact Time.

Figure 6.5 shows the effect of contact time between all gases and the catalyst. One would expect that as the contact time between catalyst and substrate increases the conversion to products would increase. This is indeed the case with niobium catalysts. As the contact time increases from 228 to 456 seconds, the conversion increases from 4% to 8%, with a slight decrease in selectivity (within experimental error). Increasing contact time from 228 to 604 seconds causes approximately a 3-fold increase in

conversion with selectivity remaining approximately constant (within experimental error). Increasing contact time from 456 to 901 seconds approximately doubles the conversion with a slight decrease in selectivity to ethylene (within experimental error).

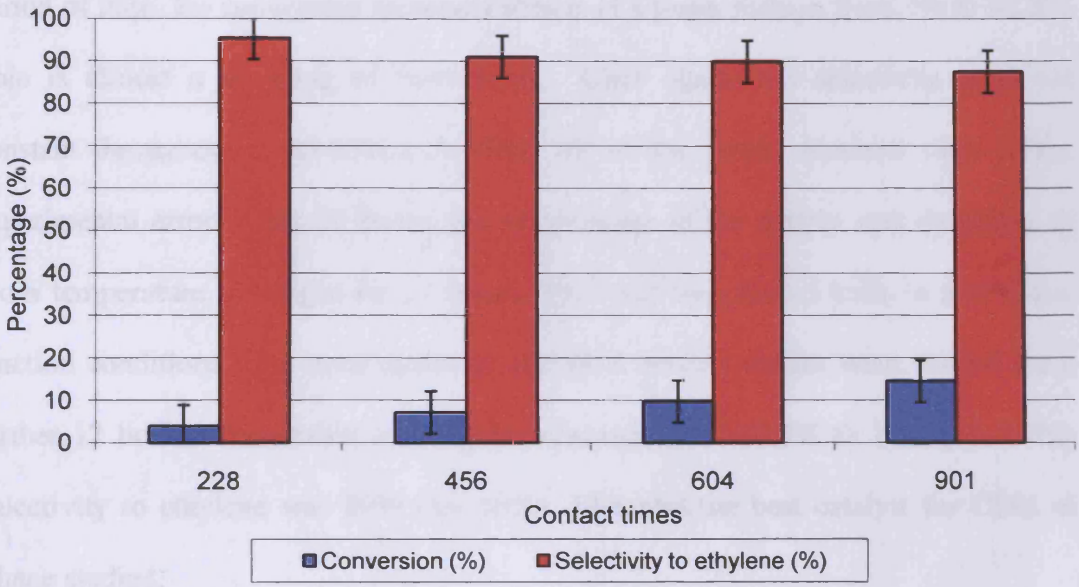

Figure 6.5 – A Graph to show conversion of ethane and selectivity to ethylene with varying contact times using a niobium phosphate catalyst prepared from the reduction using hydrogen. Analysis carried out at 500C.

6.4 Time On-line Studies.

Figure 6.6 shows conversion data for NbP-3 (niobium phosphate prepared from the reduction of niobium oxide phosphate using hydrogen). After 6 hours, the temperature of the sample was decreased to room temperature and XRD analysis was taken. XRD analysis showed that the sample had been reduced back to $NbOPO_4$ (Reference 01-070-2652, JCPDS). In this time, the conversion remained constant throughout at 7% and the selectivity to ethylene also remained constant throughout at 90% (+/- 5%).

After taking part of the sample for XRD analysis, the contact time was altered in order to remain constant at 456 seconds. The sample was again heated to 500°C and time on-line studies were carried out for a further 10 hours. Interestingly, in this period of time, the conversion increased almost in a linear fashion from 7% to 12.5%. This is almost a doubling of conversion. Once again, the selectivity remained constant throughout at 85-90% (+/- 10%) All of the results obtained were within experimental error. After 20 hours, the temperature of the system was decreased to room temperature overnight for 11 hours. This was then heated back to 500°C and reaction conditions were once again set and time on-line studies were studied for a further 12 hours. Conversion once again increased from 12.5% to 14% (+/- 10%). Selectivity to ethylene was 89% (+/- 10%). This was the best catalyst for ODH of ethane studied.

The catalyst was dark blue at the beginning of the experiment, corresponding to niobium phosphate, $NbPO_5$ (00-040-0124, JCPDS). After 6 hours, the temperature of the sample was decreased to room temperature and XRD analysis was taken. XRD analysis showed that the sample had been reduced back to $NbOPO_4$.

Post reaction, the catalyst was white in appearance. XRD analysis showed that the phase of the catalyst was orthorhombic $Nb_{1.91}P_{2.82}O_{12}$. A temperature profile for the reaction is shown in figure 6.6.

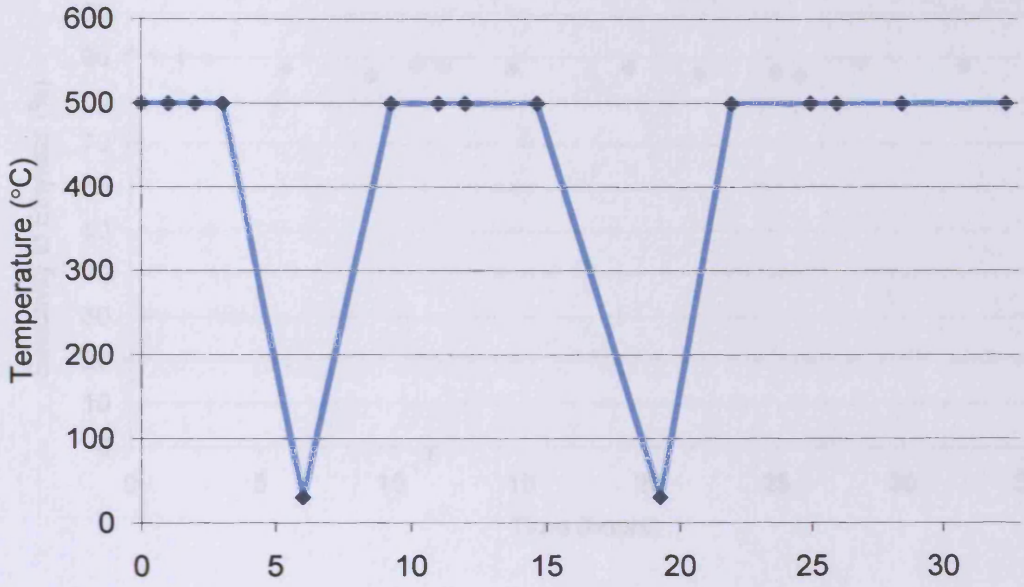

Figure 6.6 – Temperature profile for time on-line studies.

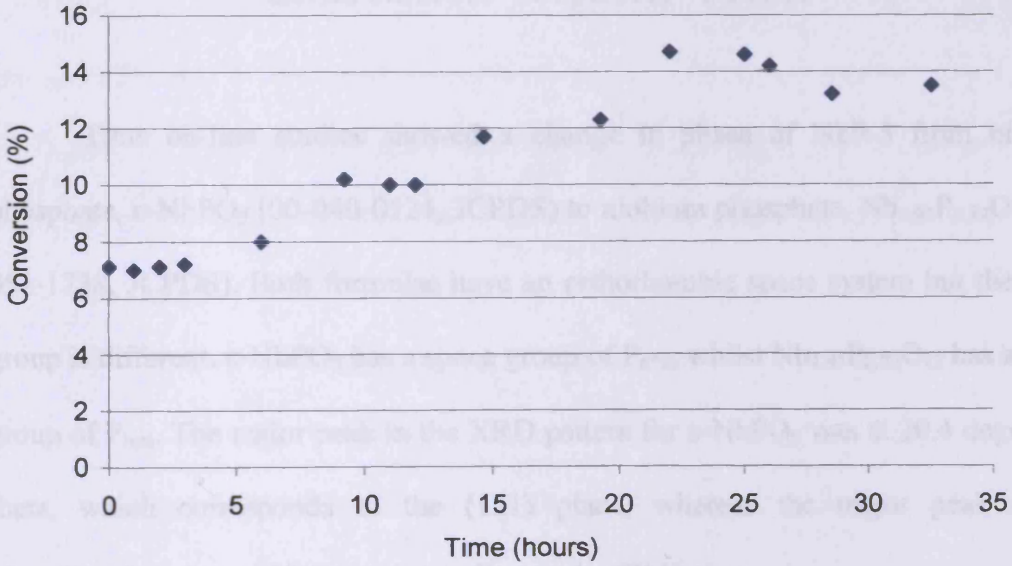

Figure 6.7 – Graph to show conversion of ethane as a function of time using $NbPO_5$ from the reduction of niobium oxide phosphate with hydrogen. Analysis carried out at 500°C. $C_2/O_2/He = 30/10/60$

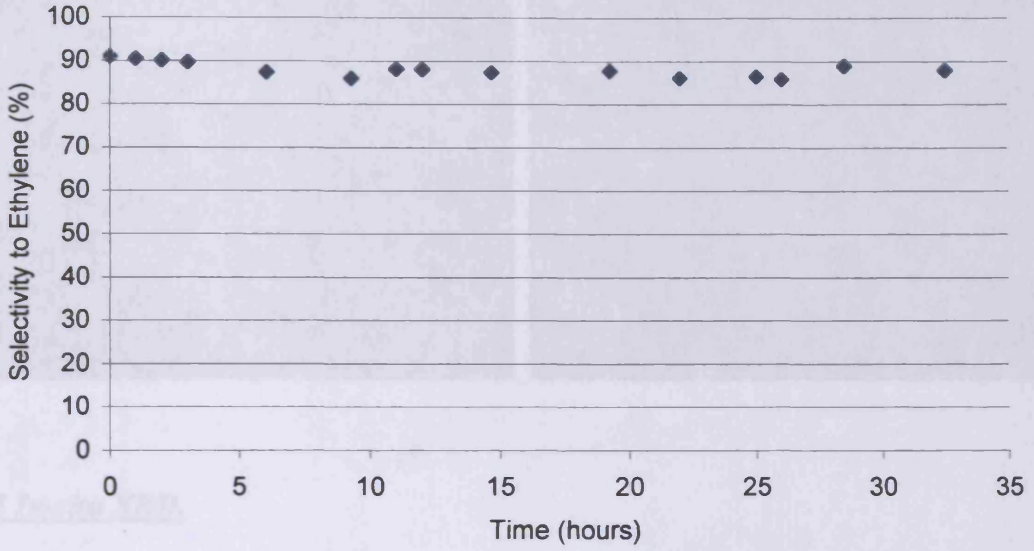

Figure 6.8 – A graph to show selectivity to ethylene as a function of time using $NbPO_5$ from the reduction of niobium oxide phosphate with hydrogen. Analysis carried out at 500°C. $C_2/O_2/He = 30/10/60$

Time on-line studies showed a change in phase of NbP-3 from niobium phosphate, ε-$NbPO_5$ (00-040-0124, JCPDS) to niobium phosphate, $Nb_{1.91}P_{2.82}O_{12}$ (00-051-1738, JCPDS). Both formulae have an orthorhombic space system but the space group is different. ε-$NbPO_5$ has a space group of P_{n*a}, whilst $Nb_{1.91}P_{2.82}O_{12}$ has a space group of P_{bcn}. The major peak in the XRD pattern for ε-$NbPO_5$ was at 20.4 degrees 2-theta, which corresponds to the (121) plane, whereas the major peak in for $Nb_{1.91}P_{2.82}O_{12}$ was at. 20.5, corresponding to the (211) plane.

The SEM images below shows niobium phosphate prepared from the reduction of niobium phosphate using hydrogen. The unused sample (left) is very similar in structure and morphology to the used sample (right) after reaction with ethane.

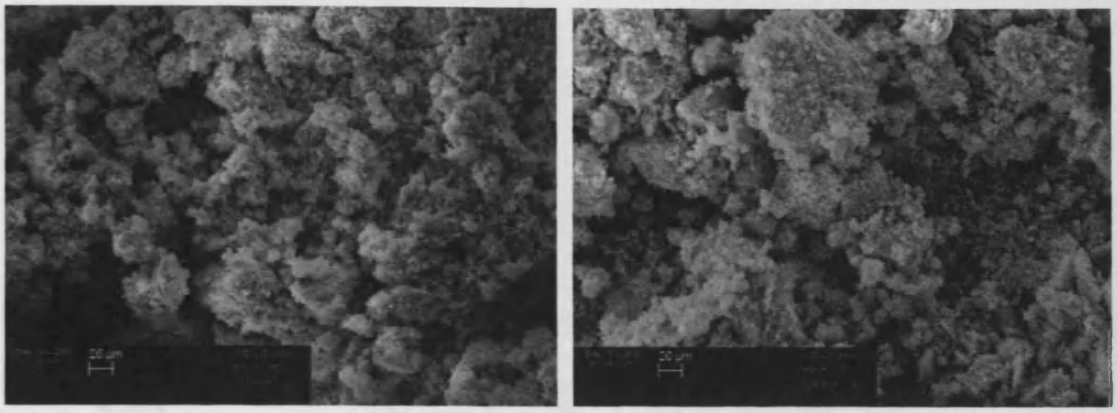

6.5 In-situ XRD.

Time on-line studies were carried out for the ODH of ethane using a niobium phosphate catalyst prepared from the reduction of niobium oxide phosphate with hydrogen. The reaction with ethane was simulated using *in-situ XRD* studies, as shown in figure 6.9. The catalyst initially was dark blue in appearance. According to XRD data, the phase of the catalyst was $NbPO_5$ (00-040-0124, JCPDS). After 6 hours, the catalyst was light blue in colour. This was still the same phase as before, $NbPO_5$ (00-040-0124, JCPDS).

The XRD pattern changes after 32.5 hours reaction with ethane. According to XRD data, the phase of the catalyst changes to $Nb_{1.91}P_{2.82}O_{12}$ (00-051-1738, JCPDS). There is a distinct change in pattern, as if the catalyst became less crystalline.

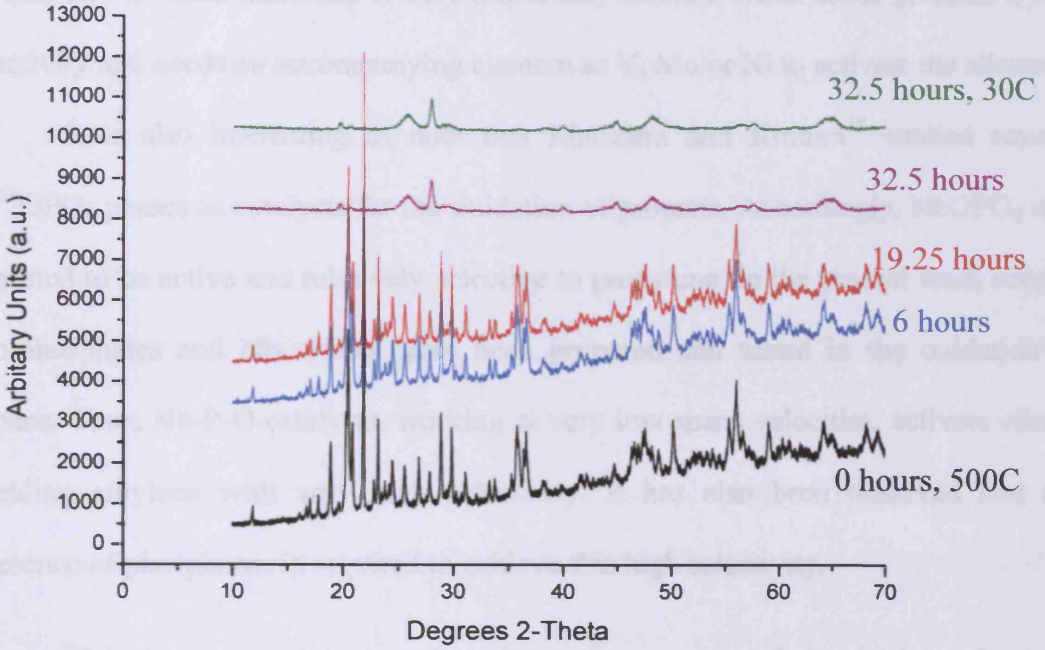

Figure 6.9 – In-situ XRD studies using niobium phosphate prepared from the reduction of niobium oxide phosphate using hydrogen. Analysis carried out at 500°C.

6.6 Discussion.

Many authors agree that the ODH process proceeds via a Mars Van Krevelen redox mechanism[5]. Early transition metal cations are necessary because their oxidation state varies in the course of the reaction. It is also accepted that the adsorption and desorption rates is related to acid-base properties.

Vanadium oxide based catalysts have been considered for many years the catalysts of choice for the oxidative dehydrogenation of ethane to ethylene[6,7,8,9,10]. However, currently mixed metal oxide catalysts containing niobium seem to perform more efficiently for this reaction. Mo-V-Nb[11], Mo-V-Te-Nb-O[12,13,14] and Ni-Nb-O[15,16,17] catalysts present higher selectivity to ethylene and can work at lower reaction

temperatures than conventional supported vanadium catalysts. Although the presence of niobium in these materials is very important, niobium oxide alone presents a low reactivity and needs an accompanying element as V, Mo or Ni to activate the alkane.

It is also interesting to note that Matsuura and Kimura[18] studied several $M^{5+}OPO_4$ phases as catalysts for the oxidation of propane. Accordingly, $NbOPO_4$ was reported to be active and relatively selective to propylene. In the present work several Nb-phosphates and Nb oxides have been prepared and tested in the oxidation of ethane. Thus, Nb-P-O catalysts, working at very low space velocities, activate ethane yielding ethylene with very high selectivity. It has also been observed that the presence of phosphorus is required to achieve this high selectivity.

Phosphorus-containing catalysts have shown a remarkably higher selectivity for the oxidative dehydrogenation of ethane to ethylene than the P-free catalysts. Thus Figure 2 shows the variation of the selectivity to ethylene with the ethane conversion for the different catalysts tested. Catalysts without phosphorus present a low selectivity to ethylene (ca 15% at 5% conversion) in contrast with those containing P (75-95% at 5% conversion).

Among the P-containing catalysts $NbPO_5$ (prepared from the reduction of niobium oxide phosphate with hydrogen) was the most selective to ethylene. The order of selectivity to ethylene of the NbP-series was as follows: NbP-3 (95% at ethane conversions of 5%) > NbP-2 (85%) > NbP-1 (78%).

Ethane activation is not due to a homogeneous gas phase process as the conversion from the blank experiments under the same conditions was negligible. The observation of ethane activation is quite unexpected taking into account that Nb_2O_5 demonstrates a low reducibility[19], as Wachs and co-workers observed that the reduction of Nb_2O_5 with hydrogen was initiated at ca. 800ºC. Catalyst reducibility

would be expected to be important as the oxidative dehydrogenation of ethane to ethylene proceeds mainly by a redox mechanism[20,21]. However, the selectivity to ethylene obtained on our Nb-oxide catalysts was relatively low.

The addition of another element, such as P, in niobium phosphate structures, has led to a remarkable increase in the selectivity to ethylene although, at this early stage of investigation, the catalyst conversion is relatively low. The explanation for the observed promoter effect of phosphorus in this reaction is not straightforward. The addition of P modifies both the acidic and the redox characteristics of the niobium oxide. For example, niobium (V) oxides have an acid strength ($H_0 \leq -5.6$), whereas niobium phosphate has a higher acid strength of $H_0 \leq -8.2$[18,19]. In particular, the acidity of the support used to produce supported vanadium oxide catalysts is an important factor for the selective oxidation of ethane to ethylene, as increased acidity was beneficial for ethylene production[22].

Figure 6.10 shows a comparison of niobium catalysts tested in this chapter in comparison to other catalysts which have high yields for the ODH of ethane. The first key point to note is that Mo-V-Te-Nb-O catalysts reach a much higher conversion in comparison to niobium catalysts. The next point to note is that niobium oxides have a very low conversion and selectivity to ethylene.

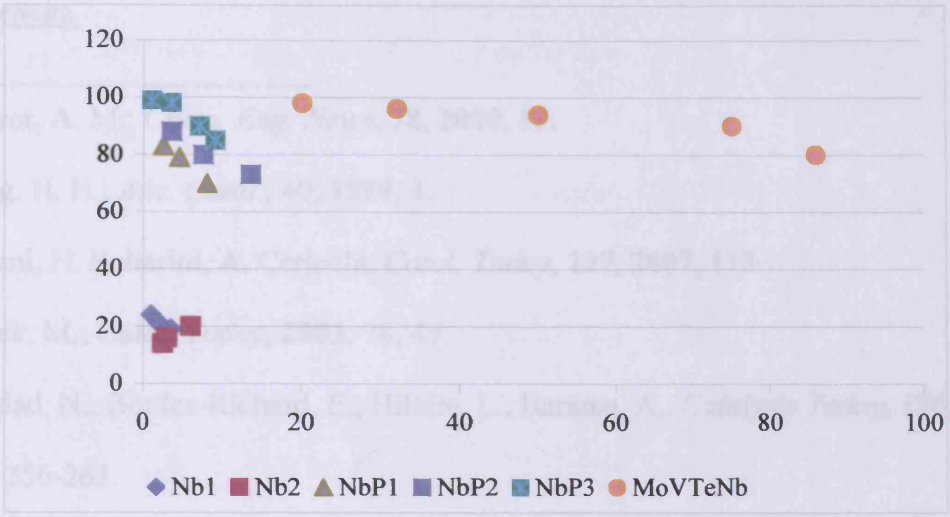

Figure 6.10 – A graph to show selectivity of ethylene as a function of ethane conversion using niobium based catalysts and comparing to MoVTeNbO catalyst.

6.7 Conclusions.

Several Nb-phosphates have been prepared, characterized and tested as catalysts for the oxidation of ethane. These catalysts have shown a very high selectivity to ethylene, although the catalytic results obtained depend on the nature of the Nb-phosphate. Orthorhombic $Nb_{1.91}P_{2.82}O_{12}$ was the most efficient crystalline phase of those investigated. In addition, it has been demonstrated that the presence of phosphorous is required to achieve this high selectivity, as Nb-oxide catalysts showed far inferior performance.

References.

[1] Thayer, A. M.; *Chem. Eng. News*, 78, **2000**, 19.

[2] Kung, H. H.; *Adv. Catal.*, 40, **1994**, 1.

[3] Cavani, N. Ballarini, A. Cericola, *Catal. Today*, 127, **2007**, 113.

[4] Ziolek, M.; *Catal. Today*, **2003**, 78, 47.

[5] Naddad, N., Bordes-Richard, E., Hilaire, L., Barama, A., *Catalysis Today*, 126, **2007**, 256-263.

[6] Bañares, M. A., Khatib, S. J.; *Catal. Today*, 96, **2004**, 251.

[7] Bañares, M.; *Catal. Today*, 51, **1999**, 319.

[8] Dai, H. X., Au, C. T.; *Current Topics Catal. vol. 3*, **2002**, 33.

[9] López Nieto, M.; *Topics Catal.*, 41, **2006**, 3.

[10] Cavani, F., Trifirò, F.; *Catal. Today*, 24, **1995**, 307.

[11] Thorsteinson, M., Wilson, T. P., Young, F. G., Kasai, P. H.; *J. Catal.*, 52, **1978**, 116.

[12] López Nieto J. M., Botella, P., Vázquez, M. I., Dejoz, A.; *Chem. Commun.* **2002**, 1906.

[13] Solsona, B., Vázquez, M. I., Ivars, F., Dejoz, A., Concepción, P., López Nieto, J. M.; *J. Catal.*, 252, **2007**, 271.

[14] Botella, P., García-González, E., Dejoz, A., López Nieto, J. M., Vázquez, M. I., González-Calbet, J.; *J. Catal.*, 225, **2004**, 428.

[15] Heracleous, E., Lemonidou, A. A.; *J. Catal.*, 237 **2006**, 162.

[16] Liu, Y.; *US Patent 7227049B2*, **2007**.

[17] Heracleous, E., Lee, A. F., Wilson, K., Lemonidou, A. A.; *J. Catal.*, 231, **2005**, 159.

[18] Matsuura, I., Kimura, N.; *Stud. Surf. Sci and Catal.*, 82, **1994**, 271.

[19] Wachs, I. E, Briand, I. E., Jehng, J. M., Burcham, L., Gao, X.; *Catal. Today*, 57, **2000**, 323.

[20] Kung, H. H., Kung, M. C.; *Appl. Catal. A: General*, 157, **1997**, 105.

[21] Blasco, T., López Nieto, J. M.; *Appl. Catal. A: General*, 157, **1997**, 117.

[22] Sun, Q., Auroux, A., Shen, J.; *J. Catal*, 244, **2006**, 1.

7. *Conclusions and Future Work.*

Various phases of niobium oxides, niobium oxide phosphates and niobium phosphates have been tested for catalytic activity using three probe reactions. The probe reactions that were chosen were methanol partial oxidation to formaldehyde, propane oxidative dehydrogenation and ethane oxidative dehydrogenation.

Niobium oxides were prepared by a variety of methods, including oxidation and precipitation reactions. Oxidation reactions produced an orthorhombic phase, whereas precipitation reactions produced a monoclinic phase, according to XRD. Surface areas measured by nitrogen adsorption were between 7 and 12m^2/g.

It was found that conversion of methanol for all niobium oxides, apart from niobium oxide produced from the oxidation of niobium ethoxide were low. Typically, conversion of methanol was <5% at 400°C. The selectivity to formaldehyde for all niobium oxide catalysts was 100% when the catalysts became active, but the complete selectivity for each catalyst decreased to varying amounts at 400°C. The catalyst with the highest selectivity to formaldehyde at 400C out of all niobium catalyst was the catalyst prepared from the oxidation of niobium metal and niobium oxide purchased from Aldrich; these gave selectivity to formaldehyde of 85%. The best niobium oxide catalyst produced was the oxidation of niobium ethoxide, which produced 72% conversion with 65% selectivity to formaldehyde. Niobium oxides have low conversion of methanol with high selectivity to formaldehyde. Niobium, oxygen and phosphorus catalysts have high conversion of methanol and high selectivity to formaldehyde.

All niobium oxide catalysts produced low conversion of propane in the oxidative dehydrogenation reaction studied. Catalysts became active at 300-350°C. The highest conversion of propane recorded using niobium oxide was 1.2% at 500°C. This was recorded using niobium oxide prepared from the precipitation of niobium chloride and urea. All other niobium oxides produced conversions of <1%. Selectivity to propene varied from 25-60% at 500°C. The selectivity to propene decreased rapidly when each niobium oxide catalyst became active. After the initial decrease in selectivity, the selectivity to propene remained constant. Niobium catalysts discussed in this investigation have low conversion of propane, whilst selectivity to propene decreases with increasing temperature.

Two niobium oxide catalysts were tested for the oxidative dehydrogenation of ethane to ethylene. Niobium oxide prepared from the precipitation of niobium chloride and urea showed the highest conversion of ethane, but a very low selectivity to ethylene. Niobium oxide which was purchased from Aldrich produced a lower conversion of ethane but a high selectivity to ethylene.

Niobium oxide phosphates were prepared using two different types of phosphoric acid. Both produced the same form of niobium oxide phosphate, according to XRD data. Also, the surface areas of the catalysts were similar. There was a large difference in catalytic activity of the catalysts for methanol oxidation. Using ortho-phosphoric acid produced approximately double the conversion in comparison to using pyro-phosphoric acid. Selectivity to formaldehyde for both catalysts was high, above 95%.

As with niobium oxides, niobium oxide phosphates showed low conversion of propane in propane oxidative dehydrogenation. Both niobium oxide phosphate catalysts showed conversion of propane of <1% at 500C, with selectivity to propene between 35 using pyro-phosphoric acid and 60% using ortho-phosphoric acid. Only one niobium oxide phosphate was tested for the oxidative dehydrogenation of ethane. This produced a conversion of ethane of 5% with high selectivity to ethylene.

Niobium phosphates were prepared by a variety of methods, mainly reduction of niobium oxide phosphate. This was performed using reduction with different alcohols and calcination under hydrogen.

The best catalyst for methanol oxidation was niobium phosphate prepared from the reduction of niobium oxide phosphate with hydrogen. This produced 90% conversion of methanol with 90% selectivity to formaldehyde at 400°C. Niobium oxide phosphates produced from the reduction of niobium oxide phosphate using alcohols produced a similarly high conversion of methanol, but a lower (<50%) selectivity to formaldehyde.

Niobium phosphates produced the lowest conversion of all groups of catalysts for the oxidative dehydrogenation of propane. Conversions of propane were <0.5% for all niobium phosphate catalysts, with selectivity to propene varying between 40 and 60%. C-H bonds on the secondary carbon will be weaker so it would be expected that propane ODH would give better results than ethane ODH. This may give an indication as to the mechanism for the ODH reaction and the way the molecule needs to bind to the active site.

Only niobium phosphate prepared from the reduction of niobium oxide phosphate with hydrogen was tested for the oxidative dehydrogenation of ethane. This produced the highest conversion of ethane with a high selectivity to ethylene.

MoVTeNb catalysts are used for the oxidative dehydrogenation of ethane. Conversion of ethane reached 80%, with 80% selectivity to ethylene. Niobium catalysts discussed in this investigation retain a high selectivity to ethylene; however conversion of ethane is considerably lower.

The introduction of phosphorous into the catalytic system enhances the activity of the catalyst for both oxidation of methanol and the oxidative dehydrogenation of ethane. However, the addition of phosphorus into the catalyst has little effect for the oxidative dehydrogenation of propane. Phosphorus increases the acidic properties of the catalyst, which enhances the catalytic activity of the catalyst. Also, structural and electronic differences could be different when phosphorus in introduced into the catalyst. Comparing niobium phosphate catalysts to vanadium phosphate catalysts, it is shown that vanadium provides redox ability, whereas phosphorous provides stability in the catalyst.

Further work is needed to develop the niobium based catalysts discussed in this investigation. Suggested future work can be summarised:

- Investigate the effect of supporting the niobium catalysts. Niobium compounds are expensive to produce and supporting niobium would reduce the cost. The mobility of niobium would be significantly reduced.

- Adding dopants (e.g. Pd) into the catalysts. As niobium compounds retain their high selectivity to desired products at higher temperatures, it would be necessary to attempt to increase the conversion of reactant with a known dopant which produces a high conversion of reactant.

- Attempting to increase the surface area of the catalysts. It is possible that as all of the catalysts in this study have a low surface area, there may only be a fraction of active sites available. By increasing the surface area of the catalyst, potentially more active sites within the catalyst would become available, increasing the conversion of reactant.

- Using chlorine-free precursors. Chloride ions are known to be a catalyst poison. By using chlorine-free precursors, it is possible that the selectivity of the catalyst and the conversion of reactants could be further enhanced.

Appendix.

4.2 Nb2(CO3)5 – Calcined to 500C

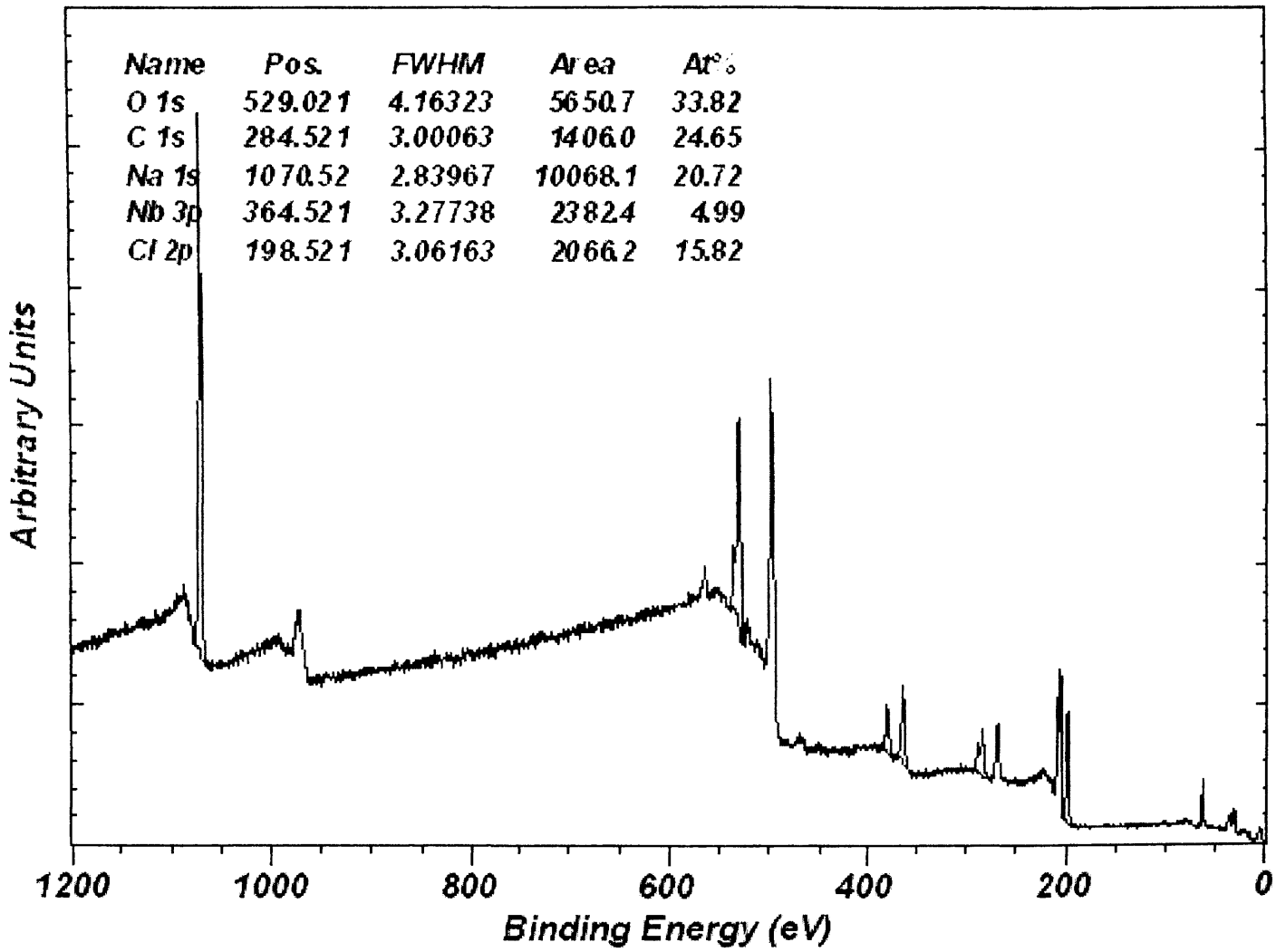

Al(a)

4.2 Nb2(CO3)5 – Calcined to 500C

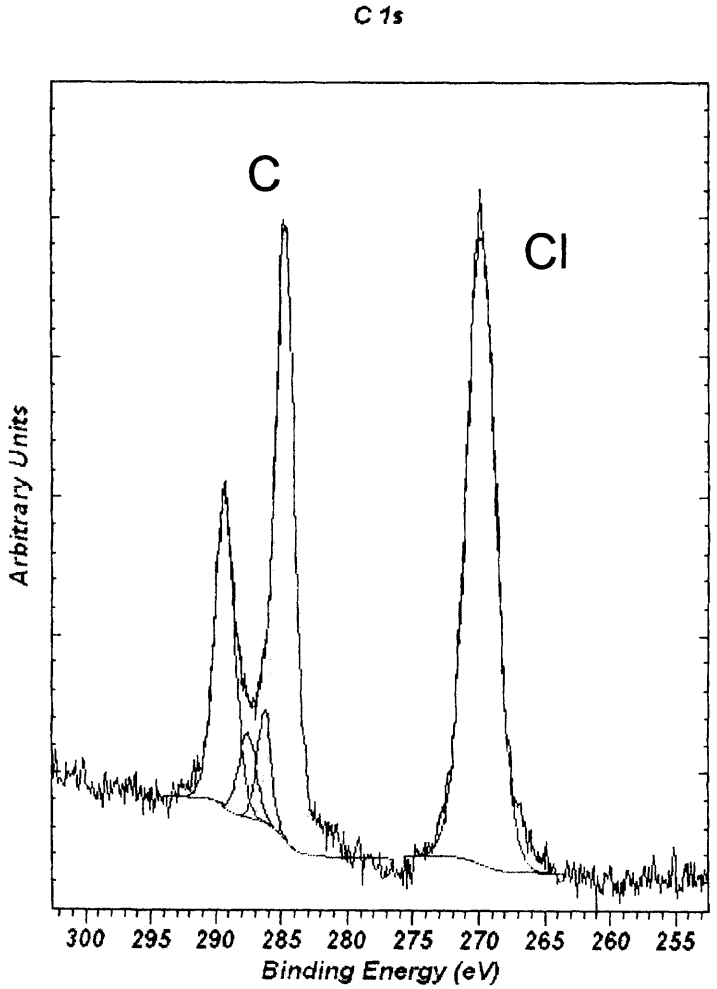

C(1s) Binding Energy	Possible Species
284.7	CHx
286.2 287.5	O-C-O and –CO- bonds
289.3	carbonate

4.2 Nb2(CO3)5 – Calcined to 500C

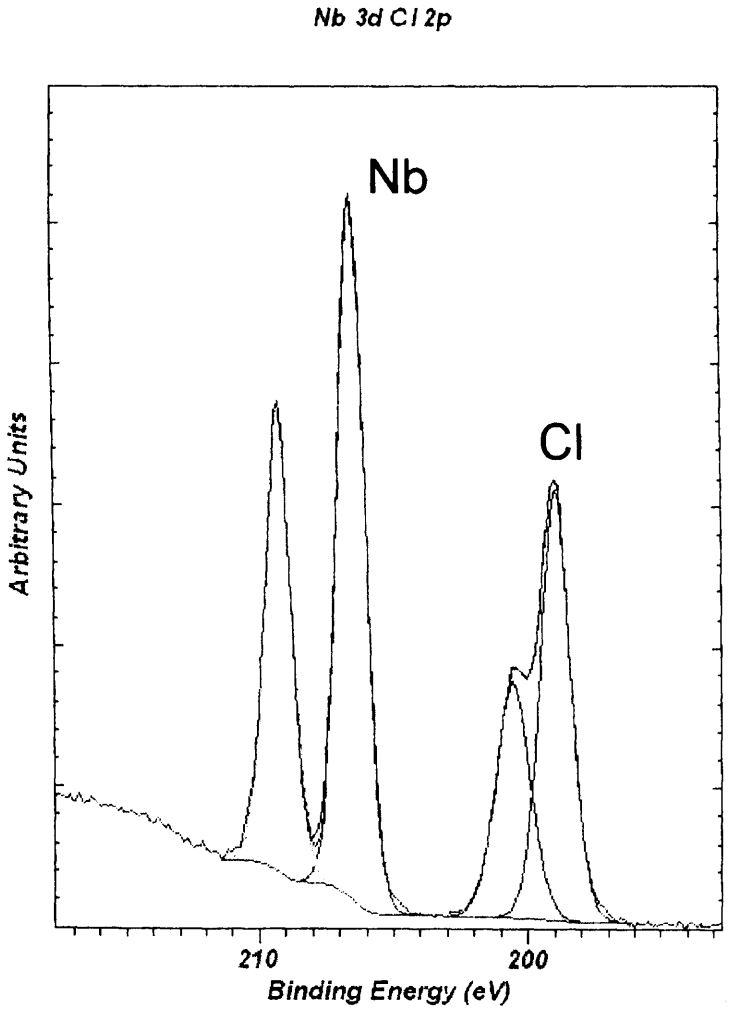

Nb(3d) 5/2 Peak Binding Energy	Ox. State
206.6	+5

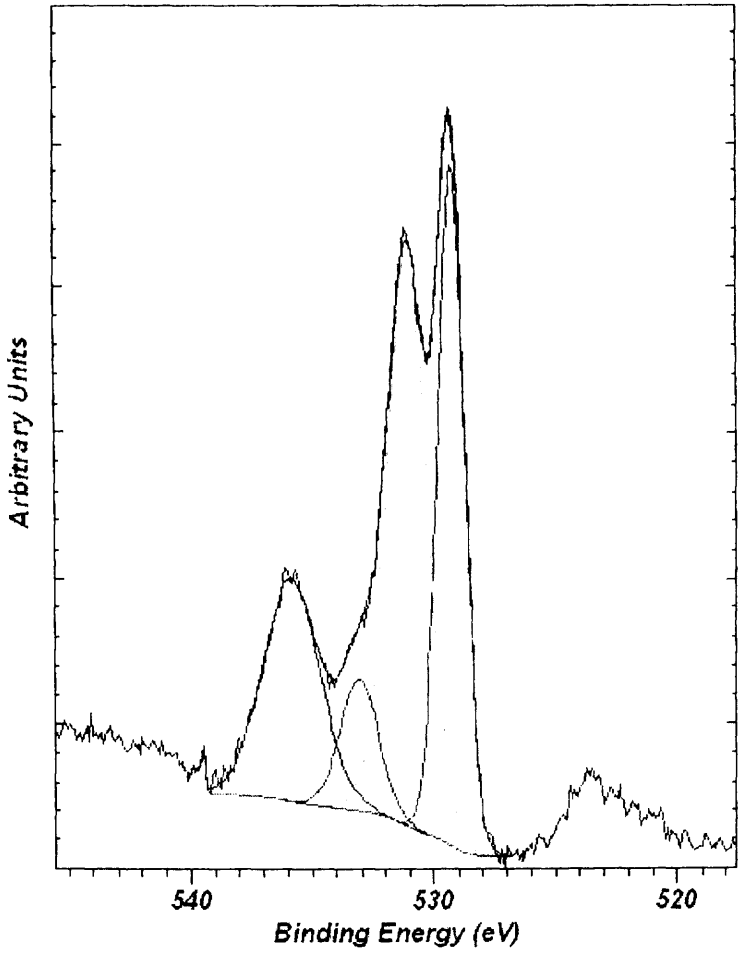

O(1s) Binding Energy	Possible Species
529.3	Oxide
531.1	OH
High Binding energy peaks	due to presence of Sodium (Na-O auger)

A1(c)

Nb_2O_5 4.2c600 – Nb2O5 from Na2CO3 Post MeOH reactor Used

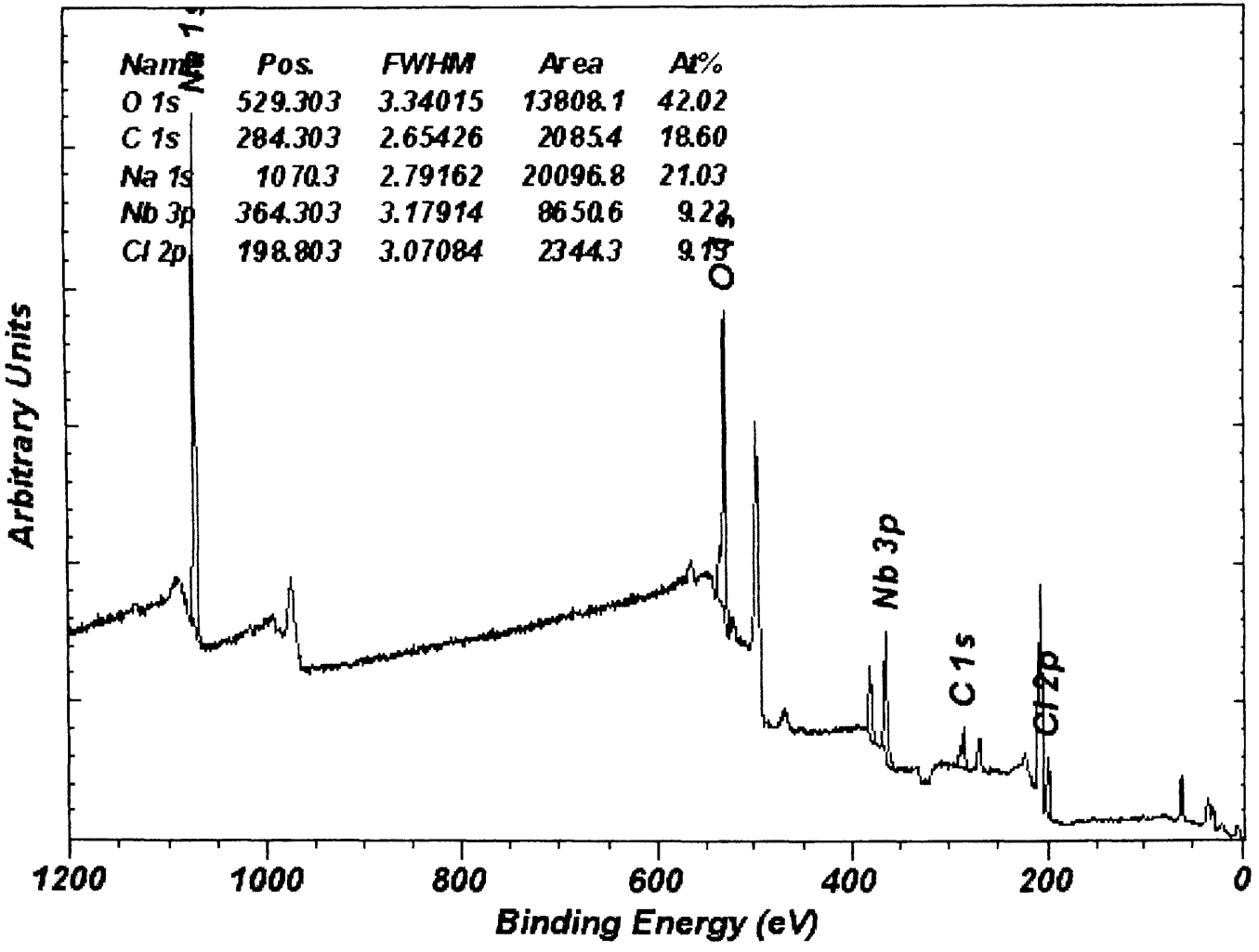

A2(a)

Nb_2O_5 4.2c600 – Nb2O5 from Na2CO3 Post MeOH reactor Used

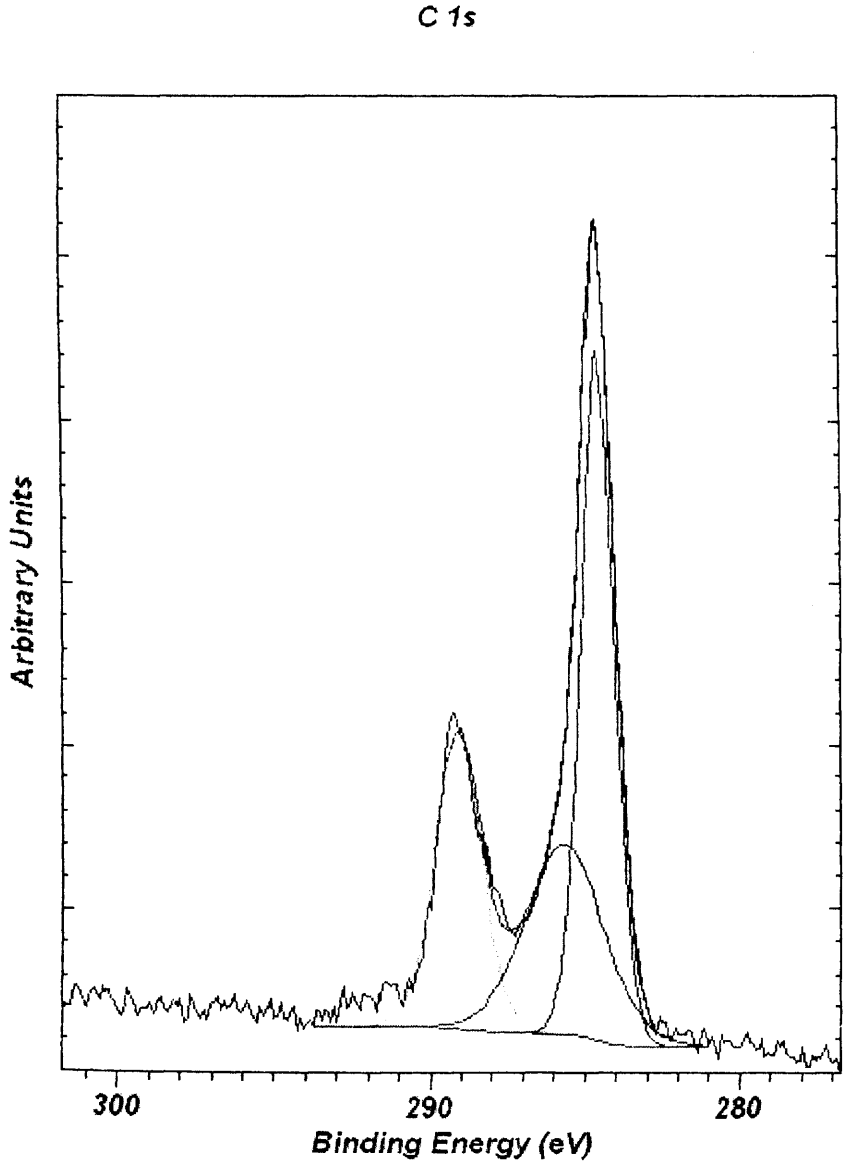

C(1s) Binding Energy	Possible Species
284.7	CHx
285.7	COx groups
289.1	Carbonate

A2(b)

Nb_2O_5 4.2c600 – Nb2O5 from Na2CO3 Post MeOH reactor Used

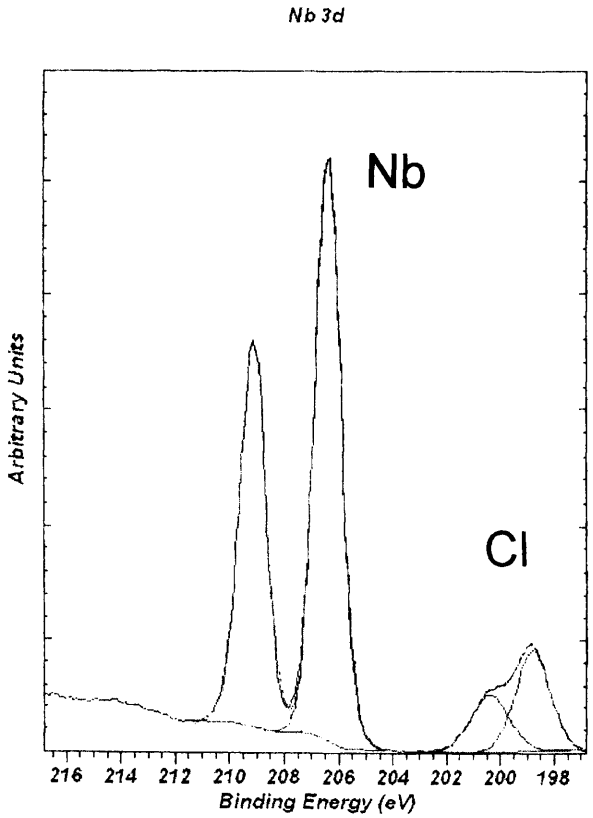

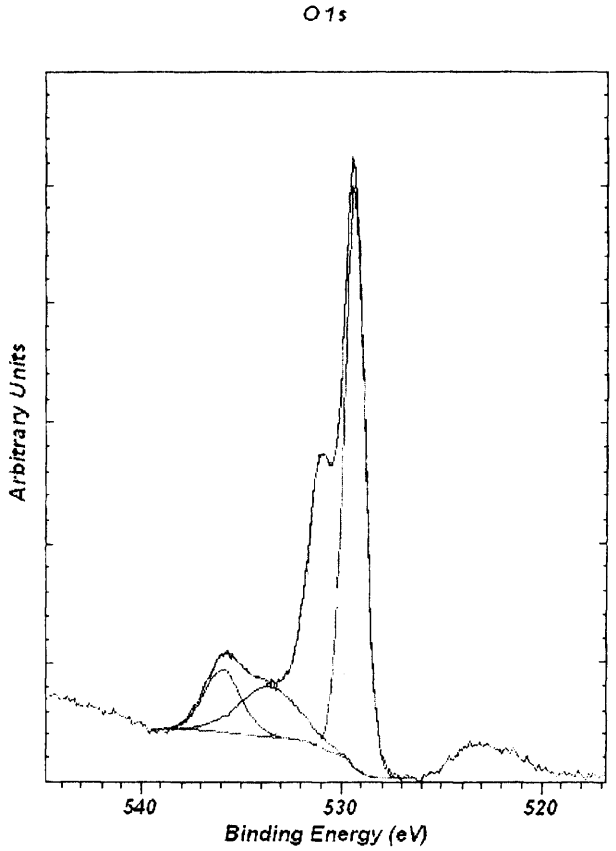

~~Nb(3d) 5/2 Peak Binding Energy~~	~~Ox. State~~
206.4	+5/+4

~~O(1s) Binding Energy~~	~~Possible Species~~
529.4	Oxide
530.9	OH or CO_3
Other high binding energy peaks	Due to presence of Sodium

A2(c)

$NbCl_5$ + urea – 500C Calcined

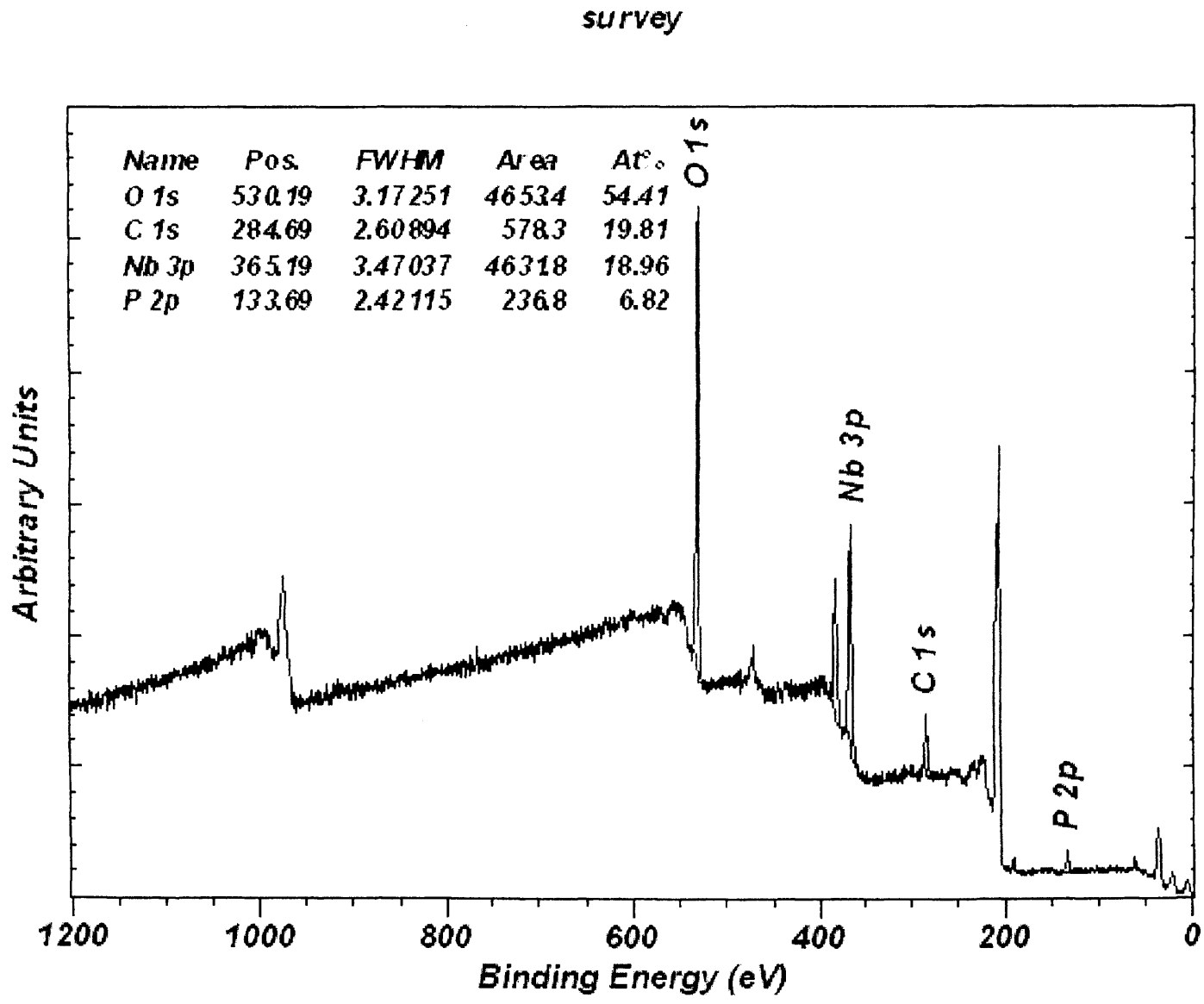

A3(a)

$NbCl_5$ + urea – 500C Calcined

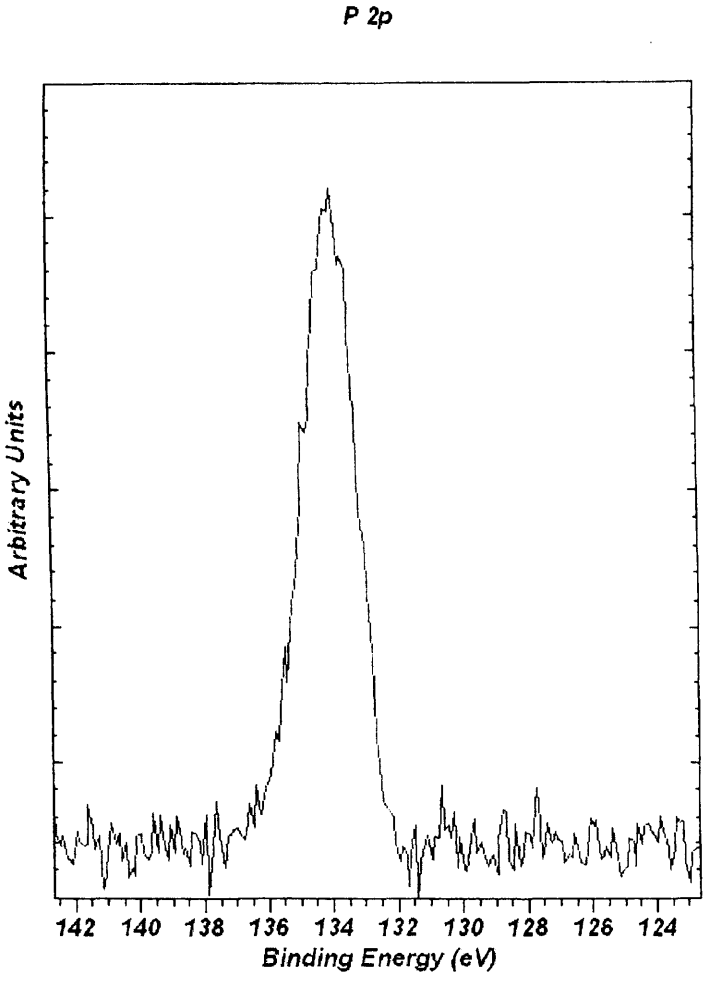

P(2p) Binding Energy	Pos. Species
134.0	$-PO_x$

A3(b)

$NbCl_5$ + urea – 500C Calcined

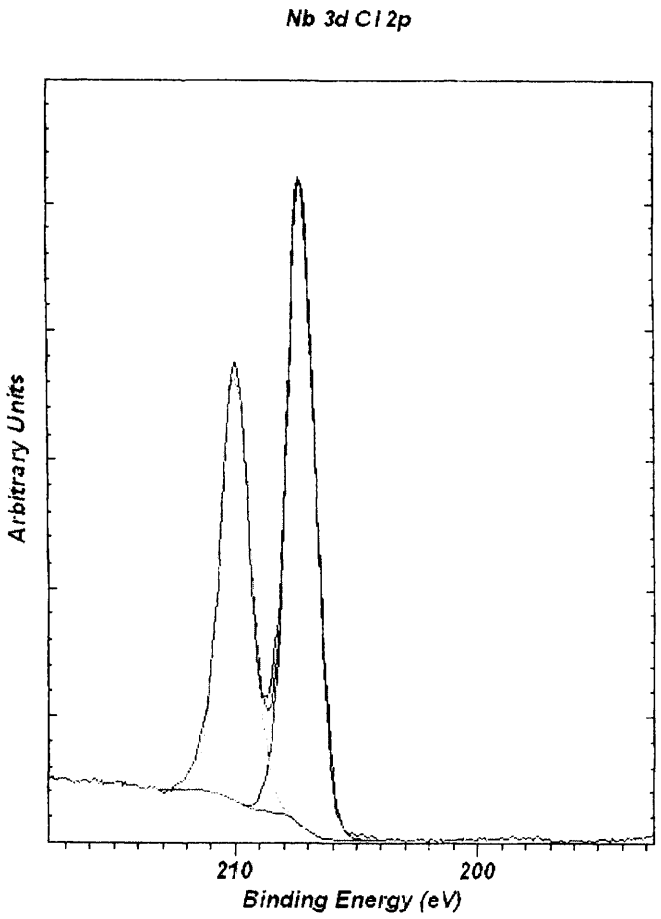

Nb(3d) 5/2 Peak Binding Energy	Ox State
207.2	+5

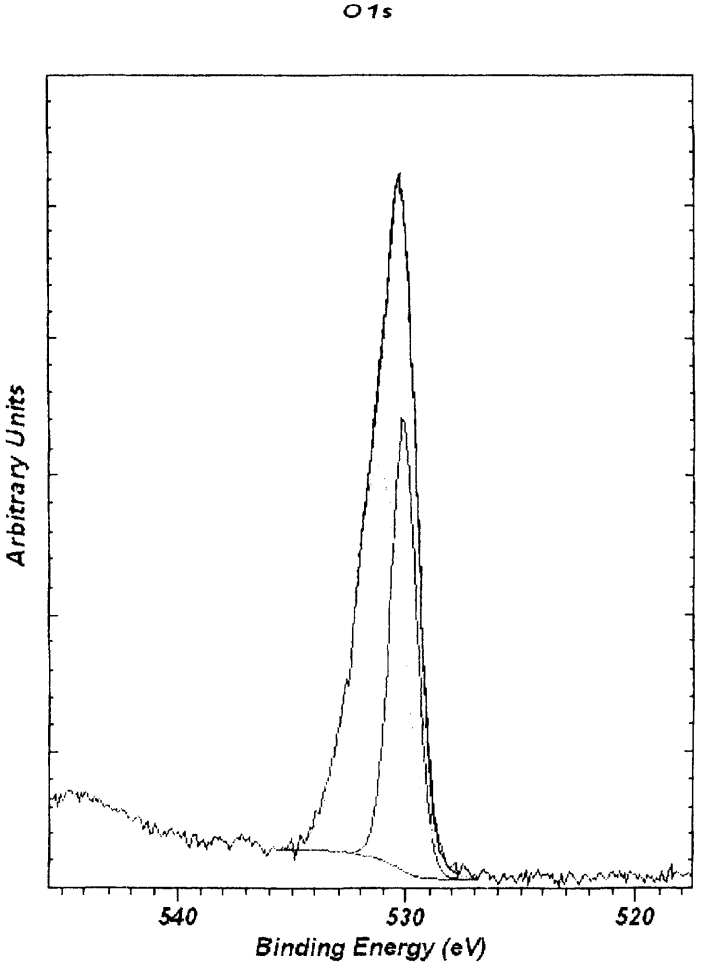

O(1s) Binding Energy	Possible Species
530.1	Oxide
531.2	OH, PO_x (small amount - broad tail)

A3(c)

Nb_2O_5 11c 600 – Nb2O5 from Urea Post MeOH reactor Used

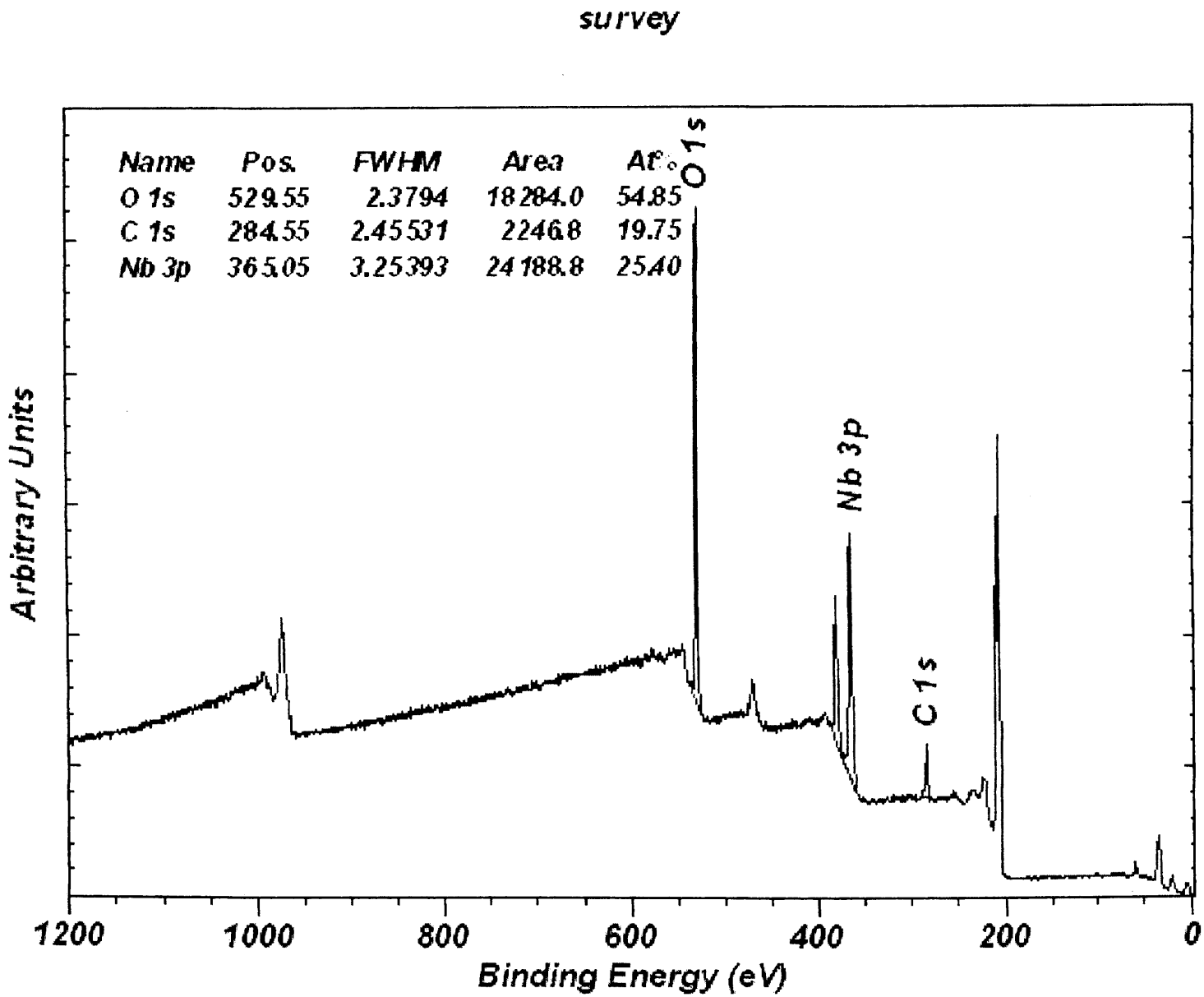

A4(a)

Nb_2O_5 11c 600 – Nb2O5 from Urea Post MeOH reactor Used

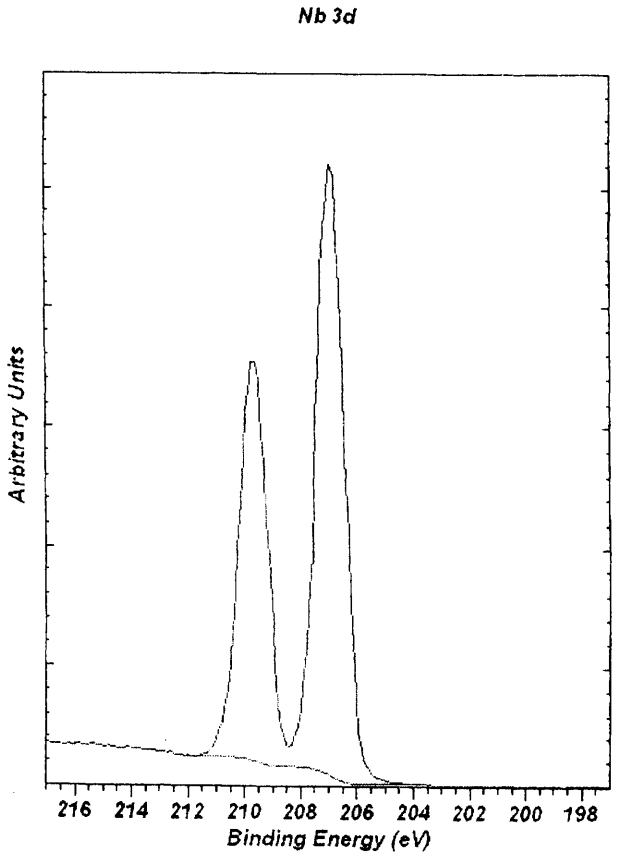

Nb(3d) 5/2 Peak Binding Energy	Ox. State
206.9	+5

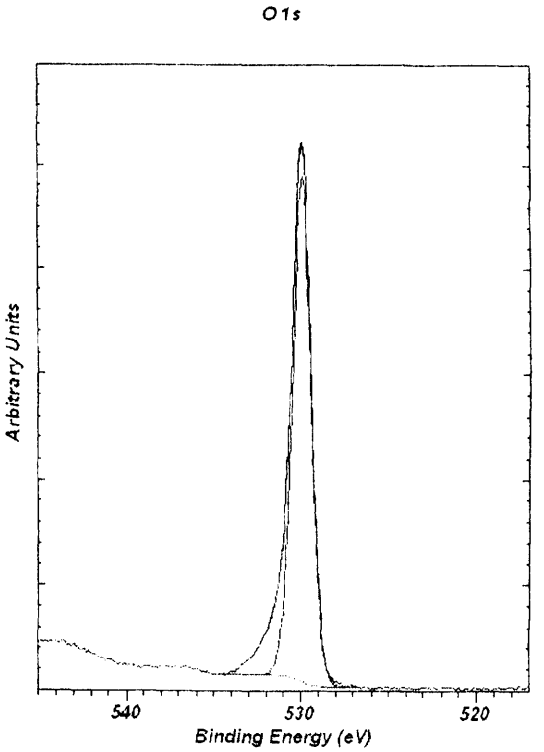

O(1s) Binding Energy	Possible Species
529.9	Oxide
531.1	OH

AH(6)

Nb -> Nb2O5 – 500C Calcined

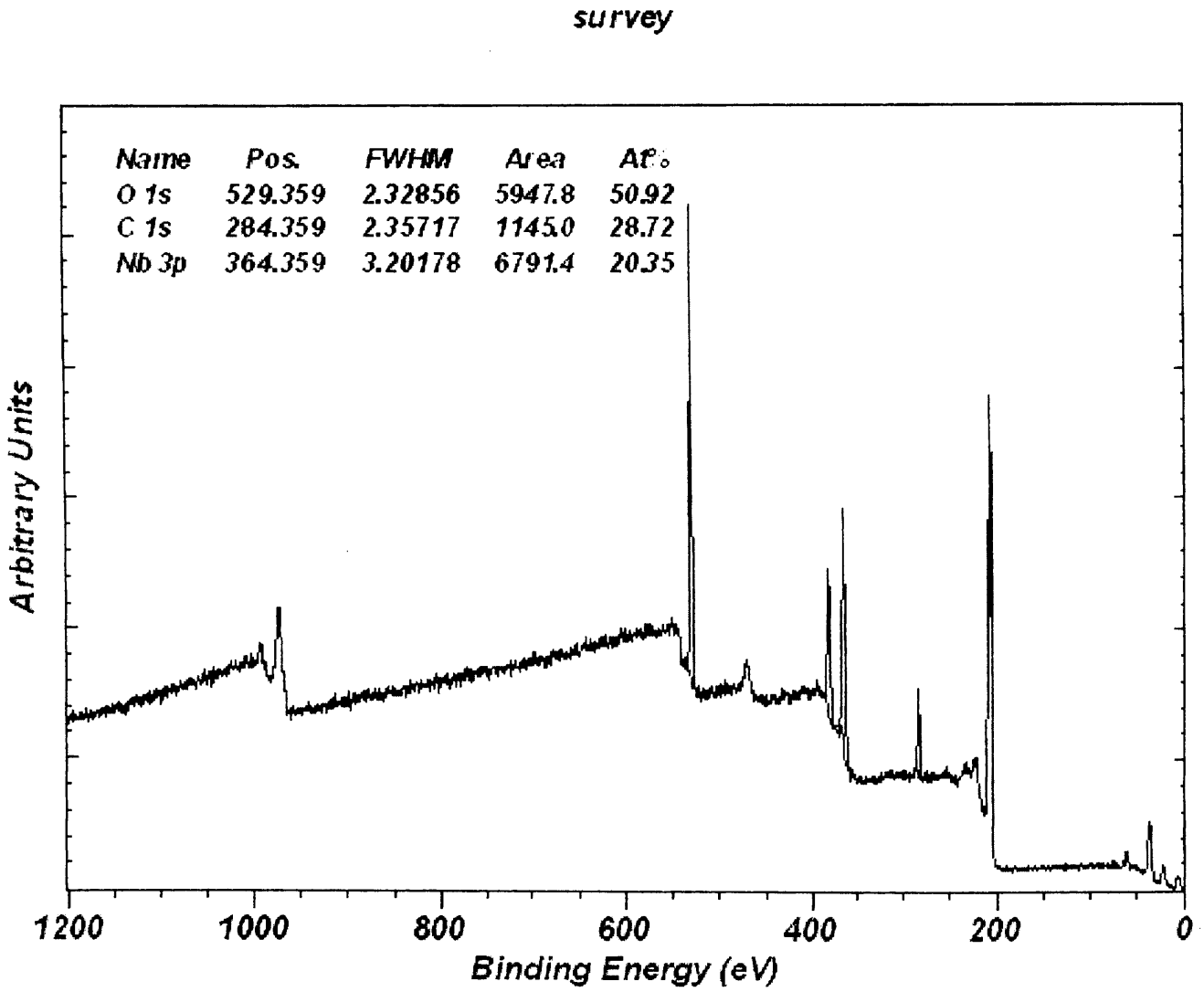

A5(a)

Nb -> Nb2O5 – 500C Calcined

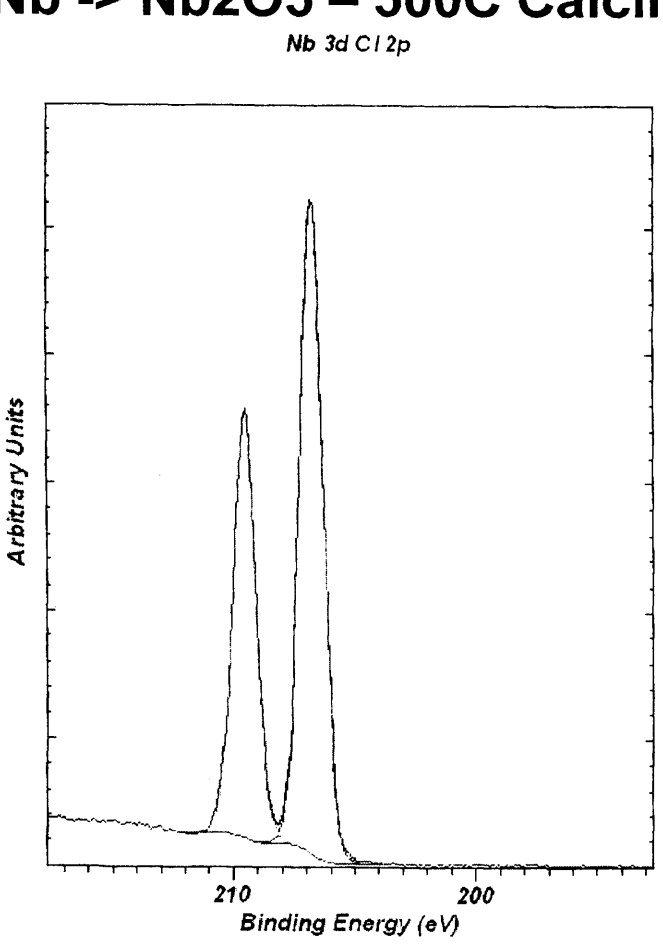

Nb(3d) 5/2 Peak Binding Energy	Ox. State
206.8	+5

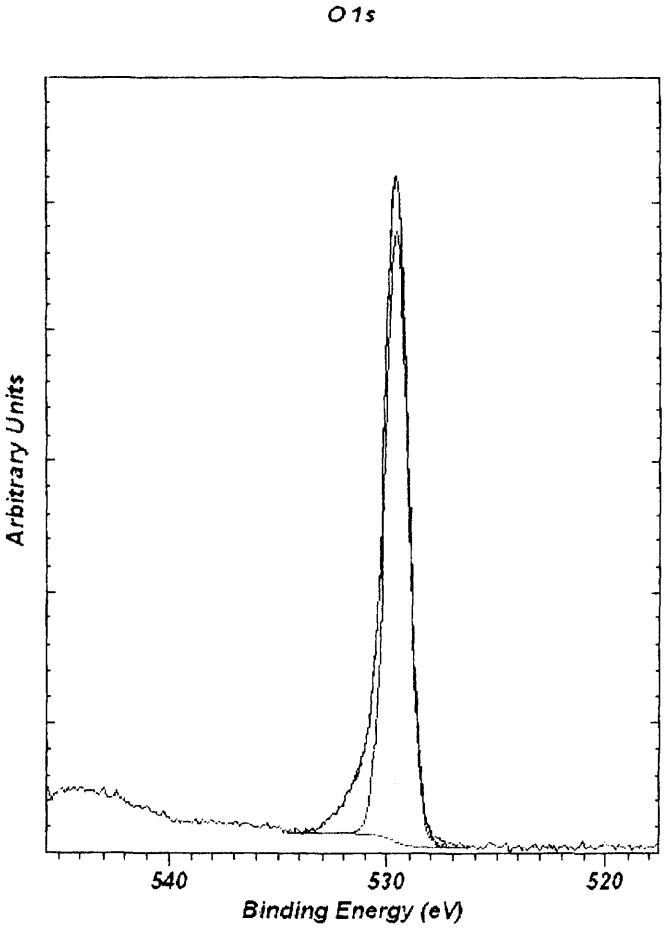

O(1s) Binding Energy	Possible Species
529.6	Oxide
530.5	OH

A5(b)

Nb-> Nb_2O_5 – Nb2O5 from Nb Post MeOH reactor Used

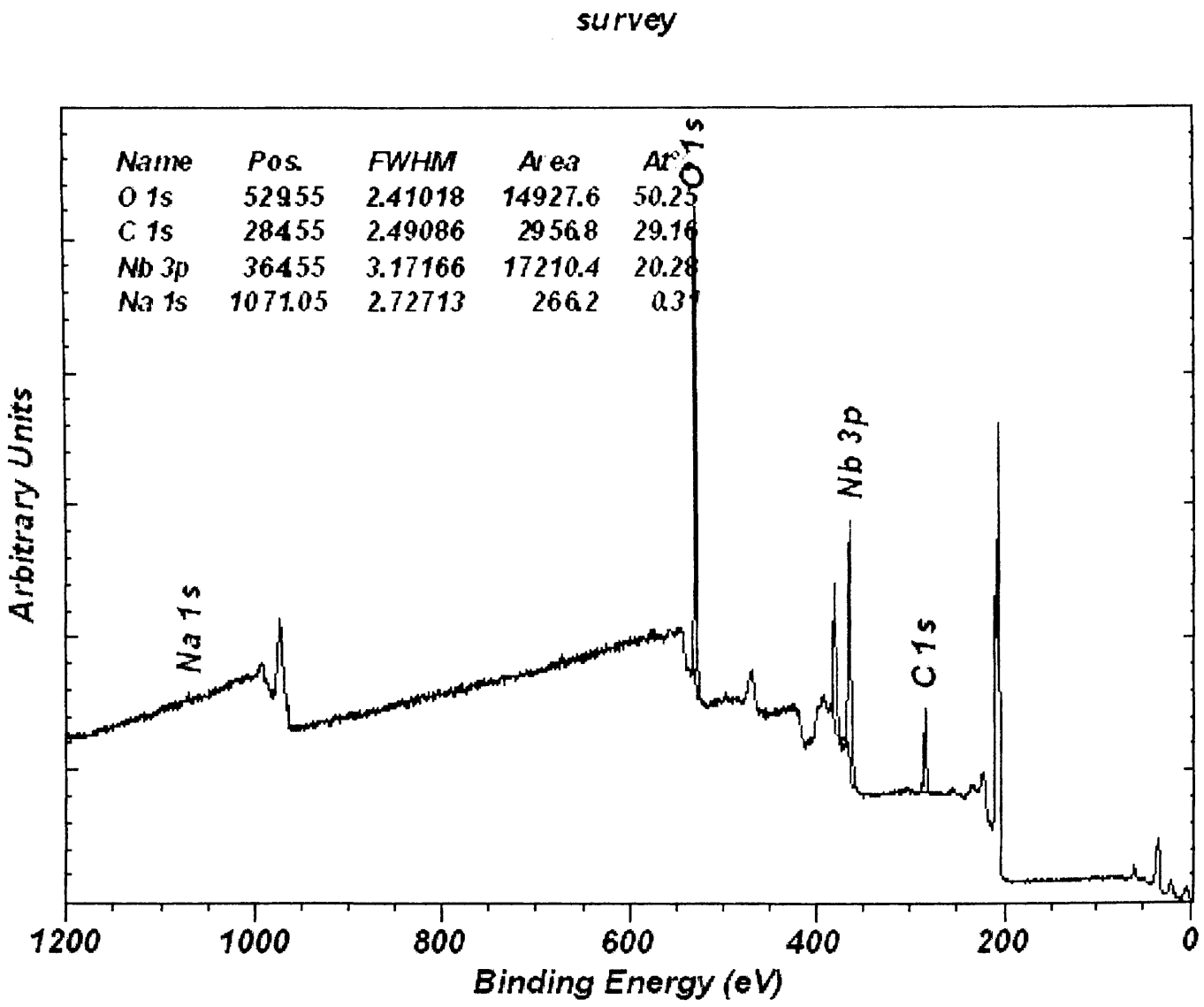

A6(a)

Nb-> Nb_2O_5 – Nb2O5 from Nb Post MeOH reactor Used

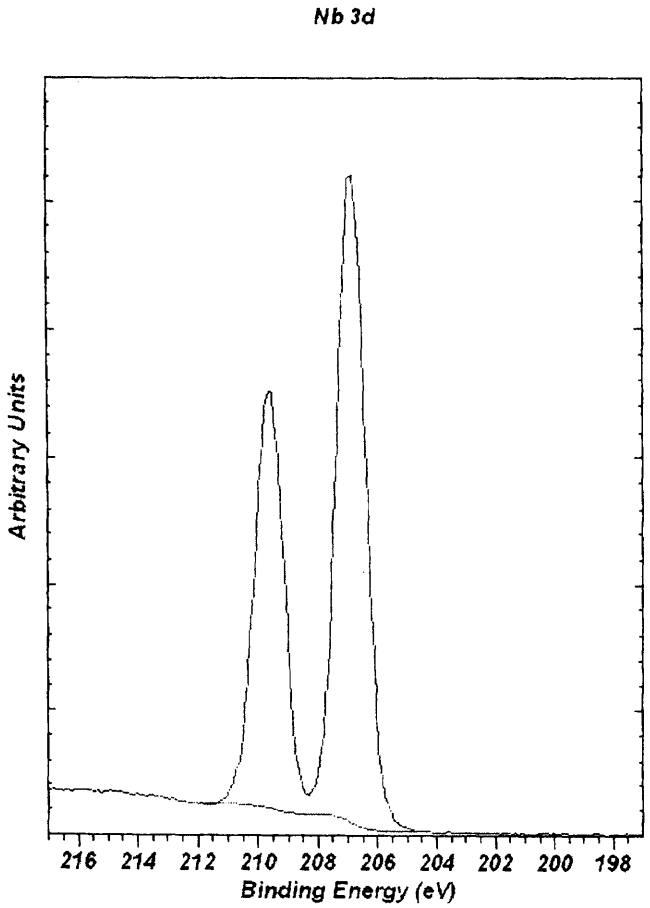

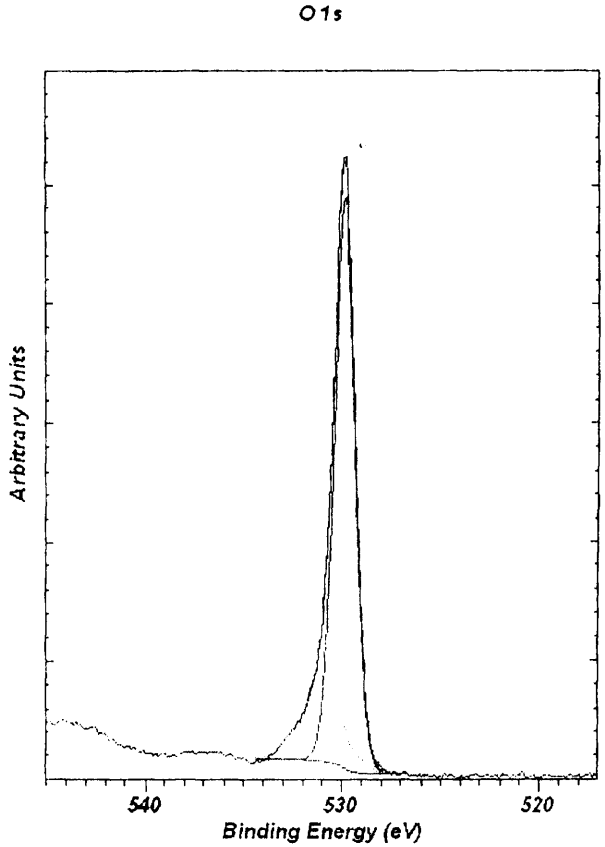

Nb(3d) 5/2 Peak Binding Energy	Ox. State
206.8	+5

O(1s) Binding Energy	Possible Species
529.9	Oxide
531.0	OH

A6(b)

Nb2O5 up 7.2c 450

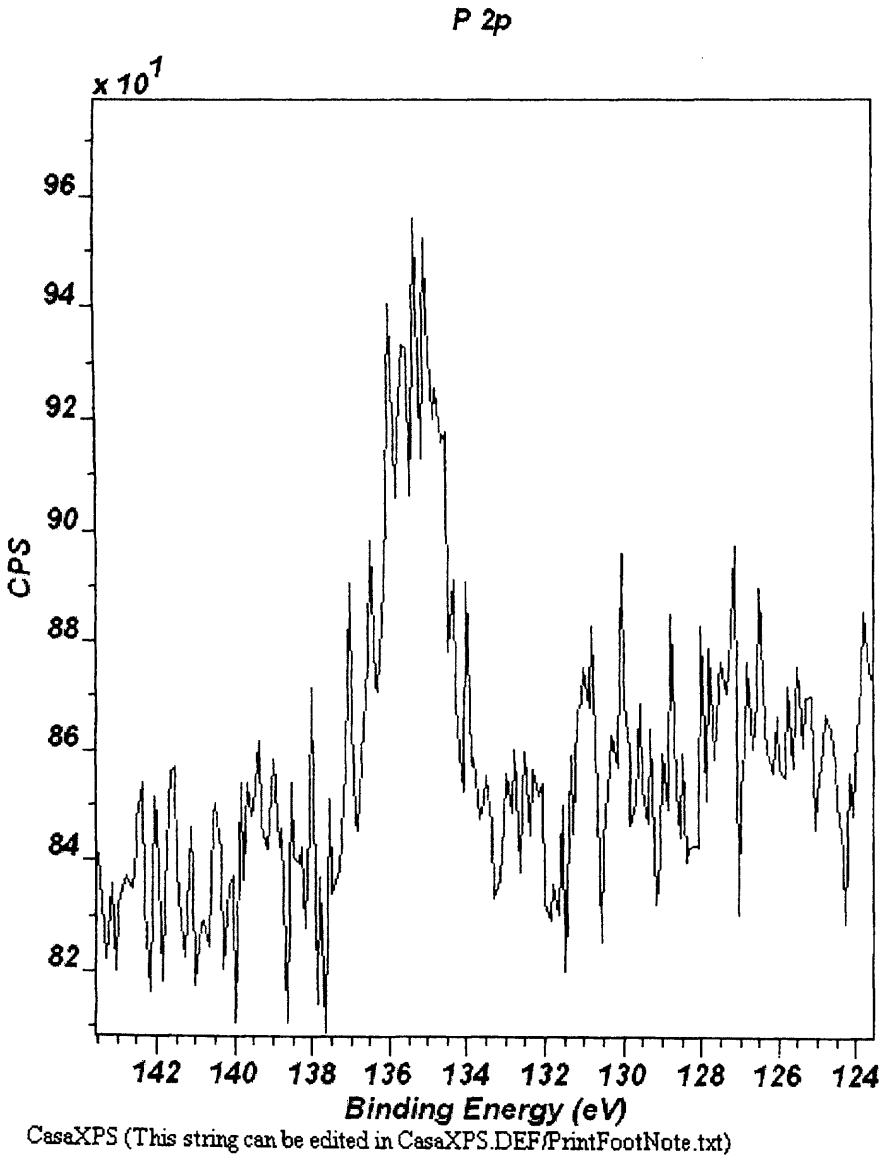

P(2p) Binding Energy	Possible Species
135.3	PO_x Contamination

A7(a)

Nb2O5 up 7.2c 450

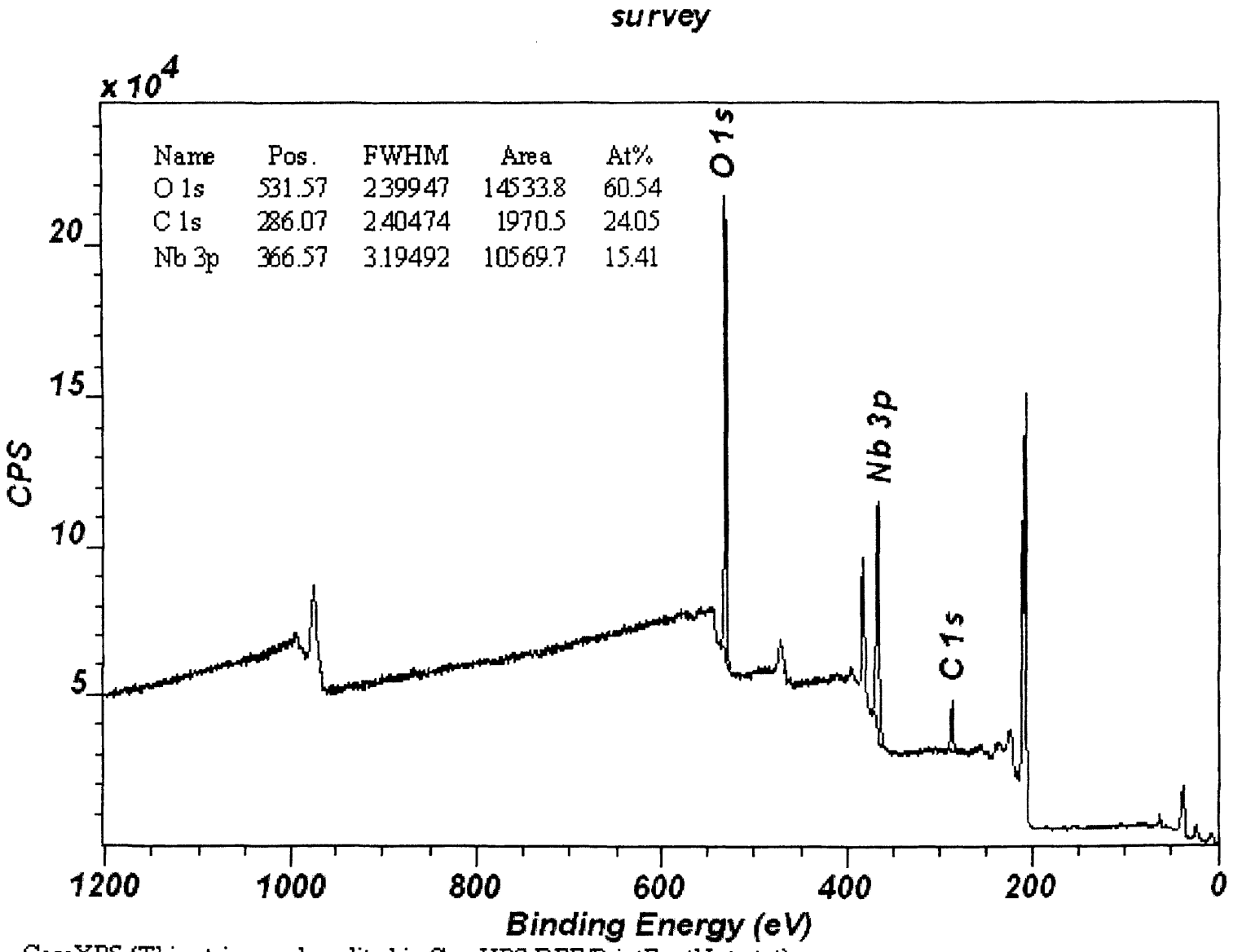

CasaXPS (This string can be edited in CasaXPS.DEF/PrintFootNote.txt)

A7(b)

Nb(OEt)5 → Nb2O5 – After heating >400 C (Contains Glass Wool)

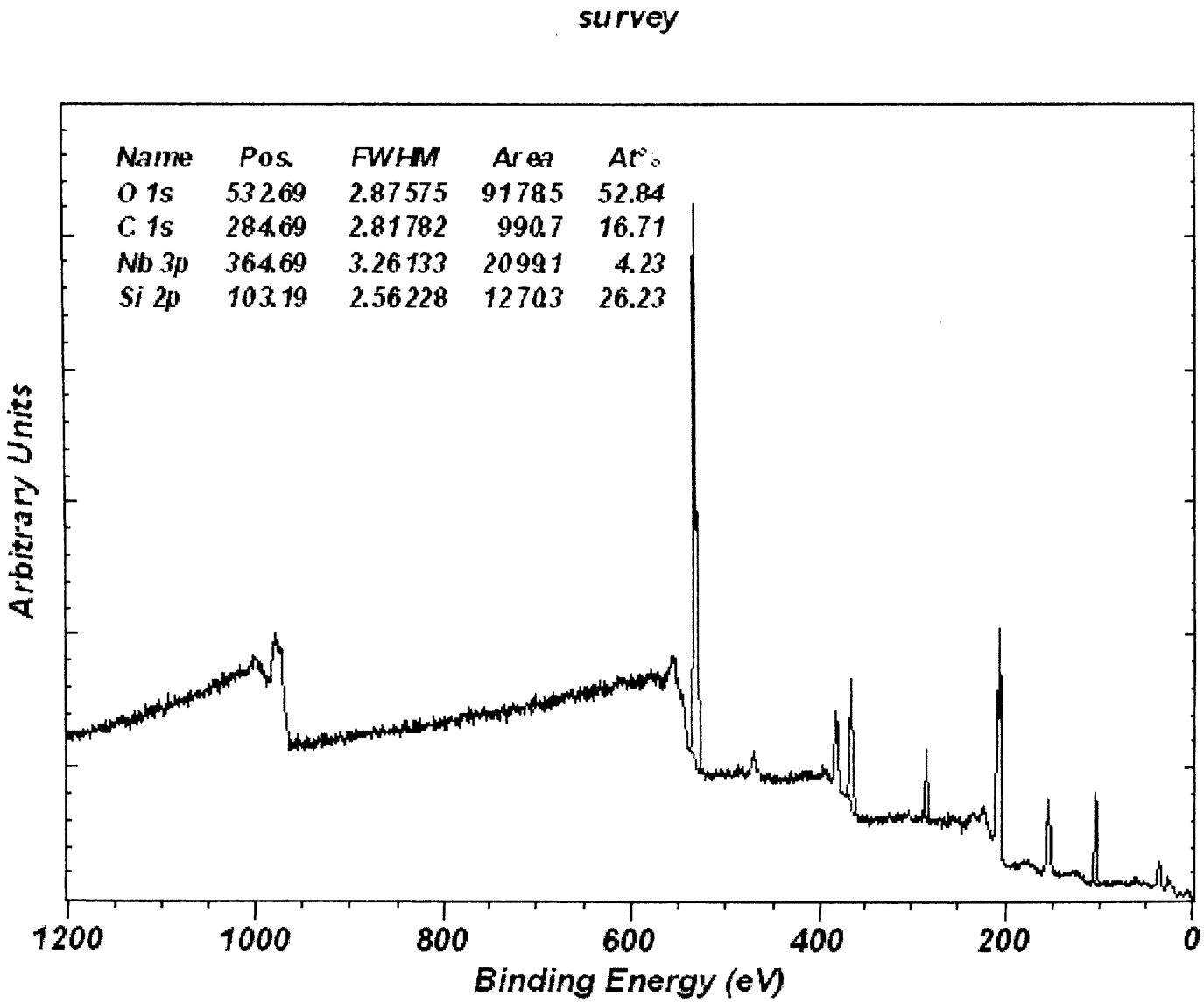

A8(a)

Nb(OEt)5 → Nb2O5 – After heating >400 C (Contains Glass Wool)

MPOH

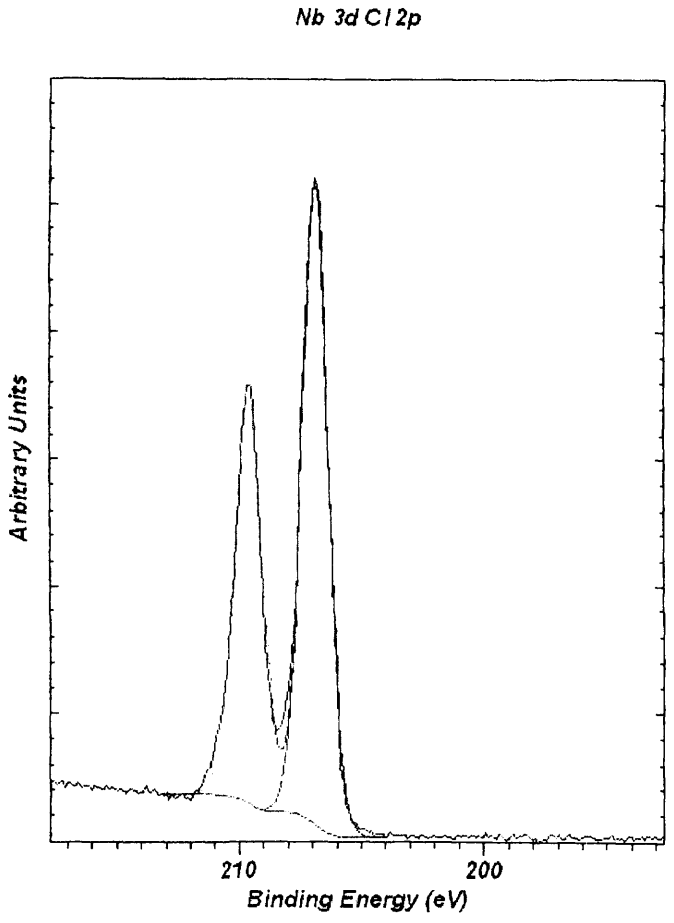

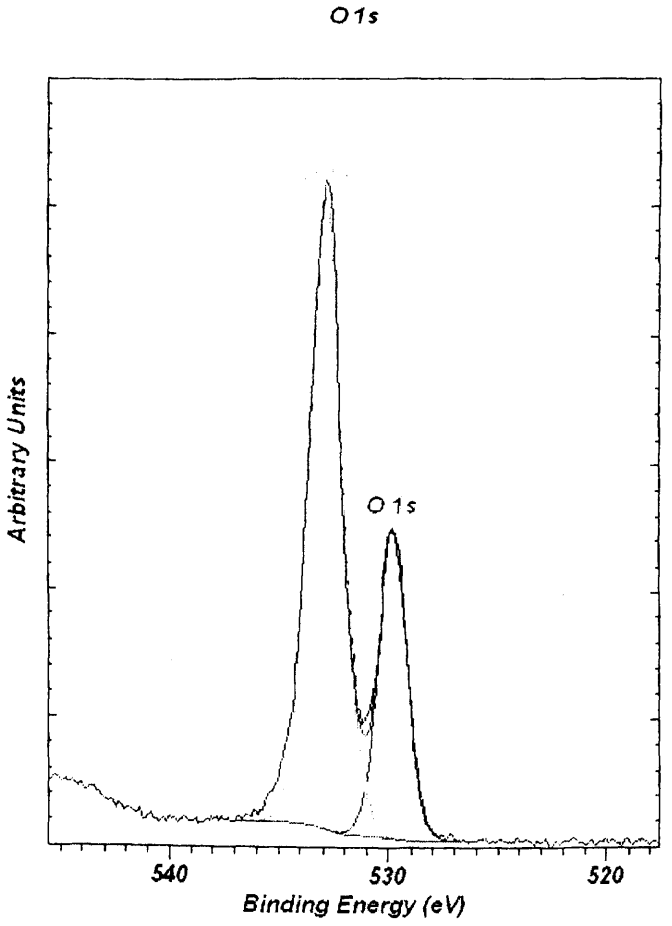

Nb(3d) 5/2 Peak Binding Energy	Ox. State
206.9	+5

O(1s) Binding Energy	Possible Species
529.9	oxide
532.8	SiO2

A8(6)

Nb2O5 Aldrich – Aldrich supplied Nb2O5

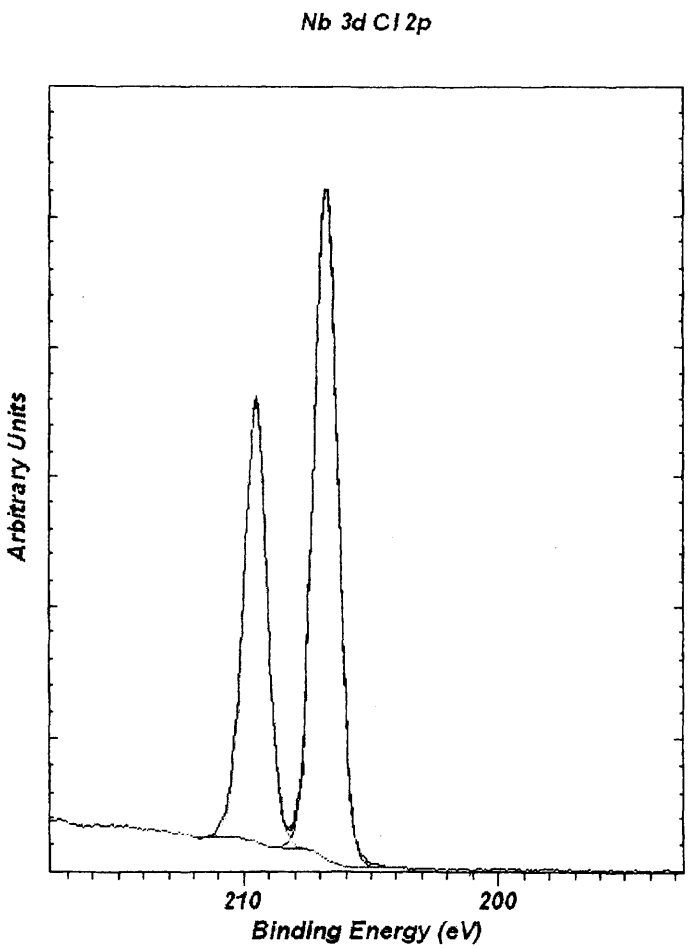

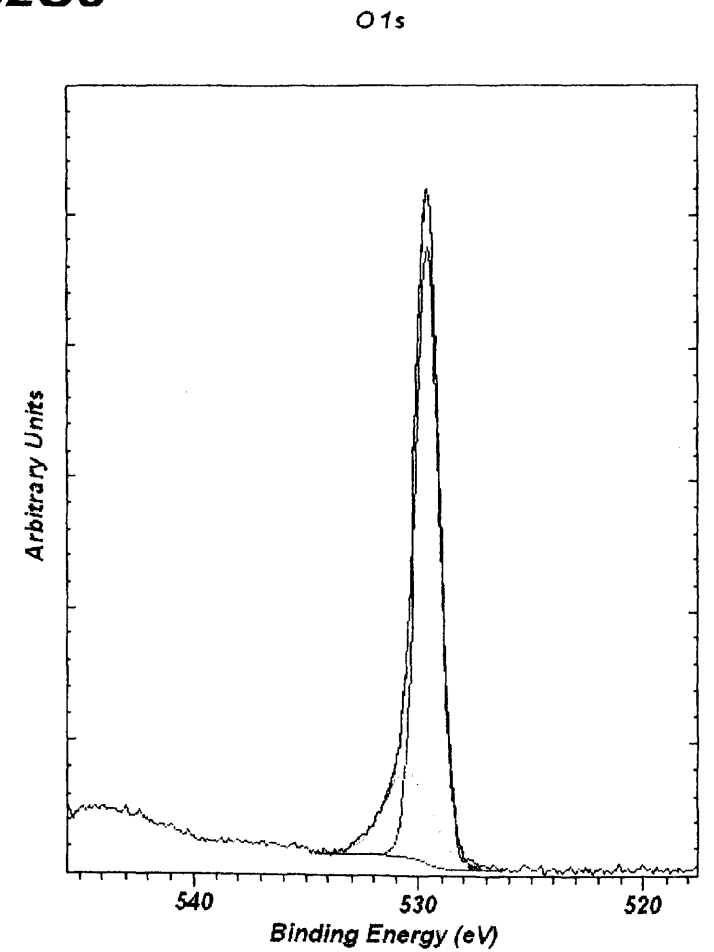

Nb(3d) 5/2 Peak Binding Energy	Ox. State
206.7	+5

O(1s) Binding Energy	Possible Species
529.7	Oxide
530.6	OH

A9(a)

Nb2O5 Aldrich – Aldrich supplied Nb2O5

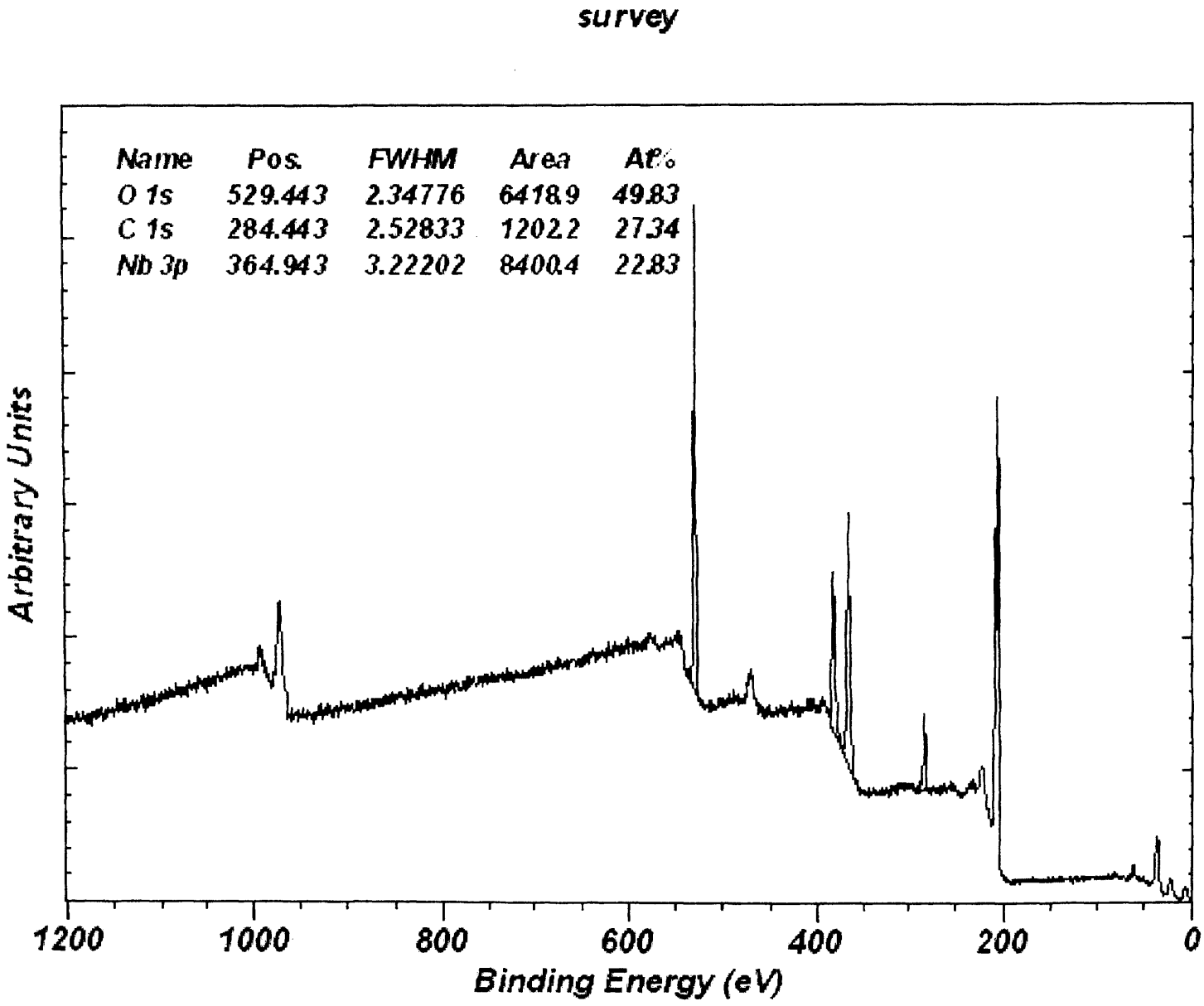

Nb_2O_5 u m – Nb2O5 from Aldrich Post MeOH reactor

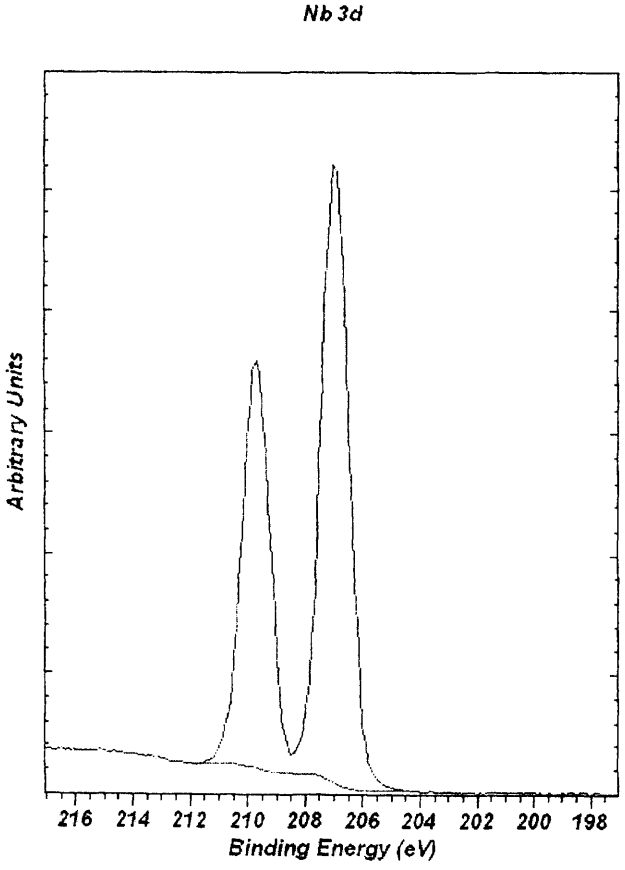

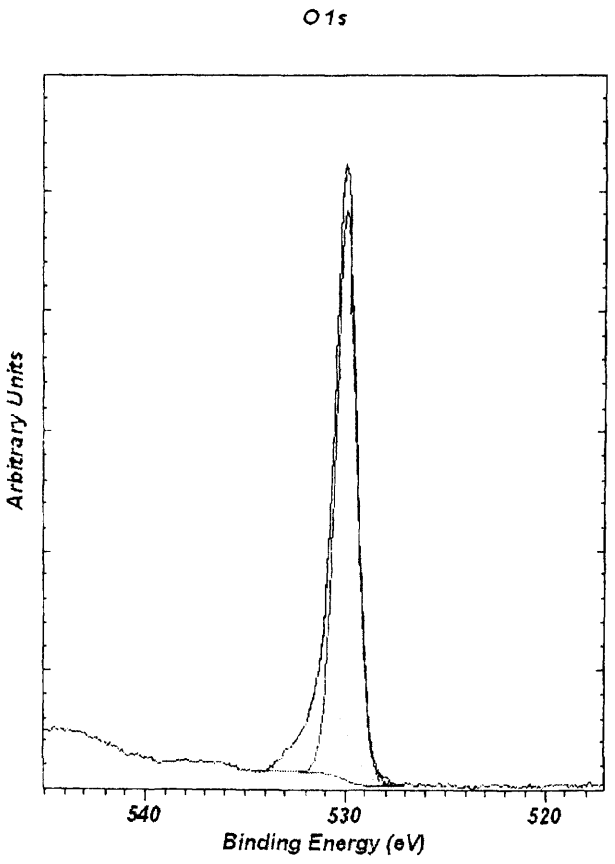

Nb(3d) 5/2 Peak Binding Energy	Ox. State
206.9	+5

O(1s) Binding Energy	Possible Species
529.9	Oxide
531.0	OH

A 10(~)

Nb_2O_5 u m – Nb2O5 from Aldrich Post MeOH reactor

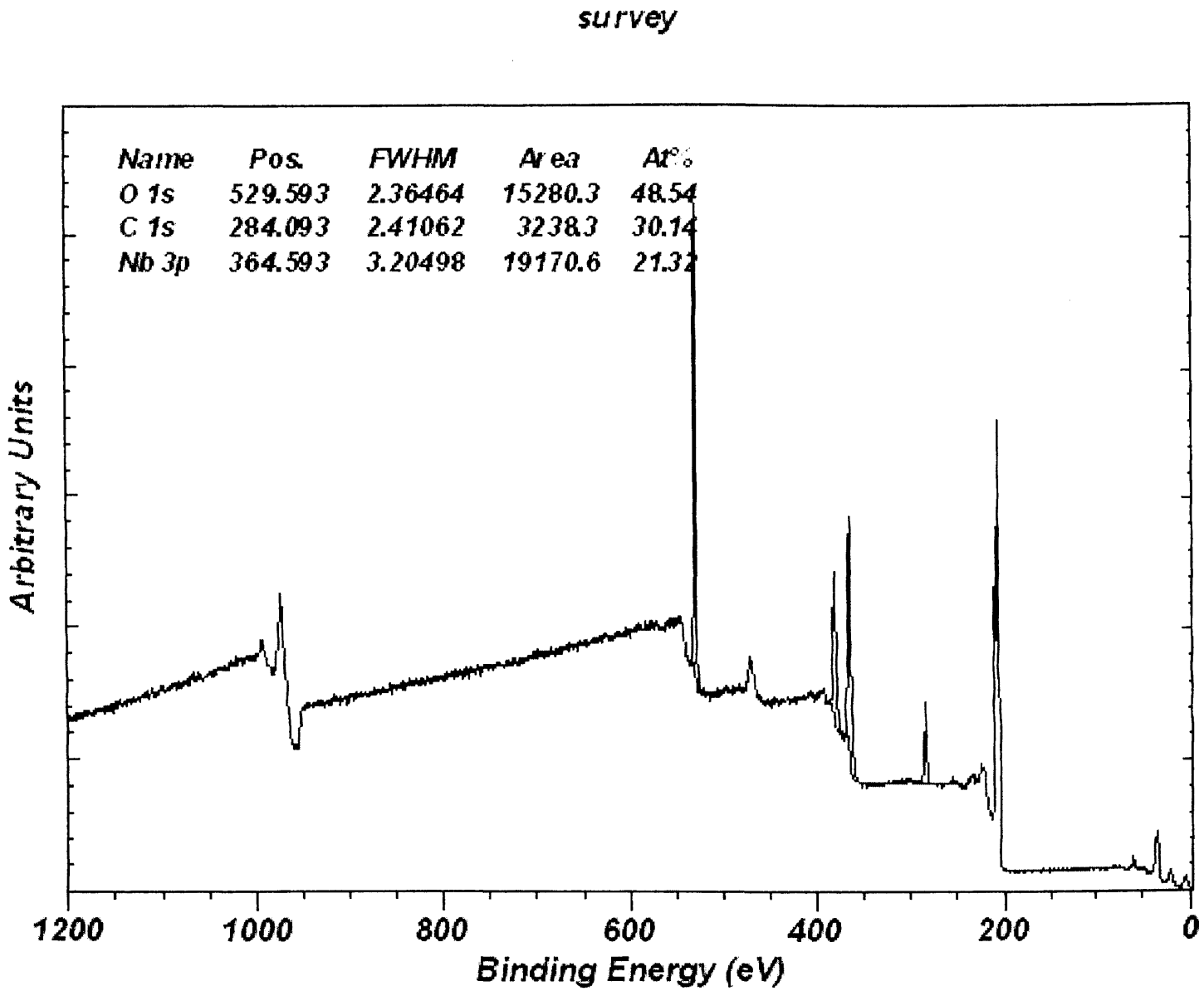

A10(b)

$NbOPO_4$ (1b) – Calcined 500C

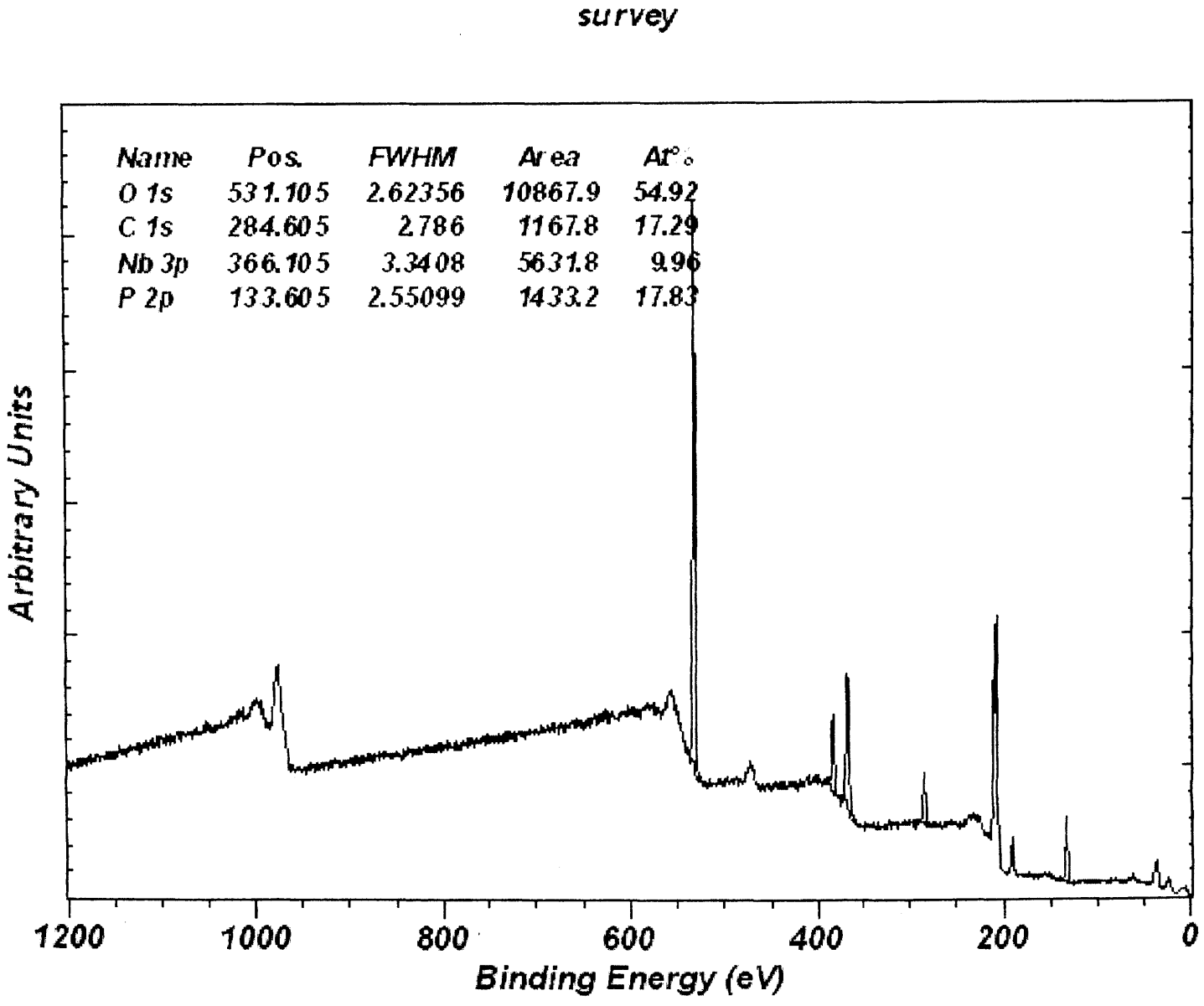

$NbOPO_4$ (1b) – Calcined 500C

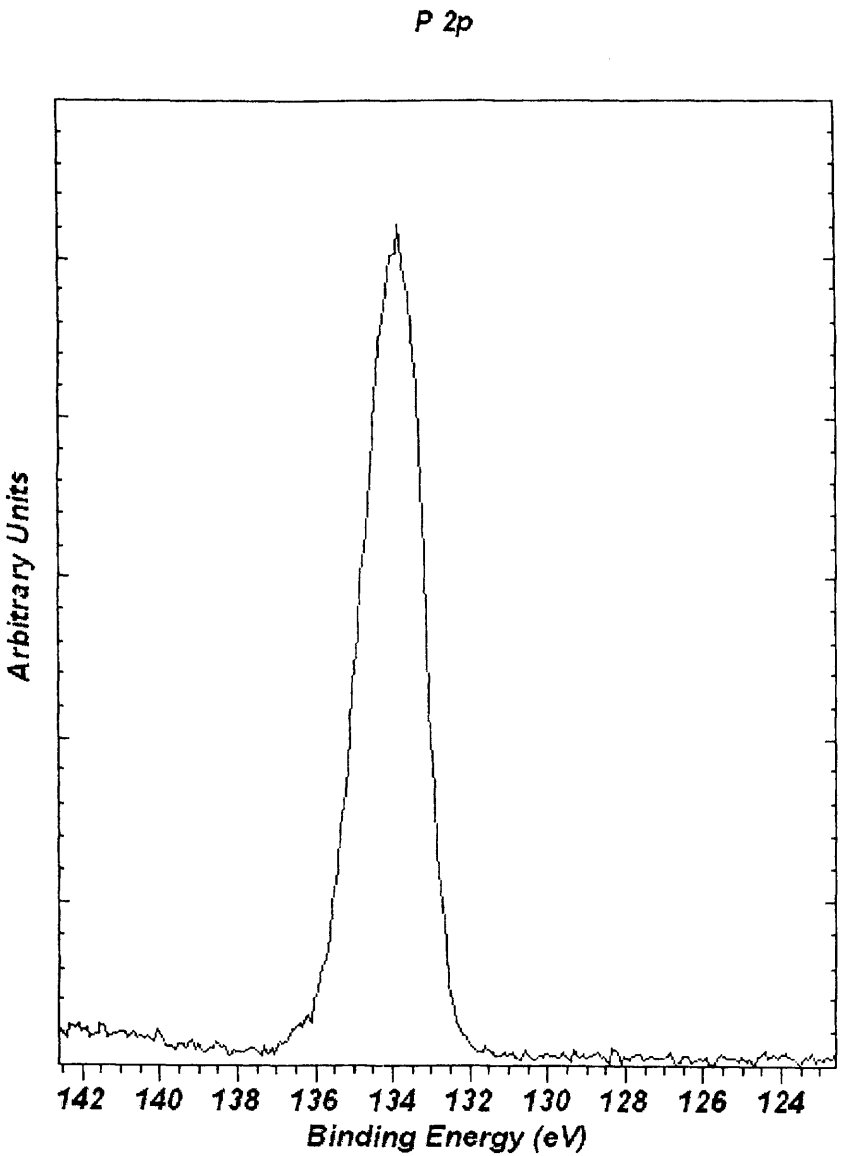

P(2p) Binding Energy	Possible Species
133.9	-POx

$NbOPO_4$ (1b) – Calcined 500C

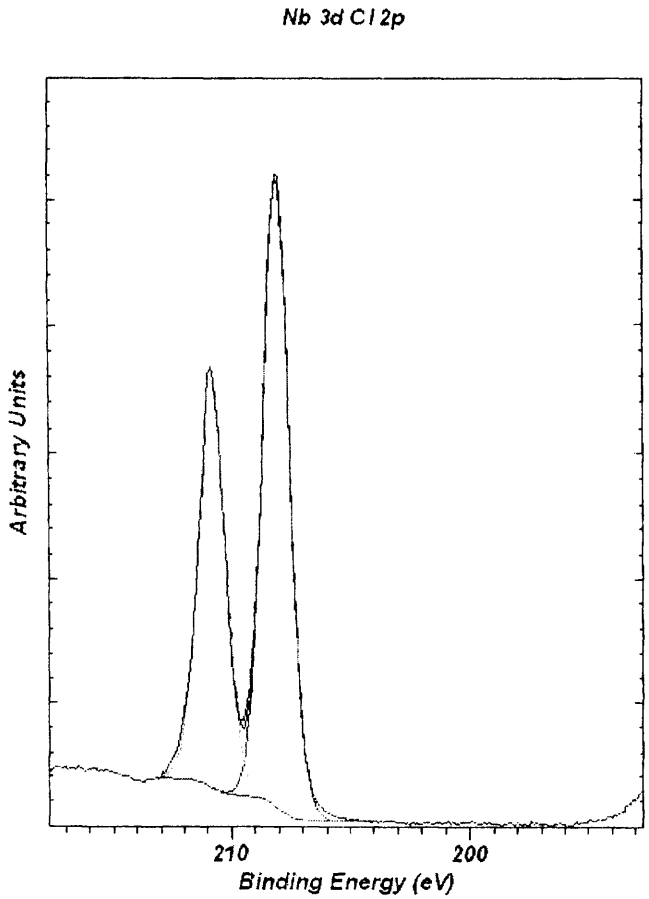

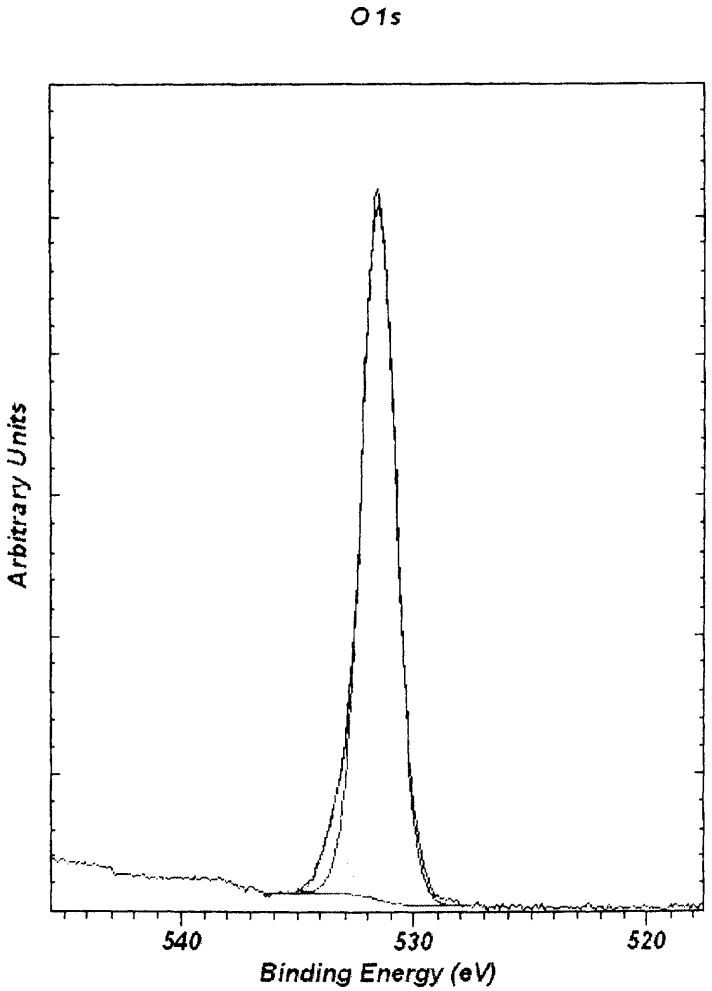

Nb(3d) 5/2 Peak Binding Energy	Ox. State
208.0	+5

O(1s) Binding Energy	Possible Species
531.5	POx
533.4	

A11(c)

1b used

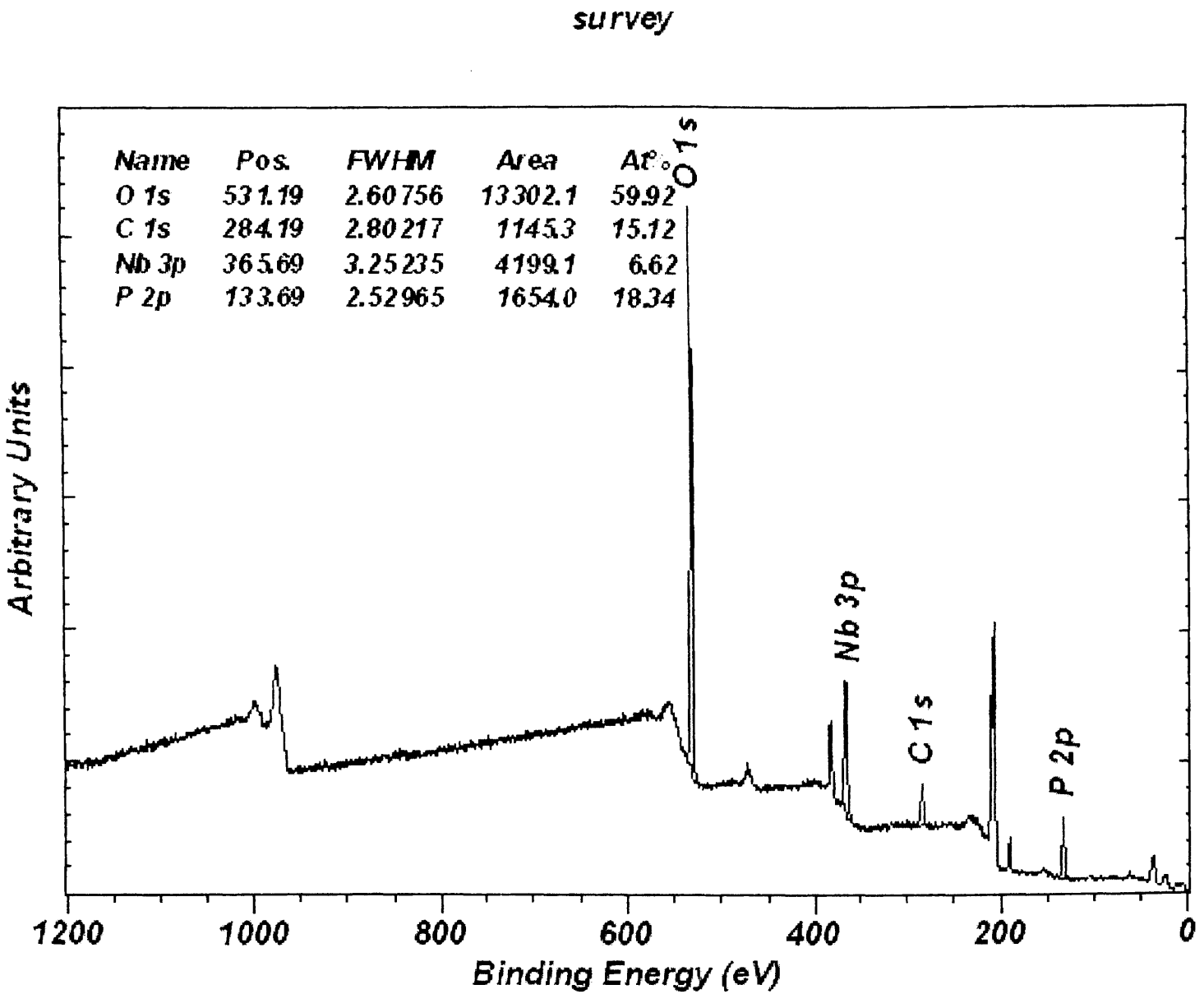
survey
Name Pos. FWHM Area At%
O 1s 531.19 2.60756 13302.1 59.92
C 1s 284.19 2.80217 1145.3 15.12
Nb 3p 365.69 3.25235 4199.1 6.62
P 2p 133.69 2.52965 1654.0 18.34
O 1s
Nb 3p
C 1s
P 2p
Arbitrary Units
1200
1000
800
600
400
200
0
Binding Energy (eV)

A12(a)

1b used

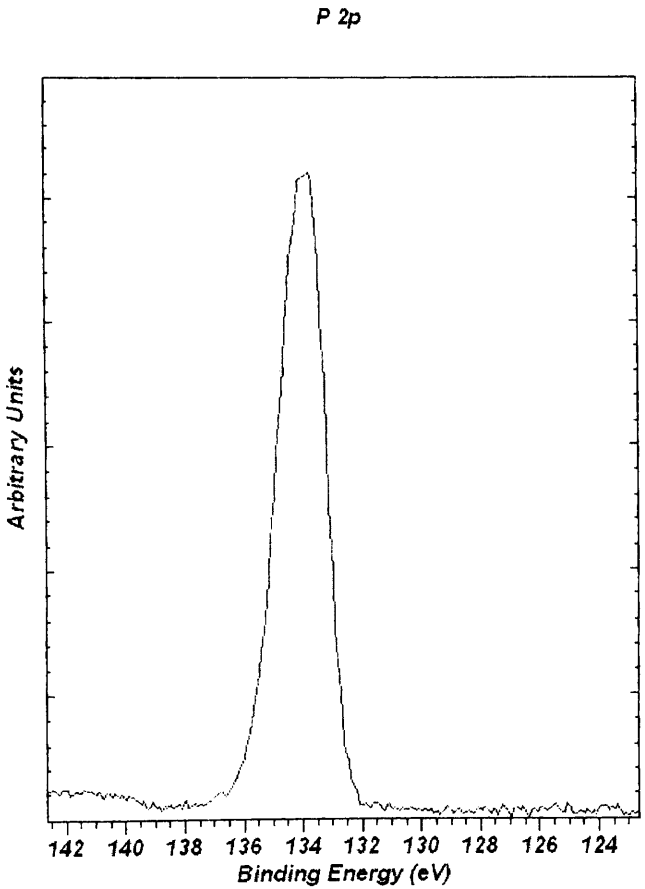

P(2p) Binding Energy	Pos. Species
134.0	$-PO_x$

A12(b)

1b used

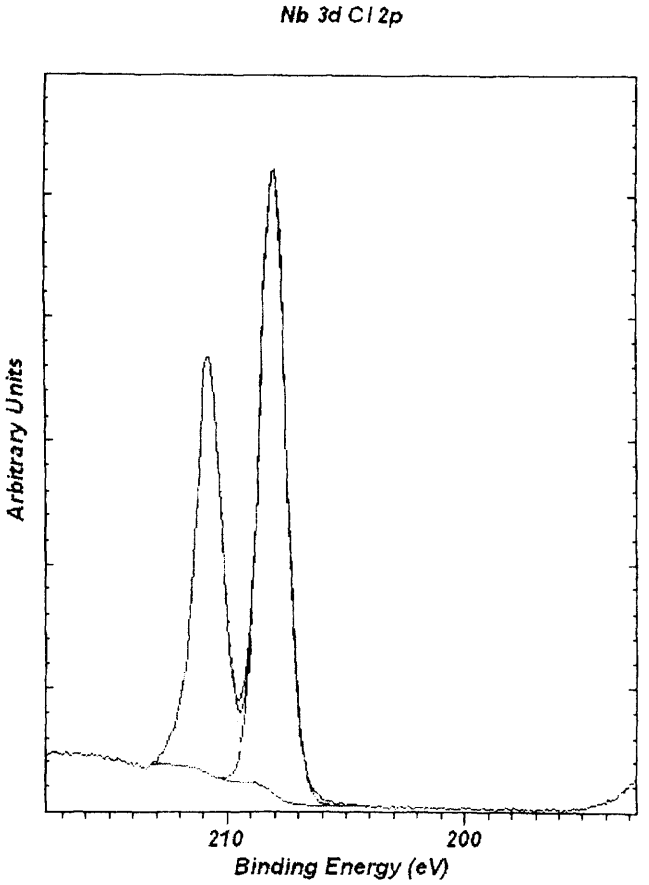

Nb(3d) 5/2 Peak Binding Energy	Ox. State
208.1	+5

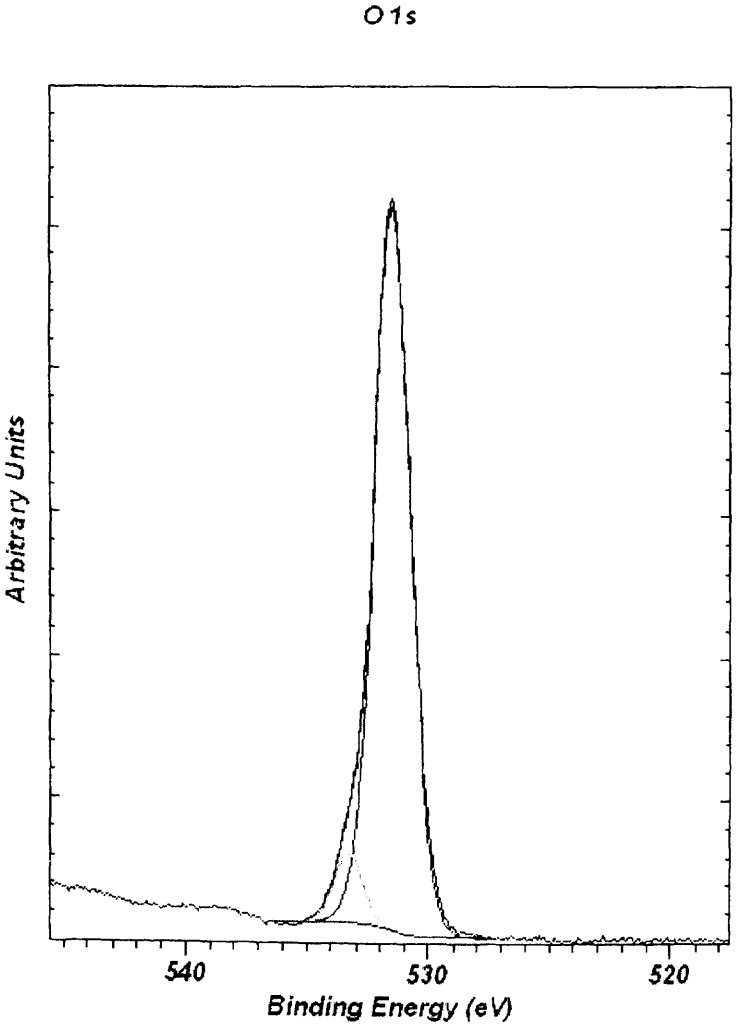

O(1s) Binding Energy	Possible Species
531.5	CO_3, PO_4, OH
533.2	

A12(c)

$NBOPO_4$ (2d) – Calcined in Air 500 C

survey

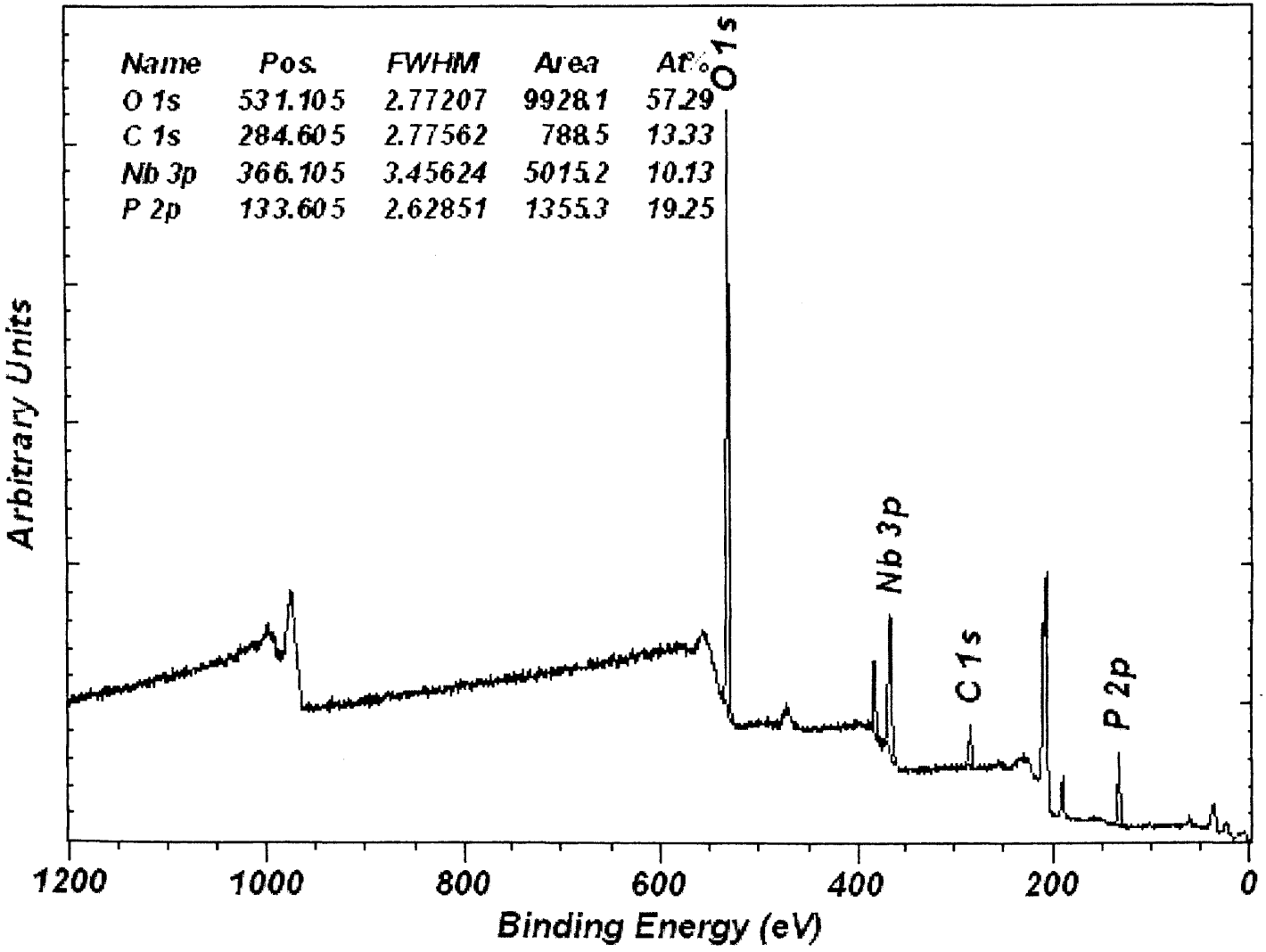

A13(a)

$NBOPO_4$ (2d) – Calcined in Air 500 C

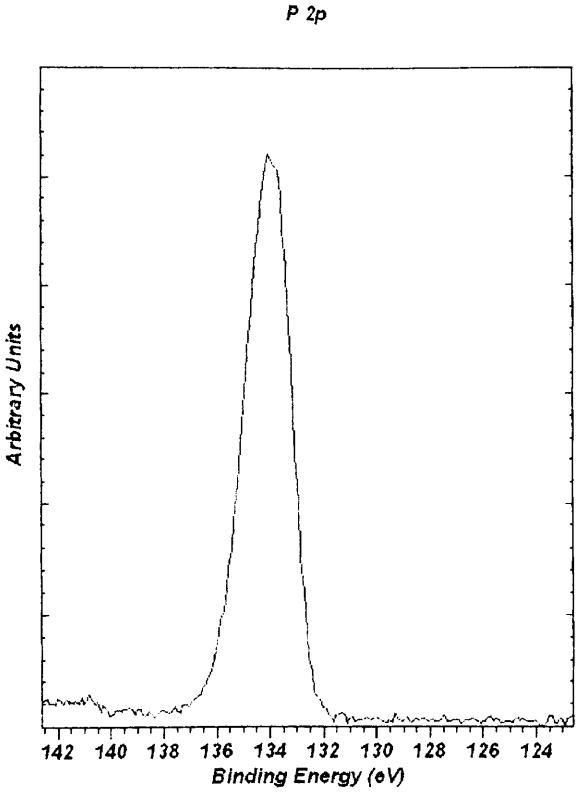

P(2p) Binding Energy	Pos. Species
134.0	$-PO_x$

$NBOPO_4$ (2d) – Calcined in Air 500 C

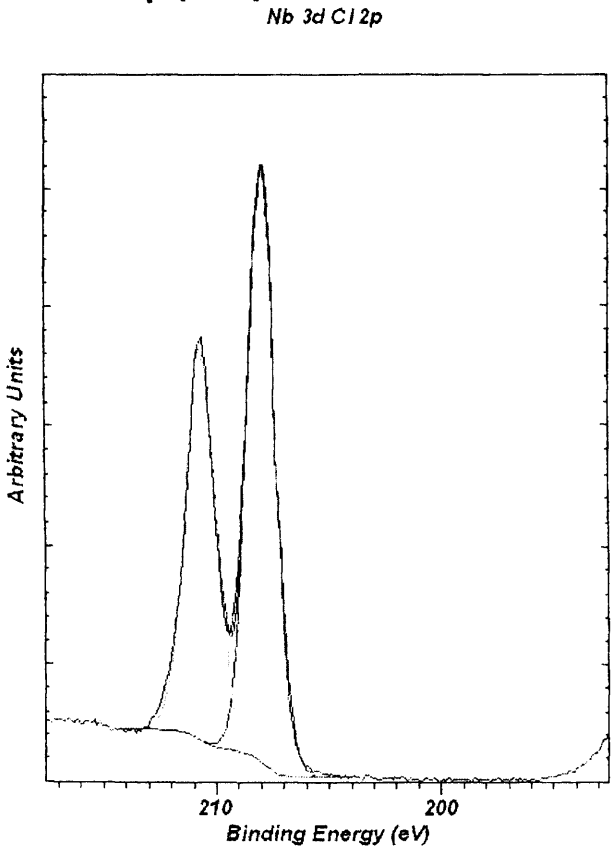

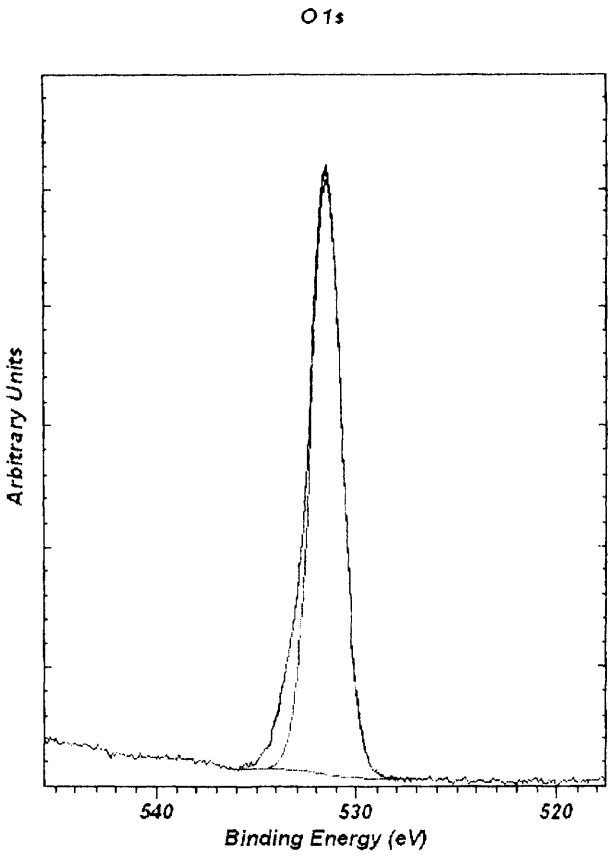

Nb(3d) 5/2 Peak Binding Energy	Ox. State
207.9	+5

O(1s) Binding Energy	Possible Species
531.5	CO_3, PO_4, OH
533.2	

A13(c)

2d used

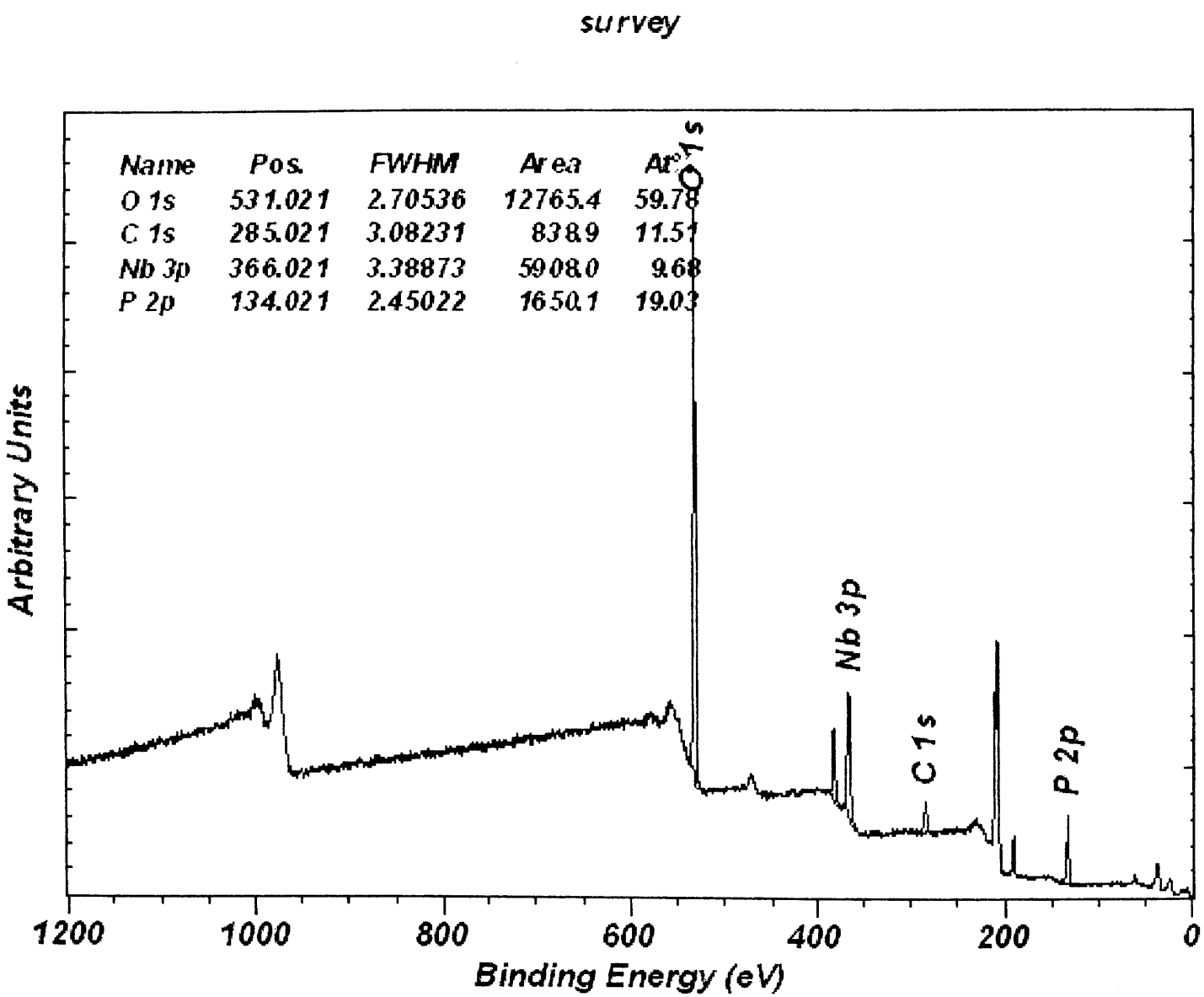
survey
Name Pos. FWHM Area At
O 1s 531.021 2.70536 12765.4 59.78
C 1s 285.021 3.08231 838.9 11.51
Nb 3p 366.021 3.38873 5908.0 9.68
P 2p 134.021 2.45022 1650.1 19.03
O 1s
Nb 3p
C 1s
P 2p
Arbitrary Units
1200
1000
800
600
400
200
0
Binding Energy (eV)

A14(c)

2d used

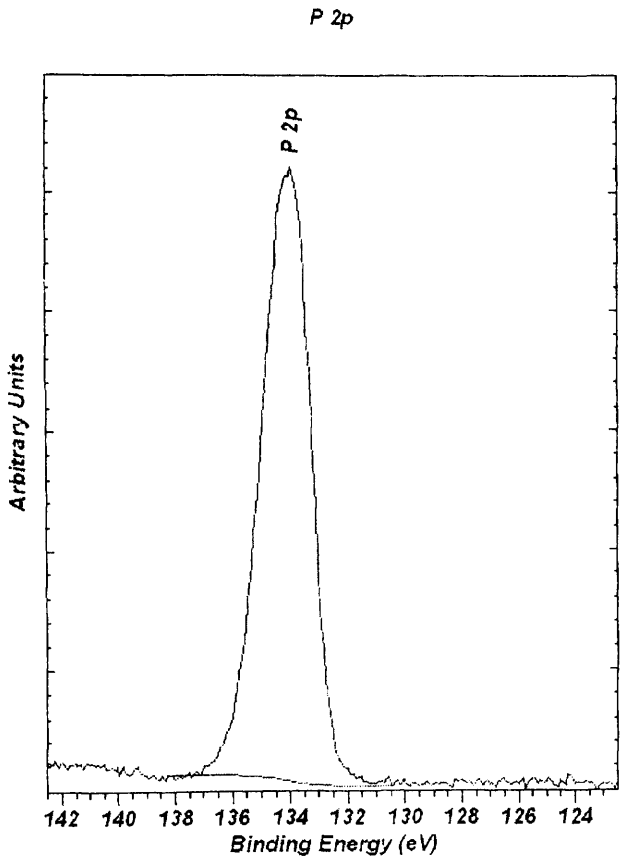

P(2p) Binding Energy	Pos. Species
134.0	$-PO_x$

A44(b)

2d used

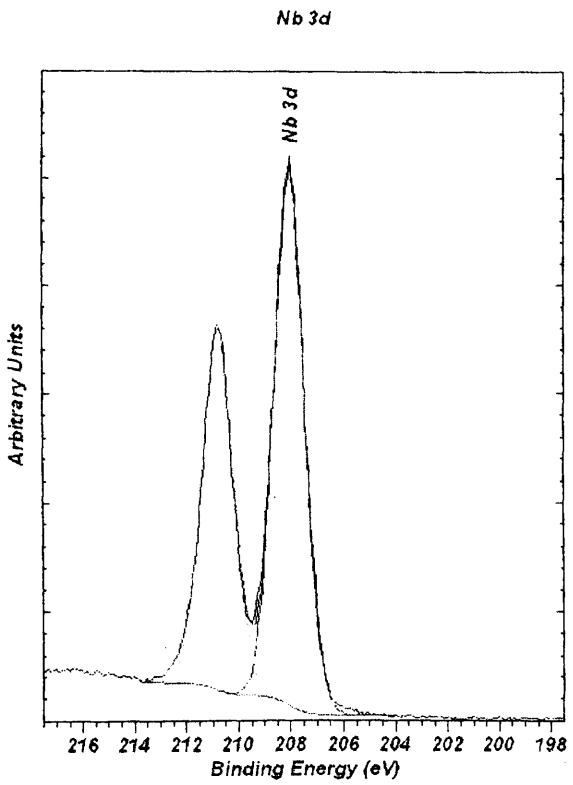

Nb(3d) 5/2 Peak Binding Energy	Ox. State
208.0	+5

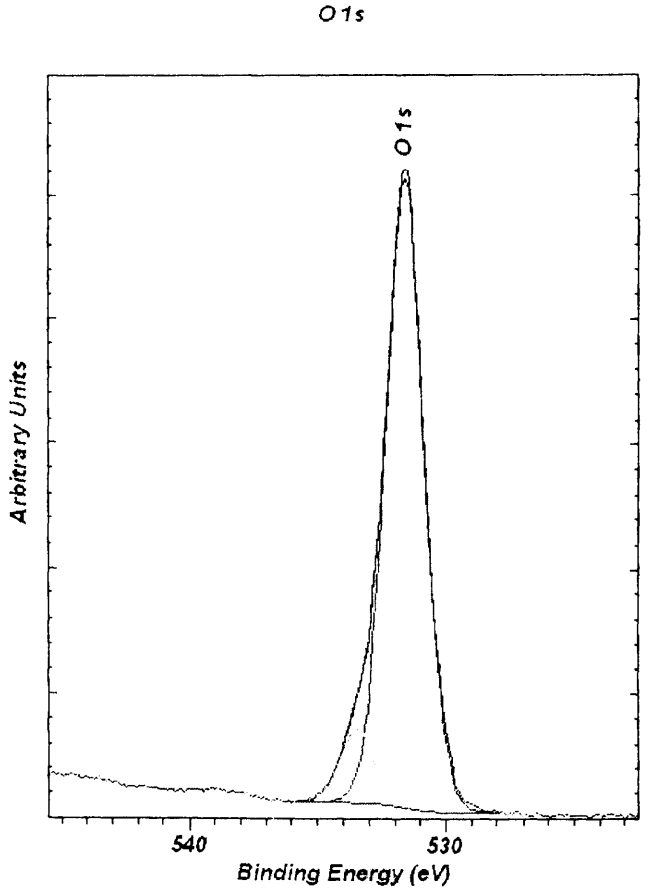

O(1s) Binding Energy	Possible Species
531.6	CO_3, PO_4, OH
533.1	

A14(c)

NbPO5 3c

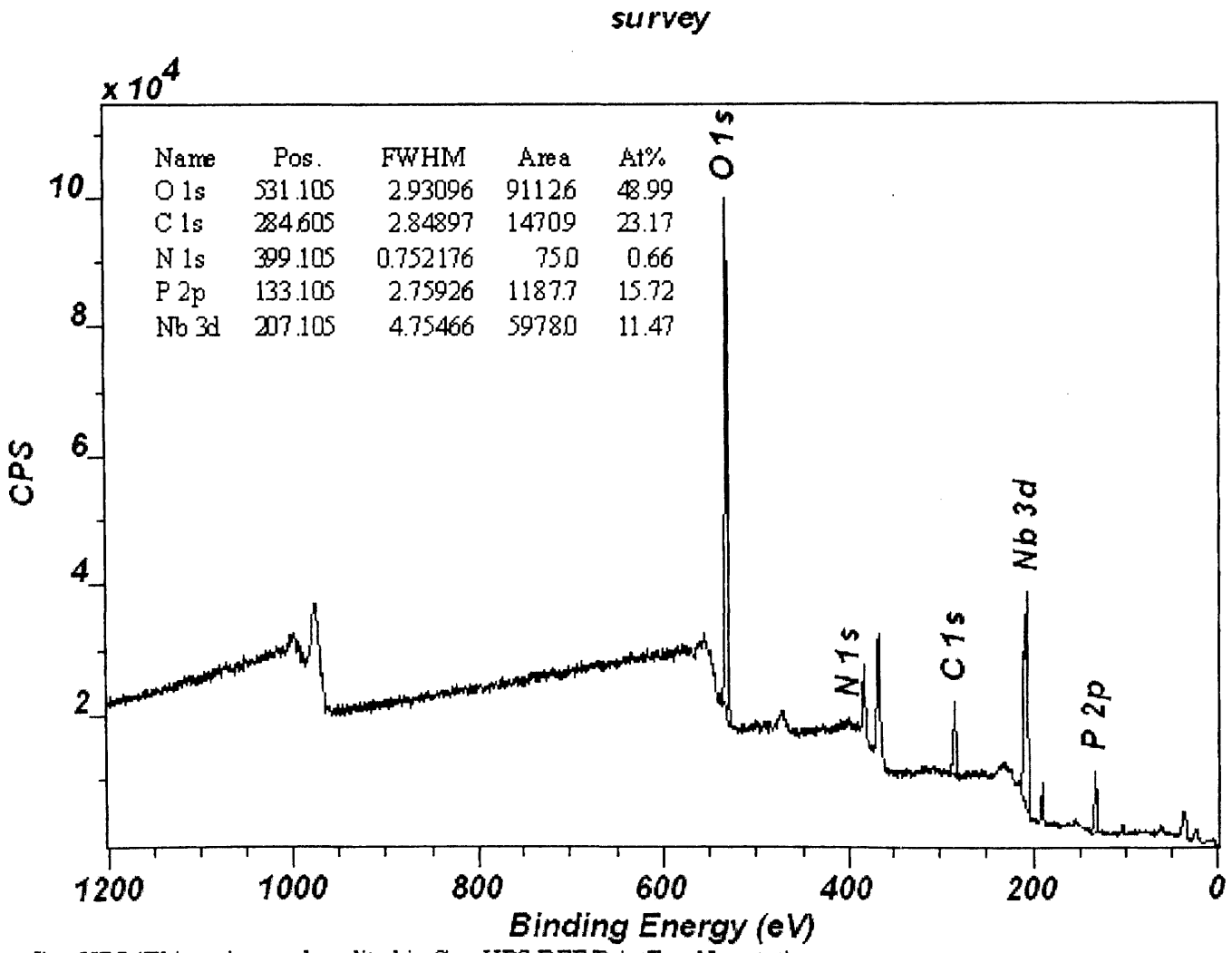

CasaXPS (This string can be edited in CasaXPS.DEF/PrintFootNote.txt)

A15(a)

NbPO5 3c

P(2p) Binding Energy	Possible Species
133.7	PO_x

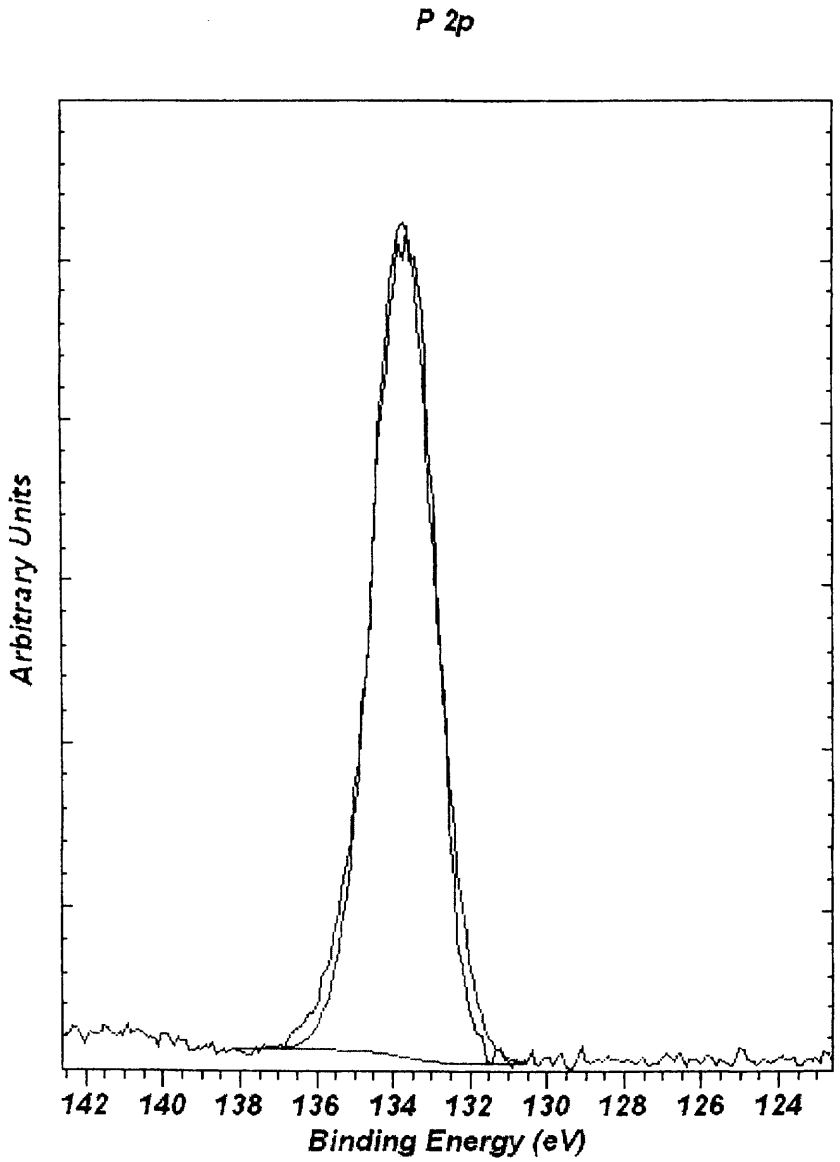

A15(b)

NbPO5 3c

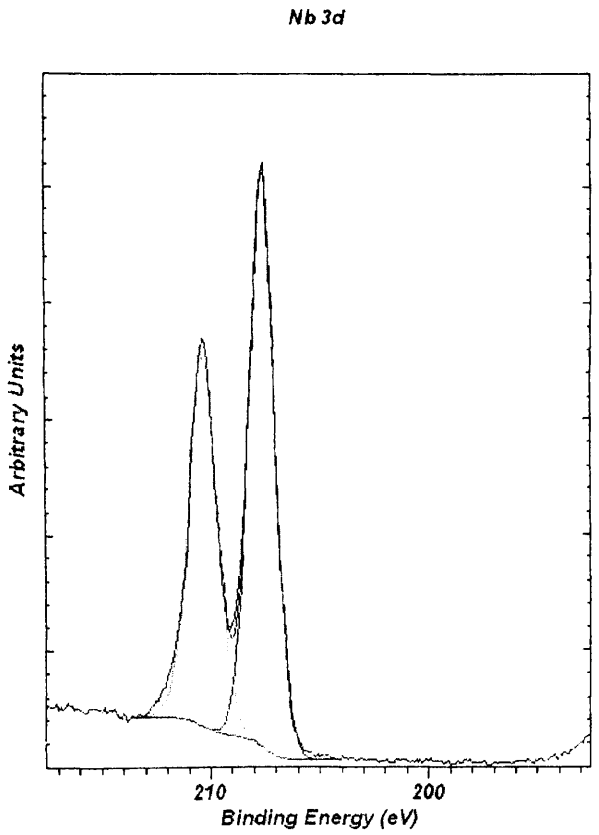

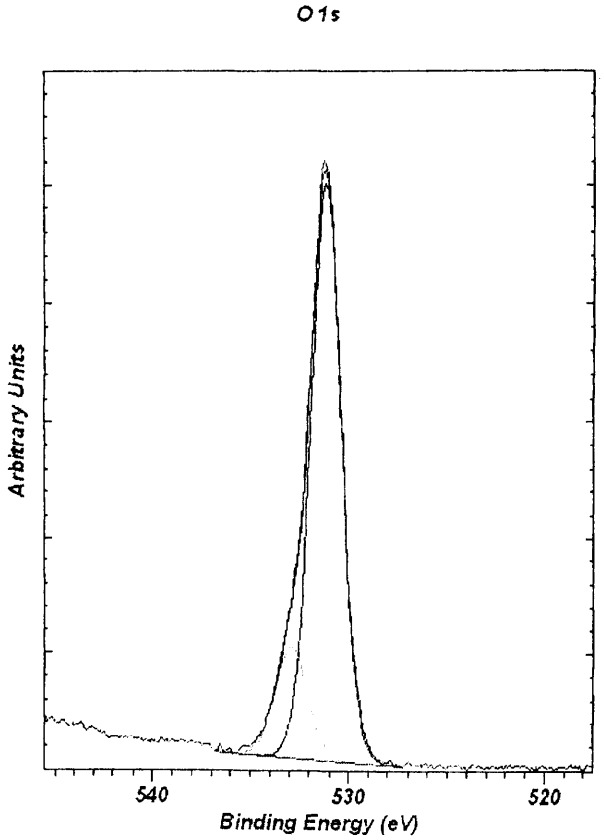

Nb(3d) 5/2 Peak Binding Energy	Ox. State
207.6	+5

O(1s) Binding Energy	Possible Species
531.2	CO_3, PO_4, OH
532.9	SiO_2 Contamination

A15(c)

$NBPO_5$ 3cu – $NbPO_5$ from I-BuOH – Post MeOH Reactor

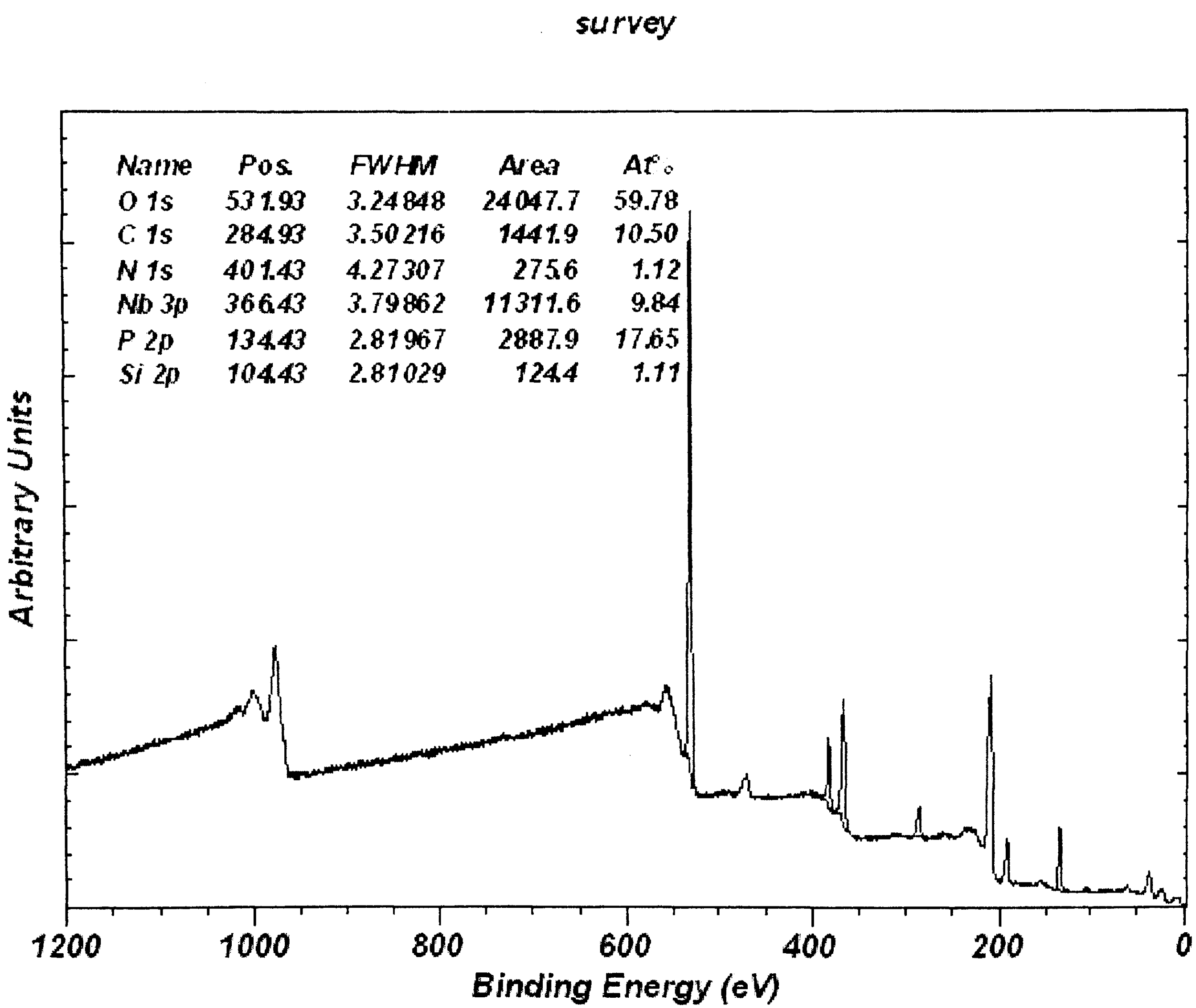

A16(a)

$NBPO_5$ 3cu – $NbPO_5$ from I-BuOH – Post MeOH Reactor

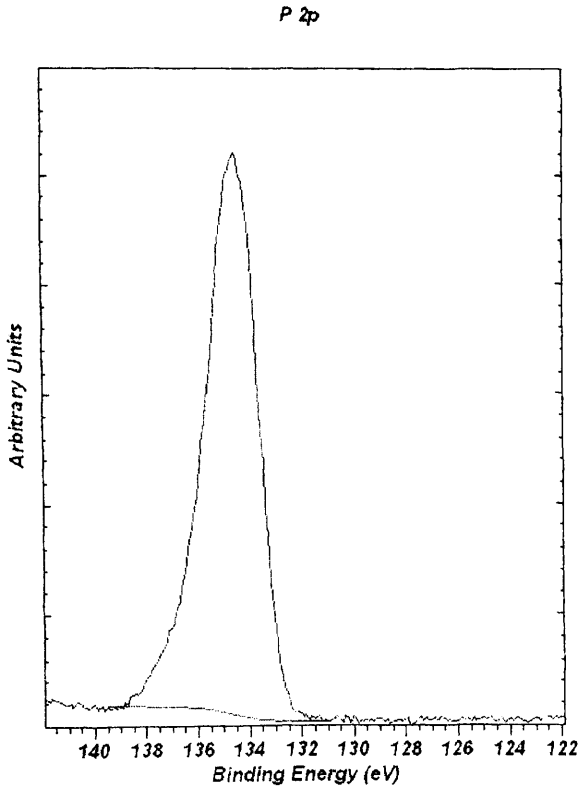

P(2p) Binding Energy	Possible Species
134.5	$-PO_{x,}$, $-P_2O_5$, -PO(OH)

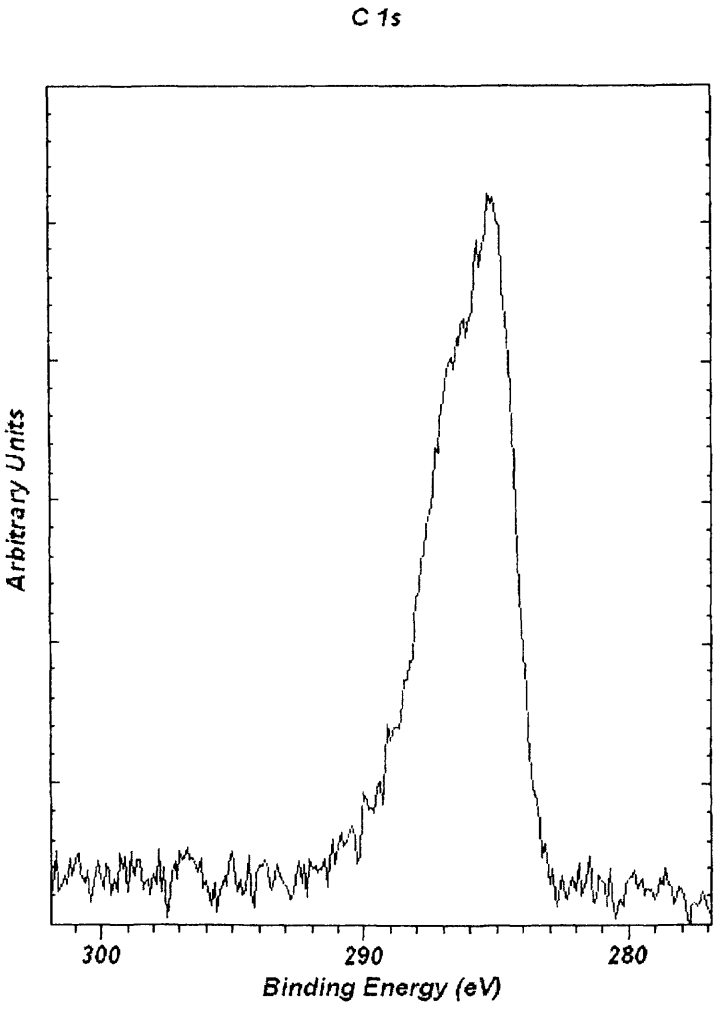

$NBPO_5$ 3cu – $NbPO_5$ from I-BuOH – Post MeOH Reactor

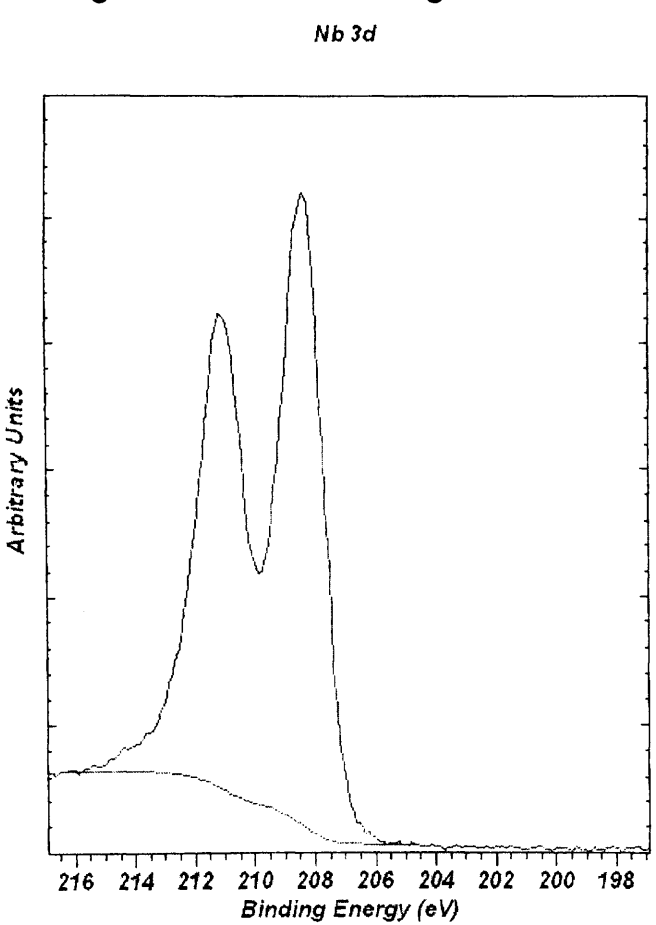

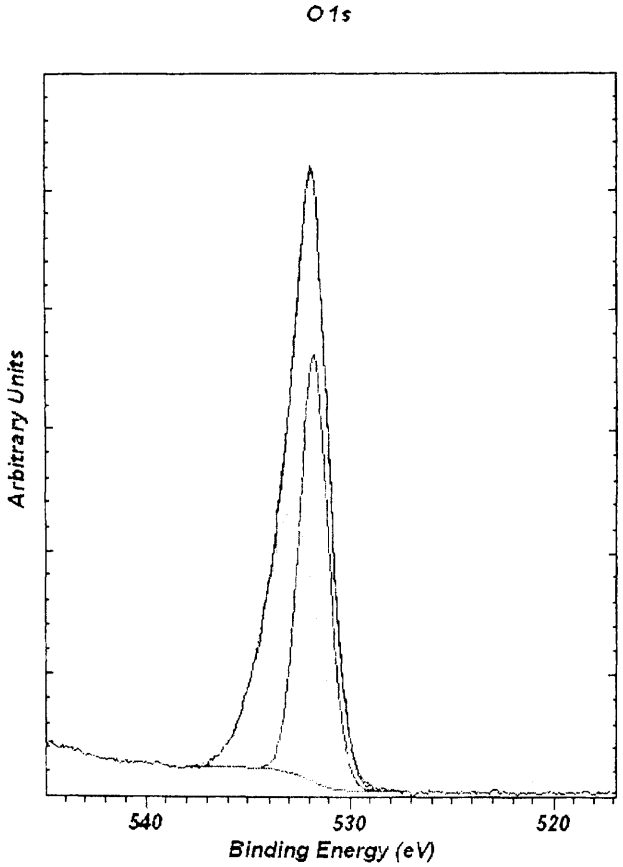

Nb(3d) 5/2 Peak Binding Energy	Ox. State
208.4	+5

O(1s) Binding Energy	Possible Species
531.7	CO_3, PO_4, OH
532.9	SiO_2 Contamination

Note for this batch of samples, there is slight charging which couldn't be alleviated, hence the broader higher binding energy tail

A16(c)

3b unused

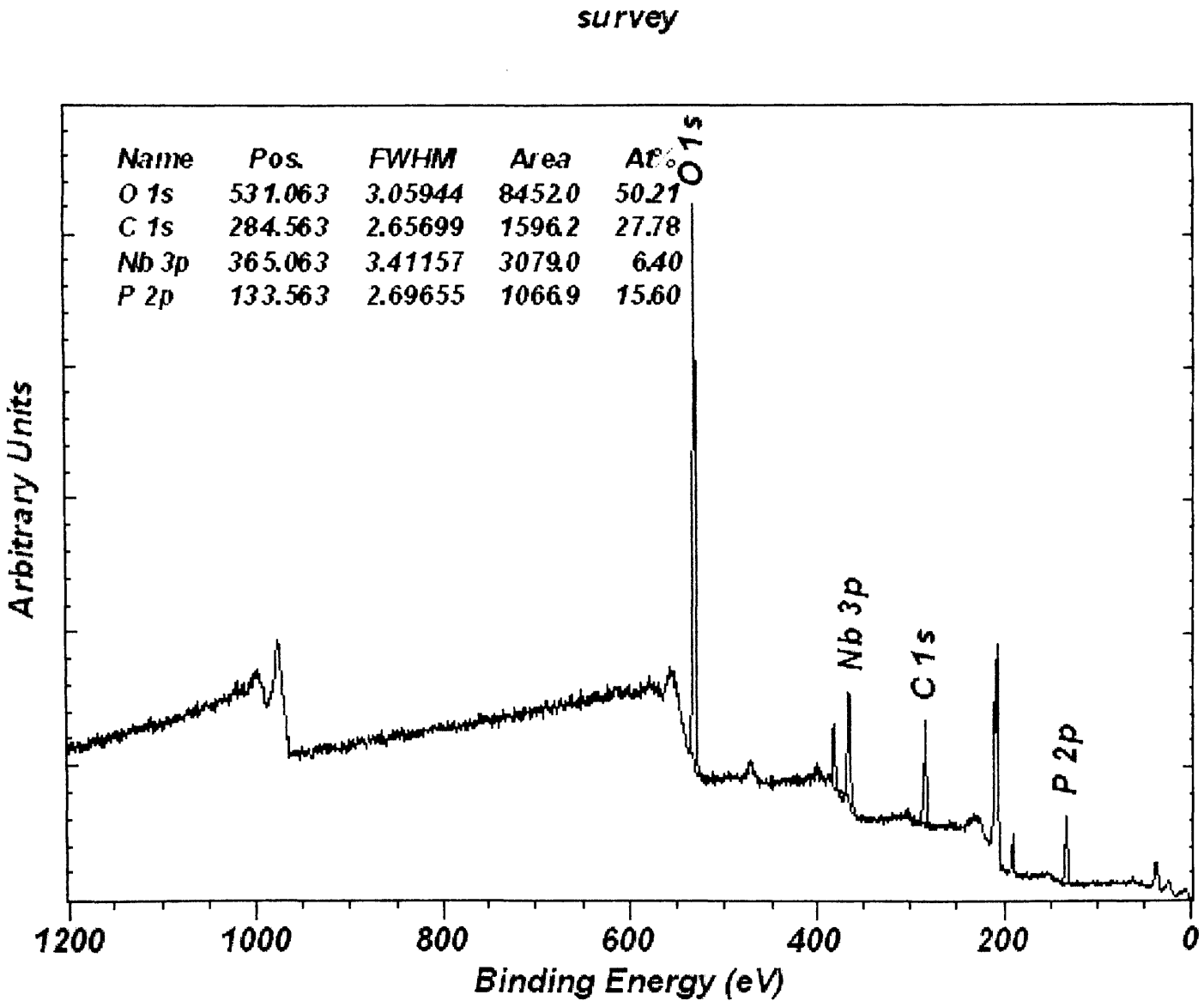

A17(a)

3b unused

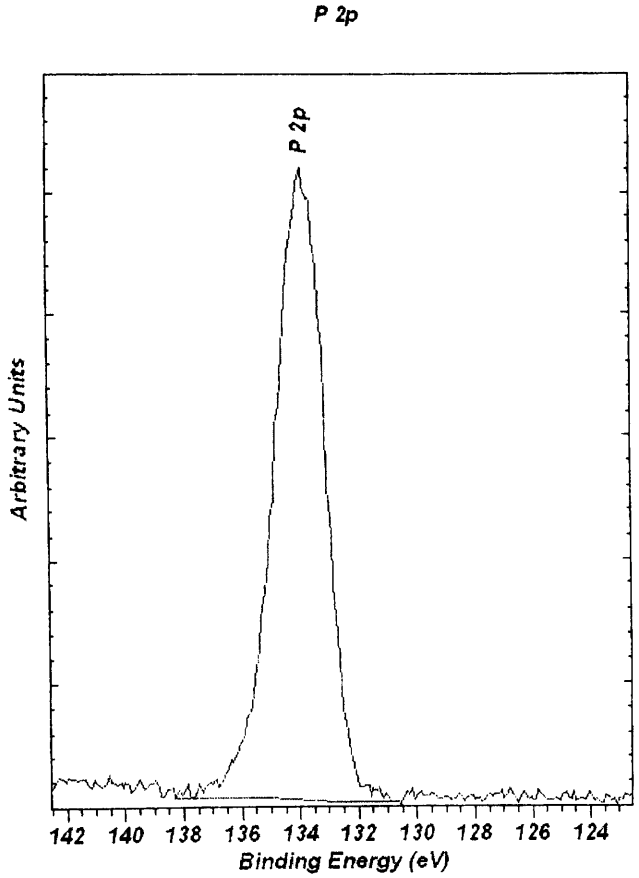

P(2p) Binding Energy	Pos. Species
133.8	$-PO_x$

A12(b)

3b unused

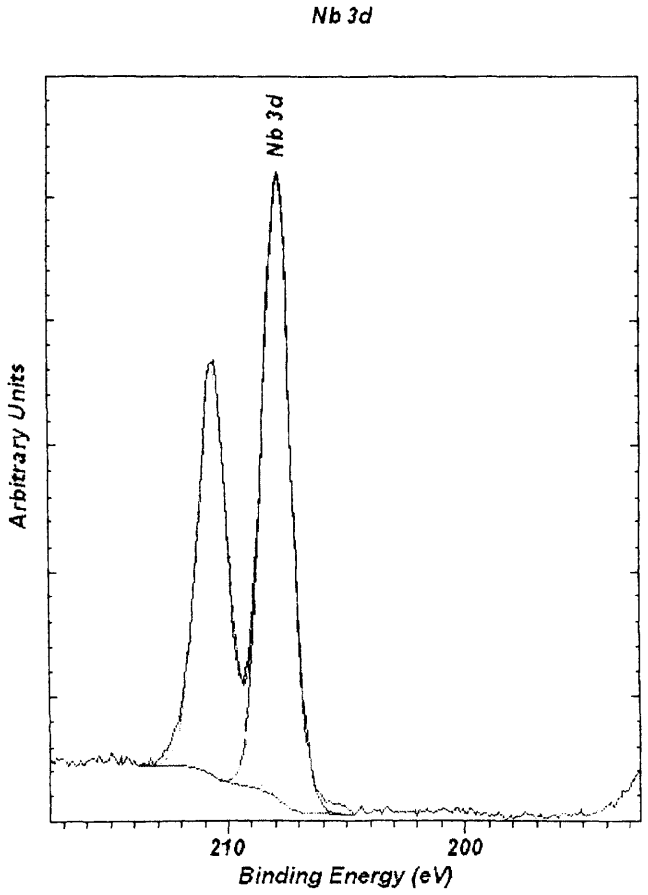

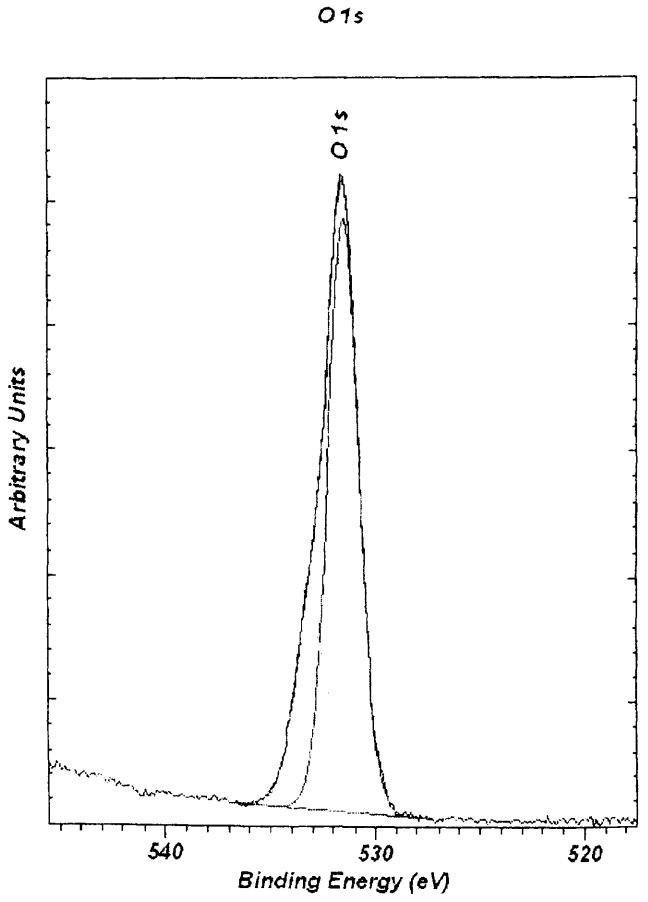

Nb(3d) 5/2 Peak Binding Energy	Ox. State
207.8	+5

O(1s) Binding Energy	Possible Species
531.5	CO_3, PO_4, OH
533.1	

A17(c)

$NBPO_5$ 3bu – $NbPO_5$from i-BuOH – Post MeOH Reactor

survey

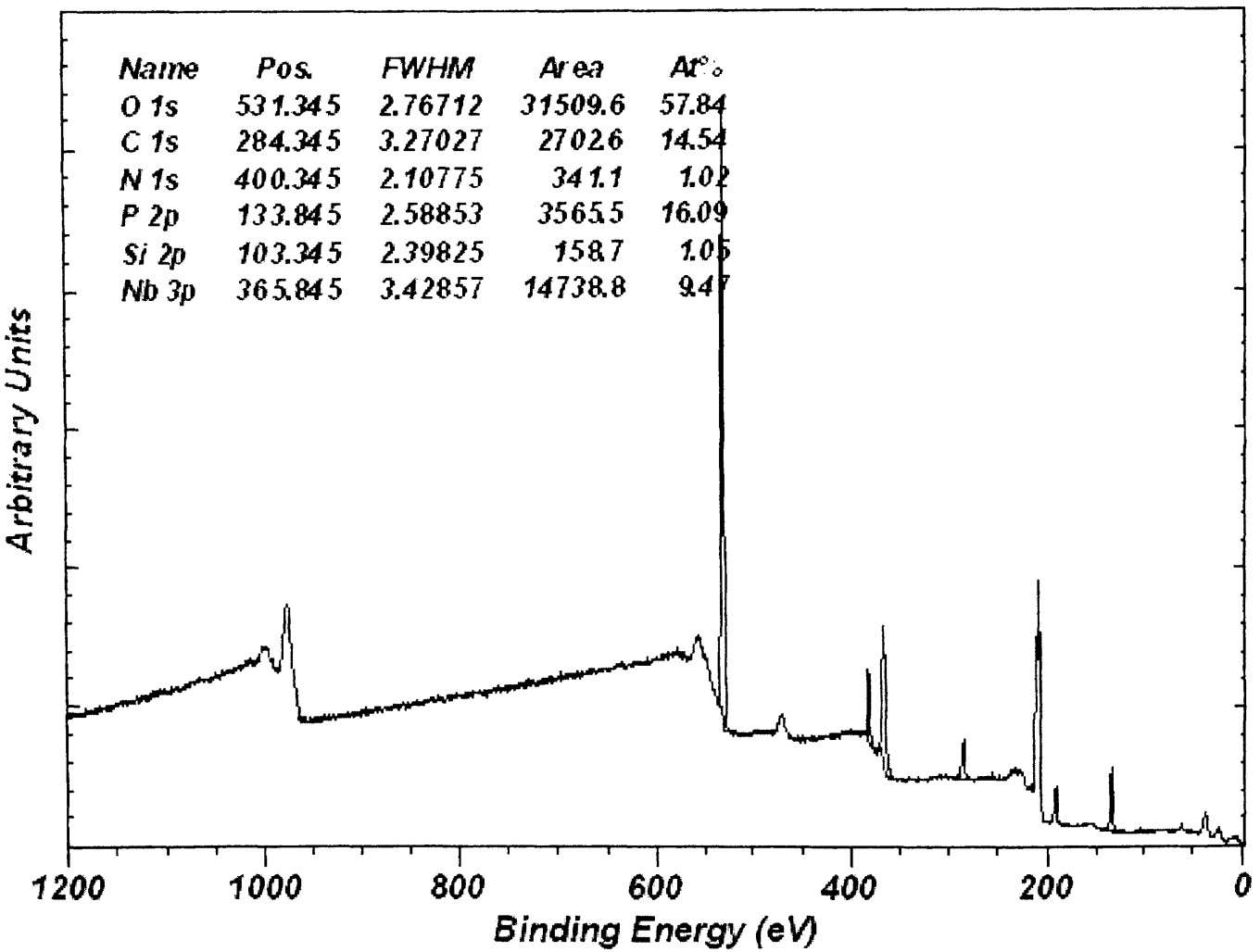

A18(a)

$NBPO_5$ 3bu – $NbPO_5$from i-BuOH – Post MeOH Reactor

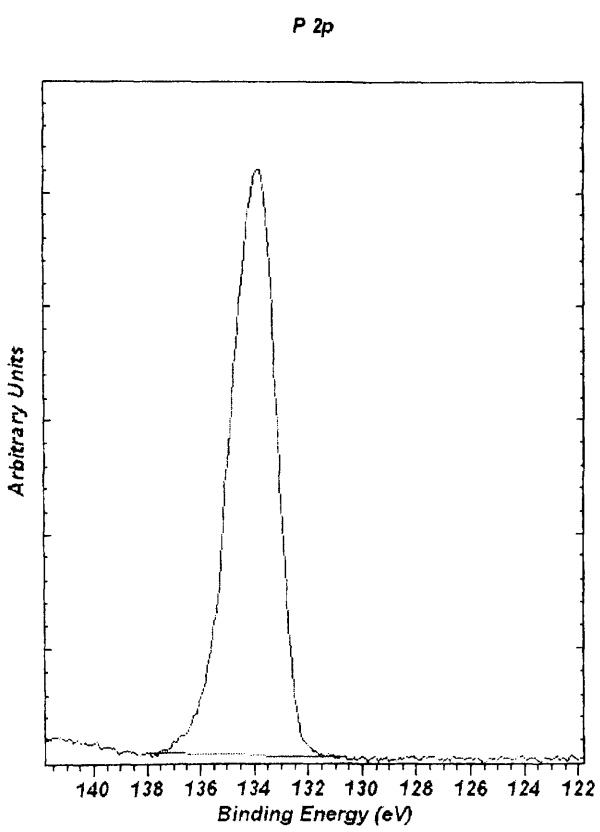

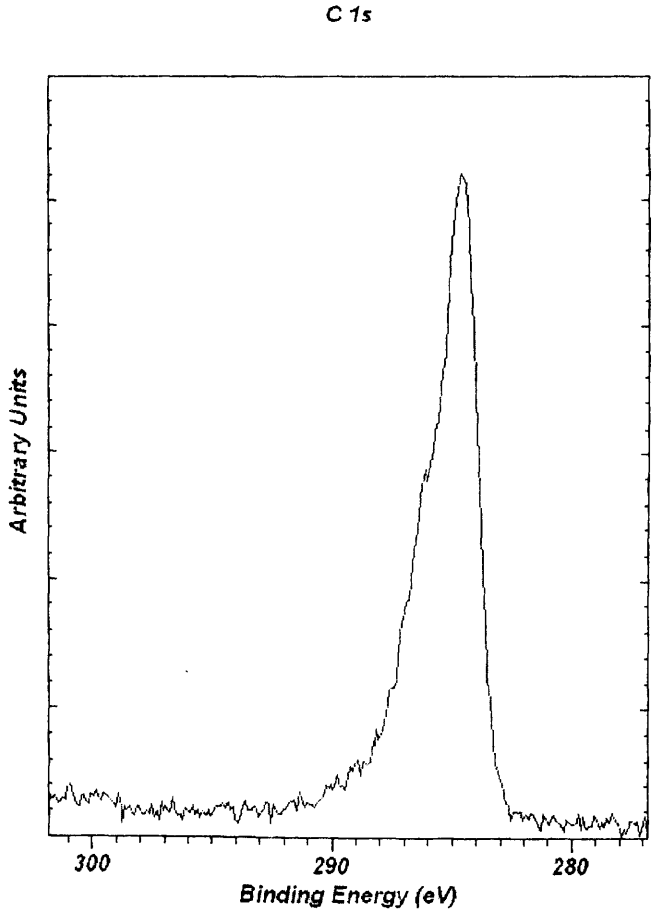

P(2p) Binding Energy	Possible Species
133.9	PO_x

A18(6)

$NBPO_5$ 3bu – $NbPO_5$from i-BuOH – Post MeOH Reactor

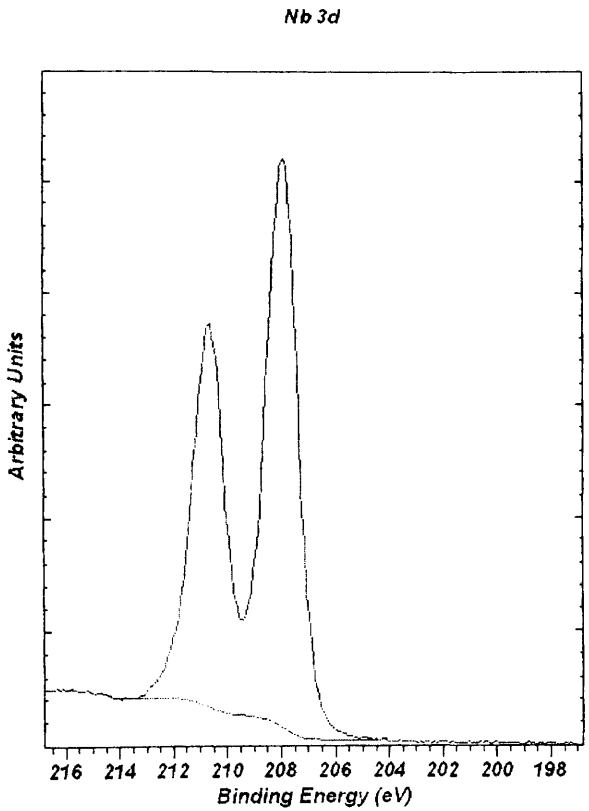

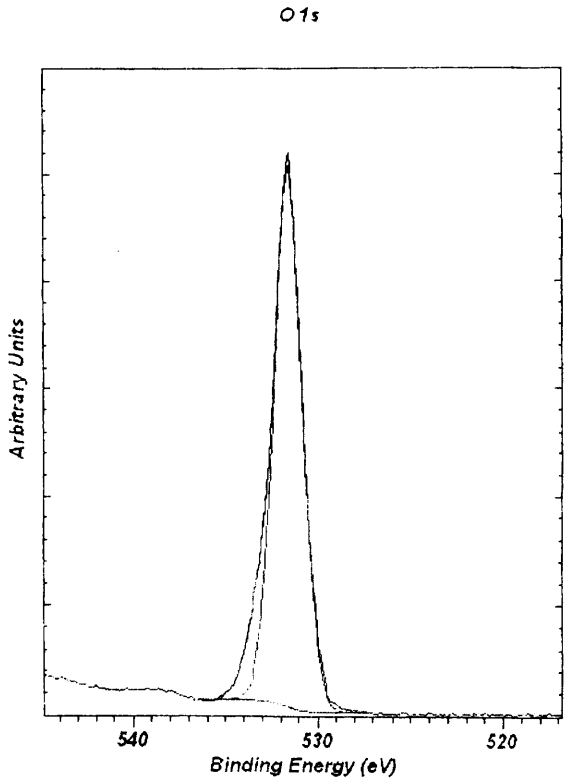

Nb(3d) 5/2 Peak Binding Energy	Ox State
208.0	+5 (*)

O(1s) Binding Energy	Possible Species
531.5	CO_3, PO_4, OH
533.3	SiO_2 Contamination

A18(c)

(*) Note: higher than expected for Nb_2O5, expect due to phosphate like groups?

8.1 unused

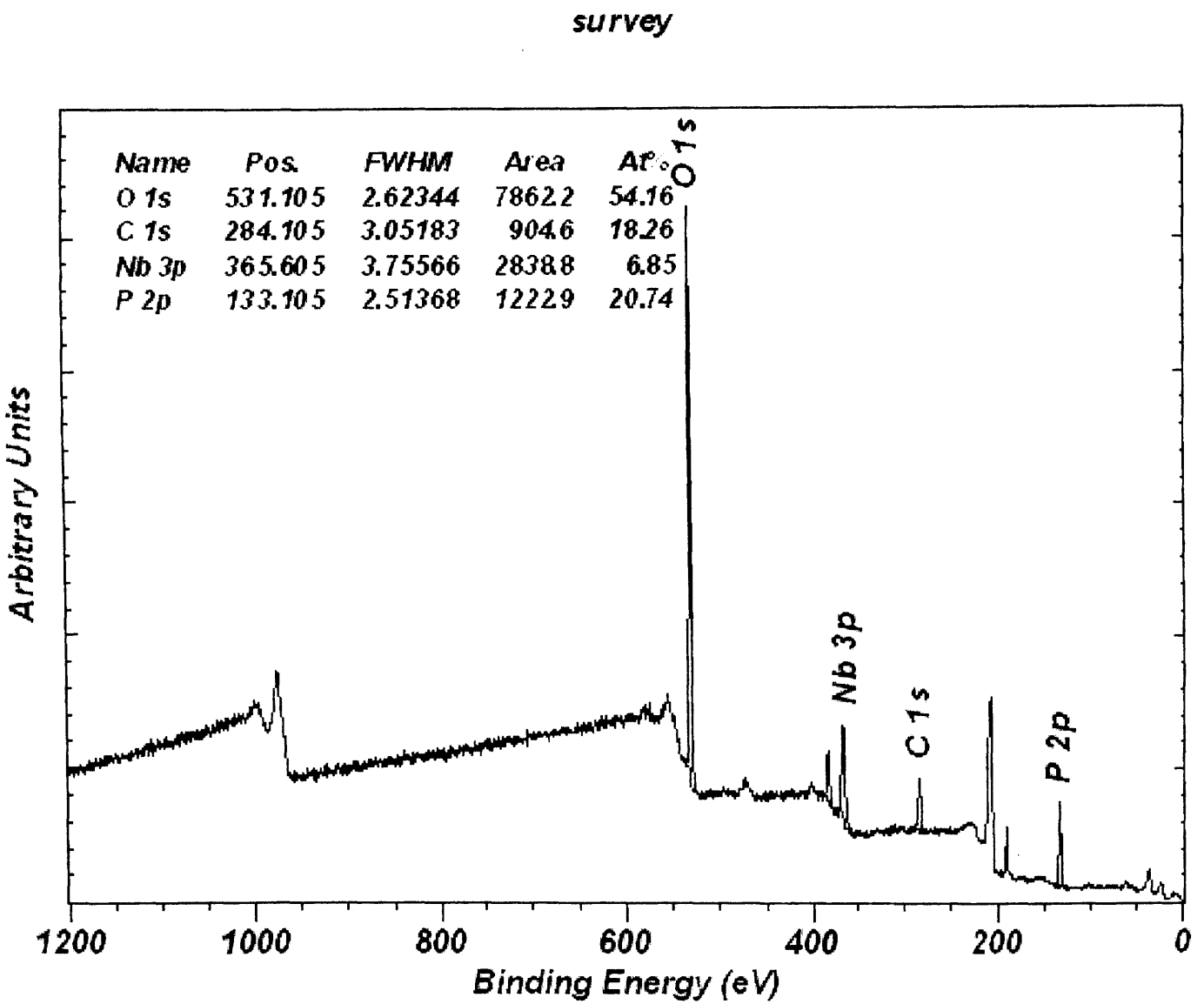

A19(a)

8.1 unused

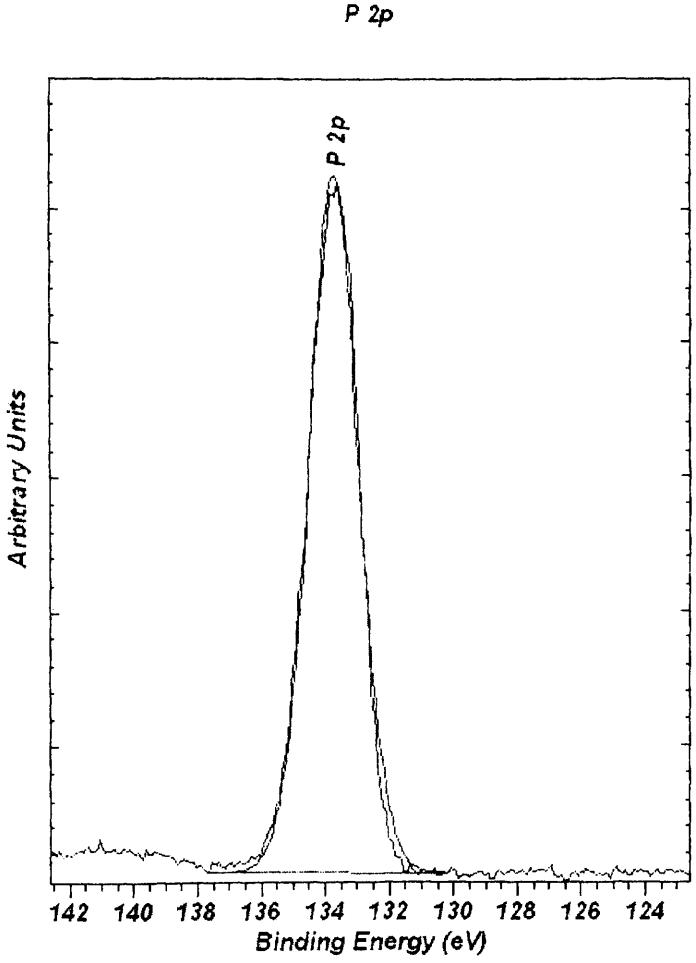

P(2p) Binding Energy	Pos. Species
133.7	$-PO_x$

8.1 unused

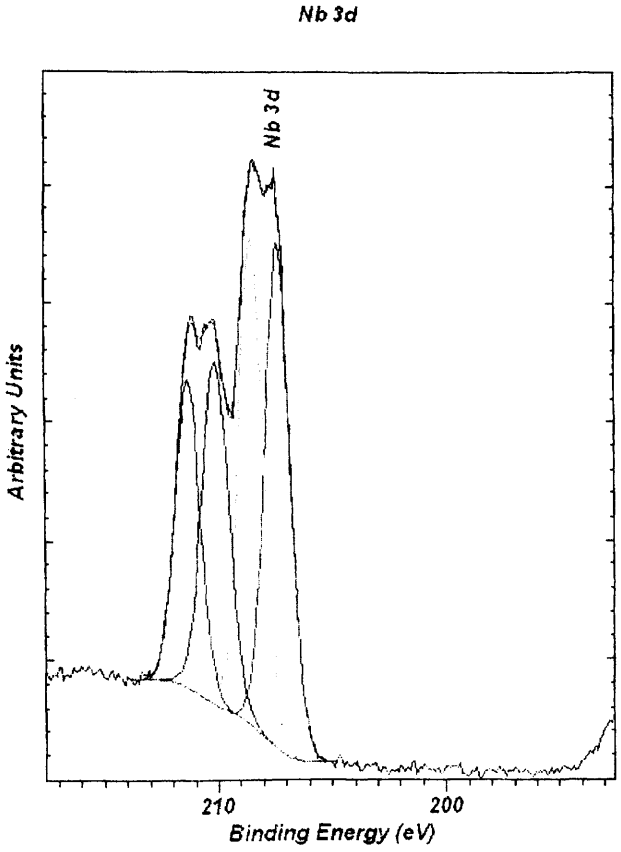

Nb(3d) 5/2 Peak Binding Energy	Ox. State
207.3	+5 (oxide)
208.5	+5 (connected to POx)

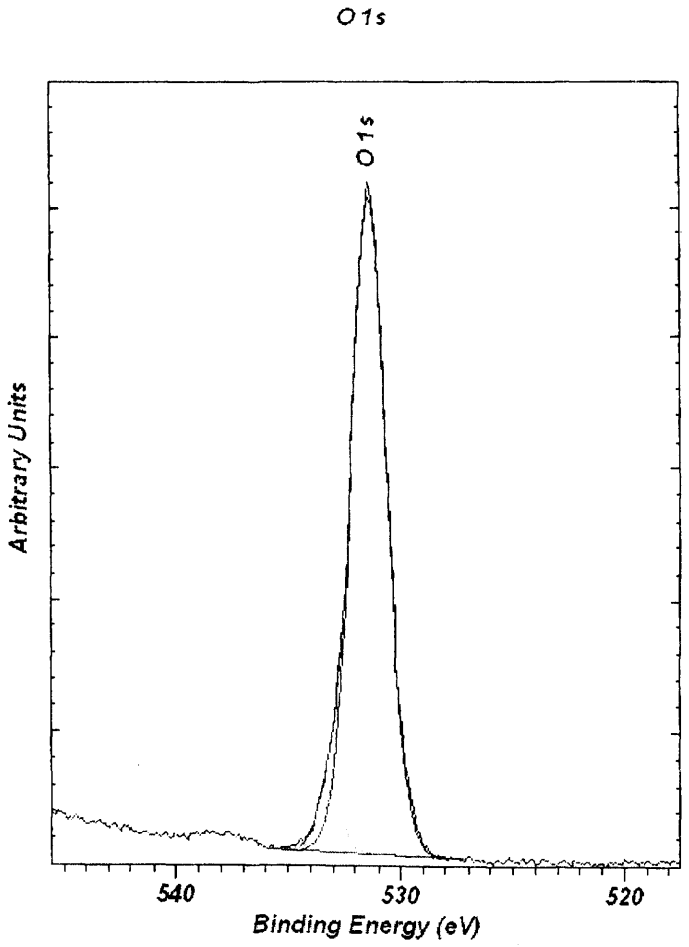

O(1s) Binding Energy	Possible Species
531.4	CO_3, PO_4, OH
533.1	

A19(c)

8.1 Calc – $Nb_2P_4O_{15}$ Post MeOH Reactor

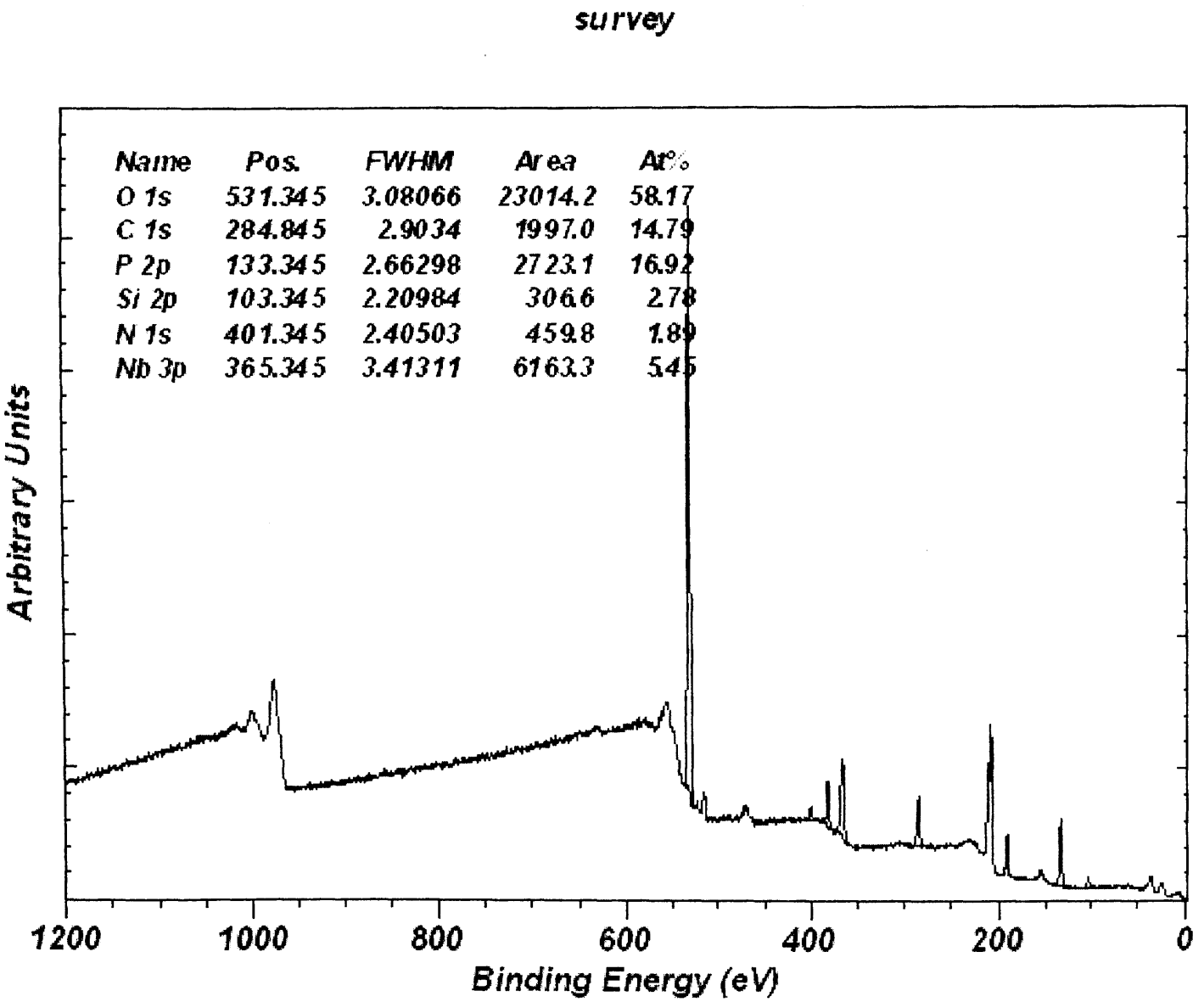

A20(a)

8.1 Calc – $Nb_2P_4O_{15}$ Post MeOH Reactor

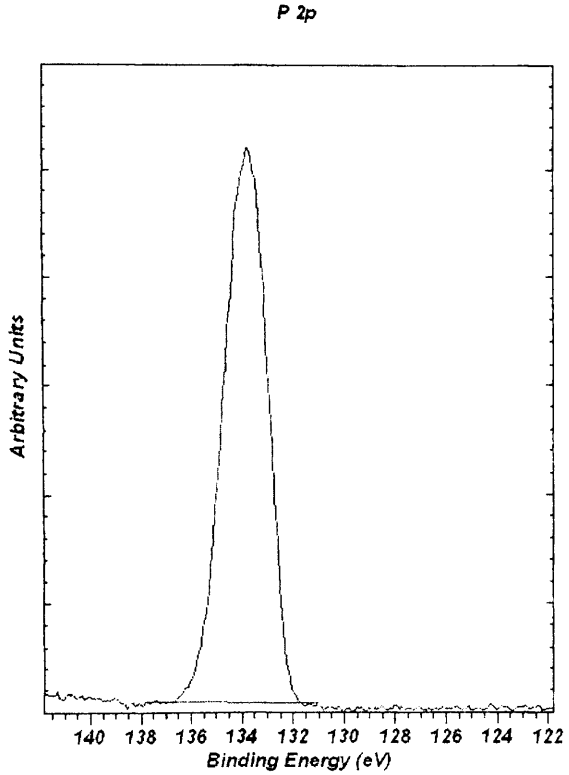

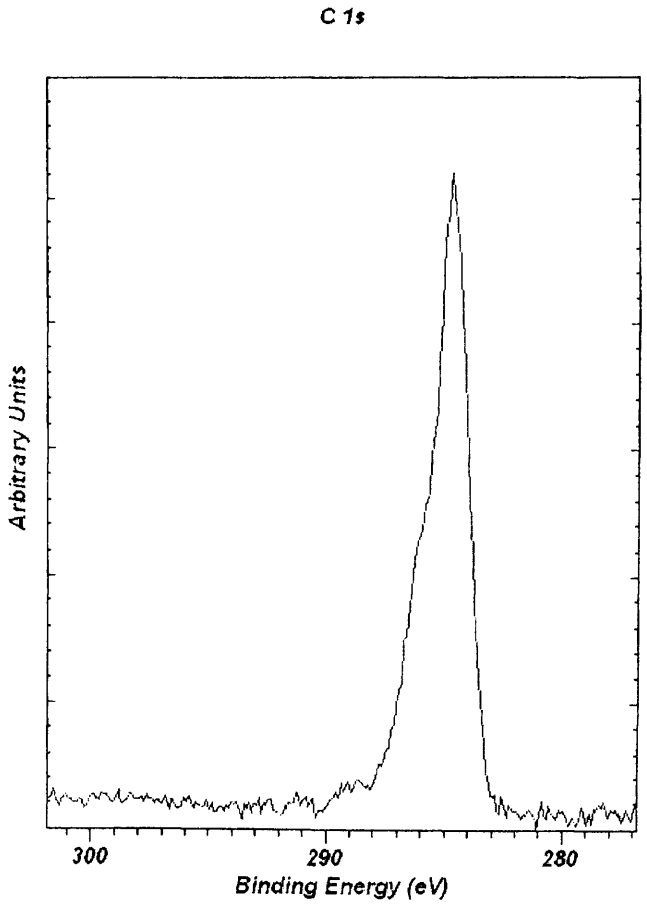

P(2p) Binding Energy	Possible Species
133.8	PO_x

A 20(b)

8.1 Calc – $Nb_2P_4O_{15}$ Post MeOH Reactor

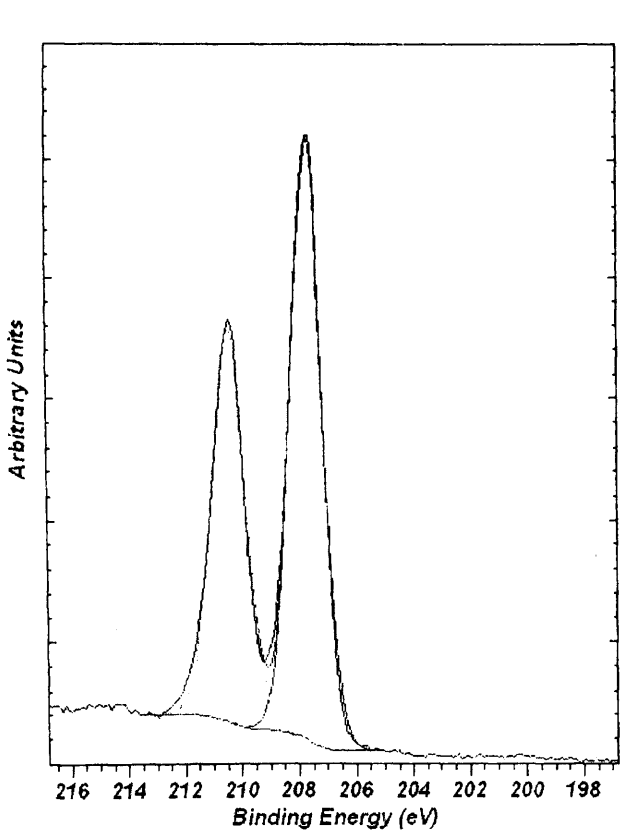

Nb(3d) 5/2 Peak Binding Energy	Ox. State
207.7	+5 (*)

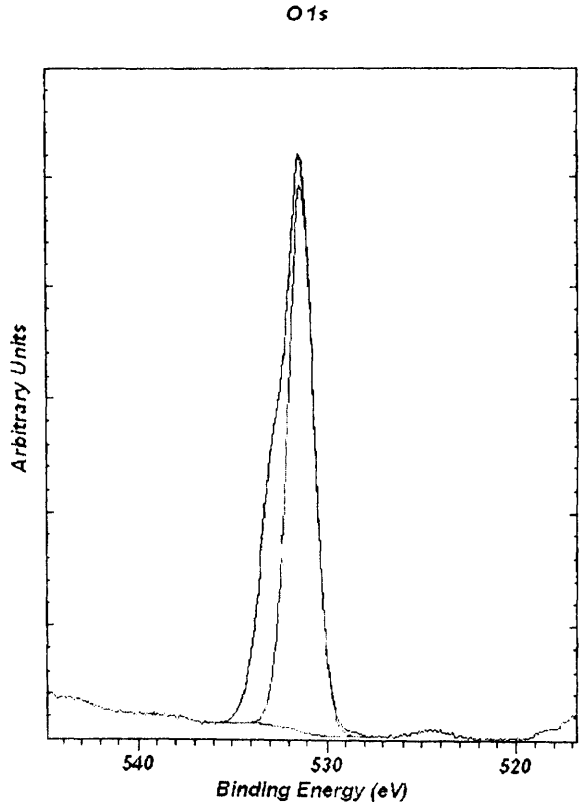

O(1s) Binding Energy	Possible Species
531.3	CO_3, PO_4, OH
532.8	SiO_2 Contamination

(*) Note: One reference points to NbO_2 (Nb +4 with same value)

A20(c)

4d – $NbOPO_4$ Calcined 500C in H_2

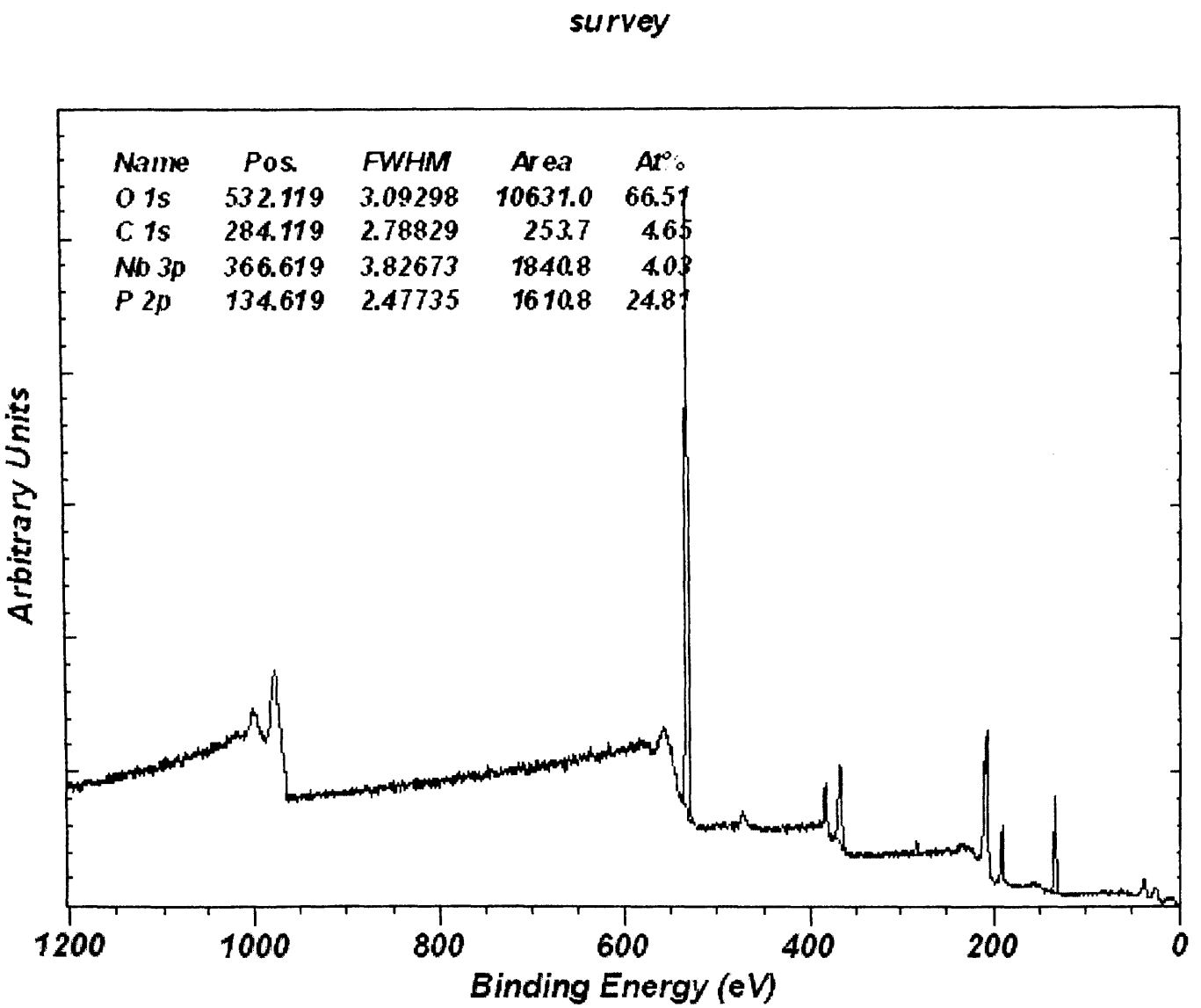

A21(a)

4d – $NbOPO_4$ Calcined 500C in H_2

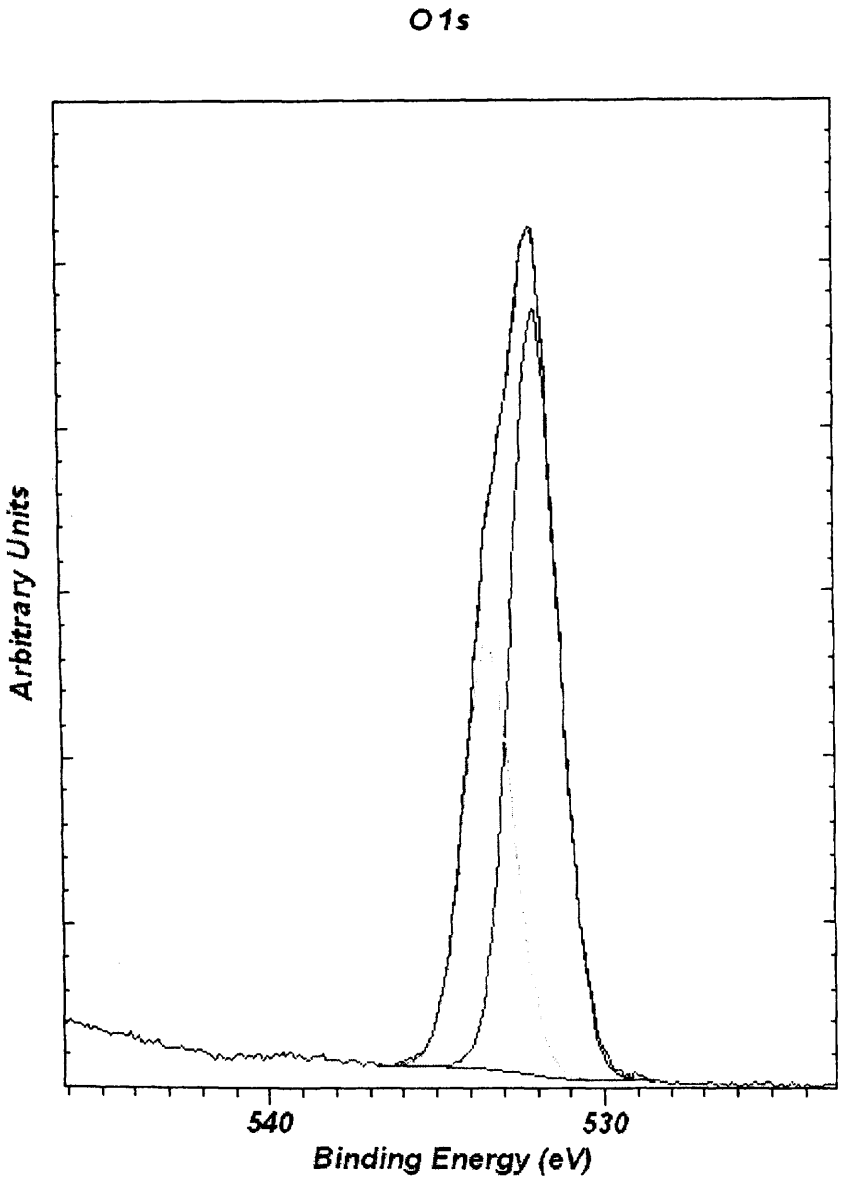

O(1s) Binding Energy	Possible Species
532.0	CO_3, PO_4, OH
533.4	

A21(b)

4d – $NbOPO_4$ Calcined 500C in H_2

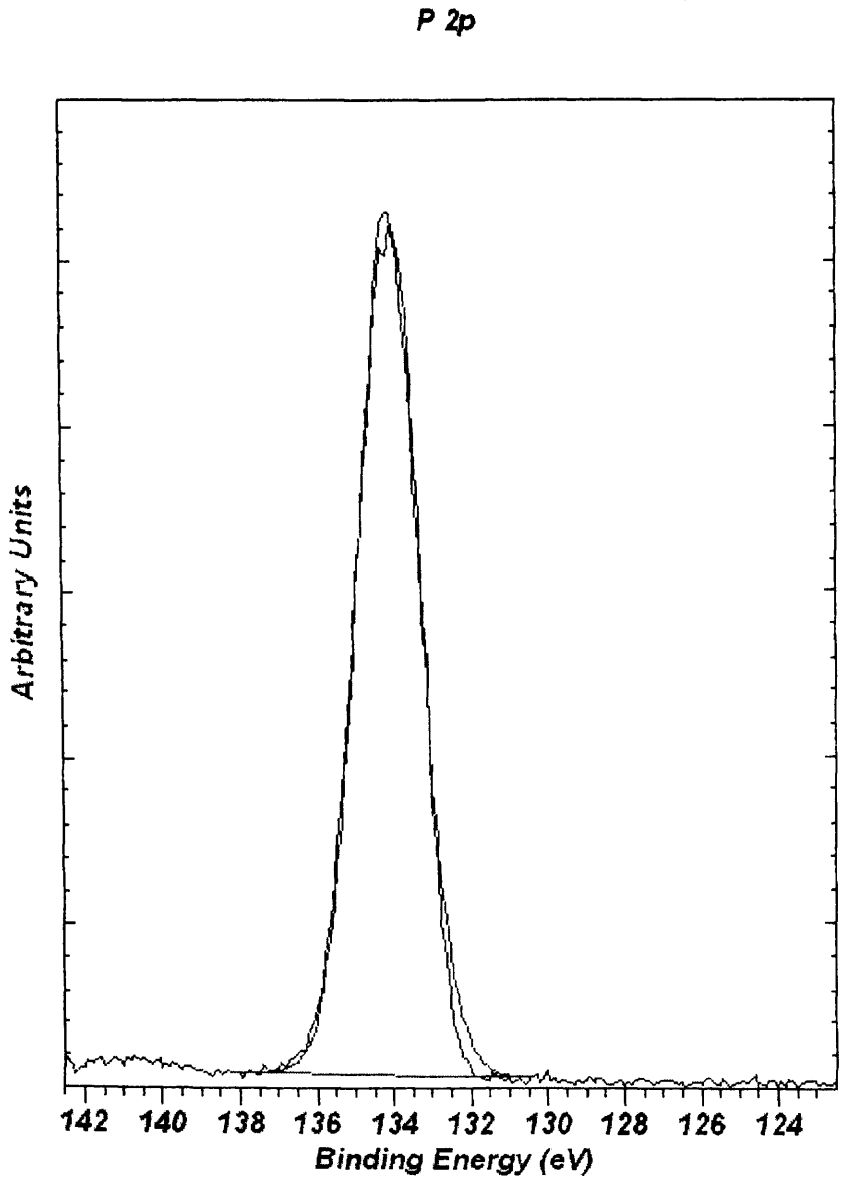

P(2p) Binding Energy	Pos. Species
134.1	$-PO_x$

A21(c)

4d – $NbOPO_4$ Calcined 500C in H_2

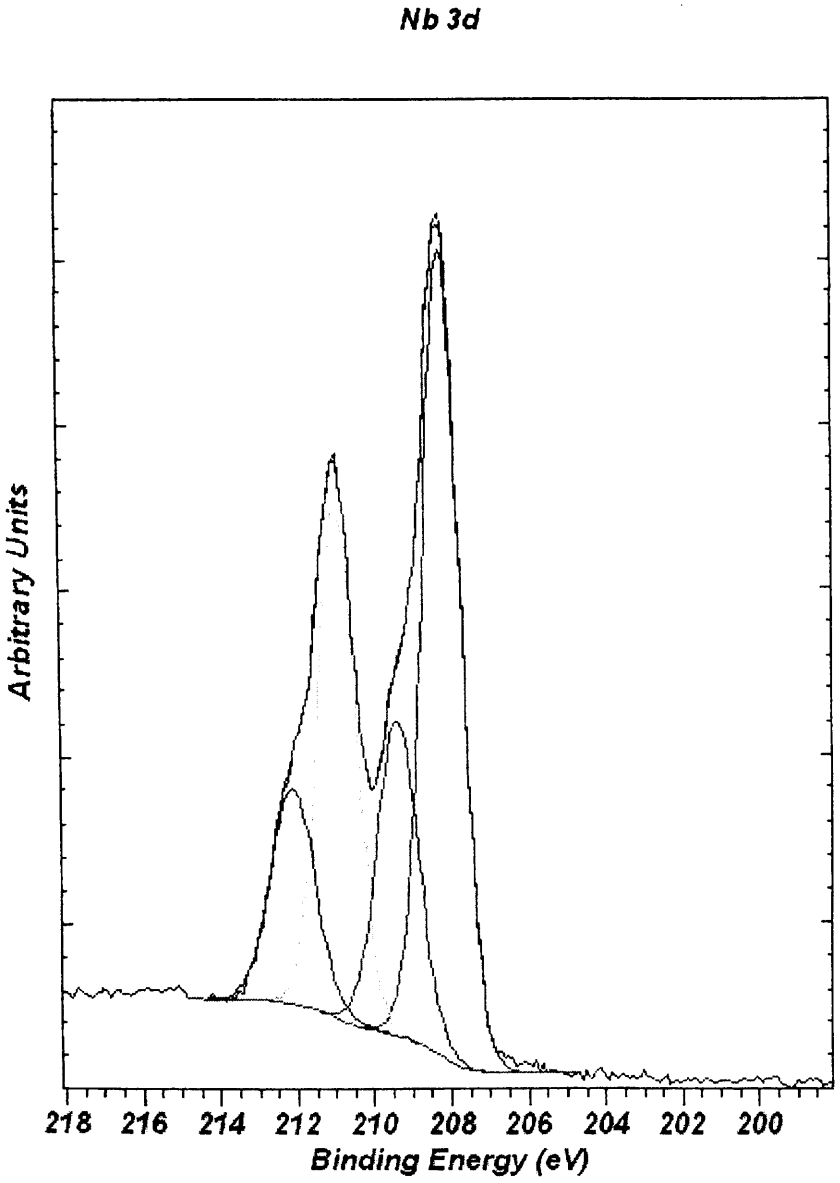

Nb(3d) 5/2 Peak Binding Energy	Ox. State
208.2	+5
209.4	Nb in highly electron withdrawing environment ?

A21 (d)

4du – Used $NbOPO_4$ Calcined 500C in H_2

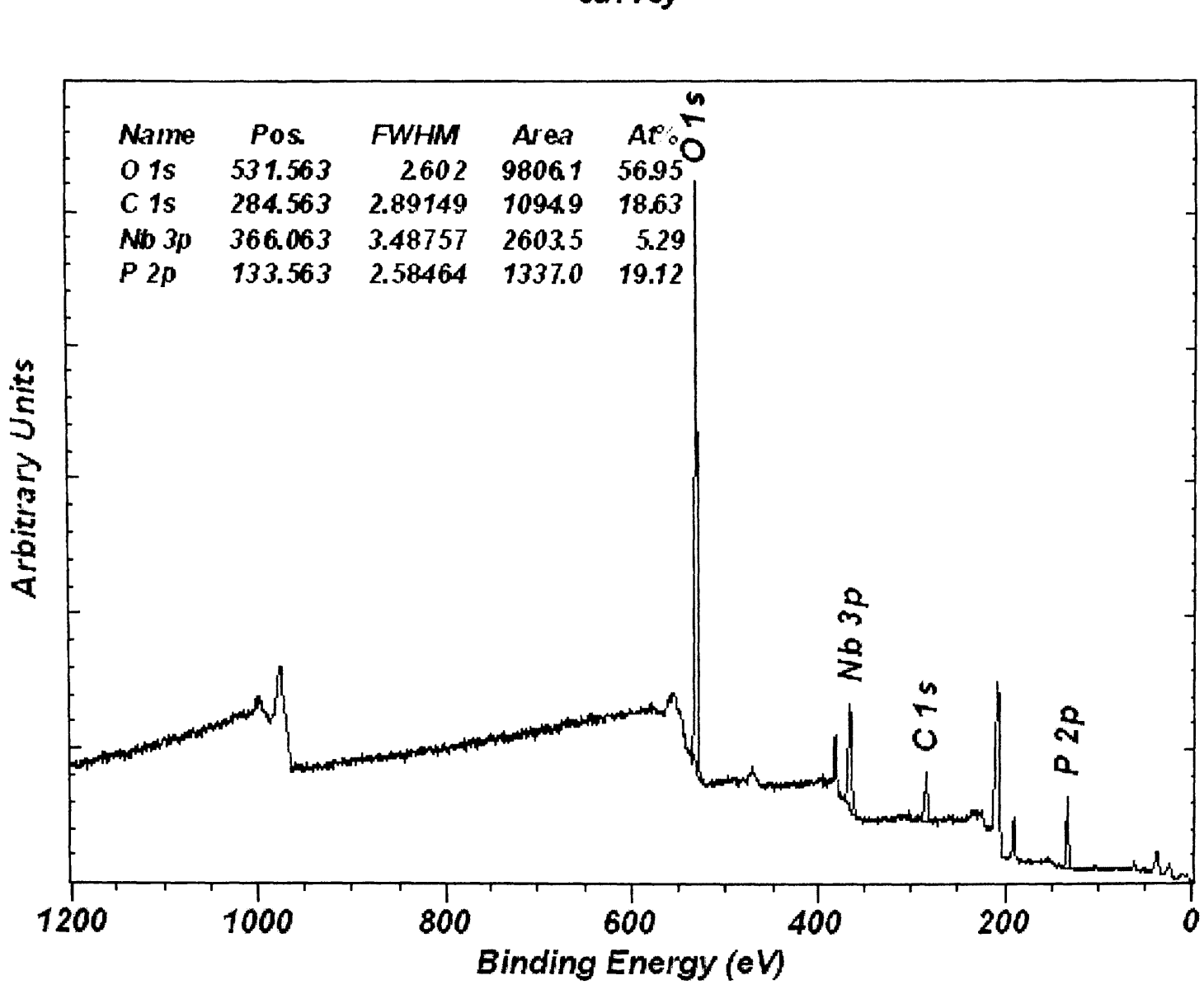

A22(a)

4du – Used $NbOPO_4$ Calcined 500C in H_2

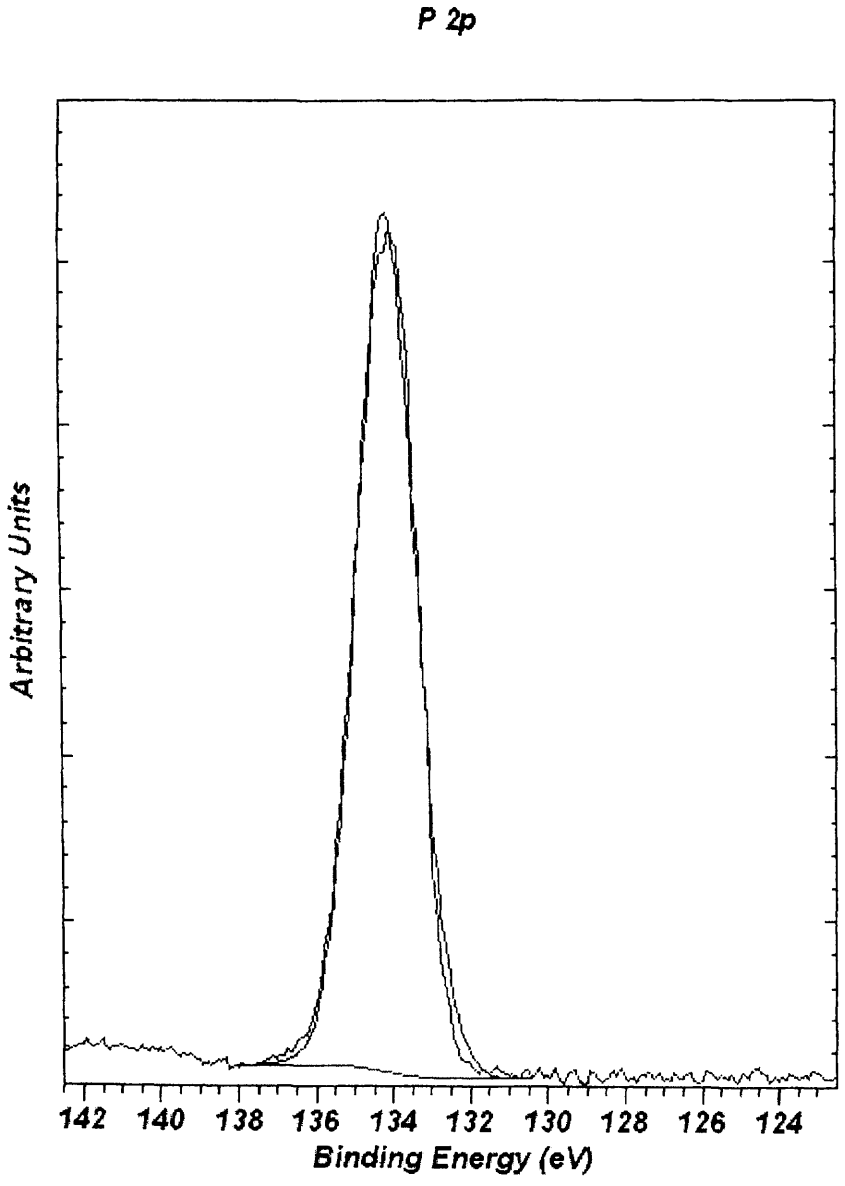

P(2p) Binding Energy	Pos. Species
134.1	$-PO_x$

A22(b)

4du – Used $NbOPO_4$ Calcined 500C in H_2

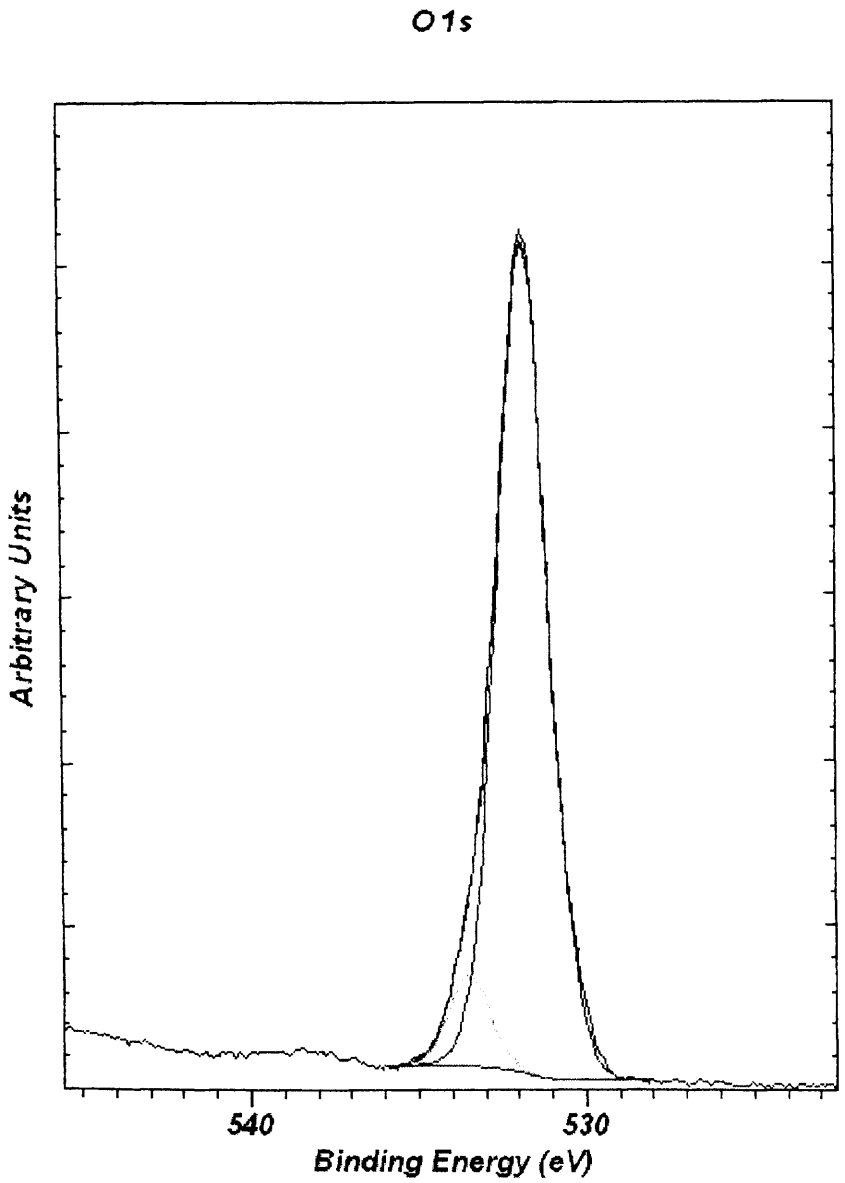

O(1s) Binding Energy	Possible Species
531.8	CO_3, PO_4, OH
533.5	

A22(c)

4du – Used $NbOPO_4$ Calcined 500C in H_2

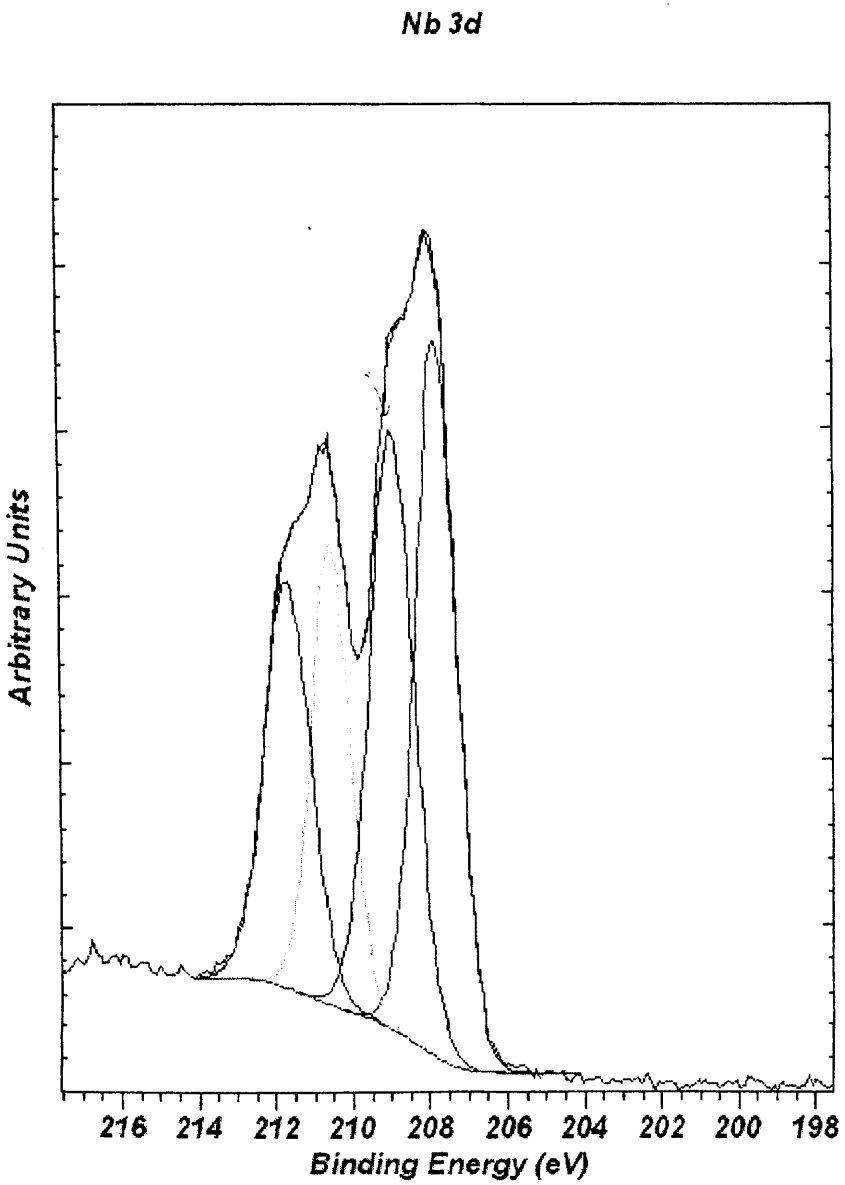

Nb(3d) 5/2 Peak Binding Energy	Ox. State
207.8	+5
208.9	Nb in highly electron withdrawing environment ?

A22(d)

Nb2O5 up 7.2c 450

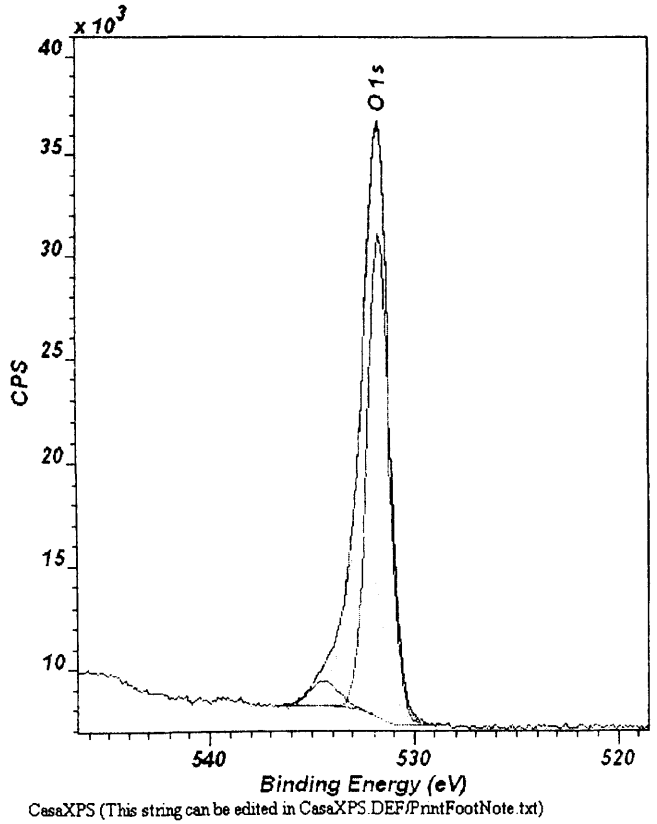

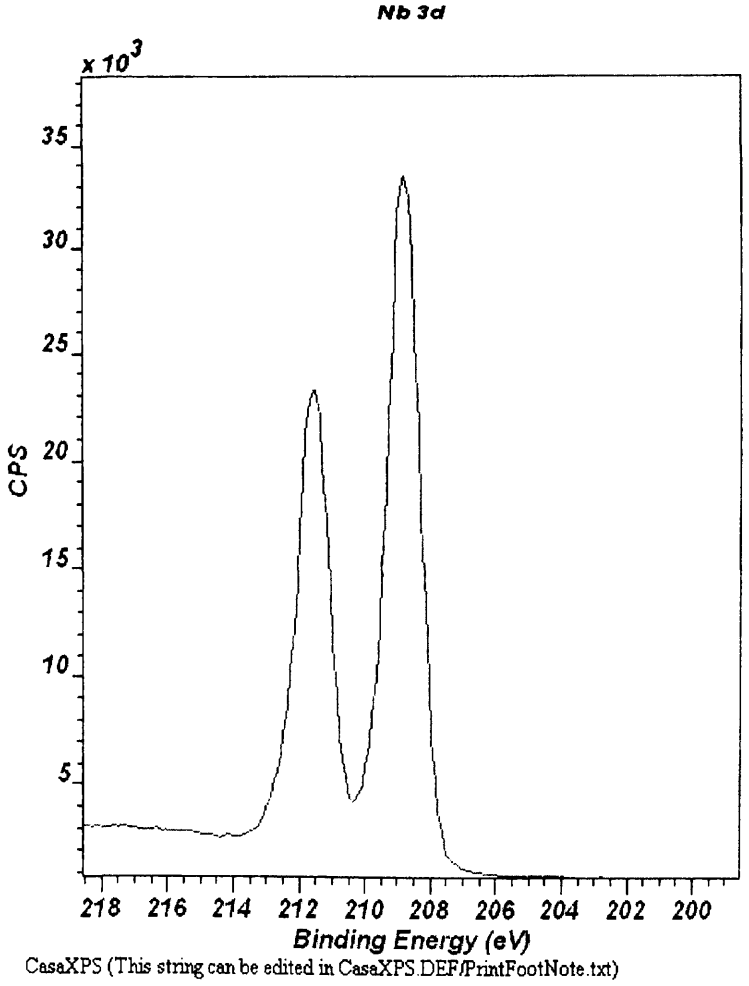

O(1s) Binding Energy	Possible Species
531.7	Oxide
532.5	SiO2 contam ?
534.4	SiO2 contam ?

Nb(3d) 5/2 Peak Binding Energy	Ox. State
208.8	+5

A23(a)

Nb2O5 up

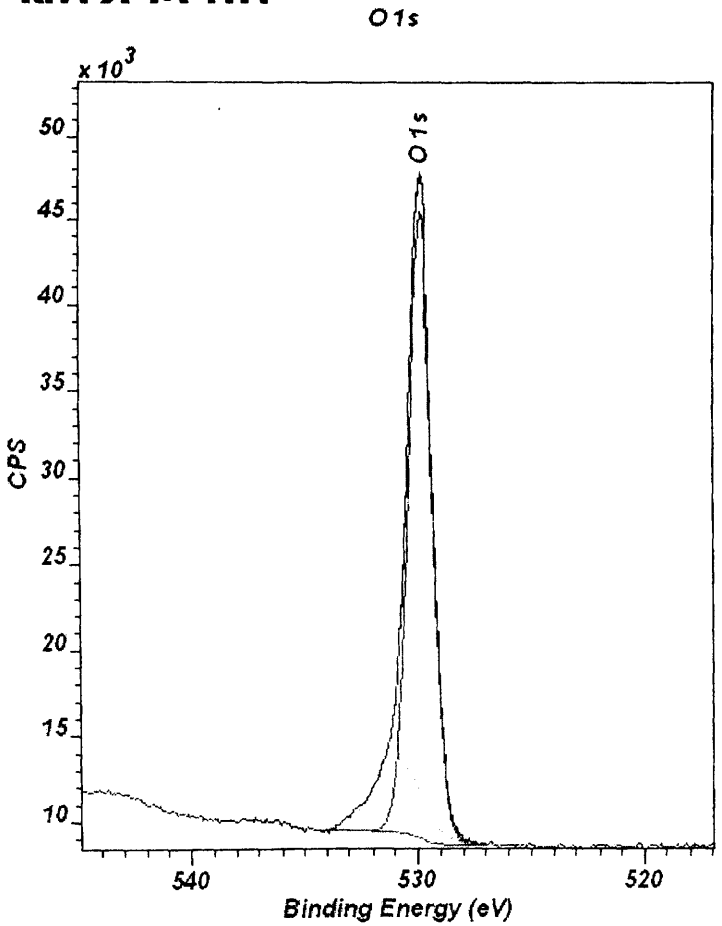

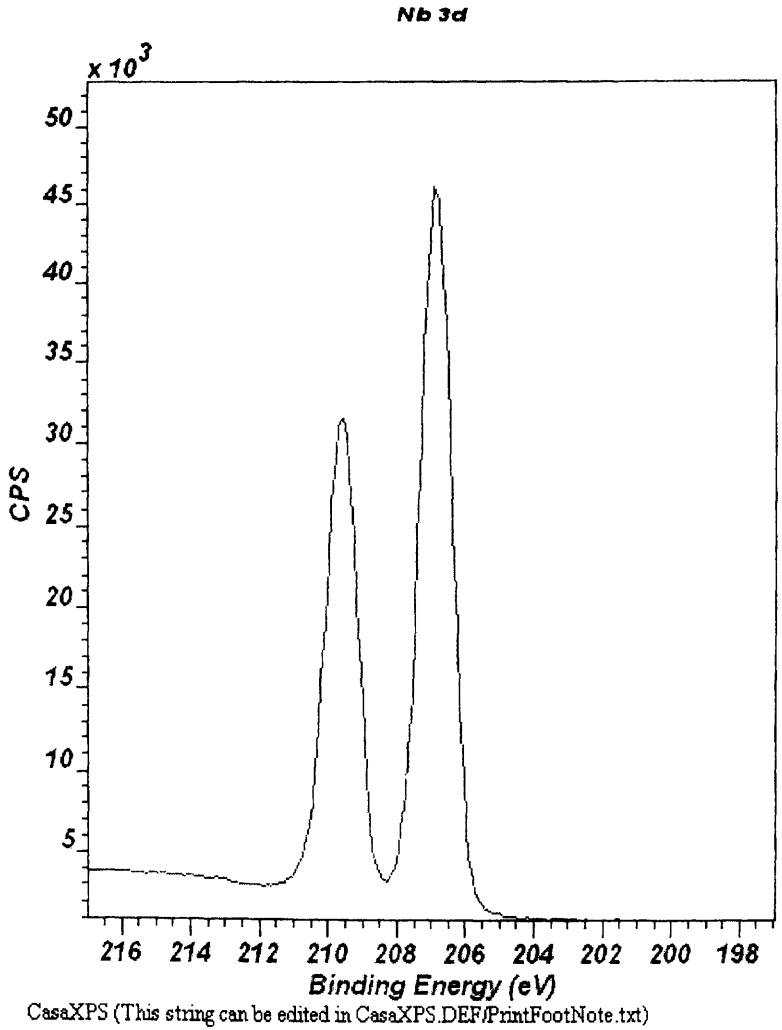

O(1s) Binding Energy	Possible Species
529.8	Oxide
530.9	OH

Nb(3d) 5/2 Peak Binding Energy	Ox. State
206.9	+5

A24(a)

Nb2O5 up

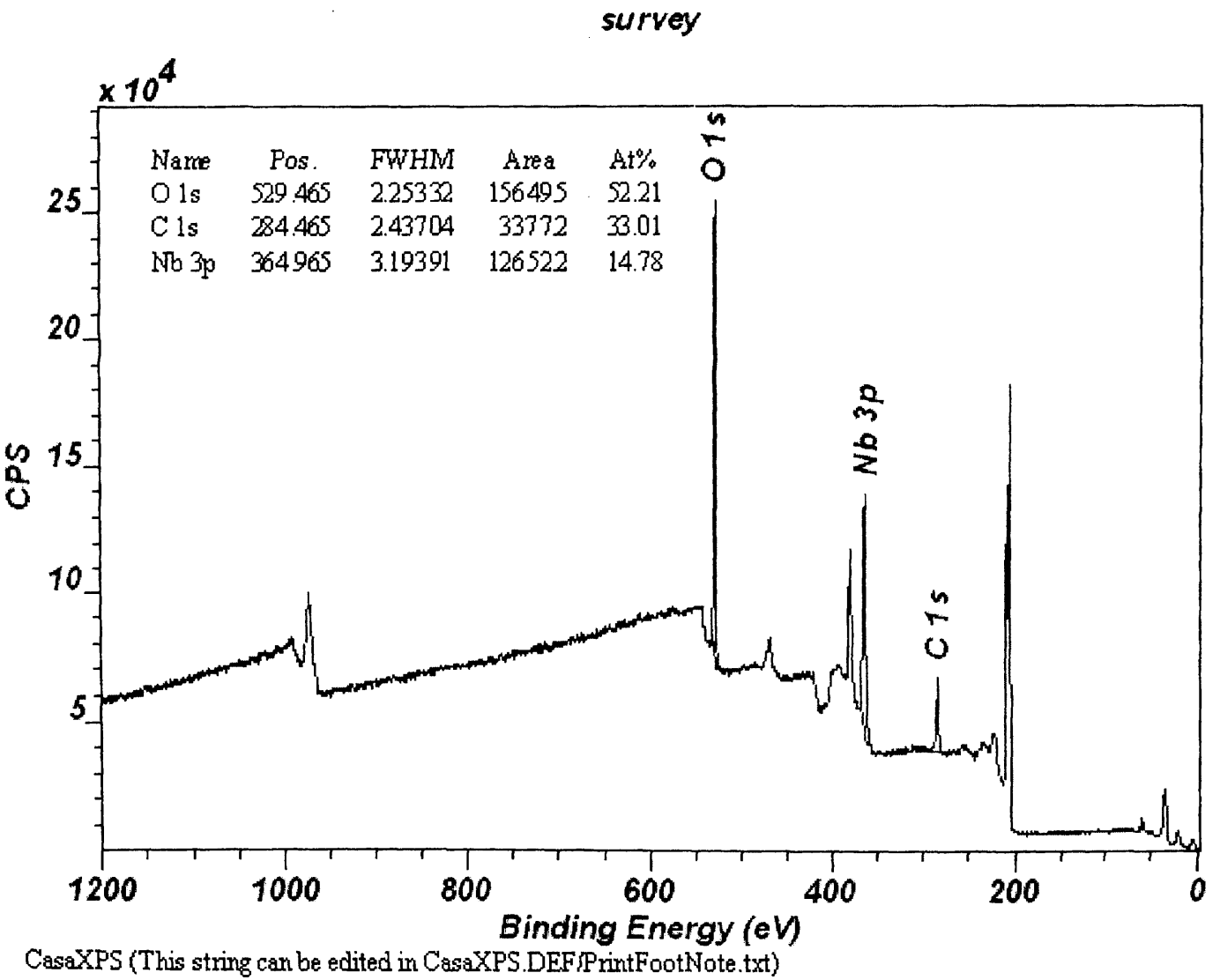

A25(a)

NbOPO4 2cup

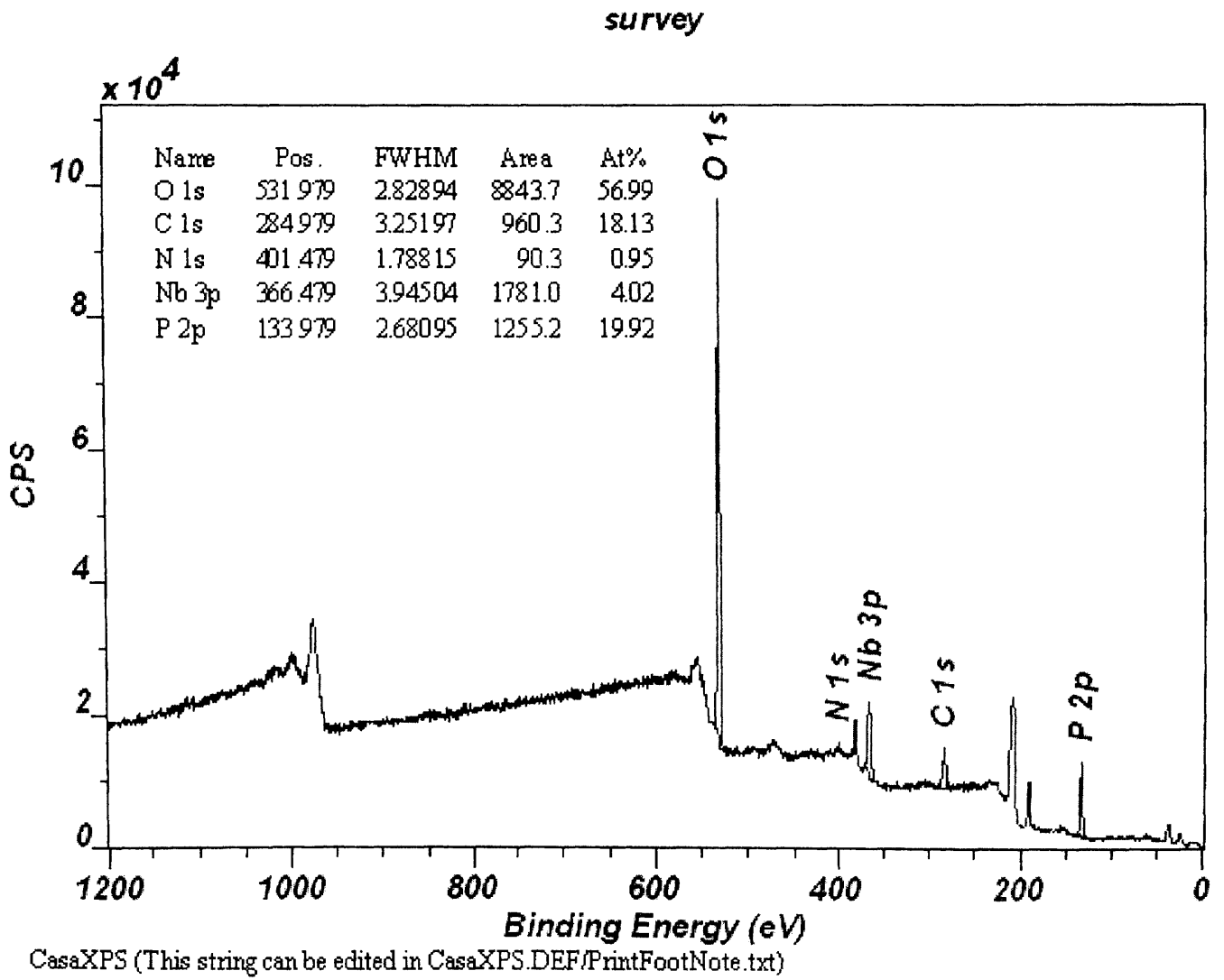

CasaXPS (This string can be edited in CasaXPS.DEF/PrintFootNote.txt)

A26(a)

NbOPO4 2cup

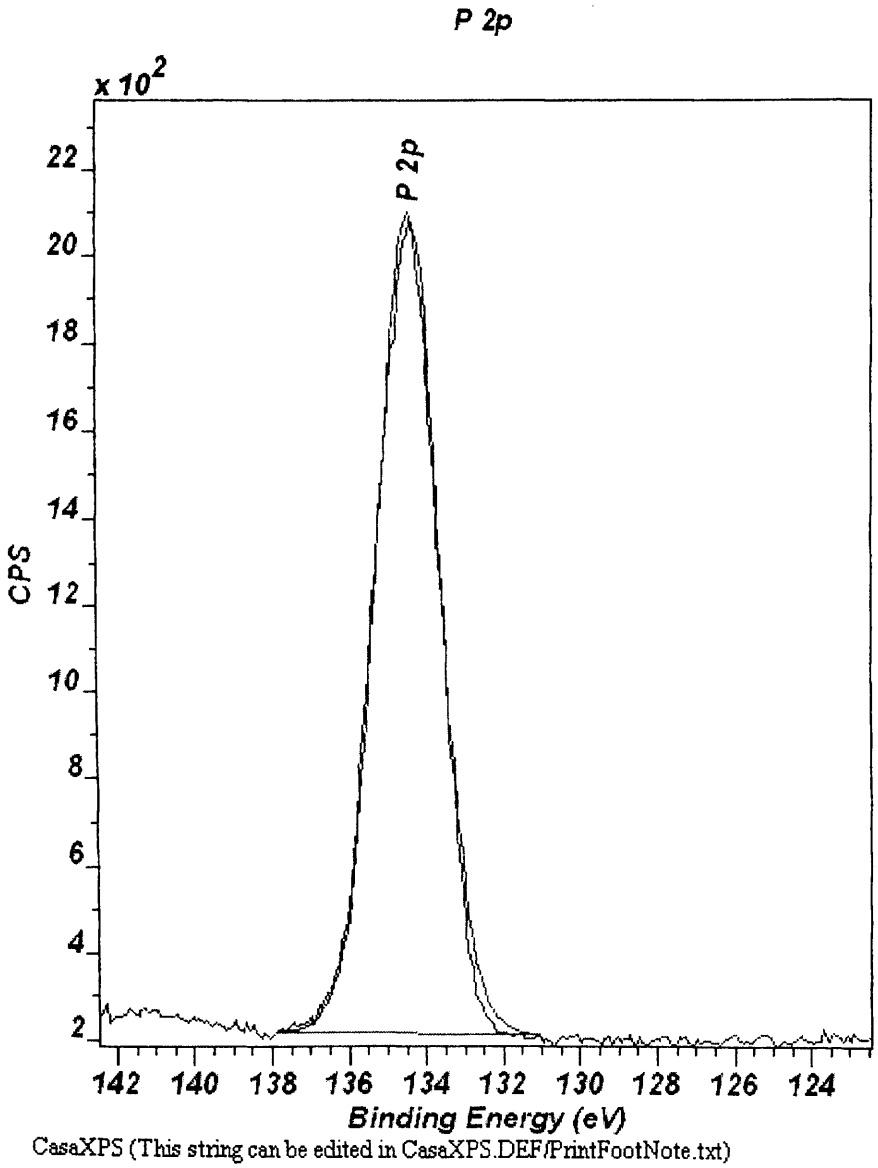

P(2p) Binding Energy	Possible Species
134.5	PO_x

A26(b)

NbOPO4 2cup

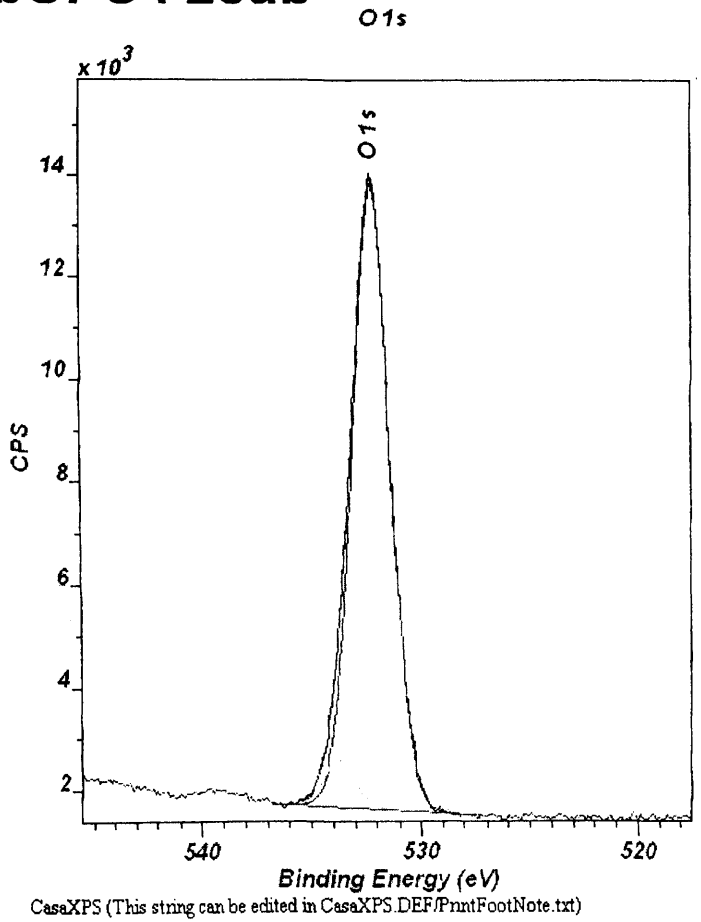

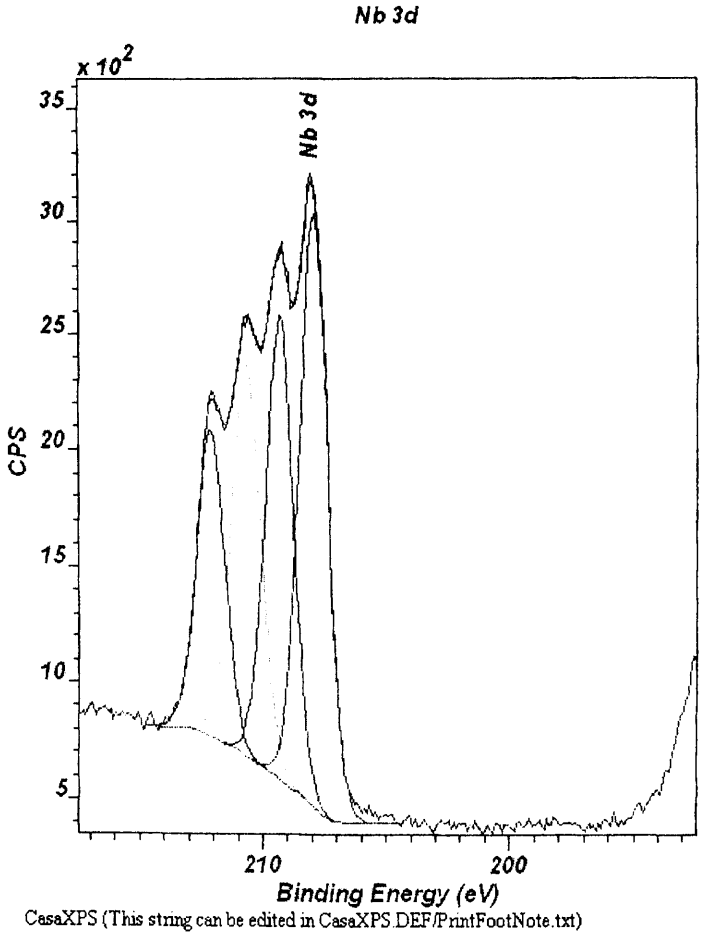

O(1s) Binding Energy	Possible Species
532.2	CO_3, PO_4
533.7	SiO_2 Contamination

Nb(3d) 5/2 Peak Binding Energy	Ox. State
207.9	+5
210.7	+5 attached to electron withdrawing group

A26(c)

NbOPO4 2cup

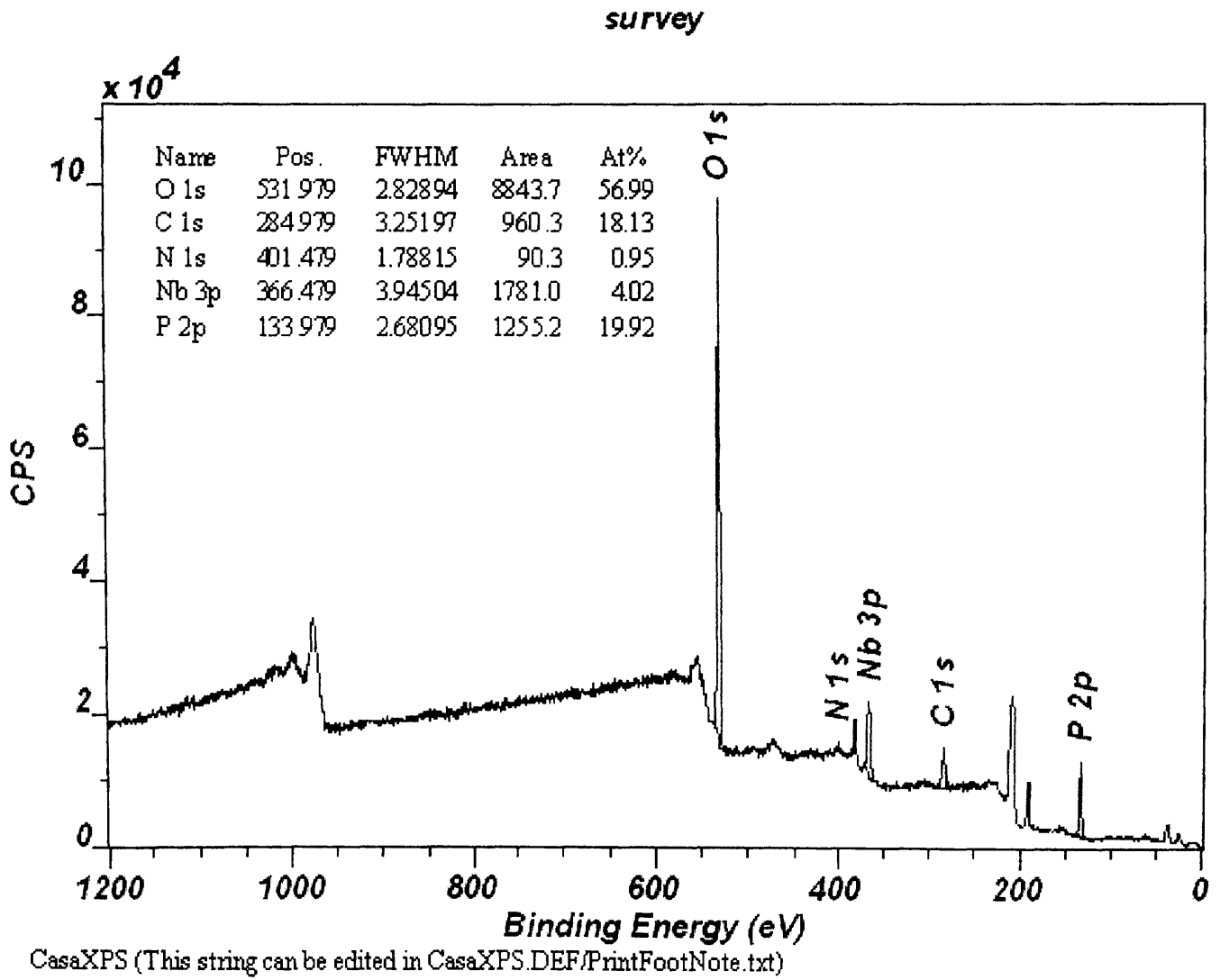

A27(c)

NbOPO4 2cup

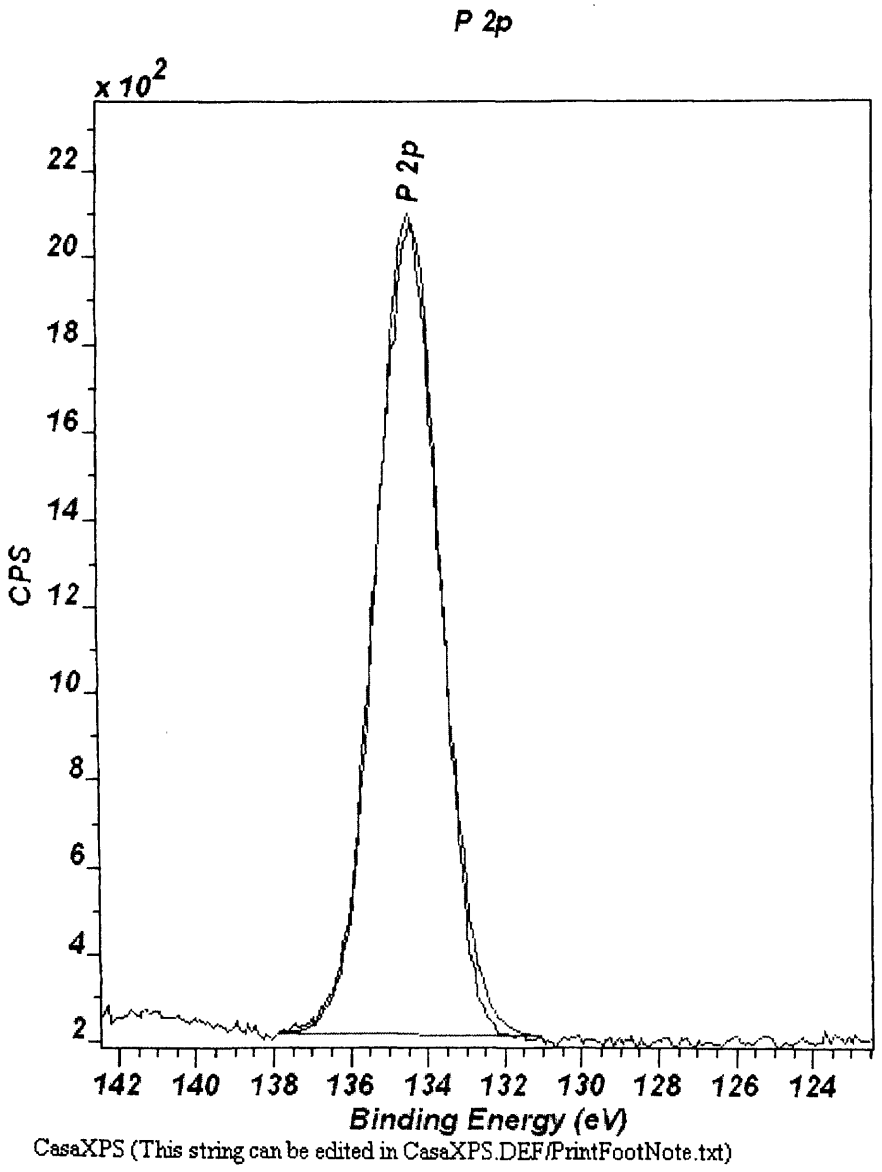

P(2p) Binding Energy	Possible Species
134.5	PO_x

A27(b)

NbOPO4 2cup

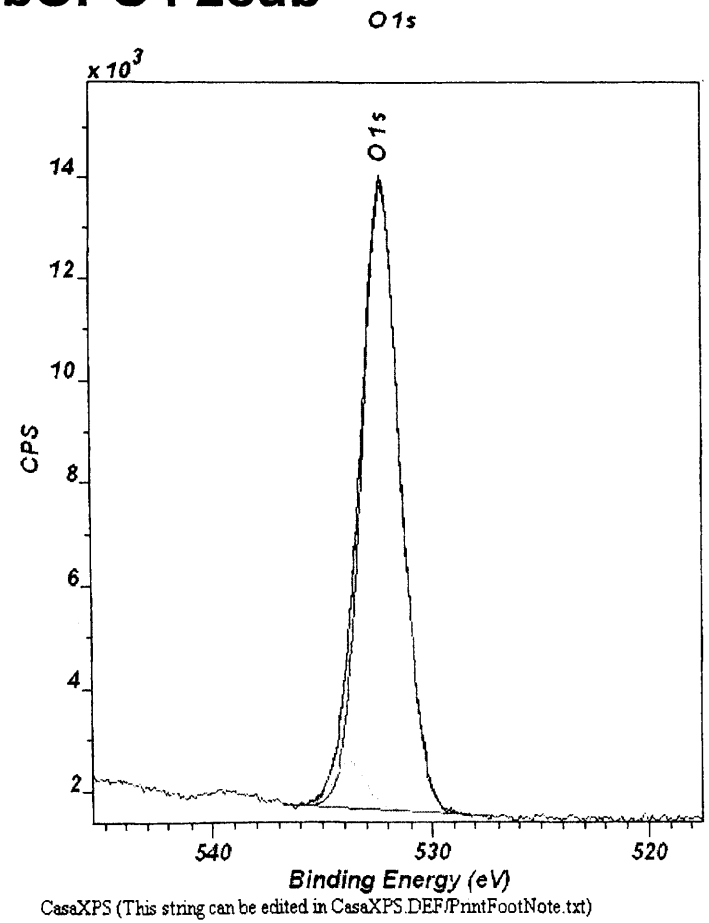

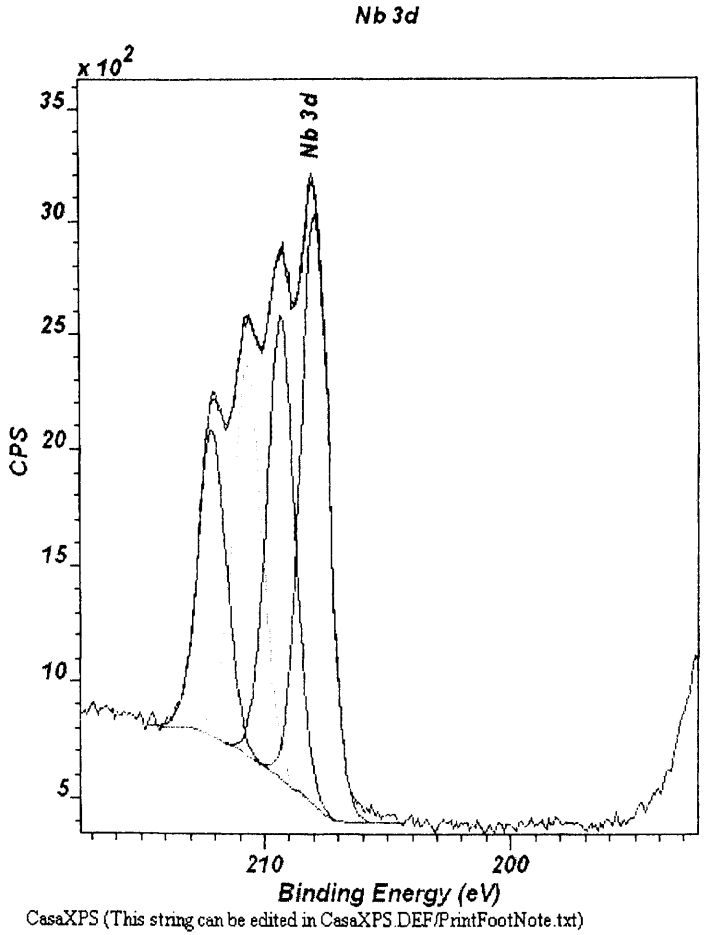

O(1s) Binding Energy	Possible Species
532.2	CO_3, PO_4
533.7	SiO_2 Contamination

Nb(3d) 5/2 Peak Binding Energy	Ox. State
207.9	+5
210.7	+5 attached to electron withdrawing group

A27(c)

NbPO5 6cup

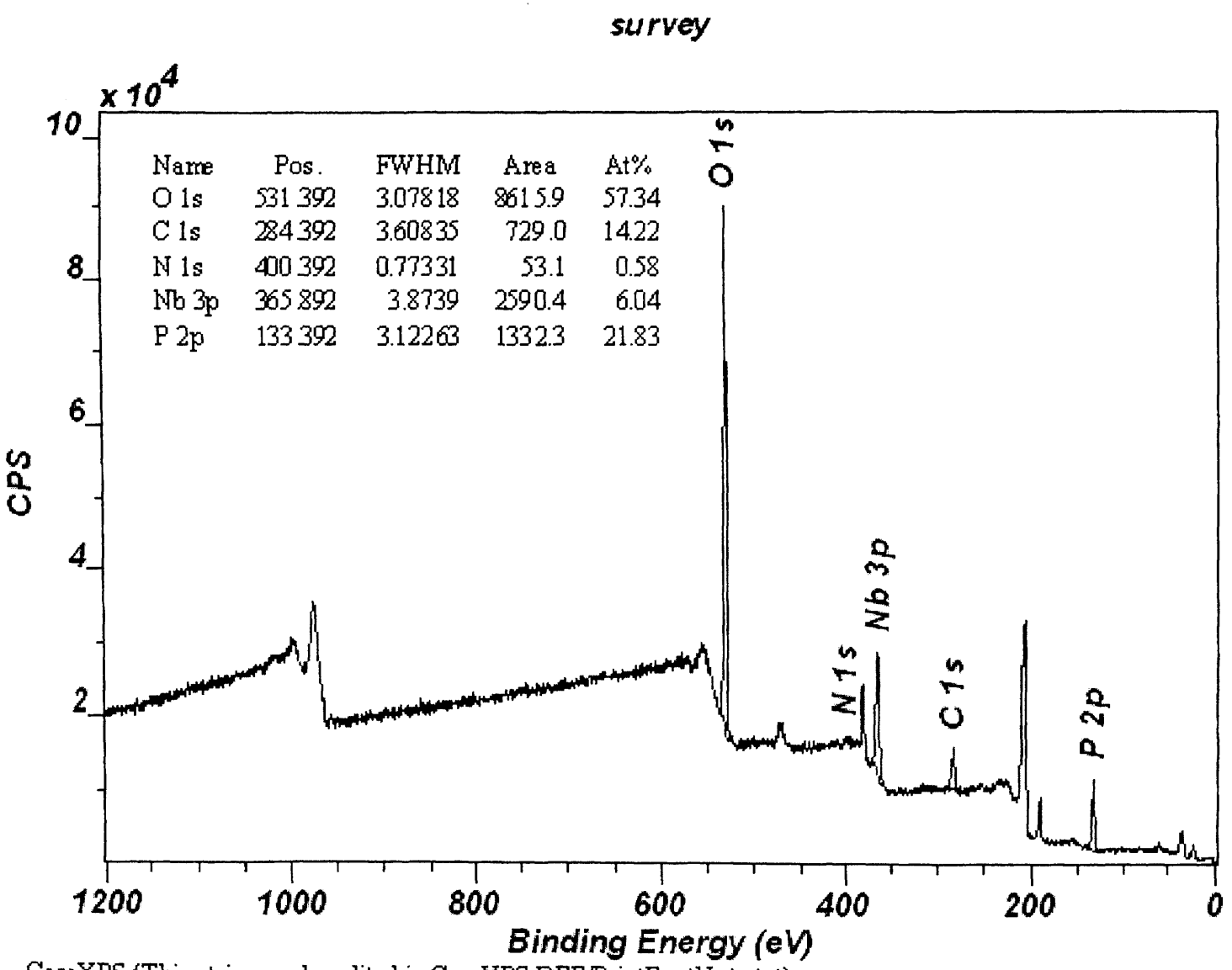

CasaXPS (This string can be edited in CasaXPS.DEF/PrintFootNote.txt)

A28 (a)

NbPO5 6cup

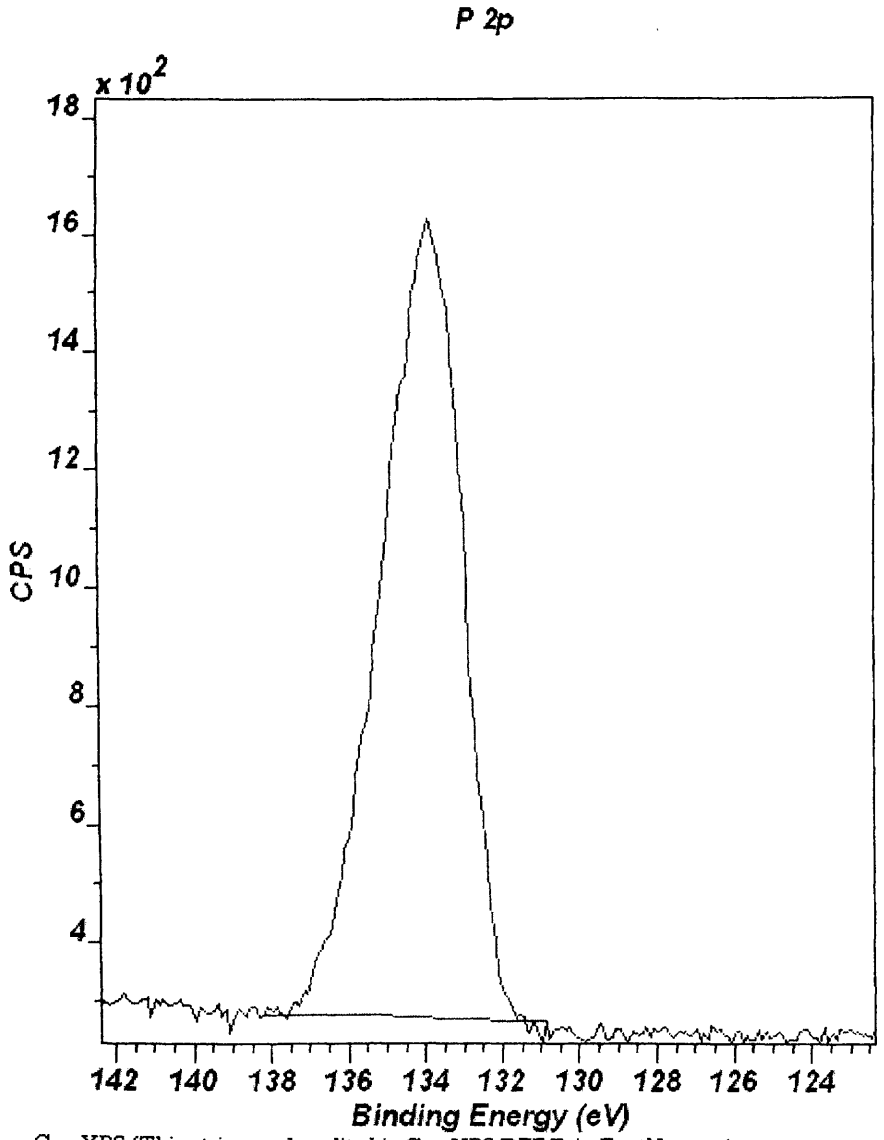

CasaXPS (This string can be edited in CasaXPS.DEF/PrintFootNote.txt)

P(2p) Binding Energy	Possible Species
133.9	PO_x

NbPO5 6cup

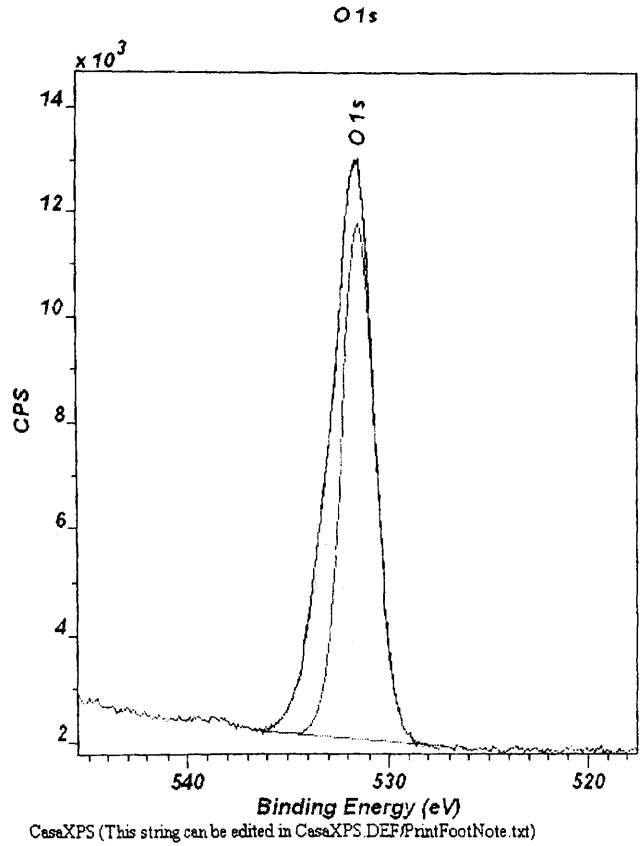

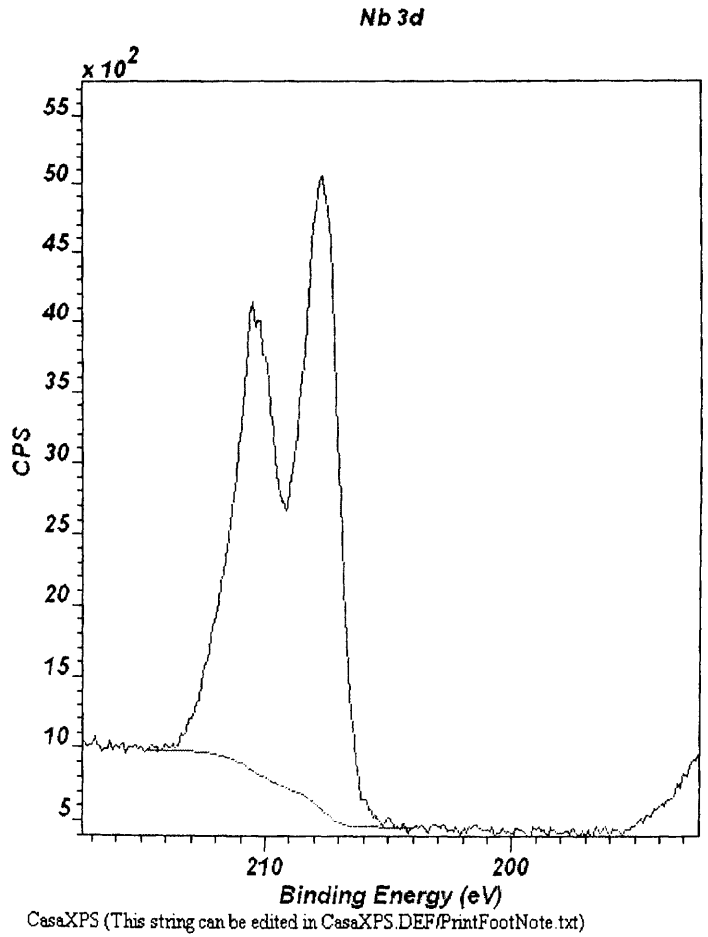

O(1s) Binding Energy	Possible Species
531.4	CO_3, PO_4, OH
532.9	PO, Water or just broadening due to

Nb(3d) 5/2 Peak Binding Energy	Ox. State
207.8	+5

A28(c)

NbP5 up

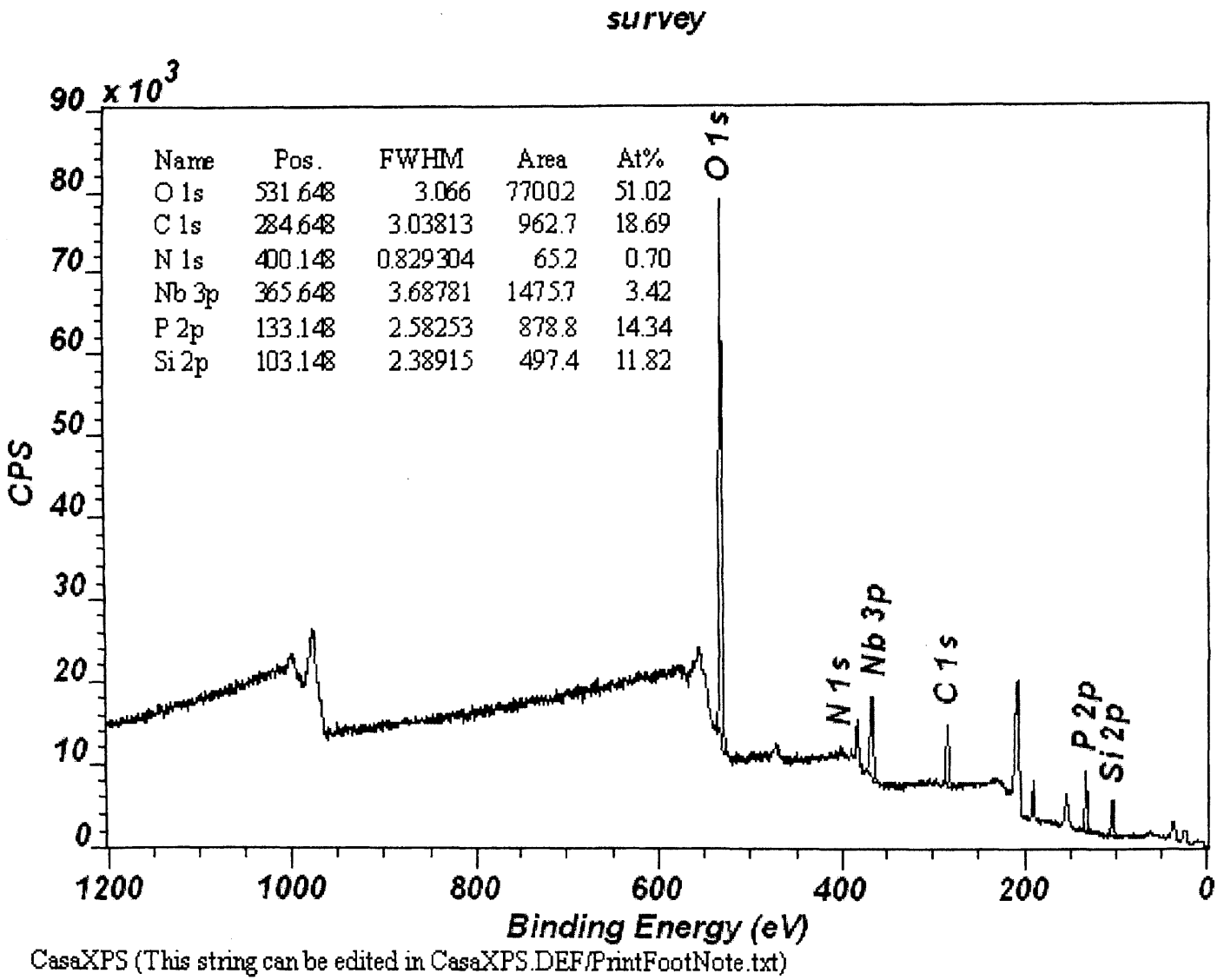
survey
90 x 10^3
80
70
60
50
40
30
20
10
0
CPS
Name Pos. FWHM Area At%
O 1s 531.648 3.066 77002 51.02
C 1s 284.648 3.03813 962.7 18.69
N 1s 400.148 0.829304 65.2 0.70
Nb 3p 365.648 3.68781 1475.7 3.42
P 2p 133.148 2.58253 878.8 14.34
Si 2p 103.148 2.38915 497.4 11.82
O 1s
N 1s
Nb 3p
C 1s
P 2p
Si 2p
1200
1000
800
600
400
200
0
Binding Energy (eV)
CasaXPS (This string can be edited in CasaXPS.DEF/PrintFootNote.txt)

A29(a)

NbP5 up

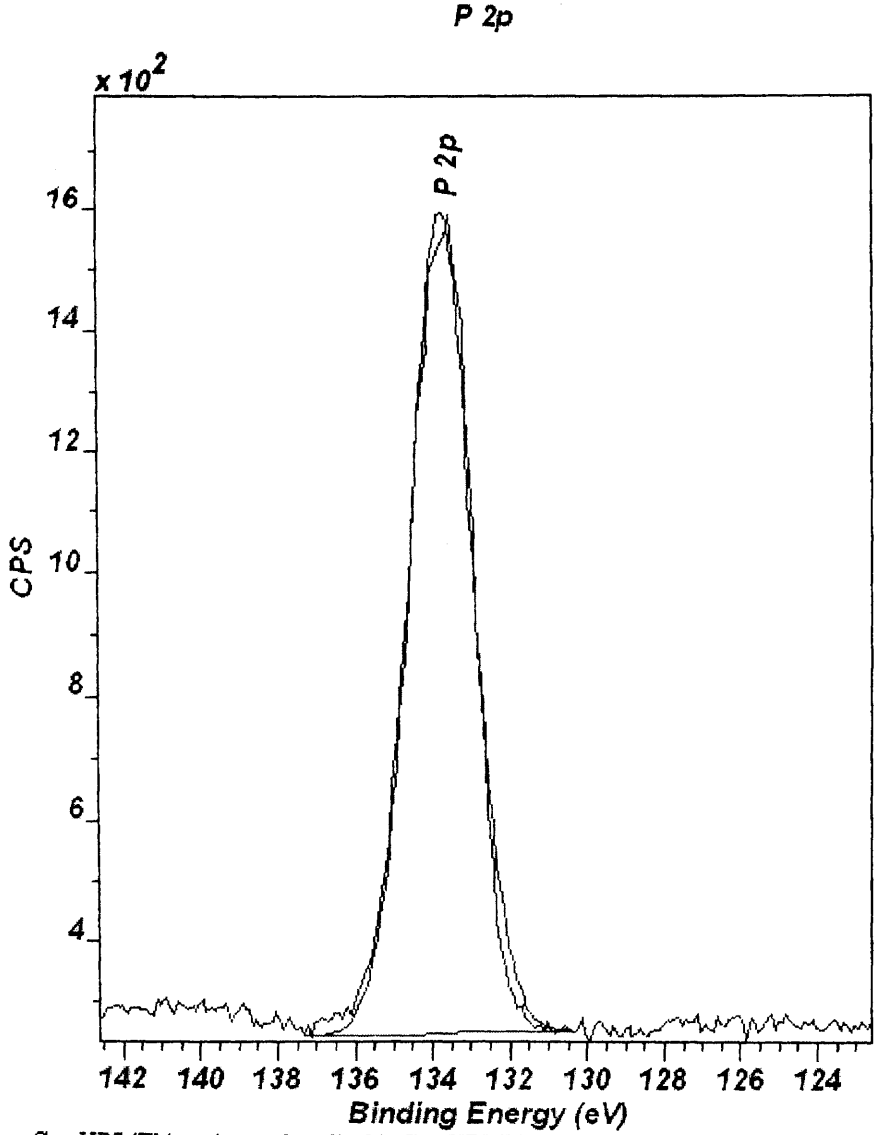

P(2p) Binding Energy	Possible Species
133.8	PO_x

NbP5up

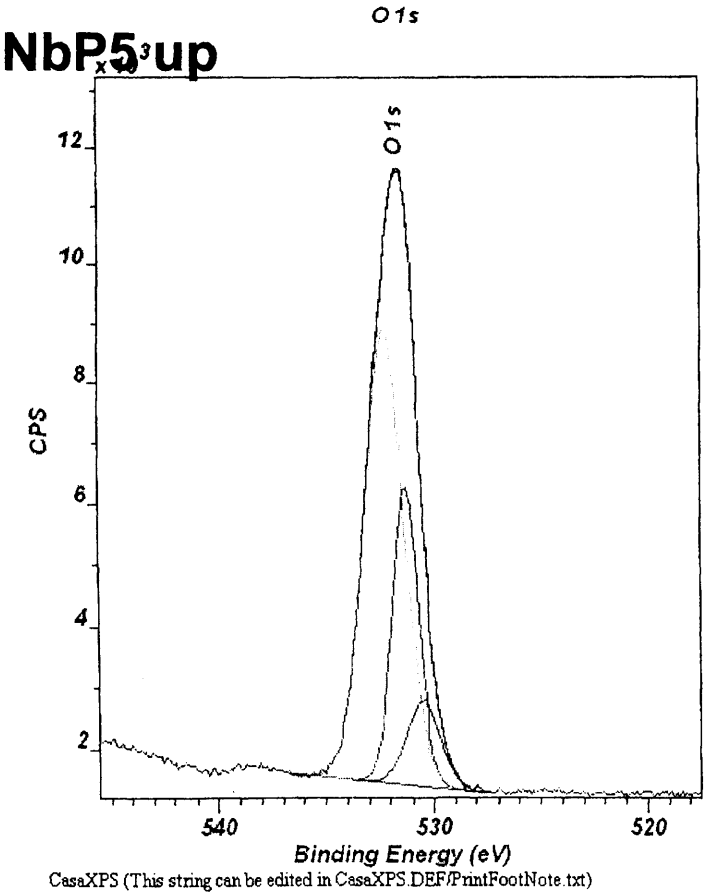

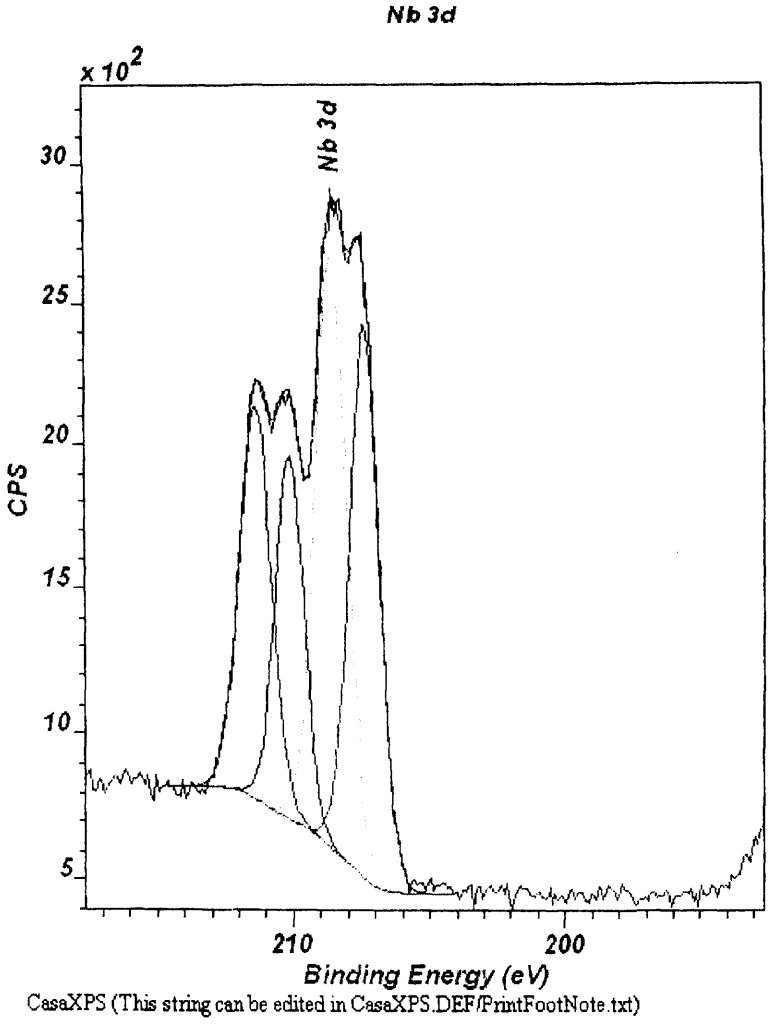

O(1s) Binding Energy	Possible Species
530.4	oxide
531.3	CO_3, PO_4, OH
532.3	PO

Nb(3d) 5/2 Peak Binding Energy	Ox. State
207.4	+5
210.1	+5 attached to electron withdrawing group

A 29(c)

NbPO5 3bup

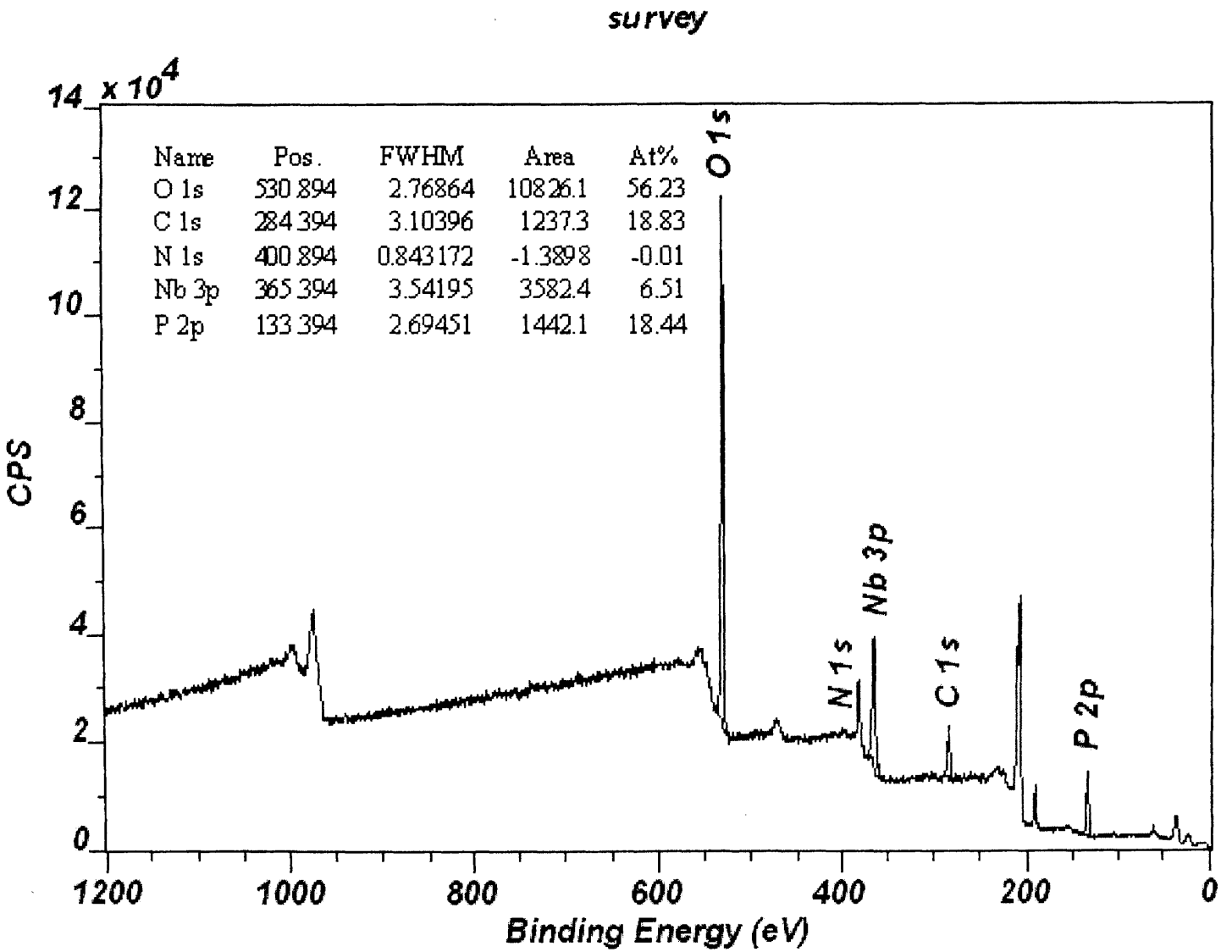

CasaXPS (This string can be edited in CasaXPS.DEF/PrintFootNote.txt)

A30(a)

NbPO5 3bup

P(2p) Binding Energy	Possible Species
133.9	PO_x

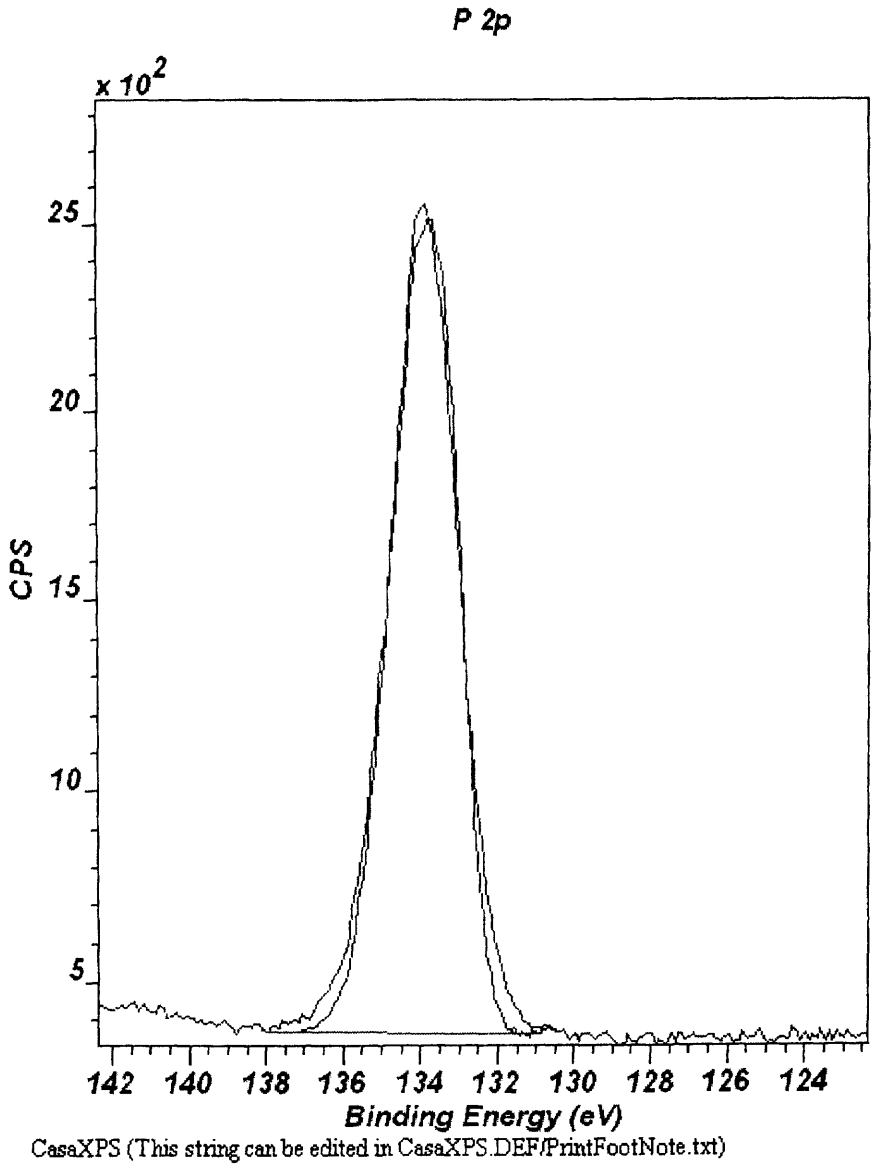

A30(b)

NbPO5 3hun

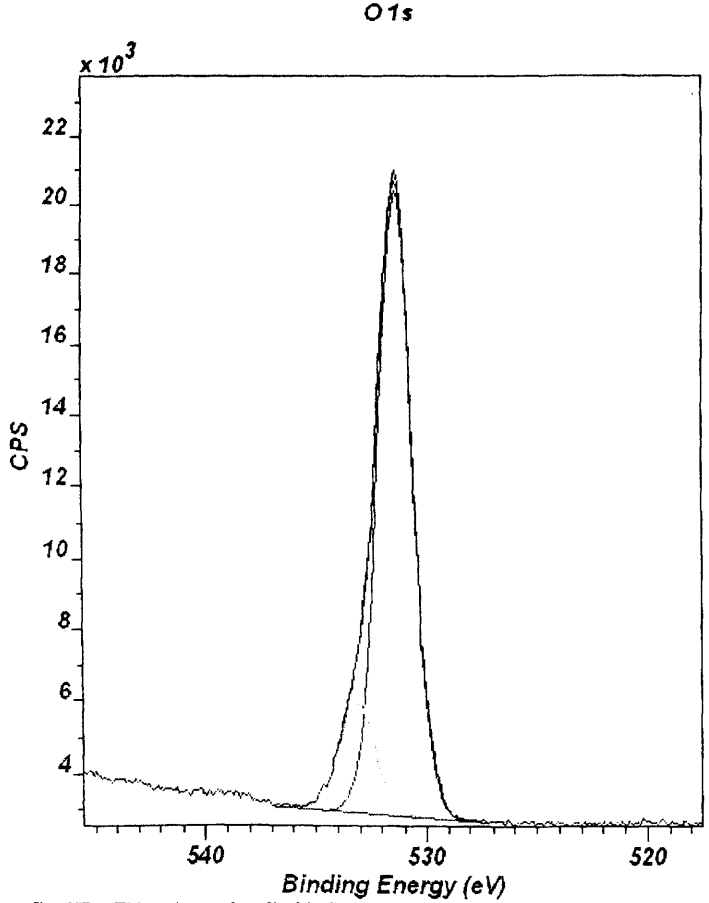

CasaXPS (This string can be edited in CasaXPS.DEF/PrintFootNote.txt)

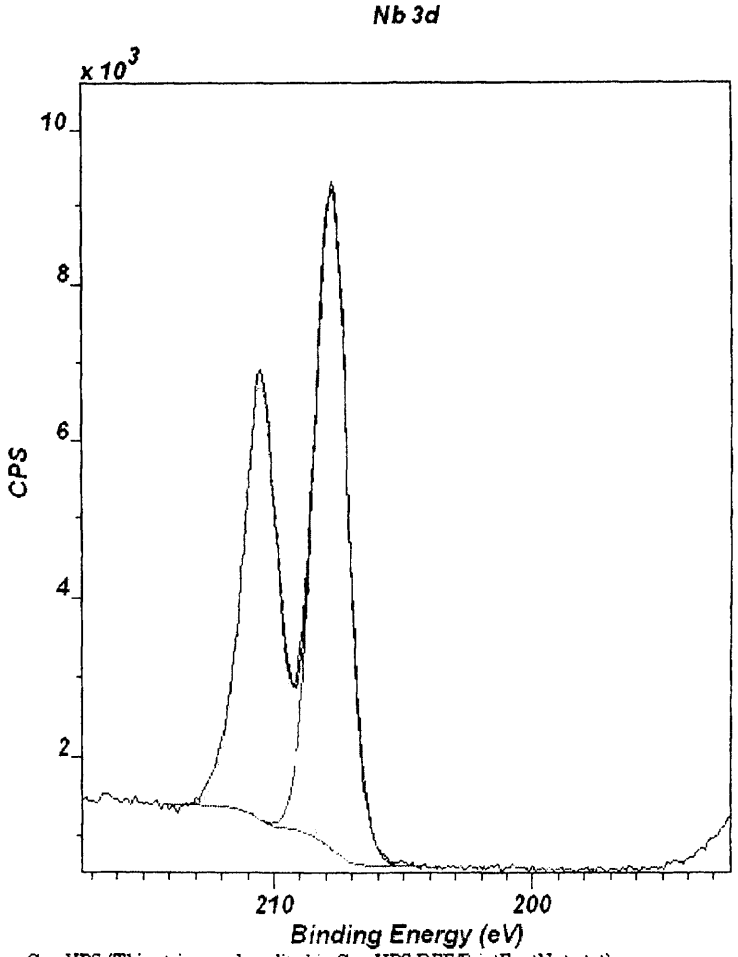

CasaXPS (This string can be edited in CasaXPS.DEF/PrintFootNote.txt)

O(1s) Binding Energy	Possible Species
531.3	CO_3, PO_4, OH
533.1	SiO_2 Contamination

Nb(3d) 5/2 Peak Binding Energy	Ox. State
207.6	+5

A30(c)

NbOPO4 6aup

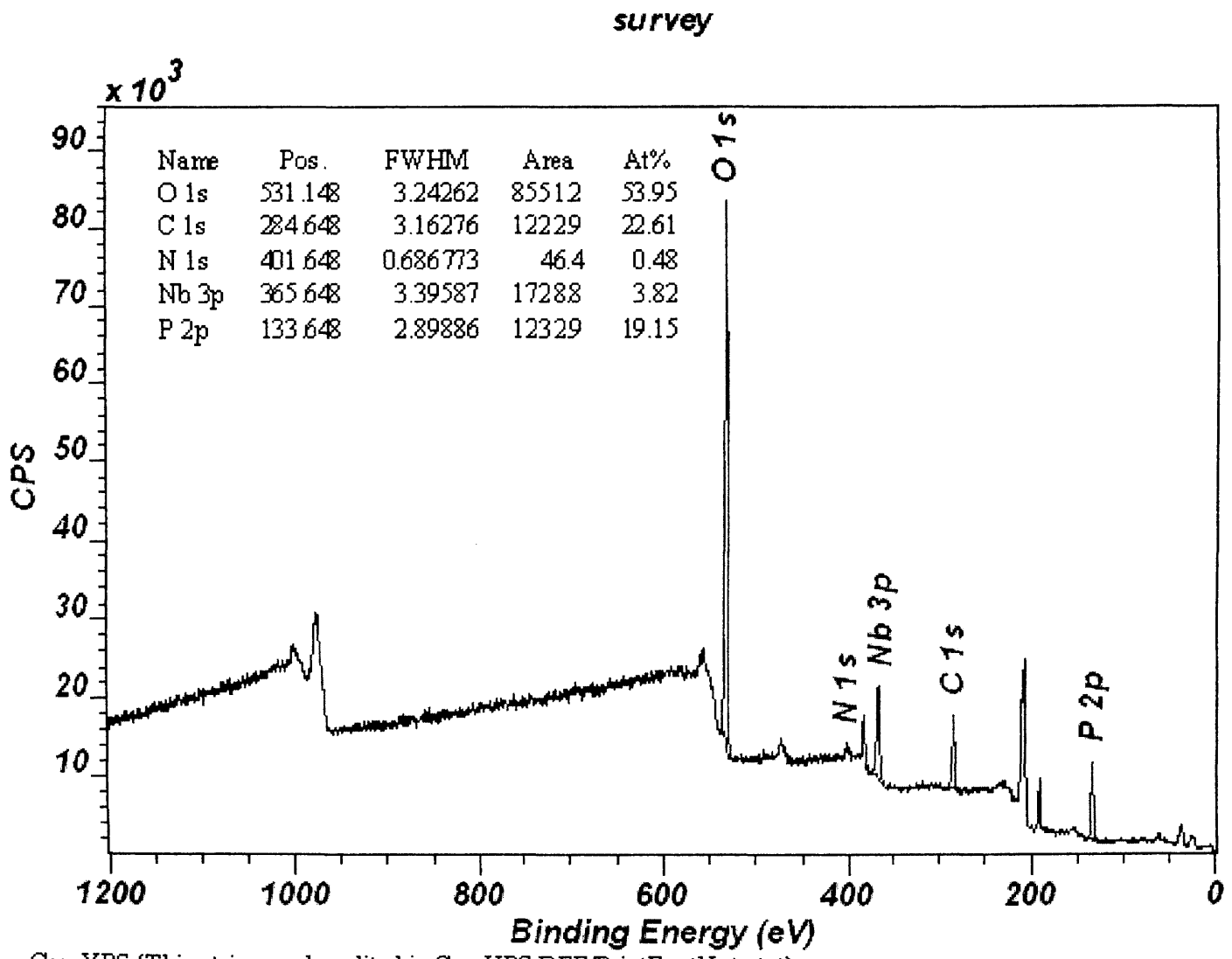

CasaXPS (This string can be edited in CasaXPS.DEF/PrintFootNote.txt)

A31(c)

NbOPO4 6aup

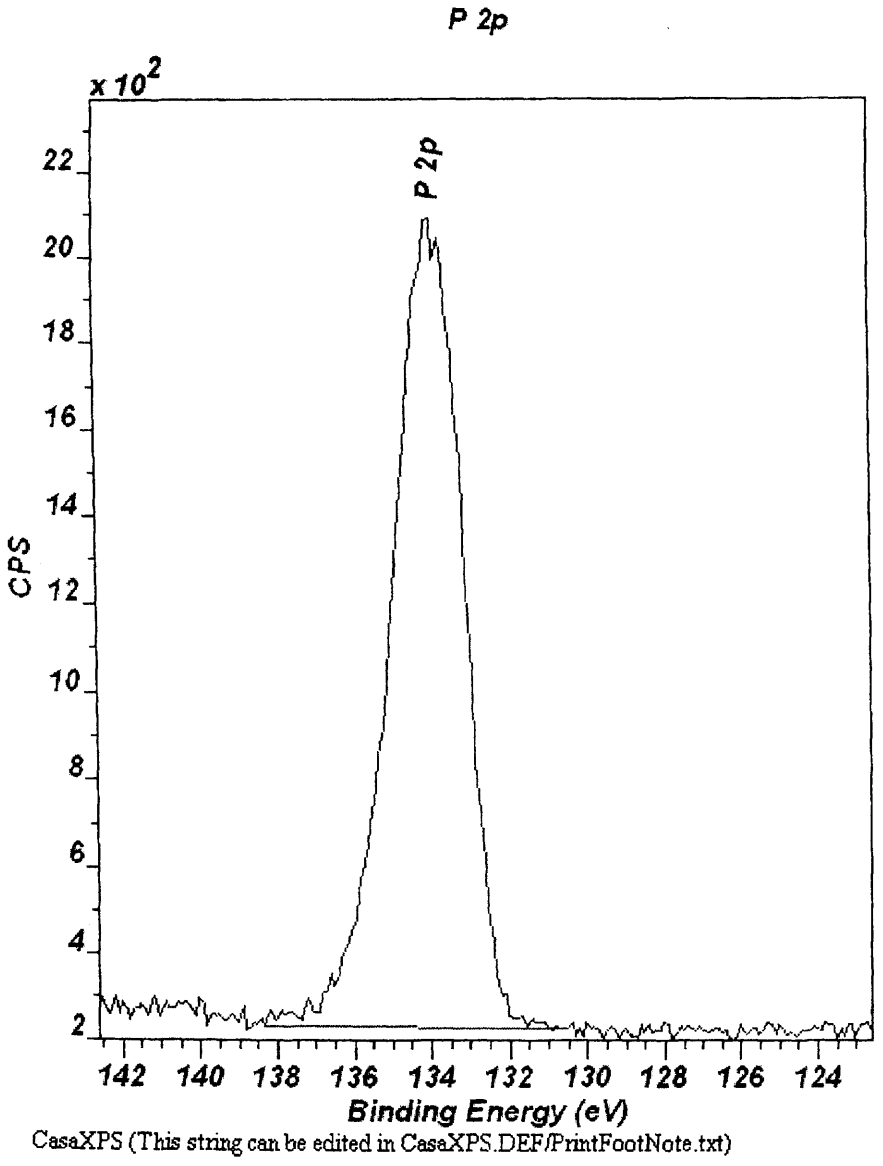

P(2p) Binding Energy	Possible Species
134.0	PO_x

A31(6)

NbOPO4 6aun

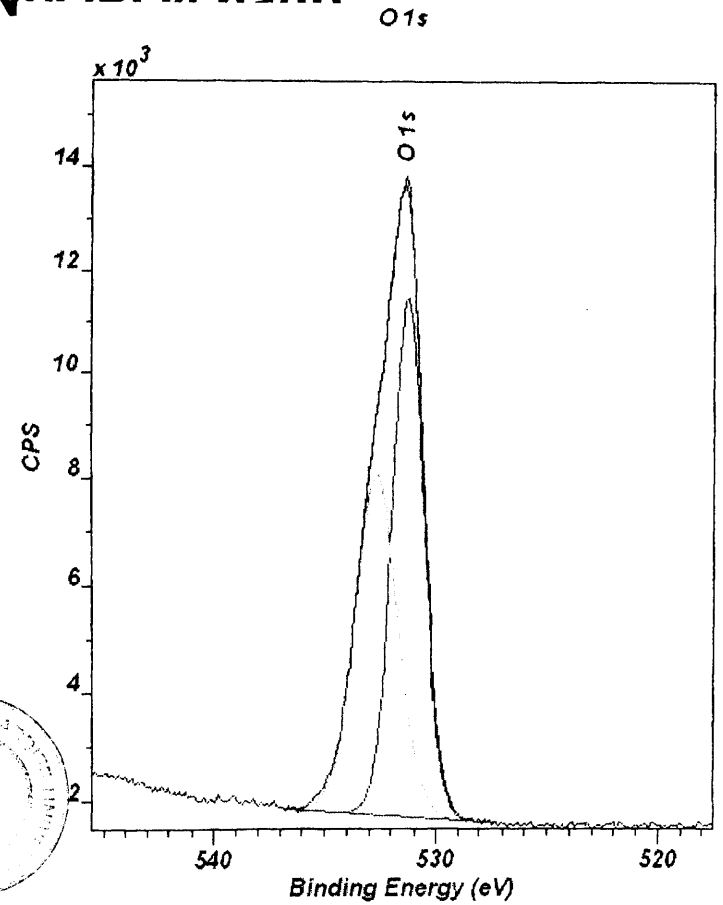

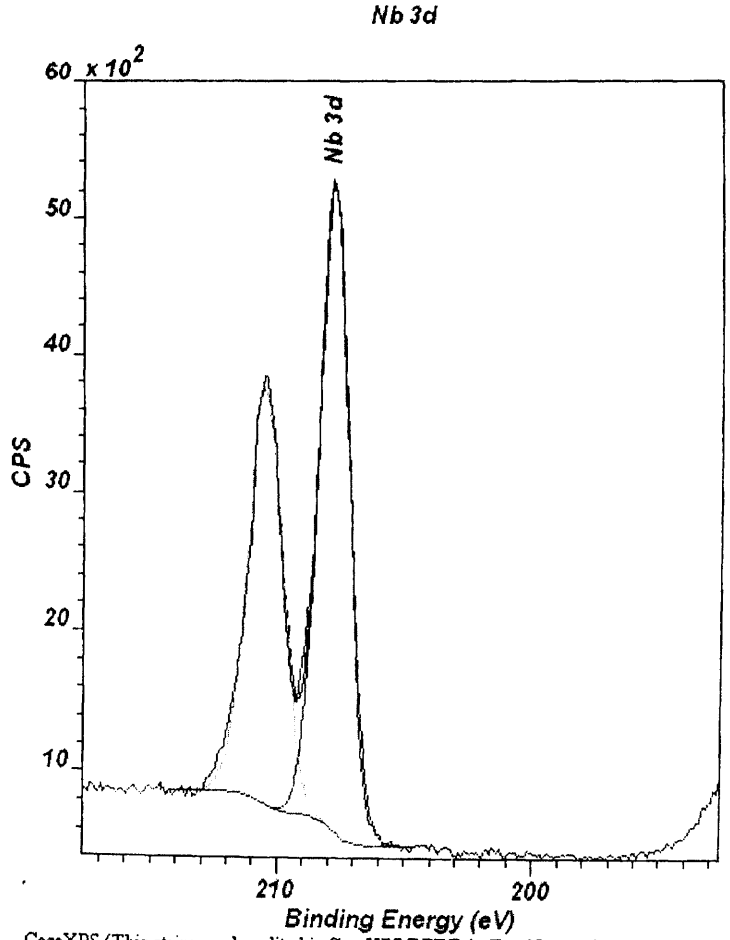

O(1s) Binding Energy	Possible Species
531.3	CO_3, PO_4, OH
532.7	PO

Nb(3d) 5/2 Peak Binding Energy	Ox. State
207.8	+5

A31(c)